Theses and Dissertations   1. Thesis and Dissertation Collection, all items

1971

The flow of dilute polymer (Polyox WSR-301) solutions past bluff bodies in the drag transition region.

Rainey, Peter Garland.

Monterey, California ; Naval Postgraduate School

http://hdl.handle.net/10945/15724

THE FLOW OF DILUTE POLYMER (POLYOX
WSR-301) SOLUTIONS PAST BLUFF BODIES
IN THE DRAG TRANSITION REGION

by

Peter Garland Rainey

United States
Naval Postgraduate School

THESIS

THE FLOW OF DILUTE POLYMER (POLYOX WSR-301)

SOLUTIONS PAST BLUFF BODIES

IN THE DRAG TRANSITION REGION

by

Peter Garland Rainey

Thesis Advisor: T. Sarpkaya

March 1971

The Flow of Dilute Polymer (Polyox WSR-301) Solutions

past Bluff Bodies in the Drag Transition Region

by

Peter Garland Rainey
Lieutenant, United States Navy
B. Met.Eng., Rensselaer Polytechnic Institute, 1963

Submitted in partial fulfillment of the
requirements for the degree of

DOCTOR OF PHILOSOPHY

from the
NAVAL POSTGRADUATE SCHOOL
March 1971

ABSTRACT

Flow of aqueous solutions of Polyox WSR-301, with concentrations of 1.0 to 200 wppm, past bluff bodies was investigated in the cylinder drag transition region of Reynolds numbers. Lift and drag forces were measured on a NACA-0024, four-inch chord hydrofoil. Drag force, pressure distribution and separation angle were measured on circular cylinders (diameters from 1/4 to 1-1/2 inch).

The polymer additive was found to alter only those drag coefficients which have a Reynolds number transition region. Two distinct types of cylinder drag transition were observed: (1) At high concentrations, transition from sub-critical to a transcritical flow occurred at the same free stream velocity independent of body diameter; and (2) at low concentrations and/or molecular weights, tripping from a sub-critical to a super-critical flow occurred at a well defined flow condition which was a function of free stream velocity, body diameter and turbulent pipe-flow friction reduction. In all cases, transition occurred earlier than that in the pure solvent. The polymer had a de-stabilizing effect on the boundary layer flow.

TABLE OF CONTENTS

LIST OF TABLES

LIST OF FIGURES

Figure

Figure

Figure

c^*	critical shear wave velocity
C_d	drag coefficient
C_p	pressure coefficient
d	diameter of circular cylinder
D	drag force
h	test section height
L	length of circular cylinder
M.W.	molecular weight
P_s	stagnation pressure
P.D.R.	per cent (pipe) drag reduction
Re	Reynolds number
Re_c	critical Reynolds number
T.R.T.	total (pump) running time
U	corrected free stream velocity
V	measured free stream velocity
Wn	Weissenberg number
wppm	weight part of solute per million of solvent
α	hydrofoil angle of attack
ε_t	total velocity correction factor
θ	cylinder angle measured from forward stagnation point
μ	dynamic fluid viscosity
ν	kinematic fluid viscosity
ρ	fluid density
τ_w	wall shear stress

ACKNOWLEDGEMENT

I. INTRODUCTION

A. SURVEY OF THE PREVIOUS INVESTIGATIONS

There has been considerable interest in fluid dynamic studies of the flow of dilute polymer solutions in water during the years since 1965 for the purpose of optimizing the speed and endurance characteristics of submerged or partly submerged bodies. The motivations for this optimization through the reduction of resistance rather than by the increase of the power and efficiency of the propulsion systems and drives came from the "Toms' effect." In 1948, Toms [Ref. 1] demonstrated that a dilute solution of polymer in a Newtonian solvent drastically reduced frictional drag under turbulent flow conditions. The discovery of Toms' effect did not arouse particular interest until the 1960's. Since then, an increasing number of experiments in chemistry, physics and fluid dynamics have been carried out. Some of the reports of these investigations contained empirical correlations, theoretical analyses based on viscoelastic models, and phenomenalogical descriptions of various mechanisms to explain the role played by polymer molecules, clusters and/or chains in reducing the wall friction, and in modifying the remainder of the flow field. Excellent surveys of such research have been presented by Hoyt and Fabula (1964) [Ref. 2], Deavors (1966) [Ref. 3], Lumley (1967) [Ref. 4], and A. White (1968) [Ref. 5].

Although drag reduction has been achieved with a great variety of substances, the most efficient additives in terms of drag effect per unit concentration appear to be high-molecular-weight, long-chain polymers. Despite the availability of considerable data on the behavior of such

13

systems, no concensus has been reached to explain the mechanism by which frictional reduction occurs. This is partly because all types of fundamental experiments have not yet been carried out to determine the number and range of parameters underlying the phenomenon, partly because polymers themselves do exhibit variations which may at times be far in excess of the experimental errors from one investigation to another, partly because some of the reported experiments did not contain all the necessary and pertinent information to enable its re-analysis, and partly because the results of some of the investigations were interpreted in the light of the ideas, parameters and models then available, thereby lacking some measurements which could not now be repeated to render the data usable. It should in all fairness be pointed out that the foregoing reasons are not peculiar to the study of dilute polymer solutions and they may be equally applicable to the growth of any new discovery.

It is generally theorized that the phenomenon is invariably bound up with the molecular nature of the polymeric materials being composed of long-chain molecules which impart pseudo-plastic and visco-elastic properties (shear modulus and viscosity) to their aqueous solutions depending on their age and degradation and the particular experimental set-up used to test their physical properties. In fact, it is the introduction of the new parameters such as concentration, molecular weight, degradation, and the dependency of the fluid's physical properties on the geometric, kinematic and dynamic character-istics of the test system that render the Newtonian constitutive equation inapplicable to the motion of these almost water-like dilute solutions. In general, it is postulated that these long-chain

molecules, when subjected to turbulent shear flows, are somehow capable of suppressing or altering the turbulent flow structure and thickening the viscous sub-layer. Whatever the mechanism, it is apparent that additional fundamental experiments will have to be carried out to sort out the most important parameters and perhaps to look more closely into the interaction of one or more polymer molecules in a fluid volume in the order of a small eddy.

Although extensive theoretical and experimental work has been carried out with internal flows where the drag is due to turbulent skin friction alone and where the flow and the wall-shear stress distribution are essentially uniform, little is known about the effects of polymers on the flow about bluff bodies where the wake contributes significantly to the total drag and where the shear stress varies significantly and the flow separation causes significant alterations in the over-all behavior of the flow. Obviously, if the polymer additives are to achieve their predicted importance in optimizing the performance of submerged or partly submerged bodies used in marine technology, it will be necessary to know their fluid dynamical properties when applied to external body flows. The current state of knowledge acquired through the study of the flow of dilute polymer solutions in pipes may not be sufficient for the understanding of form drag reduction of bluff bodies. It is quite possible that there are several mechanisms and that the rheological characteristics of the polymer solution manifest themselves in various forms depending on the local dynamic and kinematic characteristics of the flow as determined by the body shape, flow velocity, and solution age and concentration.

The earliest known experiment with bluff bodies in drag-reducing polymers was carried out by Crawford and Pruitt [Ref. 6] in 1963. They dropped 5/8-inch-diameter rubber and steel spheres in Guar gum solutions and reported that at 2,500 wppm[1] the drag on both the steel and rubber spheres was reduced. But at 5,000 wppm, only the drag on the steel sphere was less than it would be in water. Ruszczycky [Ref. 7] carried out some measurements in 1965 on the fall velocity of steel spheres in polyethylene oxide "Polyox WSR-301," using spheres of diameters from 3/8 inch to one inch in concentrations up to 15,000 wppm. He found that for all spheres with a diameter less than 1/2 inch, as the concentration was increased, the drag at first decreased, reaching a minimum between 2,500 wppm and 7,500 wppm. The largest drag reduction observed was 26% obtained with the one-inch sphere in 7,500 wppm solution. These results, although inconclusive because of their limitations and confinement to polymer solutions of very high concentrations, appear to point out that a mechanism different from that observed for turbulent flow in pipes may be in operation.

A. White [Refs. 8, 9] conducted some experiments by dropping concrete and steel spheres with different diameters into a tank which contained a WSR-301 solution. Using high-speed photography, the wake patterns and traces of the spheres were recorded. His experiments indicated that below the critical Reynolds number, where the boundary layer is laminar, the drag on a sphere is considerably reduced by adding Polyox, although drag reduction in pipe flow occurs only in the

---

[1]Weight part per million

16

<u>turbulent</u> region. White's flow visualization studies showed that delayed boundary layer separation and the small wake size with the polymer solutions are associated with the drag reduction. He further concluded, on the basis of the observations of Brennen and Gadd [Ref. 10], that the delayed laminar separation is caused by visco-elastic effects because the phenomenon seems to occur only with solutions which exhibit normal-stress-difference behavior.

Lang and Patrick [Ref. 11] observed the flow about freely falling spheres, cylinders, disks, and cones in Polyox solutions 200 to 1,000 wppm. They noted that there was drag reduction for only those bluff bodies which had a movable separation point. However, they also reported that there was no significant drag reduction for circular cylinders for Re $< 2 \times 10^4$. They further suggested that the mechanism which causes the polymer molecules to shift the separation point is not apparent and merits further investigation. In Lang and Patrick's experiments, the fall of the objects was not always steady and at times there were sudden shifts in the direction of fall. For reasons yet unknown, the drag of spheres in Polyox solutions did not follow the typical trend of sphere drag in plain water as a function of Reynolds number as far as the characteristic sharp decrease, which is due to sudden transition to turbulent separation is concerned.

Extensive studies on freely falling spheres have been conducted by Hayes [Ref. 12] and Chenard [Ref. 13]. With WSR-301, in a Reynolds number range of approximately 10^4 to 10^5, Hayes observed that there was no drag reduction at Reynolds numbers below 10^4, drag reduction increased with the Reynolds number, and the maximum drag reduction occurred in a concentration of 100 wppm for Reynolds numbers between 10^4 and 10^5.

17

James [Ref. 14] investigated the drag reduction of small circular cylinders in laminar flow of WSR-301. The use of small wires and flow speeds limited the Reynolds number range of the experiments to 100. Concentrations were varied from 8 to 220 wppm. An injected dye study was also performed which revealed viscoelastic effects of the polymer on the flow patterns around the cylinder. For the Reynolds number range encountered in this experiment, the drag coefficient increased with increasing polymer concentration when the Reynolds number was greater than a critical value, which itself was a function of concentration.

McClanahan and Ridgely [Ref. 15] towed circular cylinders through WSR-301 in the Reynolds number range of 2×10^3 to 2×10^5. They reported that the drag was increased at Reynolds numbers below 10^4. They supported Hayes' conclusions of drag reduction above 10^4 and maximum drag reduction at a concentration of 100 wppm. Fresh mixtures of the polymer solution were always used for these investigations.

Sanders [Ref. 16], based on the previously mentioned works, proposed that the drag reducing mechanism of dilute polymer solutions was due to a delay in the boundary layer separation caused by the stabilization of the laminar boundary layer. The proposed action reduced the size of the wake, which in turn decreased the drag. He further concluded that only those polymers that produce a dual terminal velocity in high concentrations have the ability to reduce drag.

Brennen [Ref. 17] investigated the effect of polymer additive on the position of the separation line on several cavitating headforms. The

apparatus consisted of a container tank and a vertical pipe which was connected to the bottom of the tank. Models were supported on a 0.15-inch-diameter sling inside the pipe, and sudden release of a flap valve at the end of the pipe provided gravity-driven flow. Velocity of the flow was controlled with a variable orifice. He used two spheres and a cylinder with respective diameters of 1/4 inch, 1/2 inch and 1/4 inch in a polymer solution of 50 wppm. Pictures taken with a high-speed camera have shown that the separation lines on the bodies in polymer solutions moved further downstream as compared to those of water. Reynolds number range for these experiments was 10^4 to 8×10^4. This study also revealed another interesting phenomenon: After a certain speed (7 fps for 1/2-inch sphere and 8 fps for cylinder) the separation line became gradually distorted into a wavy pattern. These irregularities appeared to have a lateral wave length reflected on the separation line. The wave length decreased sharply with increasing speed. Degradation produced no measurable effect on the magnitude of the spanwise wave length exhibited at a particular speed and slightly increased the critical speeds at which the various types of distortion occurred. But even for the most degraded solution, these threshold speeds were not raised by more than about 3 fps.

Luikov et al. [Ref. 18] carried out experiments with Na-Cmc solutions at high concentrations and found that the separation point moved farther downstream. They conjectured that the decrease of the resistance of the cylinder was partly due to the smaller size of the wake and partly due to a change in the character of the vortical motion in the aft region

of the cylinder. They observed notable changes in the vortex motion with the increase of the concentration of the polymer and a reduction in turbulence. They concluded that the elastic energy stored in the fluid in the polymer particles was redistributed later near the separation point and, as a result of the additional momentum provided by this redistribution, the fluid particles were able to move farther downstream against a positive pressure gradient. Barenblatt et al. [Ref. 19] measured the drag force on a rough cylinder from which highly concentrated solutions of long-chain polymers were injected. Drag reductions of 20% to 34% were achieved. Tests with glycerin injection, which did not reduce drag, showed that contraction of the wake was independent of the type of fluid injected. He therefore concluded that the contraction of the wake and the displacement of the separation point further downstream cannot conclusively explain the drag reduction phenomenon.

B. A CRITICAL DISCUSSION OF THE PROPOSED DRAG REDUCTION MECHANISMS
REGARDING THE FLOW ABOUT SUBMERGED BODIES

It is apparent from the foregoing section that the mechanisms proposed for the reduction of the drag of bodies moving through polymer solutions are less coherent and loosely related to the mechanisms for the drag reduction in pipes. This is partly because the drag reduction has been studied more extensively in conduits and additional data provide ways and means of refuting or substantiating the mechanisms proposed. Secondly, in pipe flows, the motion was essentially steady, uniform, had a uniform wall-shear distribution (somewhat affected by the polymer degradation along the length of the pipe), had no separation, no stagnation

point, no curvatures and the motion was often beyond the transition point.

The investigation of the pipe entrance region, in which convective accelerations are significant, has received even less attention than the study of external flows.

In external flows, however, the motion is unsteady due to the vortex shedding in the aft region of the cylinder, has variable shear and is accompanied by separation, stagnation, rapidly varying pressure gradient, wall curvature, and "drag crisis" at or near the transition of the laminar boundary layer to a turbulent state. Obviously, the flow about bodies introduces factors which are not encountered in the experiments conducted with pipes. Thus the relative simplicity of the pipe flows enabled the experimenters to cope with the problem in a somewhat neater way and to propose some empirical relations regarding the drag reduction. In spite of that, the present understanding does not go beyond the conjecture that the drag reduction phenomenon is an elastic interaction between polymer and turbulence. An outstanding study of drag reduction in pipes and a comprehensive discussion of the existing theories have been presented by Paterson [Ref. 20]. In summary, Paterson classified the major schools of thought as follows:

1. Aggregation Theory

According to this theory, clusters of polymer molecules stretch out in high shear regions suggesting similarities to the drag reduction obtained with fiber suspension. The migration of polymer aggregates in a manner similar to the red corpuscles in the arteries is

suggested to retard the intensification of shear layers through the exchange of momentum in the radial direction.

2. Anisotropic Viscosity Theory

The existence of elongated polymer coils is hypothesized. These coils are supposed to align with local shear, hinder momentum exchange normal to the direction of shear, and thus reduce the intensity of the turbulence. Accordingly the fluid is assumed to have two viscosities, one in the direction of shear (low) and one normal to it (high).

3. Viscoelastic Theories

a. The polymer coil possesses a characteristic relaxation time, displays a behavior solid-like for processes with a shorter time scale, a liquid-like behavior for processes with a much longer time scale.

b. The polymer molecule can act as an elastic body and absorb, store and release energy depending on the influence of the surrounding medium. Thus it is assumed that the polymer molecules extract energy from the buffer zone, store it by its own deformation, and transport it to the outer flow and release it there as the molecule returns to its equilibrium condition. In other words, the drag reduction is a unique function of the energy storable in the molecule to the turbulent energy diffusion.

4. High Effective (Tensile) Viscosity Theory

According to Paterson [Ref. 20], the observed high effective viscosity of a dilute polymer solution in an irrotational strain field is directly related to drag reduction and this high viscosity is a result of large polymer molecule deformations. Paterson presented a good deal

22

of qualitative theoretical and experimental evidence to support his hypothesis.

Paterson's most significant contribution is to show that drag reduction divided by weight concentration approaches a maximum as the concentration approaches zero, thus indicating polymer-polymer interaction (entanglement) is not necessary for drag reduction.

There are, to be sure, several other proposals regarding the drag reduction mechanism which tend to reinforce the idea of the increase of the laminar sublayer and the displacement of the buffer zone away from the wall. Be that as it may, most or all of these theories have been developed on the basis of the experimental results obtained with pipe flows and do not tend to shed any light on the observations made with flows about bodies. The instability at or near the separation point observed by Brennen, the movement of the separation point aft of the bodies where the separation point is not fixed by a sharp edge, the observation of drag reduction in laminar external flows, the change of the rate of vortex shedding, and several other observations of this type cannot readily be explained with the mechanisms so far proposed. It has been generally assumed that the viscoelasticity of the fluid plays an important role in the characteristics of the flow near the separation and that one must analyze the observations on the basis of the Reynolds, Weissenberg, and Deborah numbers. Even though the idea is appealing and is in conformity with the established dynamic similarity principles of fluid mechanics, the determination of the last two numbers is extremely difficult. The viscoelasticity of the fluid in the

Weissenberg number and the relaxation time of the fluid in the Deborah number cannot be determined in a simple manner in a way similar to that of the viscosity of the solvent. Recognizing the fact that even the viscosity of the dilute polymer solutions is shear-rate dependent and that one cannot, at least theoretically speaking, refer to a singular viscosity, the difficulties associated with the determination of the elasticity coefficient and the relaxation time become apparent. It is quite possible that the fluid which appears to have lost its viscoelasticity in a given test system may appear to exhibit viscoelastic behavior in another system. There is strong evidence to the conjecture that for a given Reynolds number, the polymers exhibit higher drag reduction in very small conduits than in larger conduits. According to the "ultimate asymptot" proposal of Virk et al. [Ref. 21], the drag reduction in turbulent pipe flow is ultimately limited by a unique asymptot and the maximum attainable drag reduction is independent of polymer type and concentration and the pipe size within the limitations of the experimental errors and within the limits of the available experimental data. There is, at present, no such information available for the flow of dilute polymer solutions about bluff bodies and it appears that additional complications introduced by the characteristics of separated flows will preclude the possibility of the existence of the ultimate drag reduction even for a given shape of body.

As mentioned previously, the motion of the separation point has been associated with the viscoelastic properties of the solution. It has also been mentioned that the measurable viscoelasticity effect

(normal stress difference) appears to vanish with aging or degradation. Should this be true, the flow of degraded solutions should not affect the wake size and since the skin friction is a very small part of the total drag of a body, the aged or degraded polymer solutions should have very little or no effect on the total drag of bodies. On the other hand, the experiments by Brennen have shown that neither aging nor degradation had any measurable effects on the magnitude of the spanwise wave length exhibited at a particular speed. It thus appears that the polymer molecules or coils, however distributed and however homogeneous, do have some other properties besides those causing normal stress difference which materially affect the flow near the separation point, cause instabilities, and alter the total drag. The experiments reported in the literature have not been systematic enough to bring out this particular aspect of the polymer solvent and flow interaction.

The foregoing summary serves to supply the means and direction to the future work in this comparatively new field. It also shows in a convincing manner that if the effect of additives is to reduce the intensity of turbulence and thus the energy loss--as observed in conduit flow--then the drag coefficient for spheres of Reynolds numbers above the ordinary critical Reynolds numbers must be larger with additives than that without the use of additives. Were the hypothesis of the "reduction or suppression of turbulence by additives" universally accept-able, then the transition in the boundary layer would have been delayed, the separation point would not have moved rearward, and the drag-coefficient would not have been considerably reduced by additives

at Newtonian Reynolds numbers far below critical. As pointed out and correctly anticipated by Sarpkaya [Ref. 22], "the anamolous .fact is that the additives in the case of bluff bodies, act, oddly enough, like a tripping wire or a turbulence generating agent." It was, in fact, Sarpkaya's proposal to the Naval Ship Research and Development Center to investigate the reasons leading to this particular anomaly that culminated in the present study. It suffices to note that the results of the extensive experimental study have substantiated the correctness of the basic hypothesis advanced in the proposal and have elucidated the significant role played by viscoelasticity in general and finite shear-wave velocity in the hydro-polymeric boundary layer in particular.

II. PREVIOUS EXPERIMENTAL WORKS ON FLOW PAST BLUFF BODIES

A. A REVIEW OF THE CYLINDER DRAG-TRANSITION REGION CHARACTERISTICS

Although the circular cylinder is a simple geometric shape, when placed in a fluid stream, the resulting flow displays many complex facets of fluid mechanics. Over a wide range of Reynolds numbers, the flow has a laminar boundary layer which separates near the region where eddies, and subsequently the vortex sheet, are formed. This vortex action drastically alters the pressure distribution and causes a drag and an oscillatory lift force.

Fluid flow around cylinders has been classified into Reynolds number regimes, each regime displaying its own peculiar characteristics. Lienhard [Ref. 23] presented a very logical classification based on vortex characteristics as shown in Fig. 1. In the lowest Reynolds number range, the drag coefficient C_d is equal to $8\pi/Re(2.002-LnRe)$, according to Lamb, and the drag force is approximately proportional to velocity. In the regime of $300 < Re < 10^5$, the drag coefficient is approximately constant at 1.2 and the drag force is proportional to the square of velocity. This type of flow, which is called subcritical by Schlichting [Ref. 24], has the typical pressure distribution shown in Fig. 2. The boundary layer remains laminar until separation. At a higher Reynolds number the Eiffel effect, a sudden decrease in drag coefficient, occurs. Flows at higher Reynolds numbers are called super-critical and display the typical pressure distribution as shown in Fig. 3. In this regime, the boundary layer becomes turbulent prior to separation.

27

U ⇒

Re < 5   UNSEPARATED FLOW

5 < Re < 40   FIXED PAIR OF VORTICES IN WAKE

40 < Re < 150   LAMINAR VORTEX STREET

150 < Re < 300   TRANSITION IN VORTEX STREET

$300 < Re \lesssim 3 \times 10^5$ TURBULENT VORTEX STREET

$3 \times 10^5 \lesssim Re < 3.5 \times 10^6$ NO VORTEX STREET TRANSITION IN BOUNDARY LAYER

$3.5 \times 10^6 < Re < ?$ BOUNDARY LAYER TURBULENT RE-ESTABLISHMENT OF TURBULENT VORTEX STREET
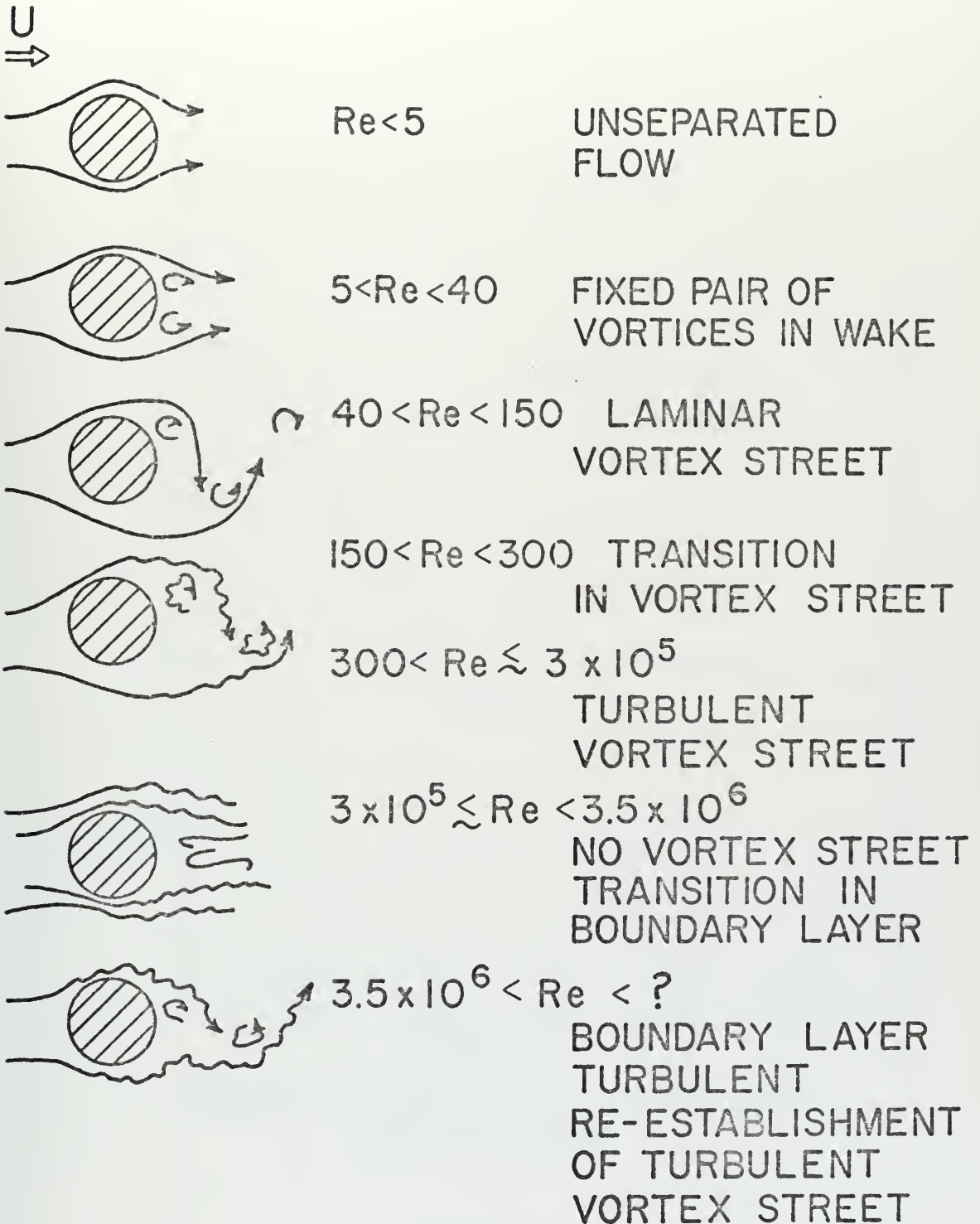
FIGURE 1: FLOW PAST CYLINDERS
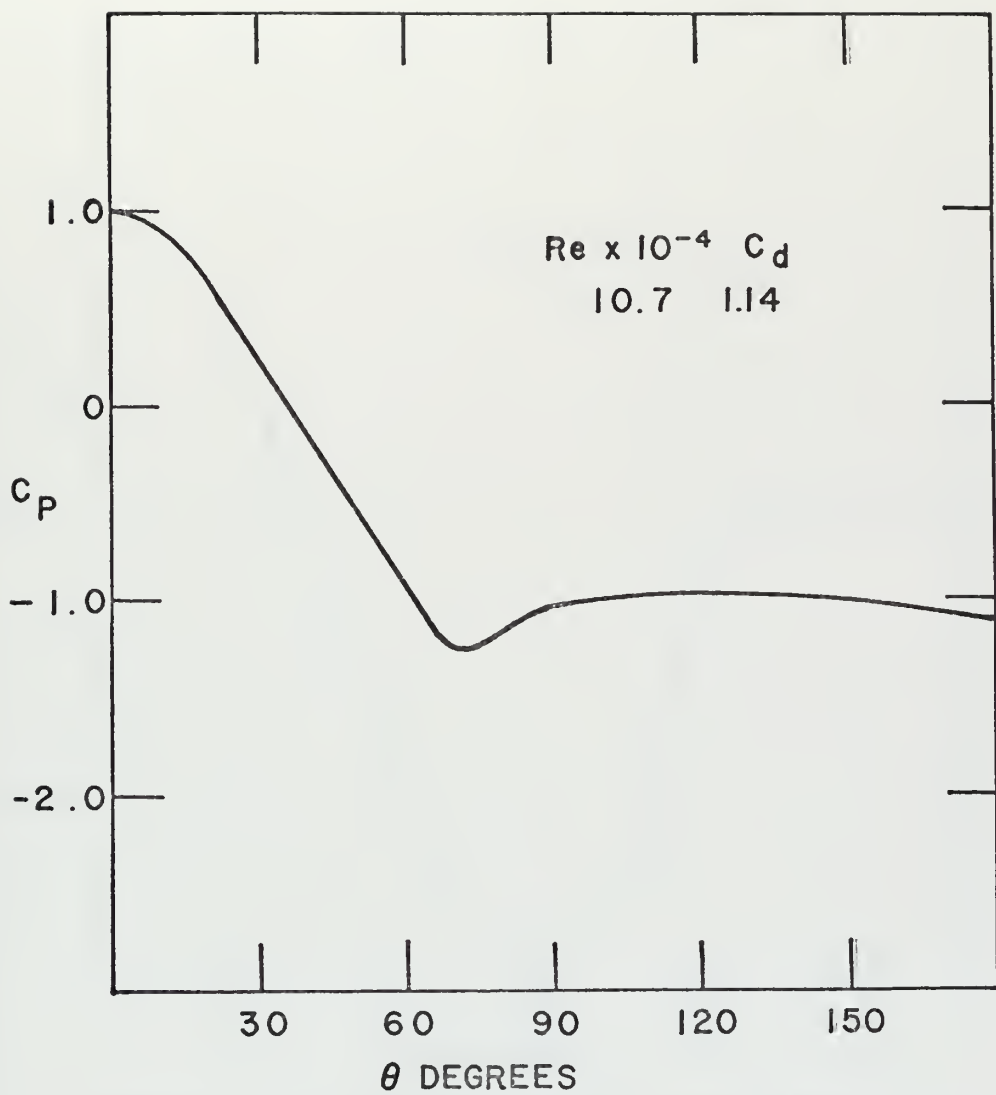
FIGURE 2: SUB-CRITICAL PRESSURE
DISTRIBUTION.

29
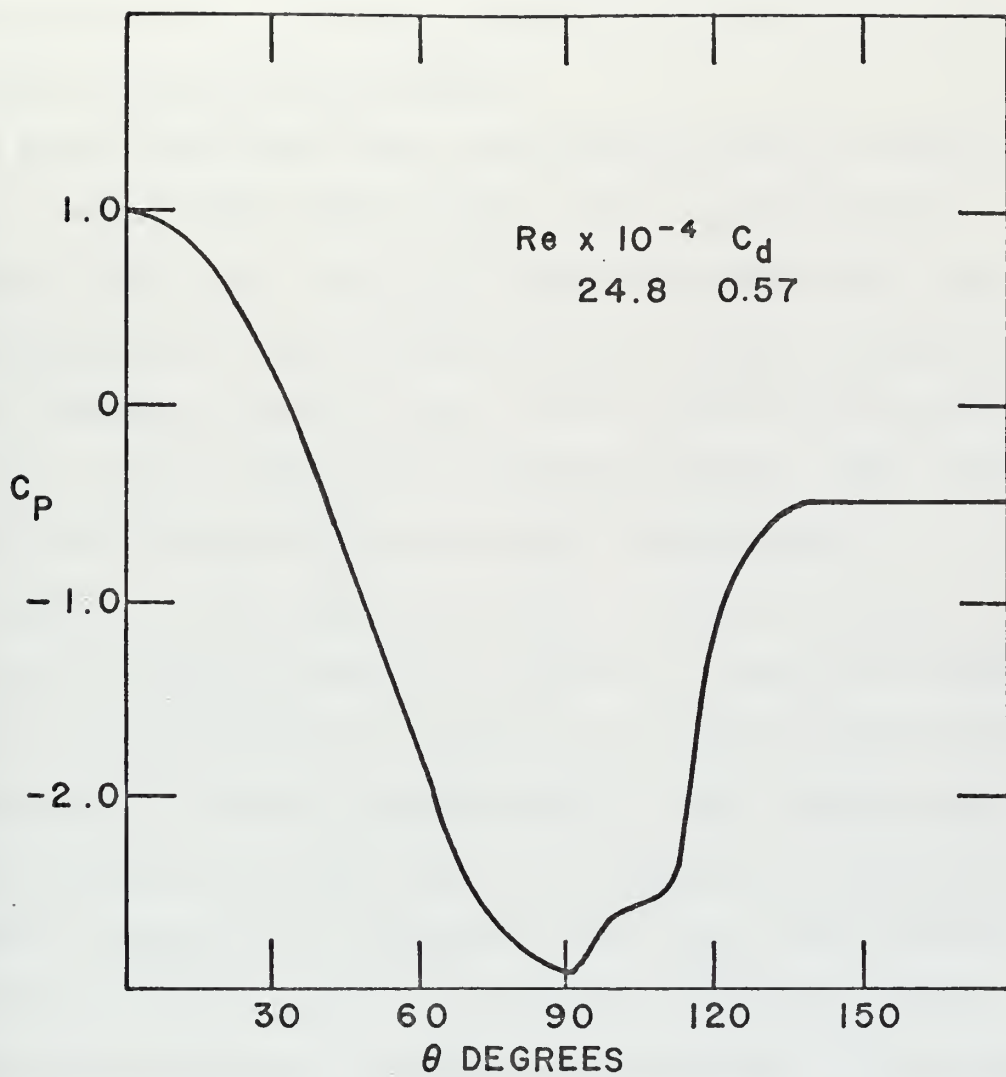
FIGURE 3: SUPER-CRITICAL PRESSURE
DISTRIBUTION.

A recent review of lift, drag, and vortex frequency data for rigid circular cylinders (in Newtonian fluid flow) has been made by Lienhard [ref. 23]. As noted by him, the drag coefficients differ from experiment to experiment, the scatter within one set of data can be appreciable, and the Eiffel effect occurs over a range of Reynolds numbers depending upon the wind tunnel used.

A graph of drag coefficient versus Reynolds number is shown in Fig. 4, for the Eiffel effect region. Data are plotted from the reports of Fage [Refs. 25, 26, 27], Delany and Sorensen [Ref. 28], and Humphreys [Ref. 29]; and include results from Göttingen open jet tunnel, various NPL tunnels, Ames 7 x 10-foot, and Harvard one-meter tunnels. As seen from the data, the critical Reynolds number for smooth circular cylinders depends upon the tunnel characteristics.

Prandtl, in 1914, demonstrated that, by mounting a thin wire ring at a short distance in front of the equator of a sphere, the boundary layer may be made artificially turbulent at a lower Reynolds number and the decrease in drag may be precipitated at a lower Reynolds number. Schlichting [Ref. 24] states that, "As a consequence of transition to turbulent flow the point of separation which lies slightly forward of the top for a laminar boundary layer moves a considerable distance in the downstream direction reducing the wake diameter." The narrower wake causes a rise in back pressure (pressure recovery) which results in a reduced drag.

Fage and Warsap [Ref. 27], in 1929, reported the effects of artificially created turbulence and surface roughness on the drag of cylinders. Their results are shown in Figs. 5, 6, 7. The artificial

31
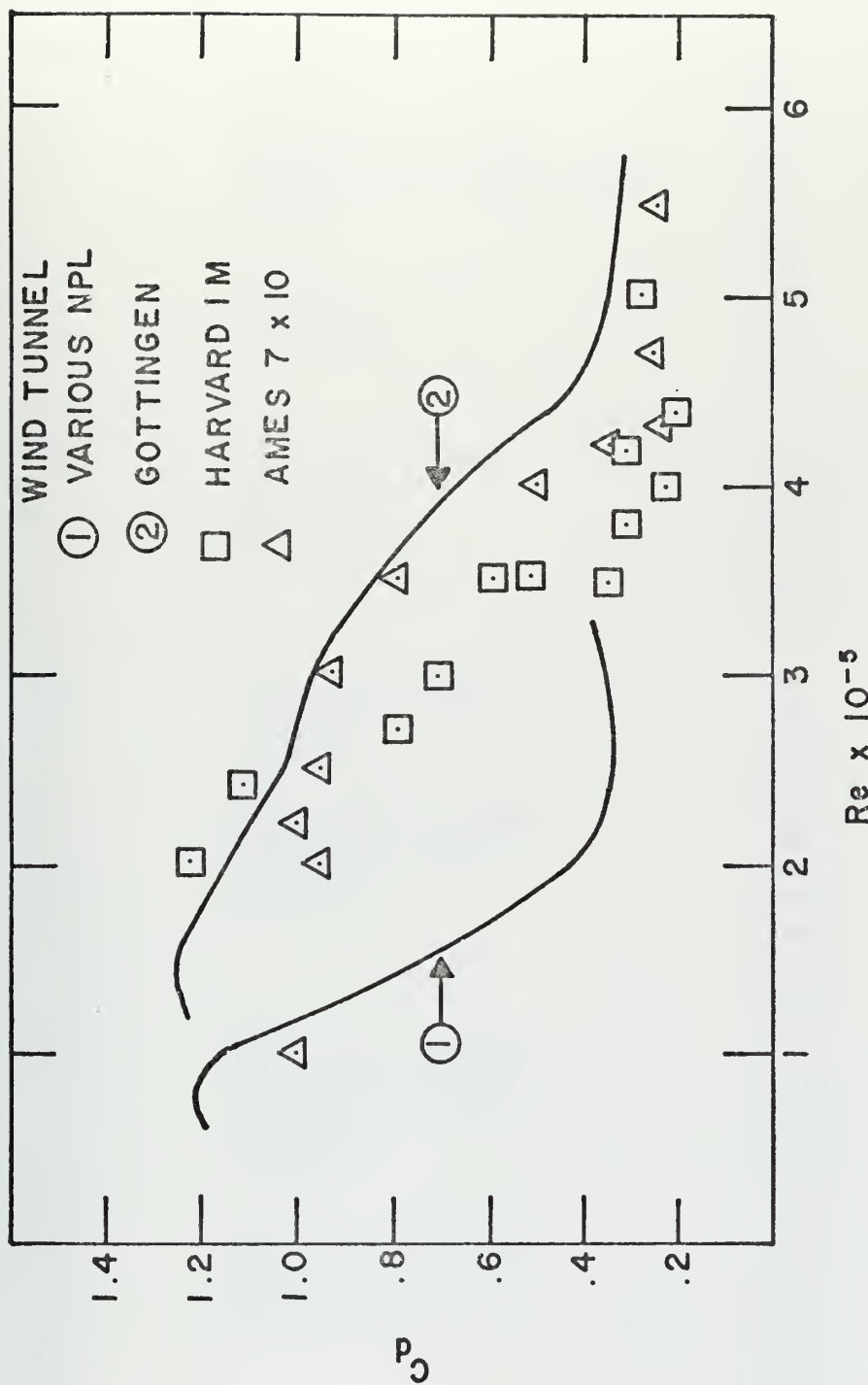
FIGURE 4: C_d TRANSITION REGION FOR CIRCULAR CYLINDERS.

TABLE I

C_d vs. Re in the Eiffel Effect Region

Ref.	Comments	C_d	Re x 10^{-5}
25	Göttingen open jet tunnel (values from plot) d=80 mm	1.22	1.18
		1.25	1.47
		1.20	1.74
		1.15	2.04
		1.08	2.30
	d=42 mm	1.05	2.46
	d=300 mm	.88	3.4
		.4	4.56
		.31	4.76
26	NPL 4-ft. tunnel corrected d=5.89 in. d=2.93 in.	.504	2.12
		.746	1.66
		1.174	1.06
		1.213	1.06
		1.204	.83
		1.188	.60
25	NPL Duplex tunnel corrected (1.07) d=23 in.	.19	3.0
		.256	4.8
		.274	7.2
		.312	9.6
	NPL 7-ft. #2 tunnel corrected (1.04) d=9 in. by Relf	.866	1.41
		.682	1.65
		.394	1.88
		.318	2.12
		.356	2.35
		.326	2.59
		.342	2.84
	NPL 4-ft. #1 tunnel corrected (1.14) d=9 in. by Relf	1.006	1.18
		.750	1.41
		.330	2.12
		.328	2.35
		.328	2.84
	NPL 4-ft. #2 tunnel corrected (1.14) d=8.9 in.	1.122	1.025
		.906	1.25
		.406	1.88
		.346	2.70
		.392	3.31
		.710	1.43
		.544	1.63
		.560	1.65
		.300	2.36

TABLE I (cont.)

Ref	Comments	C_d	Re x 10^{-5}
29	Harvard closed	1.22	2.0
	one-meter tunnel	1.15	2.3
	d=6 in.	1.1	2.4
	selected values from	1.15	2.5
	graph	.7	3.0
	with open-end gap	.78	2.7
		.5	3.5
		.58	3.5
		.34	3.5
		.30	3.6
		.30	3.8
		.30	4.2
		.30	5.2
		.30	5.8
		.20	4.44
		.22	4.0
		.23	5.0
	with double gasket seal	1.15	1.8
		.9	2.6
		.3	4.2
28	Ames 7 x 10-ft. tunnel	1.0	1.0
	corrected for wall effect	.95	2.0
	and Mach #	1.0	2.2
	d=4 and 12 in.	.95	2.5
	selected values from	.92	3.0
	graph	.90	3.3
		.80	3.5
		.50	4.0
		.36	4.2
		.24	4.3
		.24	4.7
		.26	4.7
		.28	4.7
		.24	5.5
		.26	5.5
		.28	5.5

FIGURE 5: EFFECT OF TUNNEL TURBULENCE INTENSITY

35
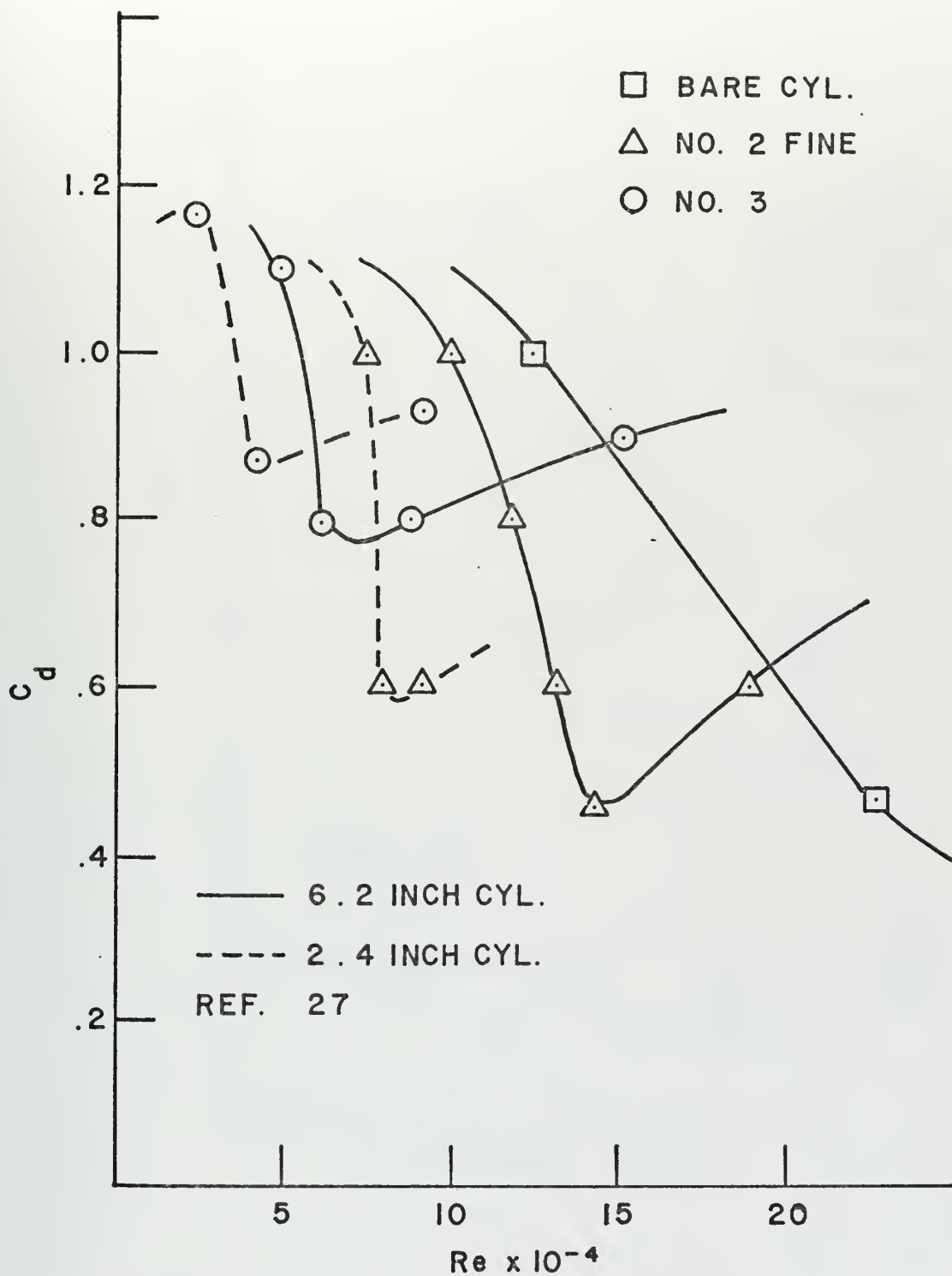
FIGURE 6: C_d vs Re EFFECT OF ROUGH
SURFACES.

36
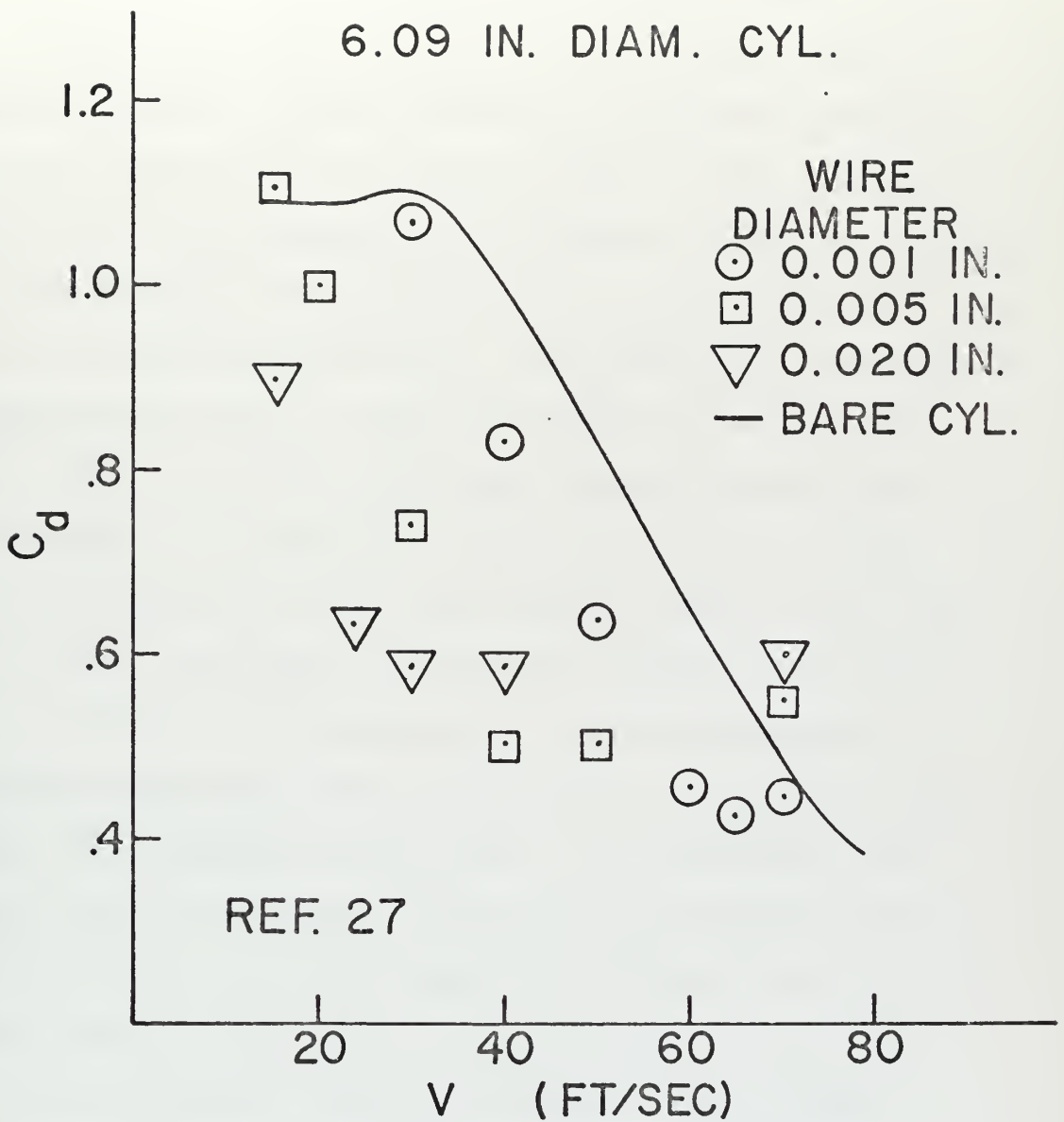
FIGURE 7: EFFECT OF
TRIPPING WIRE

turbulence was created by rope netting of 0.25-inch diameter and a mesh of 1.5 inches. As seen in Fig. 5, the effect of upstream turbulence is to shift the transition curve to lower Reynolds numbers as turbulence intensity (nearness of netting) increases while maintaining the same transition characteristics (shape of curve). However, the effects of surface roughness and tripping wires alter the transition characteristics: The earlier the Eiffel effect occurred, the higher the value of drag coefficient in the supercritical flow regime.

Humphreys [Ref. 29], in 1960, investigated the boundary layer on a cylinder in the Eiffel effect region visually and with a hot wire anemometer. He reported that "the breakdown of the periodic wake into a turbulent one, with large concurrent drops in both force (lift and drag) coefficients, has long been connected with boundary layer transition prior to separation; but this has been explored further and specifically tied to the appearance of a particular kind of mixed flow." Humphreys further noted that "with threads on the cylinder surface, this becomes a stable span-wise pattern of cells in the conclusion that such cells, composed of turbulent fluid of various shapes and varying sizes, are for the bare (smooth) cylinder the first sign of developing transition at critical Reynolds number." In the same year, Roshko [Ref. 30] investigated the flow past an 18-foot cylinder in a pressurized wind tunnel at Reynolds numbers of 10^6 to 10^7. At the highest Reynolds numbers, the drag coefficient rose to about 0.7, period vortex shedding was re-established and
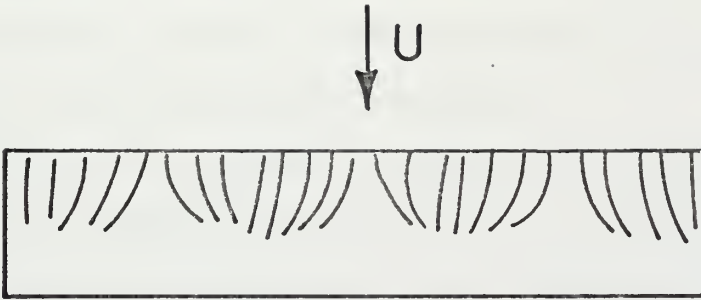
REF. 29

FIGURE 8: THREADS SHOWING
SPANWISE CELL STRUCTURE
AT CRITICAL REYNOLDS NO.

a unique pressure distribution was measured as shown in Fig. 9. He proposed that in the supercritical range (Eiffel effect region) there is a laminar separation bubble followed by turbulent separation, and in the transcritical range (Re > 5 x 10^6) the separation is purely turbulent. It can be conjectured from the two works cited above that in the transcritical range, the turbulent cell structure no longer exists, turbulent separation reaches a stationary point, still on the back of the cylinder, and C_d becomes nearly constant.

The drag force on a cylinder is composed of two components: The area integral of surface shear stress and the area integral of normal pressure. The surface shear stress is the predominant contributor to drag, only in unseparated flow, and becomes insignificant above a Reynolds number of approximately 1,000. Although the effect of viscosity on flat plates is skin friction, the significant effect of viscosity on bluff bodies is the generation of eddies forming a wake.

Since the skin friction is negligible, the drag reduction must be accomplished by altering the pressure distribution. The "inviscid fluid" pressure distribution or the d'Alembert solution is the ultimate in drag reduction, i.e., zero drag force. Any mechanism which results in increasing the pressure coefficient on the back side of the cylinder will result in apparent drag reduction. In Newtonian fluids, one such mechanism is the transition to turbulent flow. As shown by Fage, either increasing the turbulence level in the free stream or creating turbulent boundary layer by fine tripping-wires on rough surfaces results in lowering the Reynolds number at which the drag crisis occurs. "It would
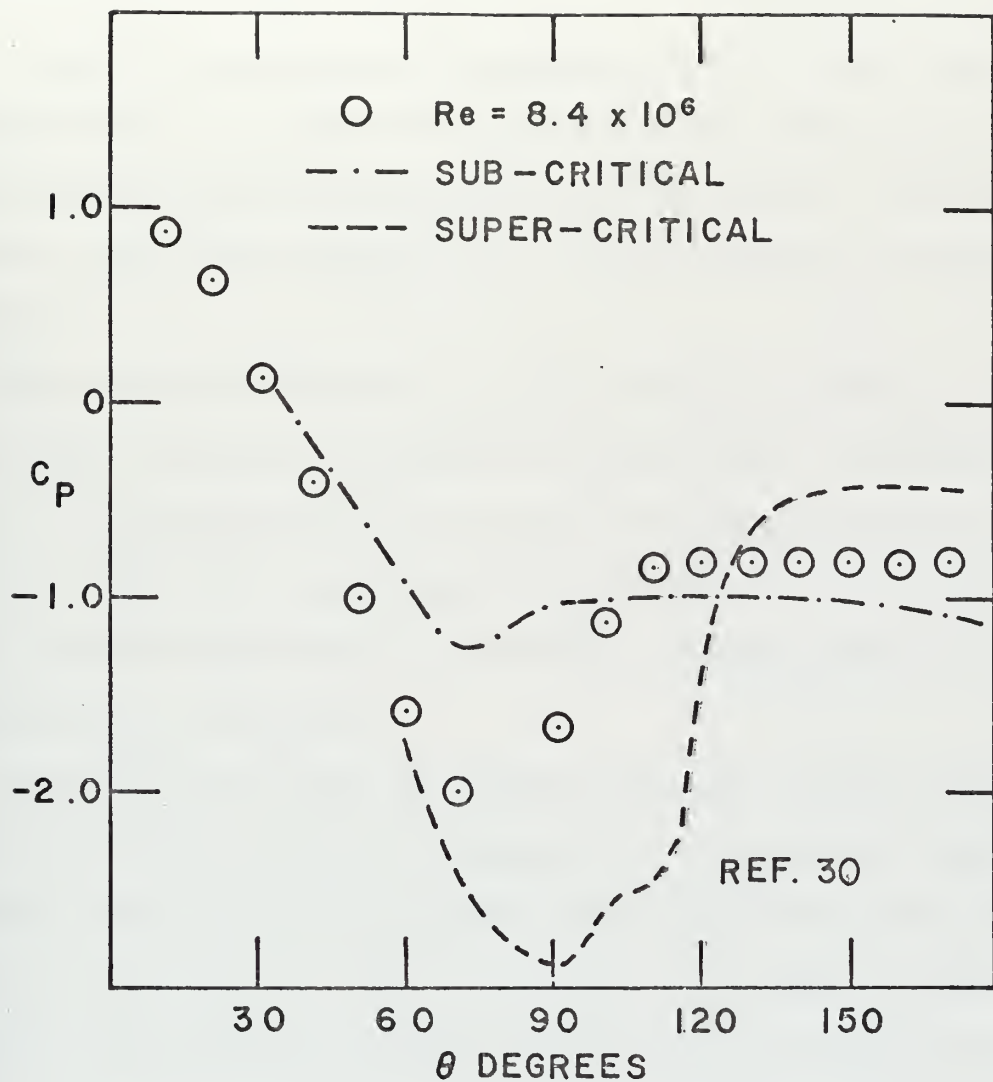
FIGURE 9: TRANSCRITICAL PRESSURE DISTRIBUTION.

41

appear that these orderly changes (in drag coefficient) in response to systematic changes in the disturbing influences preclude any idea that the flow which has been considered is of a critical nature even though it is sensitive to extraneous disturbances" [Ref. 27]. When Humphreys placed threads on a cylinder to visualize the flow, there resulted an altering of the Eiffel effect region as seen in Fig. 10. The "stabilizing" of the three-dimensional cell pattern resulted in apparent drag reduction.

The pressure distribution can also be altered by centrifugal forces. Measurements performed by Luthander and Rydberg [Ref. 31] show that the region of the Eiffel effect for a sphere is strongly dependent upon the rotation factor $U/R\omega$. According to these researchers, "the centrifugal forces have the same effect as an additional pressure gradient directed to the plane of the equator."

It can be inferred from the foregoing that one or more of the proposed drag reduction mechanisms [aggregations of molecules (roughing elements); viscoelastic extra normal stresses (modified pressure gradient), or high tensile viscosity (threads)] can trigger an instability and alter the Eiffel-effect Reynolds-number range and characteristics. Thus, in the final analysis one has to understand the inception of the instability of flow in the boundary layers and establish a relationship between the observed instability mechanism and the role played by the additives in enhancing or inhibiting that instability.

B. A REVIEW OF THE STABILITY CHARACTERISTICS OF FLOW ABOUT CYLINDERS

In the last ten years, considerable information has been obtained about the stability characteristics of flow about circular cylinders
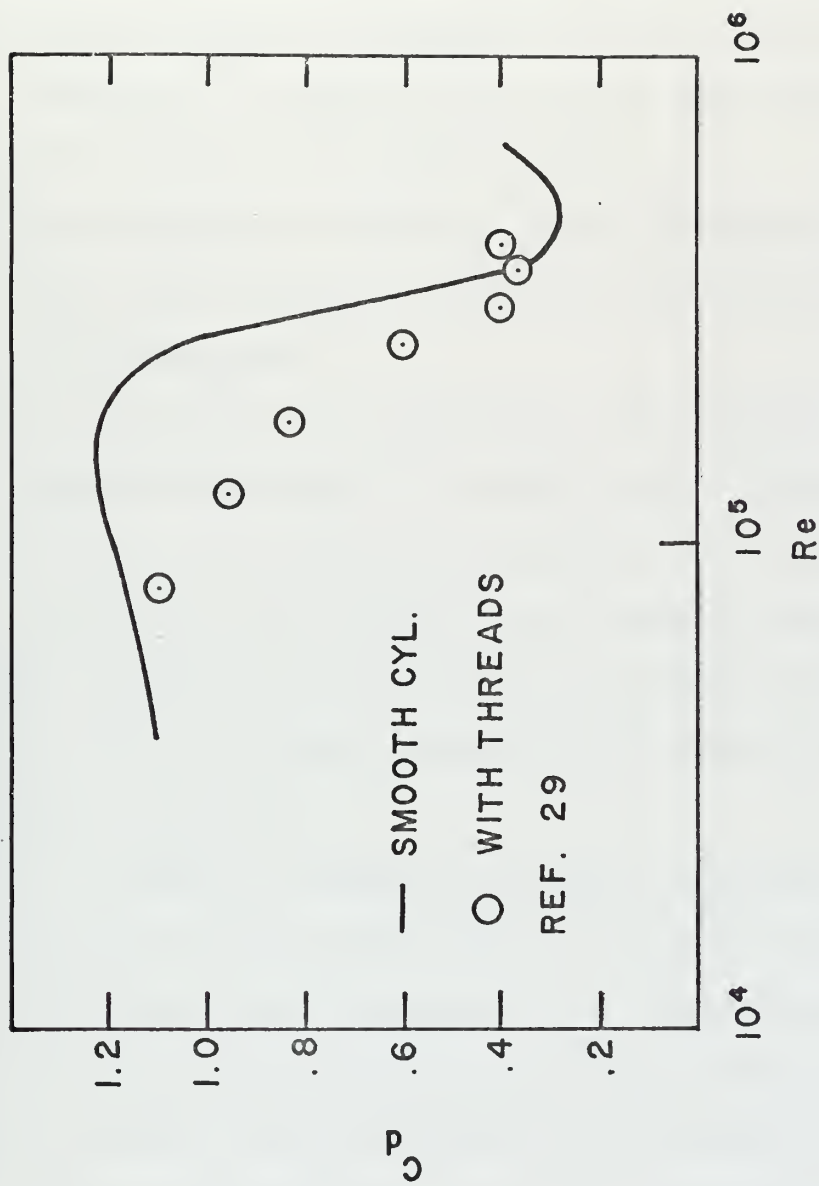
FIGURE 10: C_d vs Re EFFECT OF THREADS.

43

A synopsis of three of the most recent works [Refs. 32, 33, 34] is given below:

Petarka and Richardson [Ref. 32], based on the study of the effect of a sound field on the flow and heat transfer about a circular cylinder for an Re in the order of 10^4, assert the following:

(1) The shear layers that separate from the cylinder surface are intrinsically unstable but the rate of amplification of disturbances depends on the Reynolds number.

(2) In the absence of externally imposed disturbances, the separated shear layer develops its instability by rolling up into a train of discrete cores.

(3) In the presence of a sound field, with a frequency close to that naturally occurring in the shear layer, the growth of the instability in the shear layer is enhanced, with the processes of vortex fusion and possibly vortex breakdown being detectable.

Dale and Holler [Ref. 33], based on the study of forced oscillation of a circular cylinder in water flow and review of the pertinent literature, stated that:

(1) It is generally accepted that laminar-to-turbulent transition occurs in the free shear layer of a circular cylinder immediately downstream of separation at a Reynolds number of 10^5. As Re decreases, the transition zone moves downstream.

(2) Sinusoidal velocity fluctuations which precede transition amplify and subsequently develop into turbulence. These fluctuations or waves, originate in the attached boundary layer and are sensitive to external perturbations.

(3) Transition vortices shed from both sides of the cylinder

   simultaneously with opposite circulation.

(4) Their frequency is directly related to the free stream velocity

   divided by the boundary layer thickness at the point of separation.

   Kestin and Wood [Ref. 34] examined the stability of the uniform

flow approaching a two-dimensional stagnation region formed on a

cylinder immersed in a cross flow. They determined analytically,

and supported with experimental evidence, that the resulting flow

is one in which a regularly distributed system of counter-rotating

stream-wise vortices is super-imposed on the basic pattern of stream-

lines. The spacing of these vortices (L) was determined to be a

unique function of the boundary layer thickness:

$$L = K(\pi d/Re^{\frac{1}{2}})$$

The analytical estimate of K was 1.79 whereas the measured value of

K ranged from 1.56 at zero turbulence level (extrapolated) to 1.27 for

a free stream turbulence level of 6%.

These experiments, which were conducted in a wind tunnel over a

Reynolds number range of 5×10^4 to 2.5×10^5, confirmed that the flow

pattern consists of standing, span-wise repetitive cells of width L

equal to the instability wave length. Their cores are located slightly

outside the edge of the classical boundary layer and extend transversely

across the stagnation line.

Flow visualization studies indicated that this pattern is well defined

and persists up to the separation line. Although no attempt was made to

concurrently measure drag forces and/or separation angle or extend the

Reynolds number range past the drag crisis region for understandable reasons, it is apparent that the turbulent cells examined by Humphreys in the drag crisis region, are related to the stream-wise vortices examined by Kestin and Wood.

C. A REVIEW OF THE ANOMALOUS BEHAVIOR OF FLOW OF DILUTE POLYMER SOLUTIONS ABOUT BLUFF BODIES

In addition to well documented reduction of drag for bluff bodies in the Reynolds number range of 10^4 to 10^5, several other anomalies have been reported in the behavior of polymer flow past bluff bodies.

One of the most unusual departures from Newtonian fluid flow is Sanders' report of a dual terminal velocity in sphere drop tests in laminar flow [Ref. 16]. As he stated, "At first it was hard to believe that this dual terminal velocity behavior was real, but further experimentation revealed that this effect was always observed when the right combination of sphere size and solution concentration was used."

The effect was observed in the laminar flow, (Re $\leq 10^4$), of the dilute Polyox solutions at high concentrations (0.1 to 1%). Sanders correlated the dual terminal velocity effect with the ratio of maximum shear stress to concentration for the Stokes flow of Polyox WSR-301 about spheres. Stable states existed for values of this ratio less than 58,000 ergs/gm and greater than 100,000 ergs/gm. In between, dual terminal velocity resulted; the sphere would steady at a high terminal velocity and suddenly jump to a lower terminal velocity, at a Reynolds number based on water less than 10^4.

James [Ref. 14] observed another anomaly in the flow of dilute Polyox solutions of far reaching engineering importance: The Nusselt number was independent of velocity for small wires above a critical velocity in the order of 10^{-1} fps for a 50 wppm solution.

Brennen [Ref. 17] speculated that the irregularities in the separation line may be due to a span-wise distribution of hairpin vortices in the attached flow, which would not normally (in a Newtonian fluid) occur in the presence of a strong stream-wise acceleration. He observed that, "It appeared that it (dilute polymer solution) could cause marked instabilities in the attached flow around a sphere and cylinder which were then reflected in the irregularities of the separation line and cavity surface as the disturbances were convected downstream."

Gadd [Ref. 35] observed that concentrations of Polyox WSR-301 greater than 10 wppm reduced the eddy-shedding frequency of a wire while Separan and Guar gum did not. The large reduction in frequency was accompanied by proportionate increase in amplitude.

Kalashnikov et al. [Ref. 36] conducted similar tests with wires of 0.17 and 0.57 mm diameter in 100 wppm Polyox solutions and found that the eddy shedding frequency is lower for Polyox, the frequency decreases as wire size increases, and that the first vortices appear at a lower Reynolds number. The vortex intensity was found to be lower for fresh solutions but when a solution lost its (measurable) viscoelastic properties, the frequency of the vortex shedding became somewhat higher with a considerable increase in amplitude of oscillations. They conjectured that the intensity of inertial vortices increases in solutions containing

47

inelastic associates, while in elastic solutions the vortex intensity decreases.

Apparently, an anomaly exists between the behavior of degraded solution in pipe flow and in bluff body flow. As cited in the introduction, the entire subject of degradation entails significant contradictions. As an example of a well documented experiment, A. White [Ref. 9] observed that over a six-day period the drag coefficient of a 1/2-inch sphere at Re of 2×10^4 in a 30 wppm solution of Polyox WSR-301 increased from 0.324 to 0.455 (for water, it was 0.475.) while the friction factor in the 0.09-inch pipe did not change (apparently remaining at a maximum drag reduction).

The data of McClanahan and Ridgely [Ref. 15], obtained by towing cylinders in dilute Polyox solutions, contain two deviations from the previously reported behavior of spheres in drop tank tests at comparable concentrations; at 10 wppm Polyox WSR-301, the two-inch diameter cylinder displayed the dual value drag coefficient at Reynolds numbers of 5×10^4 to 6×10^4 followed by decreasing drag coefficients at higher velocities, and the drag coefficients above the Reynolds number of 8×10^4 in the 10 wppm solution were almost as low as with 100 wppm and much lower than at 50 wppm.

An analysis of their data by this writer revealed that at higher concentrations, the drag coefficient was primarily a function of velocity and independent of cylinder diameter. With few exceptions, there are striking examples of excellent fit to the assumption of $C_d = f(V)$.

A similar analysis was conducted of all available sphere data for concentrations of Polyox WSR-301 from 60 to 200 wppm, in the Reynolds number range of 4×10^3 to 2×10^5 (TABLE II). The result was that in the range of Reynolds numbers where the drag coefficient in a Newtonian fluid is approximately constant, in the fresh polymer solutions it is principally a function of velocity. C_d is 0.45 to 0.35 in the velocity range of 2 to 4 fps, 0.35 to 0.25 in the velocity range of 4 to 6 fps, and approximately 0.25 from 7 to 12 fps (the highest velocity found in the literature for drop tests with Re less than 2.5×10^5).

It is apparent from the foregoing that the introduction of relatively minute amounts of long-chain polymers into a Newtonian solvent not only causes modifications in the usually expected flow pattern and resulting forces on bodies, but also some additional and hitherto unknown phenomena. These will be discussed in connection with the presentation of the test data.

TABLE II

Sphere Drop Tests in Polyox WSR-301 Solutions of Concentrations

60 to 200 wppm

D in.	Re x 10^{-4}	C_d	V fps	$pV^2(Re)^{-\frac{1}{2}}$ lb/ft^2	Conc. wppm	Ref.
5/16	1.2	.32	4.6	.385	100	16
3/8	1.6	.28	5.1	.410	100	16
1/2	2.4	.25	5.8	.434	100	16
1	7.5	.25	9.0	.590	100	16
7.75	20.0	.44	3.1	.045	60	8
3	20.0	.23	8.0	.287	100	50
1/4	.7	.38	3.3	.260	200	11
1/2	2.0	.32	4.8	.326	200	11
3/4	5.0	.26	8.0	.545	200	11
1	6.0	.25	7.2	.424	200	11
1.5	12.5	.23	10.0	.565	200	11
2.0	20.0	.21	12.0	.640	200	11
2.5	25.0	.23	12.0	.575	200	11
1/4	.65	.36	3.1	.240	120	9
1/2	2.0	.28	4.8	.325	120	9
.56	2.66	.29	5.7	.400	75	41
.625	2.85	.28	5.5	.360	75	41
.44	1.67	.33	4.6	.330	75	41
.375	1.33	.35	4.3	.320	75	41
.75	3.8	.27	6.0	.370	75	41
.345	.58	.40	2.0	.105	100	41
.375	1.17	.42	3.8	.270	100	41
.44	1.51	.38	4.2	.290	100	41
.625	2.41	.315	4.4	.250	100	41
.75	3.46	.315	5.4	.310	100	41
.56	2.79	.355	6.0	.430	100	41

III. EQUIPMENT AND PROCEDURE

A. EQUIPMENT

1. NPS Water Tunnel

The experiments were performed in a recirculating water tunnel (Fig. 11) of approximately 500 gallons' capacity fitted with a test section four inches wide, eight inches high, and 16 inches long. A low-rpm, high-capacity, 14-inch-diameter-discharge, centrifugal pump circulated the fluid at test-section velocities of 5 to 25 fps. Grids were specifically not used to minimize polymer degradation. Three flow straighteners were welded into the 14-inch pipe elbow which preceded the 5:1 nozzle section. These proved sufficient to provide a test section velocity profile which remained uniform from 0.5 to 7.5 inches with a standard deviation of 1.8%.

Associated with the tunnel are a 150-gallon stainless steel storage tank, a small recirculating pump and filter system, and a 15-gallon head tank 12 feet above the test section centerline.

2. Test Specimens

An NACA 0024 aluminum hydrofoil with a four-inch chord length was used to investigate the effect of polymer solutions on lifting bodies (Fig. 12).

Aluminum cylinders of diameters of 3/4 inch, one inch and 1-1/2 inch and a one-inch flat plate, placed across the width of the test section, were used to evaluate the effect of polymer additives on the drag coefficient of bluff bodies.

A   air vent
CP centrifugal pump
M   motor
N   nozzle section
SC speed control
TS test section

1   to 15-gallon head tank
2   from filter system
3   to drainage, filter and storage
    systems, and from fill line
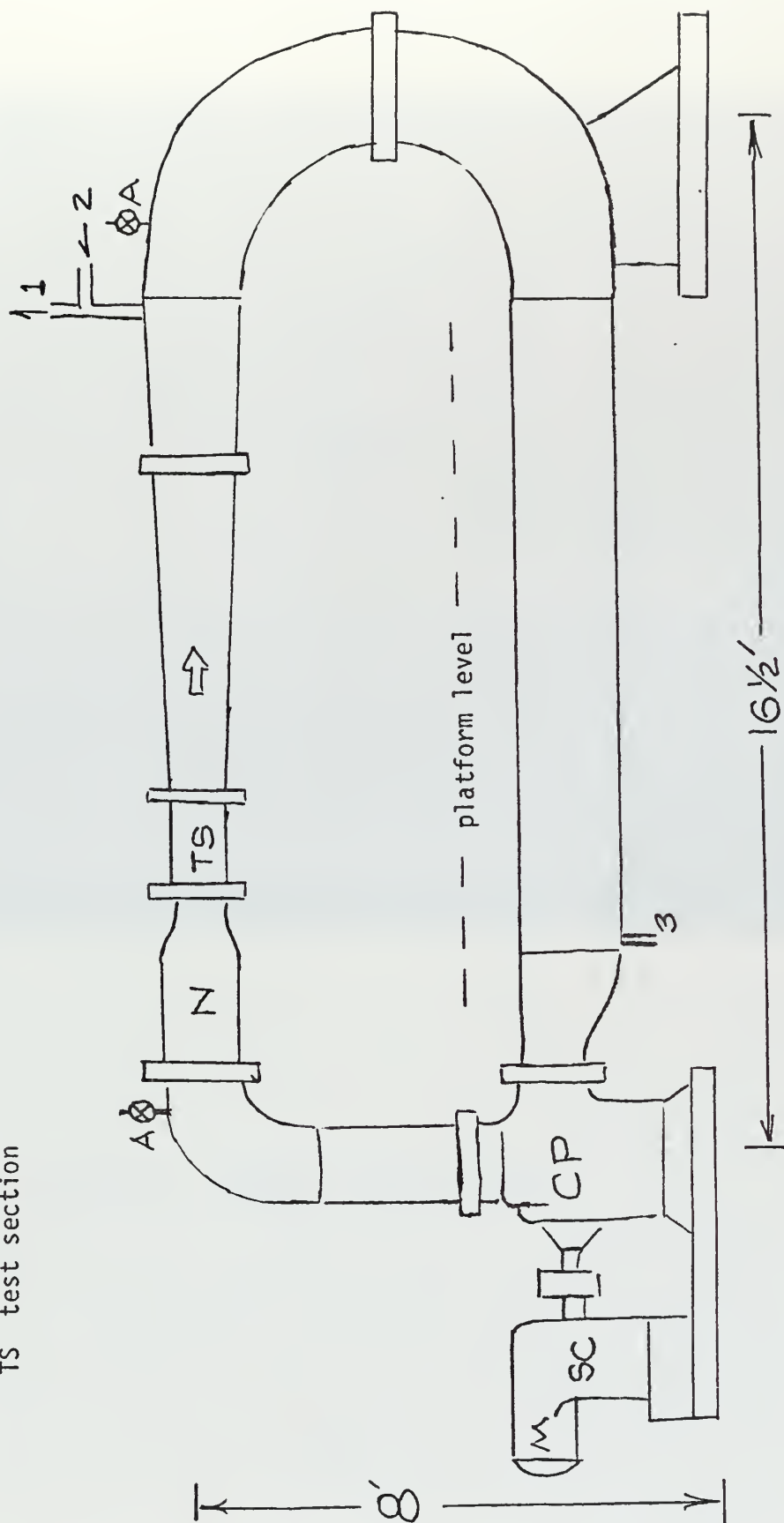
Figure 11: NPS Water Tunnel

52
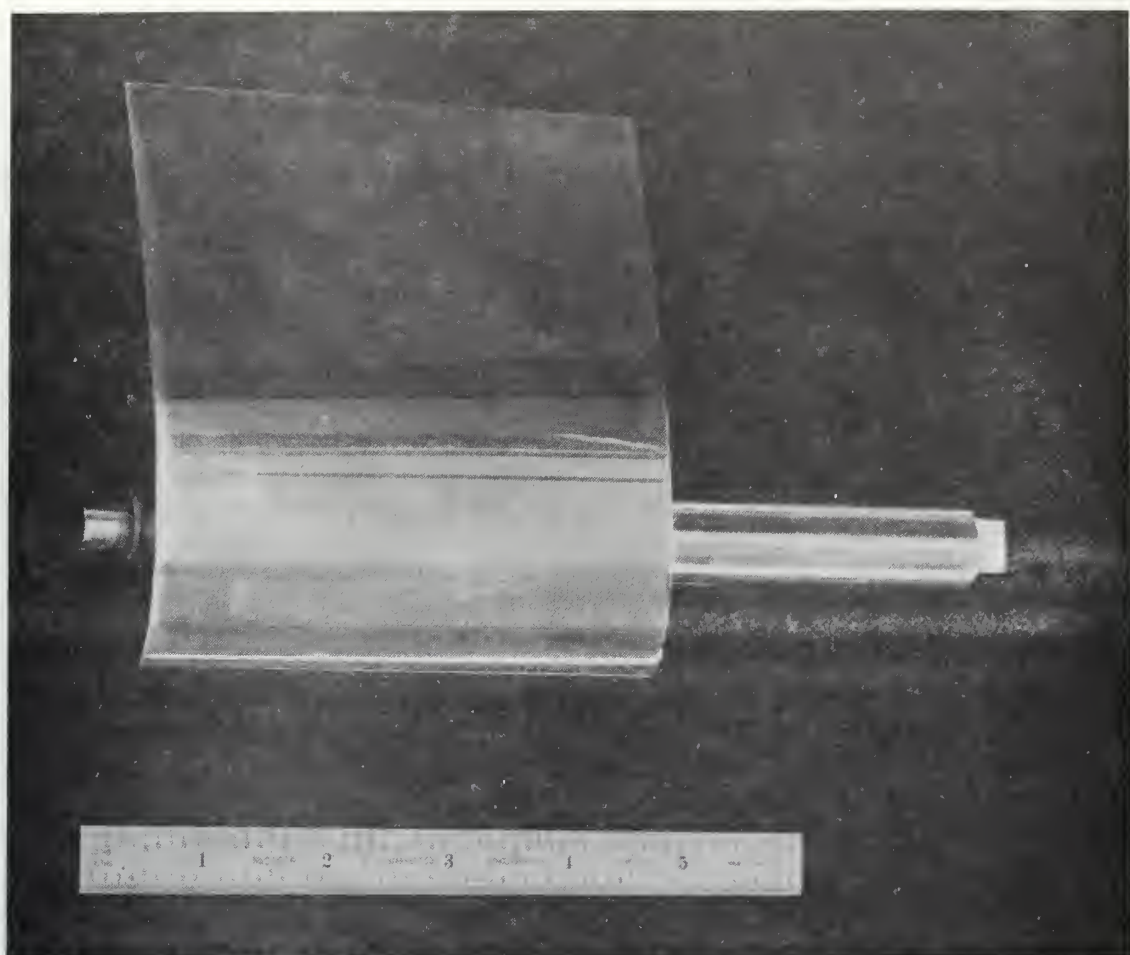
Figure 12: Hydrofoil Test Specimen

53

Local pressure measurements and flow visualization studies were conducted with a 1/4-inch-diameter brass tube and 1/2-inch, one-inch and 1-1/2-inch-diameter plexiglass cylinders. A small bore hole (three degrees of arc) drilled radially from the cylinder surface, at the mid-span, served as the total pressure tap. Static pressure was measured at the entrance of the test section with a wall tap.

The end conditions differed between the cylinders used for direct drag measurements and those used for pressure measurements (Fig. 13). All of the aluminum specimens were mounted with one end held by a self-aligning bearing imbedded in one plexiglass window, and one end passing through the other plexiglass window into the cantilever beam system. All of the plexiglass cylinders extended through both tunnel windows. They were fitted with "O" rings which permitted rotation to any desired angle yet sealed the passage through the tunnel walls.

3. Instrumentation

The lift and drag forces acting on the hydrofoil were directly measured with a strain gage fitted cantilever beam system (Fig. 14). The drag force acting on the cylinders and flat plate was directly measured on a separate strain gage fitted cantilever beam (Fig. 15). All of the bridges used four active gages (SR-4) and each beam was fitted with a redundant bridge circuit to maximize reliability. Static calibration of the instrument exhibited a 1% interference; a 50-pound load on the lift measuring beam produced a deflection on the drag measuring beam equivalent to a 0.5-pound load on that beam.

54
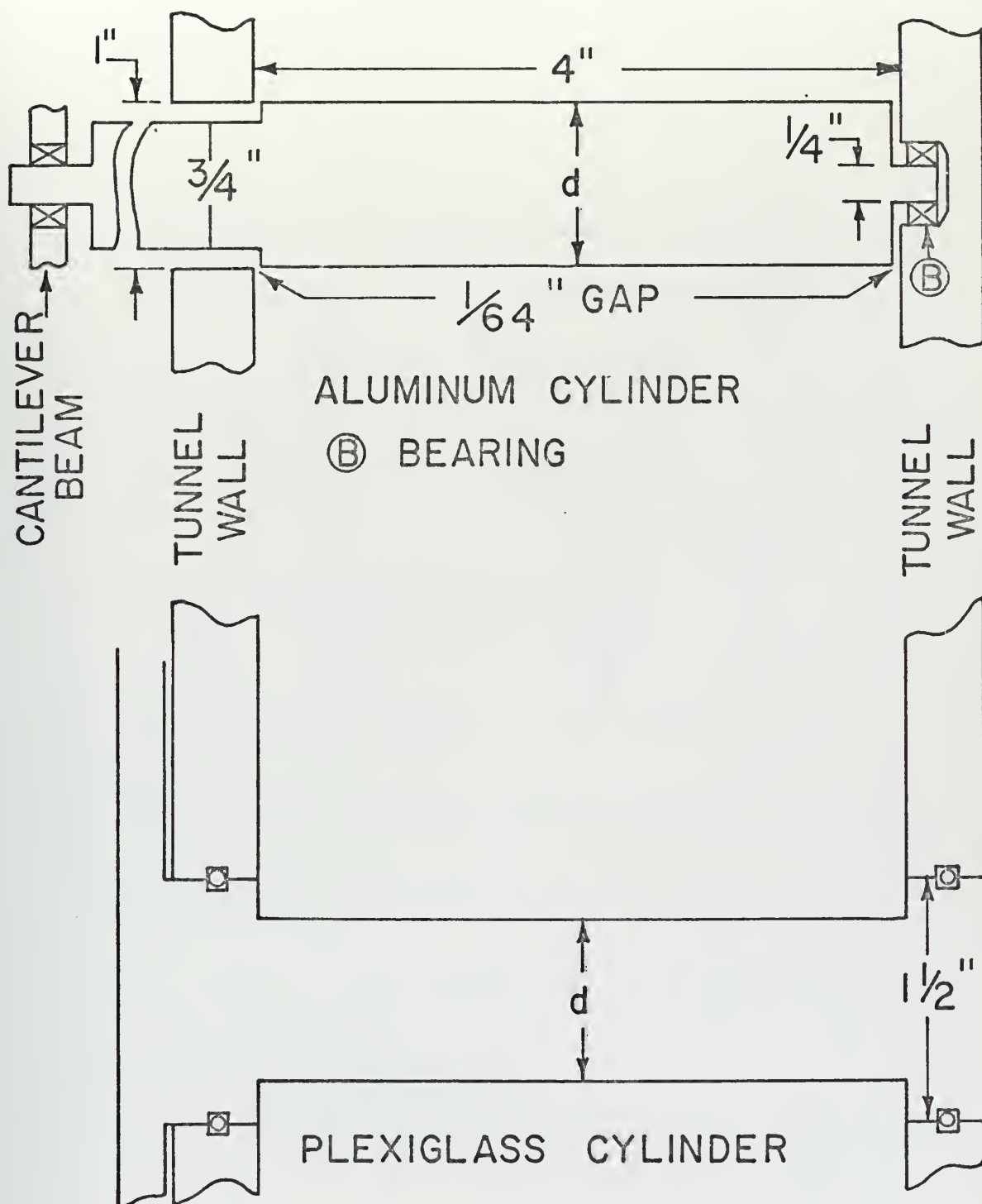
FIGURE 13: COMPARISON OF
CYLINDER END CONDITIONS
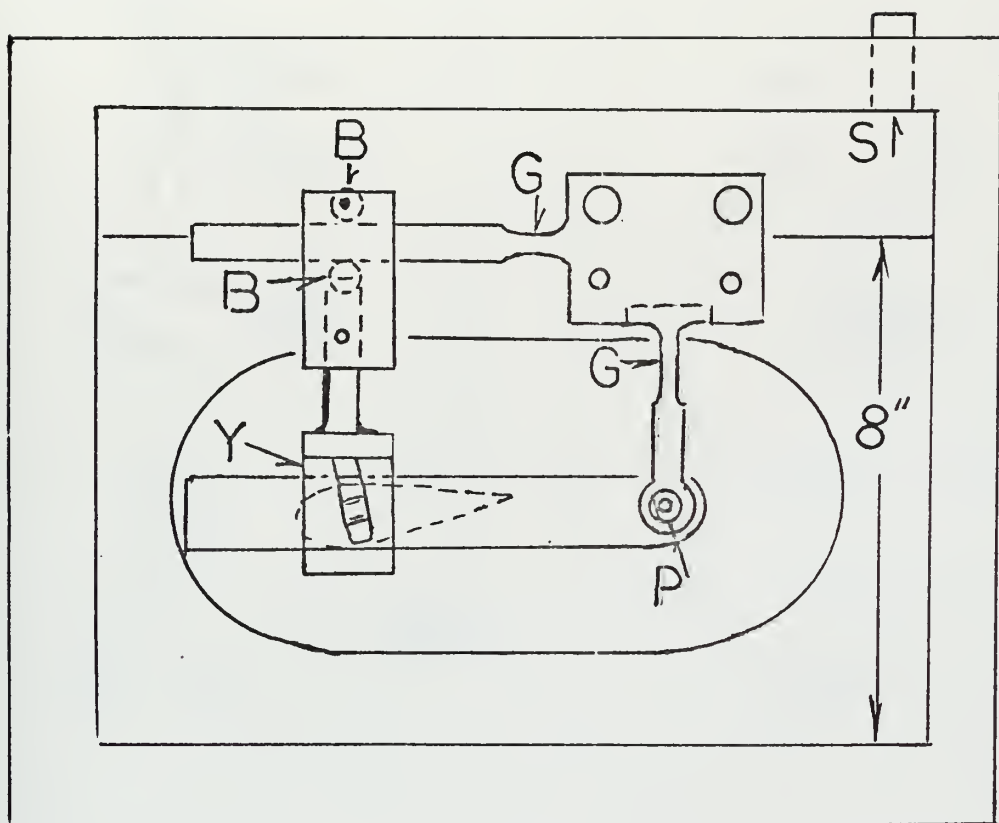
B   bearing
G   4 gages each side
P   pin and bearings
S   cable-way stuffing tube
Y   angle setting yoke

Figure 14:   Lift and Drag Force Measuring Beam System

SECTION A-A
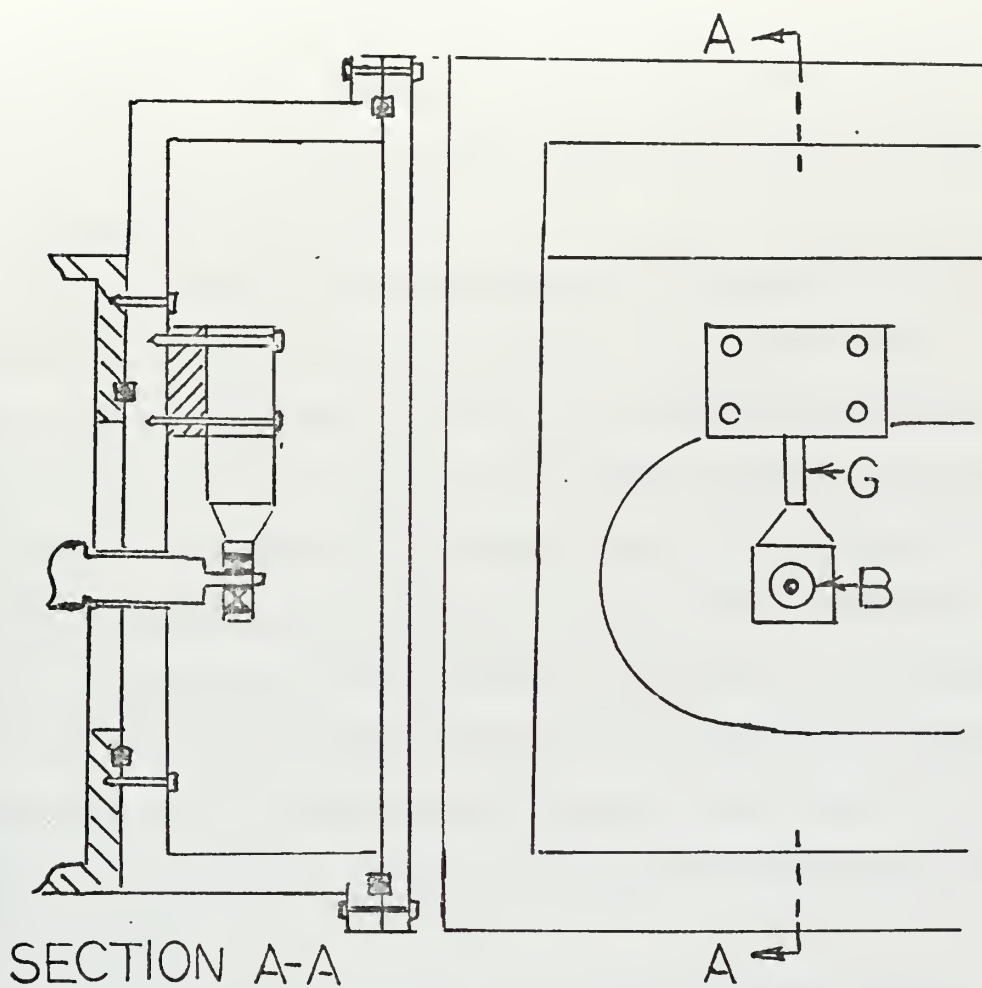
B bearing
G 4 gages on each side

Figure 15: Drag Force Measuring Apparatus

Differential pressure measurements were made with a Pace trans-
ducer (model KP-15) with a range of 0 to 25 psig.

The output of each strain-gage bridge and the pressure trans-
ducer was fed into dual-channel Hewlett Packard strip-chart recorders.

4. Turbulent Pipe Rheometer

For the purpose of correlating the effectiveness of the poly-
mer solution in turbulent pipe flow with that in external flows, a
turbulent-flow pipe rheometer, identical in principle to that used by
W. D. White [Ref. 37], was furnished by Professor Sanders. It consist-
ed basically of a 0.073-inch I.D. stainless steel pipe connected at
one end to a reservoir and at the other end to a 100 cc graduated
syringe. The syringe was driven through a worm-gear box by a variable
speed motor. The pressure drop across a six-inch length of the pipe
was measured by a Pace transducer and recorded on an H-P strip chart
recorder. The duration of the flow was measured with an electric timer.

5. Polymer

The water-soluble polymer, Polyox WSR-301, Blend 8051 F,
manufactured by Union Carbide, was the polymer used for all the data
reported herein.

B. PROCEDURE

1. Rheometer Operation

First, the temperature of the fluid in the rheometer reservoir
was measured. Then the syringe was lowered slowly to the 120 cc level
as it was filled from the reservoir. The motor was started at a pre-
selected speed by closing a relay. As the syringe plunger passed the
100 cc mark, the electric timer was manually started. At the 20 cc

mark, the relay was released, instantly stopping the timer and
shutting off the motor. The pipe friction factor was then calculated
from the measured pressure drop, flow rate, and temperature.

The Fanning friction factor for tap water (f_t) was determined for
the Reynolds number range from 3,950 to 5,660. This data (Appendix A)
established the reference values for computing the per cent pipe drag
reduction (P. D. R.) relative to laminar flow caused by a polymer
solution. The tap water friction factors had a systematic error of
approximately 3% below the expected smooth pipe value. The error in
repeatability was on the order of ±2%.

The polymer solutions were tested in the Reynolds number range of
4800 ±300. The Reynolds numbers reported herein are based on the
viscosity of water at the measured temperature. The value of pipe
drag reduction for each sample of polymer solution was calculated from
the value of the tap-water friction factor corresponding to the Reynolds
number of the test.

$$P. D. R. = 100 \times (f_t - f)/(f_t - 64/Re)$$

Conversion to absolute pipe drag reduction can be made by multiplying
the values of P. D. R. reported herein by .65. Ten-liter sample solu-
tions of 10 wppm Polyox WSR-301 were prepared without stirring in
order to establish the characteristics of this batch of Polyox in a
condition as virgin as possible. The master solution, after aging
approximately 20 hours, was used to prepare diluted solutions of concen-
trations from 10 to 0.1 wppm. The P. D. R. was determined for this
range of concentrations. The repeatability of this experiment was then
spot checked.

Tunnel samples were tested for fresh solutions as well as for
solutions taken every half-hour of pumping. Sufficient sample was

59

withdrawn from the tunnel to allow three flushes of the rheometer prior to two pipe tests.

2. Polymer Mixing in the Tunnel

Preliminary investigations [Ref. 38] indicated that the most satisfactory mixing technique would be the direct feeding of the polymer powder into the tunnel. The water level was set at the middle of the test section. A funnel was installed through a fitting on top of the test section. The weight of dry Polyox was measured to ±0.01 gm on a laboratory balance for samples of 10 gm or less. For larger samples a laboratory scale of accuracy ±0.5 gm was used. The powder was slowly sprinkled into the water as the pump ran at its lowest speed. The total pumping time (TRT) reported for each solution includes this mixing time. All solutions were then aged for approximately 24 hours.

The following procedure was followed unless otherwise noted: All solutions were made fresh (i.e., not made by diluting a previous solution) with the solutions of the highest concentration prepared first for each part of the test program. After each solution was dumped, the tunnel was flushed twice prior to mixing the next lower concentration. Water data was taken after chemically treating the tunnel water with potassium bichromate, allowing 72 hours to degrade any residual polymer, and then flushing three times with water.

For the case when distilled water was used to prepare a 5 wppm solution, the tunnel was flushed with 1,200 gallons of distilled water prior to filling the tunnel and storage tank.

3. Hydrofoil-- Direct Measurement of Lift and Drag Force

The lift and drag forces acting on the NACA 0024 hydrofoil were measured at the nominal angle settings of 0, 3, 6, 9 and 12 degrees. The actual measured angles were .7, 3.7, 6.3, 9.6, and 11.7 respectively.

The apparatus used to measure the force was calibrated by static loading of the hydrofoil with the angle of attack set at zero degrees. Calibration was repeated each time the tunnel was emptied.

The actual, unfiltered output from each strain-gage bridge was observed on the strip chart recorders. The mean force was obtained by switching in the capacitance time-averaging circuit internal to the recorder. In those cases where the oscillations still appeared, the capacitance was switched out and the estimated mean of the actual fluctuating signal was used.

The tunnel velocity was determined from the measured stagnation pressure on a 3/4-inch diameter cylinder which was inserted into the tunnel for this purpose. The cylinder was then retracted and the dynamic forces on the test body were measured. This method of determining the free stream velocity was used in preference to a Pitot tube since the Pitot tube used to measure the tunnel profile in water broke at the location where it penetrated through the tunnel wall after only a few hours of pumping. It was expected that the pressure anomaly common to dilute polymer solutions could be avoided with a velocity probe of relatively large radius. In spite of that, however, a pressure anomaly was found to exist for fresh solutions of concentrations 100 wppm and greater.

The transducer used to measure the differential pressure between the total stagnation pressure (on the 3/4-inch cylinder) and the test section entrance wall was calibrated with the standard water-manometer technique each time the force apparatus was calibrated.

The test procedure consisted of first measuring in tap water the forces acting on the hydrofoil throughout the tunnel velocity range for each angle. After each test, the water level was reduced to a sufficiently low level (by gravity feeding 100 gallons of water into a storage tank) to allow the installation of the desired angle setting yoke. The amount of water withdrawn was then pumped back into the tunnel and the test program was continued. Each set of data was obtained in an increasing order of pump speeds, and then repeated in a reverse order. Prior to and after taking each data set, the recorder balance and zero setting were checked. The entire test program was repeated with tap water. This established the reference data with which the forces produced in the flow of polymer solutions could be compared.

A 100 wppm solution was prepared in which the hydrofoil was tested in the following order of angle settings: 9, 12, 6, 3, 0, 12, 9. The hydrofoil lift and drag forces were then measured in a 25 wppm solution in the following order of angle settings: 0, 9, 3, 12. Another 25 wppm solution was prepared in which data were taken with an angle setting of six degrees.

A nut-and-bolt locking device was added to the angle setting yoke in order to eliminate the possibility of an undesirable oscillatory force or an apparent increased oscillatory lift force on the

hydrofoil. The lift force was then measured in tap water with the angle set at six degrees nominal, 4.5 measured. This was repeated at the same angle in a 200 wppm solution. After two hours of pumping, the solution was diluted 4:1 (producing 21 P. D. R.) and the lift force measurements were repeated. Again the solution was diluted 4:1 (producing 7 P. D. R.) and the test procedure was repeated. Finally, the tunnel was flushed and filled with tap water and the test procedure was repeated. This concluded the hydrofoil test program.

4. Cylinder--Direct Measurement of Drag Force

The procedure followed for the direct measurement of the drag experienced by the cylinders was similar to that followed for measurements on the hydrofoil. The test program was essentially as follows:

(1) Each cylinder was tested in water;

(2) Each cylinder was tested in separate 100 wppm solutions;

(3) The one-inch diameter cylinder was tested in a 25 wppm solution;

(4) Each cylinder was tested in separate 5 wppm solutions;

(5) The one-inch cylinder was tested in a 5 wppm solution prepared with distilled water;

(6) The one-inch cylinder was tested in a 2.5 wppm solution; and finally,

(7) The one-inch cylinder was tested in a 1 wppm solution.

The drag force was also measured on a sharp-edged, one-inch flat plate placed perpendicular to the flow in tap water and 100 wppm solutions.

5. Cylinder--Measurement of Pressure Distribution

The pressure distribution was measured on the one-inch-diameter cylinder in solutions of 100, 25, and 5 wppm. The local dynamic pressure

on the cylinder surface was measured at five-degree intervals around the mid-circumference. The angle setting was measured on a two-inch radius circle which allowed the measurement of the angle to an accuracy of ±0.5 degrees.

The tunnel centerline velocity was determined from the front stagnation pressure. No pressure anomaly was observed with these cylinders, even at 100 wppm.

The drag coefficient was calculated from the pressure distribution as described in Ref. 38.

The front stagnation pressure and rear pressure were measured on a one-inch flat plate placed perpendicular to the flow. Three-sixteenths-inch pressure taps were placed at the front and rear center of the plate. The dynamic pressures were measured in water, fresh 100 wppm solution, and again in water. The front pressure was insensitive to the polymer concentration, i.e., no pressure anomaly was observed.

6. Cylinder Separation Angle Measurements

Concurrent with the determination of pressure distributions, the angle of separation on the centerline of the cylinder was observed by dye injection from the cylinder surface. The reported angle is the minimum angle at which separation occurred. The location of separation was measured by injecting dye aft of the separation point and them rotating the cylinder forward while reducing the injection rate until two degrees aft of the apparent separation point. The dye injection rate was then reduced to a minimum and the actual separation point observed. The reported separation angle is considered to be accurate to within

64

±1 degree in those cases where separation was steady. In the case of the unsteady separation (to be discussed later) caused by the flow of degraded solutions, the reported minimum separation angle is considered to be reliable to within ±3 degrees.

7. Tunnel Correction Factors

Tunnel correction factors were not applied to the data obtained with the hydrofoil.

The standard tunnel corrections for wake and solid blockage were applied to the cylinder (and flat plate) drag data in order to compare the cylinder drag coefficient curve obtained in the NPS tunnel in tap water with the data reported in Section III.

These tunnel correction factors have been uniformly applied to all drag coefficients. The measured forces and stagnation pressures, uncorrected drag coefficients, and corrected drag coefficients and corresponding corrected Reynolds numbers are tabulated in Appendix A.

The total correction factor (e_t) is the sum of the solid-blockage correction factor and the wake-blockage correction factor

$$e_t = \frac{\pi^2}{12} \left(\frac{d}{h}\right)^2 + \frac{1}{2} \left(\frac{d}{h}\right) C_d \quad ,$$

where $\frac{d}{h}$ is the ratio of cylinder diameter to test section height (eight) inches) and C_d is the corrected drag coefficient defined by

$$C_d = 2D/(\rho U^2 L d) \quad ,$$

where D is the drag force acting on the cylinder, L is the cylinder length (four inches), and U is the corrected free-stream velocity given by

$$U = V(1 + e_t) \quad ,$$

65

where V is the velocity determined from the measured stagnation pressure P_s.

The drag coefficients are plotted as a function of the corrected Reynolds number

$$Re = Ud/\nu \quad ,$$

where ν is the kinematic viscosity of <u>water</u> at the measured fluid temperature. The actual solution viscosities were not measured and theoretical corrections based on polymer concentrations and estimated molecular weight were not applied. The common practice of reporting the drag coefficients obtained in dilute polymer solutions as a function of water Reynolds number has been followed in the presentation of the data.

The pressure distributions are plotted in terms of corrected pressure coefficients C_p. Since the free stream velocity was determined from the stagnation pressure, the reported values of C_p are the ratio of the local dynamic pressure to the front stagnation point dynamic pressure. The total tunnel correction factor was applied to obtain the corrected pressure coefficient [Ref. 39]

$$\text{(corrected)} \quad C_p = 1 - \frac{1 - C_p}{(1 + e_t)^2}$$

The uncorrected and corrected pressure coefficients are tabulated in Appendix A.

66

IV. PRESENTATION OF DATA

A. PRELIMINARY DISCUSSION

The stagnation pressure measured on the 3/4-inch-diameter cylindrical velocity probe was found to be lower in fresh polymer solutions with a concentration of 100 wppm than the pressure measured at the same pump speed in fresh solutions of lesser concentrations. This pressure anomaly rapidly disappeared with increased TRT, the pressure at the lowest pump speed requiring the greatest pumping time to return to normal.

The reduced stagnation pressure may have been caused by a decrease in the free-stream velocity in the test section (i.e., reduced pump efficiency). However, in a subsequent test, the stagnation pressure was measured on a one-inch flat plate placed perpendicular to the flow at the lowest test-section velocity in a fresh solution of 100 wppm Polyox, it did not, within experimental error, change over a two-hour run and did not differ from data obtained with tap water. Since this set of experimental conditions produced the largest pressure error in the direct-drag-measurement experiments, (Fig. 16) it is reasoned that the high concentrations of polymer did not significantly alter the pump characteristics. In addition, as seen in Fig. 16, the "error" increased with the blockage factor. If it had been caused by either clogging of the pressure tap or by only local normal-stress effects on the probe, the "error" would have been independent of the test-body blockage factor. It apparently is due to some type of distortion of the velocity field in the vicinity of the cylindrical probe.
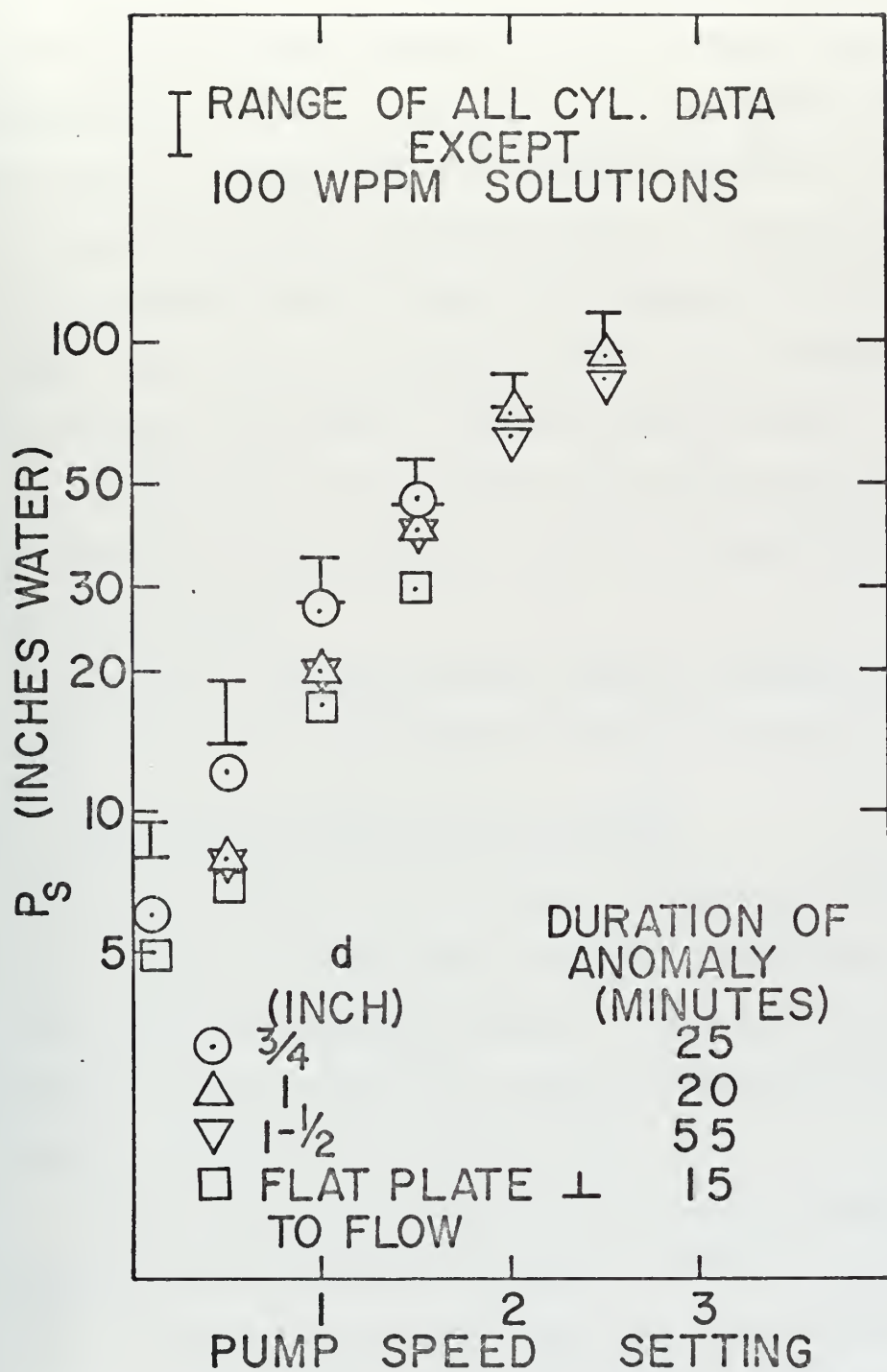
FIGURE 16: PRESSURE ANOMALY
WITH FRESH 100WPPM SOLUTIONS

A discussion of experimental errors is presented in Appendix B. The probable total per cent error in pressure measurement (exclusive of the pressure anomaly discussed) was ±5%. The per cent error in the determination of the lift force was also in the order of ±5%. The per cent error in the measurement of hydrofoil drag force is expected to be larger at low velocities partly because of bearing friction and partly because of the relatively small magnitude of the drag. At larger angles and higher speeds, the drag error is expected to reflect the lift-drag interference on the force balance system.

The anticipated per cent error in the drag force on the cylinders and flat plate is on the order of ±10% at the lowest speed to ±5% at the highest speed.

The error in reported per cent pipe-drag reduction was set by the uncertainty of the water friction factor at ±2 P. D. R.

B.   POLYOX WSR-301 PIPE FRICTION REDUCTION

The data obtained from the master solutions #1, #4, and #5, tabulated in TABLE III, established the optimum pipe-friction reduction capability for the undegraded polymer. Laboratory samples #2 and #3 indicated that the pipe-friction reduction capability at low concentration is reduced with increased aging.

The per cent pipe-drag reduction was found to be proportional to concentration for concentrations equal to and less than 1 wppm (Fig. 17). For concentrations above 5 wppm, the P. D. R. was approximately constant at 80. Preliminary investigations had revealed that above approximately 25 wppm, the P. D. R. decreases when concentration is increased.
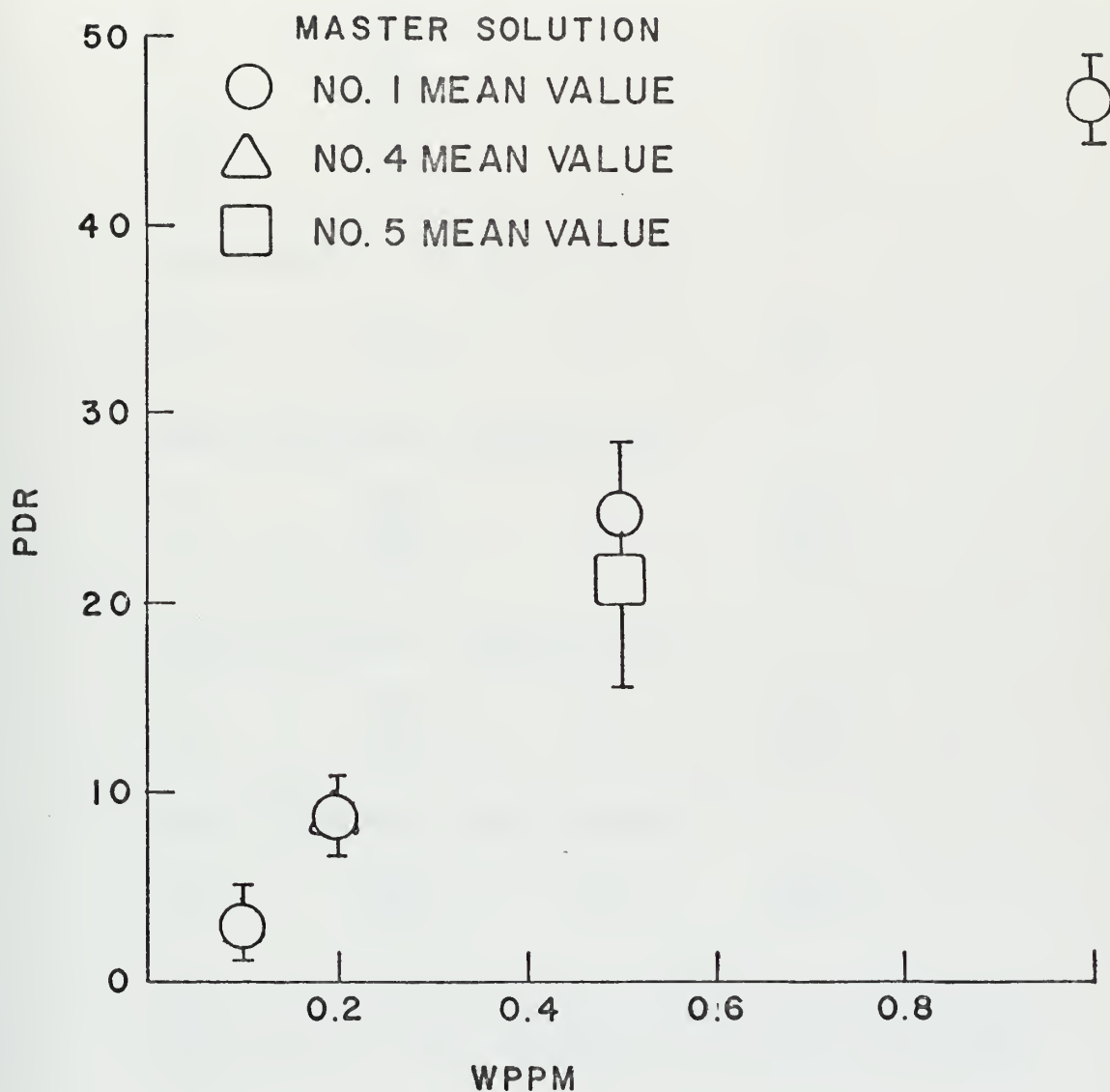
FIGURE 17: PDR vs WPPM
POLYOX WSR-301
LABORATORY SOLUTIONS

70

TABLE III

Laboratory Sample Polyox WSR-301 Solutions

Conc. wppm	$\overline{P.D.R.}$	N	s.d.
Master solution #1	aged 20 hours		
10	80.0	4	0.0
5	81.4	4	0.8
1	46.8	4	2.3
0.5	24.5	4	3.9
0.2	8.7	4	2.0
0.1	3.2	4	1.9
Master solution #2	aged 36 hours		
10	87.0	4	1.2
5	66.6	4	3.6
Master solution #3	aged 60 hours		
10	82.4	4	1.0
5	88.0	4	0.7
1	38.0	4	4.7
Master Solution #4	aged 24 hours		
10	82.0	2	1.0
0.2	8.7	4	2.5
Master solution #5	aged 18 hours		
10	79.9	4	0.8
0.5	21.4	5	5.9

$\overline{P.D.R.}$ is the mean of N number of data from the rheometer tests and s.d. is the root mean of the sum of the errors squared.
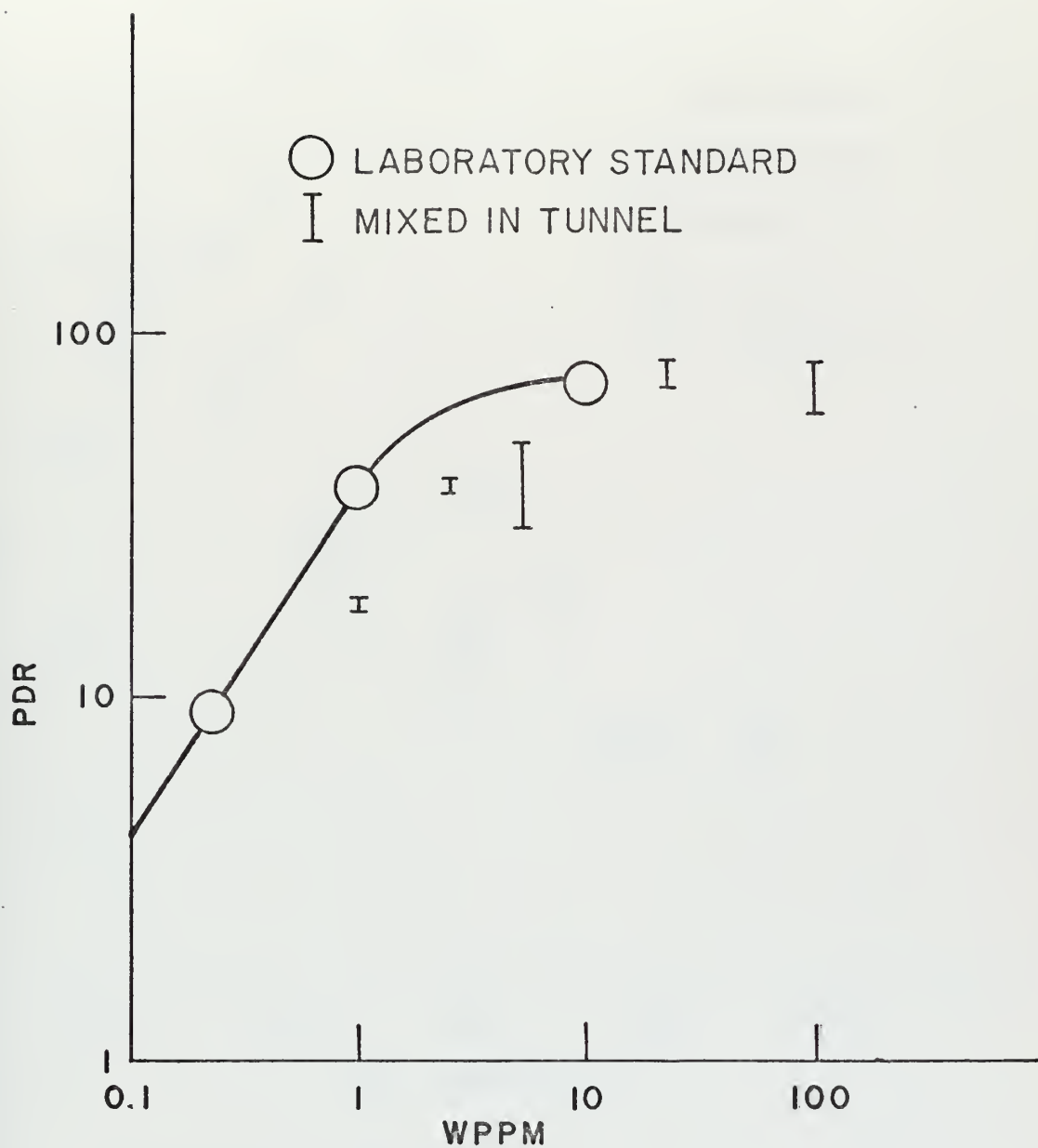
FIGURE 18: PDR vs WPPM
FOR FRESH TUNNEL SOLUTIONS

.073 IN. DIAMETER PIPE
Re ~ 5000
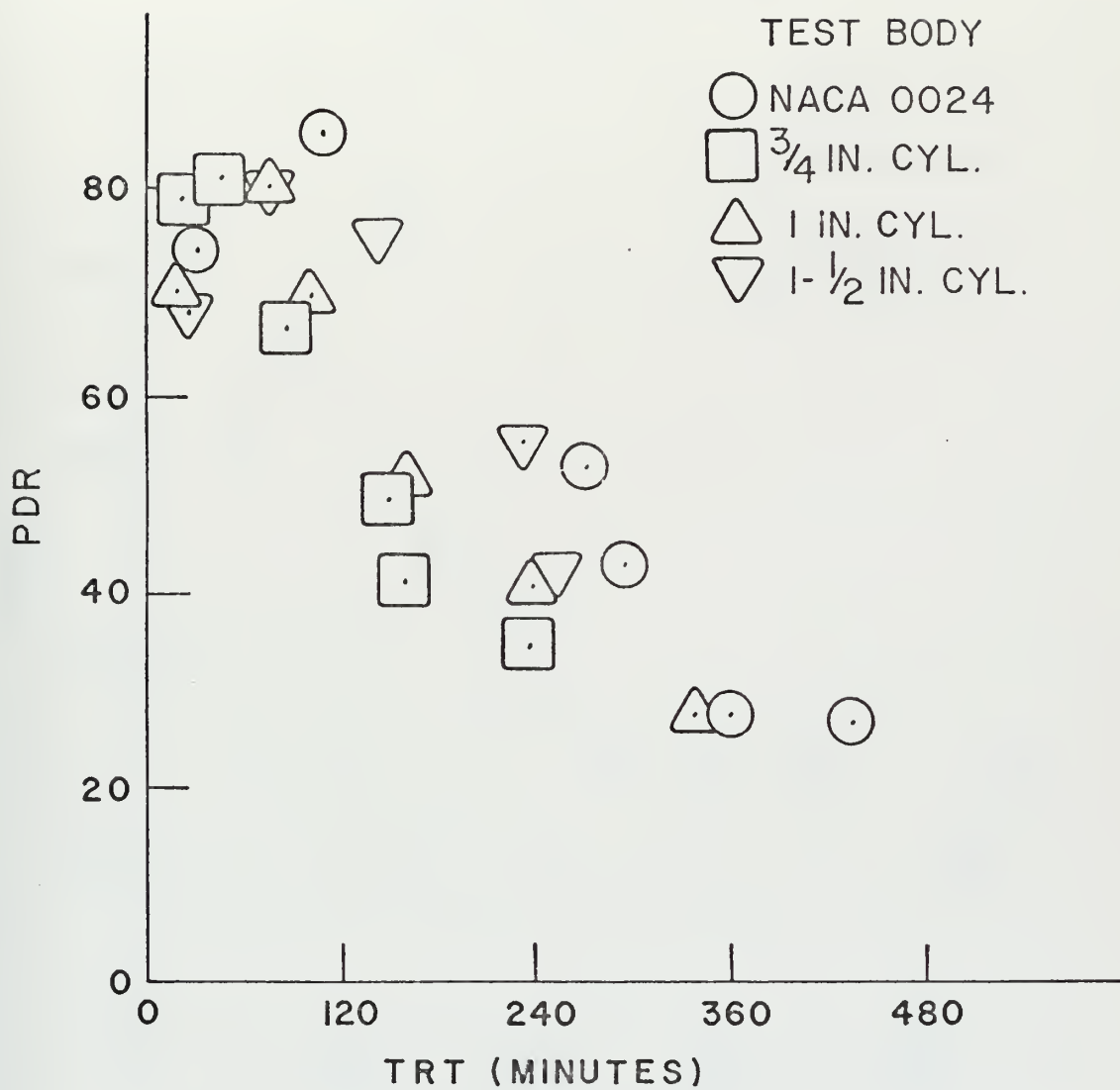
FIGURE 19: PDR vs TRT
100 WPPM POLYOX WSR-301

73

.073 IN. DIAMETER PIPE
Re ~ 5000

FIGURE 20: PDR vs TRT
25 WPPM POLYOX WSR-301

.073 IN. DIAMETER PIPE
Re ~ 5000

SOLVENT
○ DISTILLED WATER
□ TAP WATER
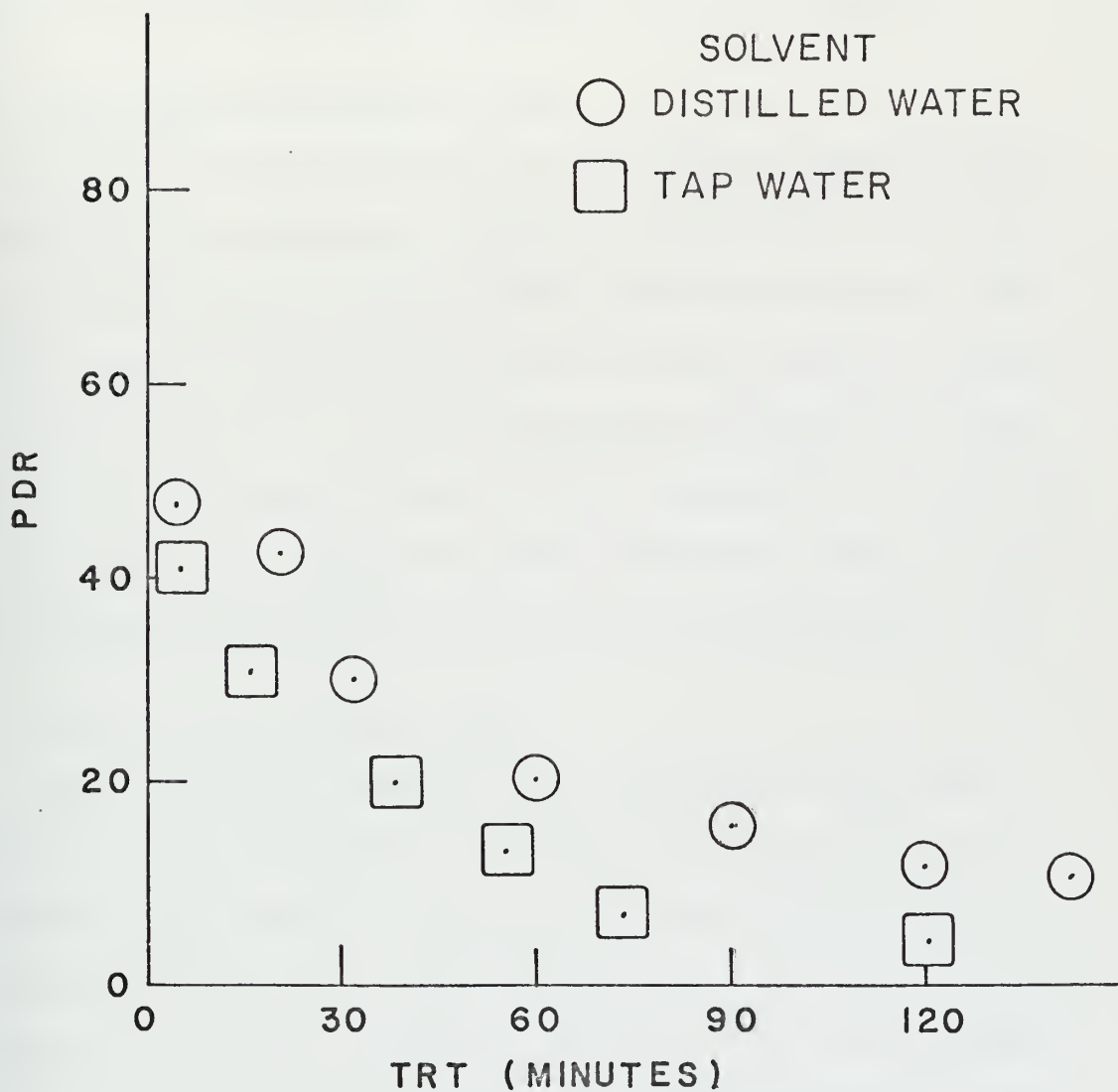
FIGURE 21: PDR vs TRT
5 WPPM POLYOX WSR—301

75

The pipe friction reduction of solutions mixed in the tunnel and aged 24 hours is compared with the standard in Fig. 18. In the range where P. D. R. is sensitive to concentration, it is apparent that the solutions mixed in the tunnel are degraded as compared to the laboratory samples.

The degradation curves, P. D. R. versus total running time, are shown for 100, 25 and 5-wppm solutions in Figs. 19, 20, and 21.

C. FLAT PLATE PERPENDICULAR TO FLOW

The data obtained with the flat plate when the pressure anomaly existed are not plotted but are tabulated in Appendix A. The drag coefficients obtained in 100-wppm Polyox solutions which were sufficiently pumped to eliminate the pressure anomaly but still displayed very high values of P. D. R. are compared with the fresh water data in Fig. 22. The corrected values narrowly scatter about the expected value of 2.0 and fall within the actual (corrected) values of 1.8 to 2.3 reported by Roshko [Ref. 40] and Delany and Sorensen [Ref. 28].

D. HYDROFOIL LIFT AND DRAG FORCES

The dilute Polyox solutions had no discernible effect upon the mean forces produced on the hydrofoil (Figs. 23 to 33). The apparent slight increase in lift at a six-degree angle of attack in the 200-wppm solution is most probably due to the pressure anomaly previously described. The apparent decrease in lift and corresponding 20% increase in drag at a nine-degree angle of attack in a relatively fresh 100-wppm solution was not repeatable. The data were taken by monotonically increasing the pump speed. Two data taken by decreasing the speed fell relatively much closer to the reference

76
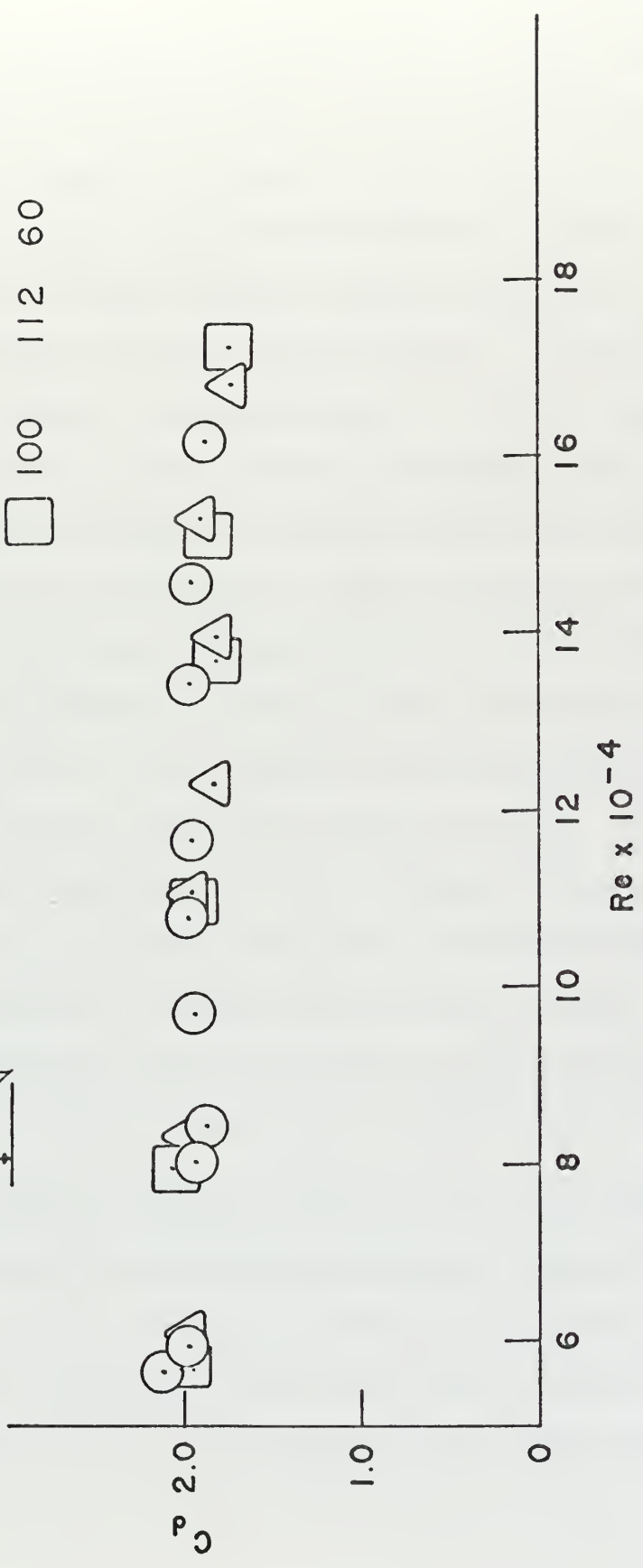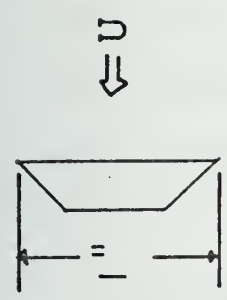
FIGURE 22: C_d vs Re FOR FLAT PLATE

77

water values, thus indicating a friction problem with one of the bearing surfaces which was alleviated at the highest speed. Subsequent values of lift force were slightly lower than the water values without a corresponding increase in drag force.

The only significant difference between the forces on the hydrofoil in water and in polymer solutions was the presence of a larger amplitude of oscillations in lift in polymer solutions. In order to conclusively determine that this increase was due to the flow of polymer solution rather than just to the loosening of the angle-setting clamp in the force-measuring apparatus, the angle was set at six degrees and a 200-wppm solution was prepared. After the data were obtained at 200 wppm, the solution was diluted 4:1 with the result of noticeable reduction in the amplitude of lift oscillation. The solution was further diluted 4:1 which further reduced the amplitude of lift oscillation. Then the tunnel was flushed and filled with water. The strip chart recordings of the first set of data (200-wppm fresh) are compared with that obtained last (water) in Fig. 34. If the oscillations were due to the loosening of the angle-setting clamp, the last set of data should have shown larger oscillations than the first set of data. This was not the case as seen from the figure cited above.

E.   DRAG FORCE ON CYLINDERS IN DILUTE POLYMER SOLUTIONS

The drag force was measured on 3/4-inch, one-inch and 1-1/2-inch diameter cylinders with tunnel velocities ranging from approximately 7 to 25 fps. Drag coefficient versus Reynolds number for tap water is presented in Fig. 35 and compared with the data previously obtained
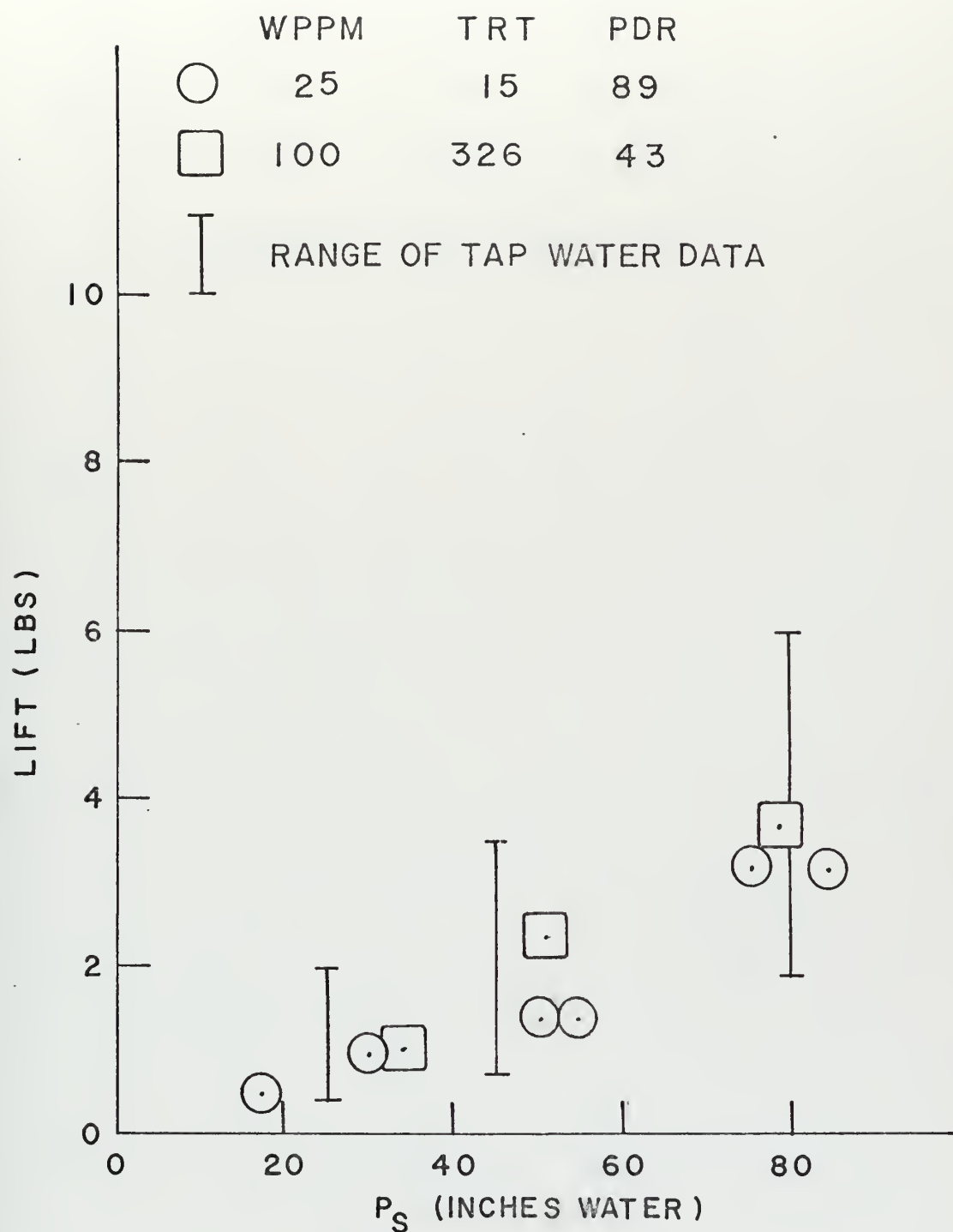
FIGURE 23: LIFT vs P_S
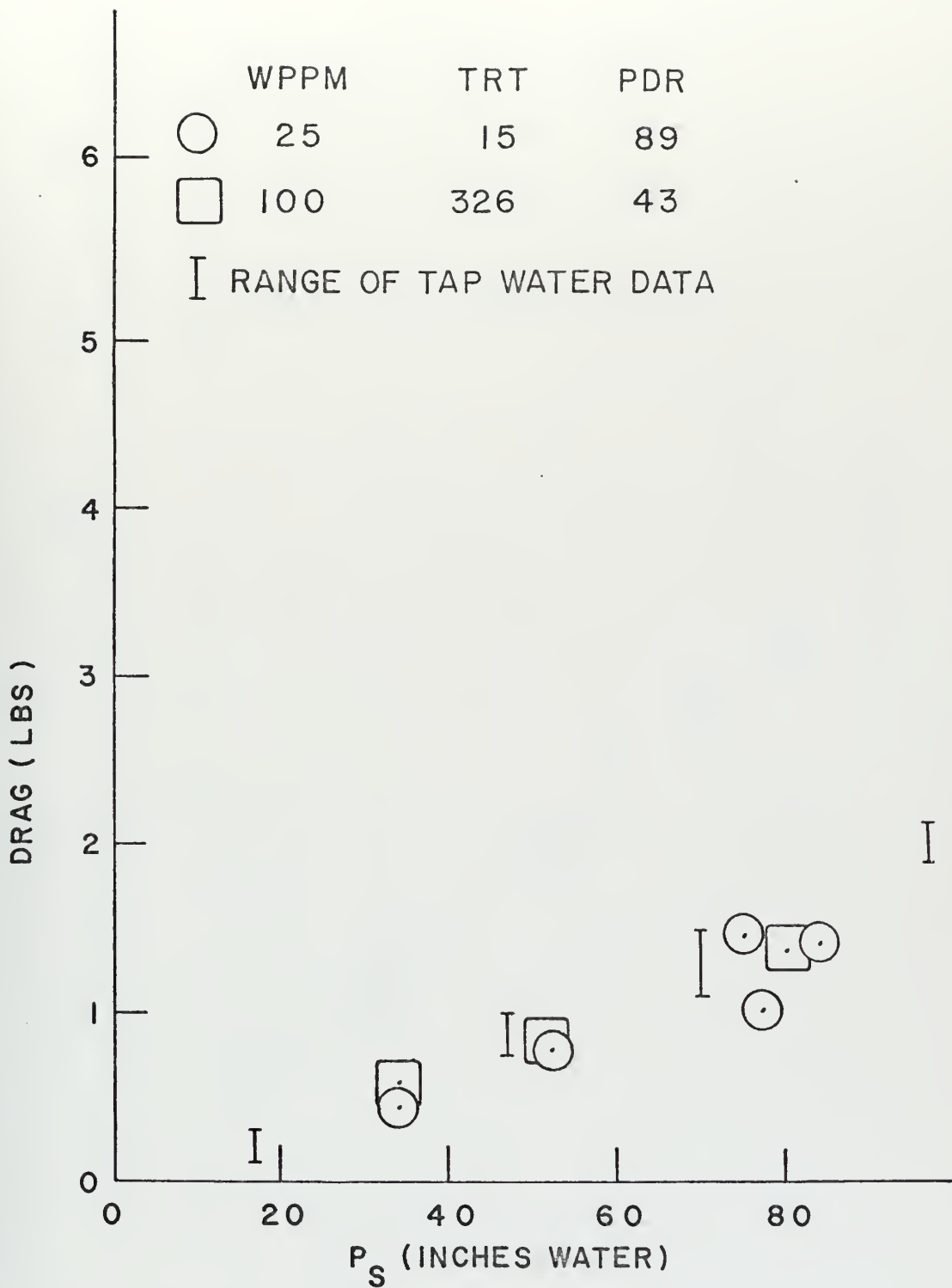
α = 0 DEGREES (NOMINAL)

FIGURE 24: DRAG vs P_S

$\alpha \doteq 0$ DEGREES (NOMINAL)
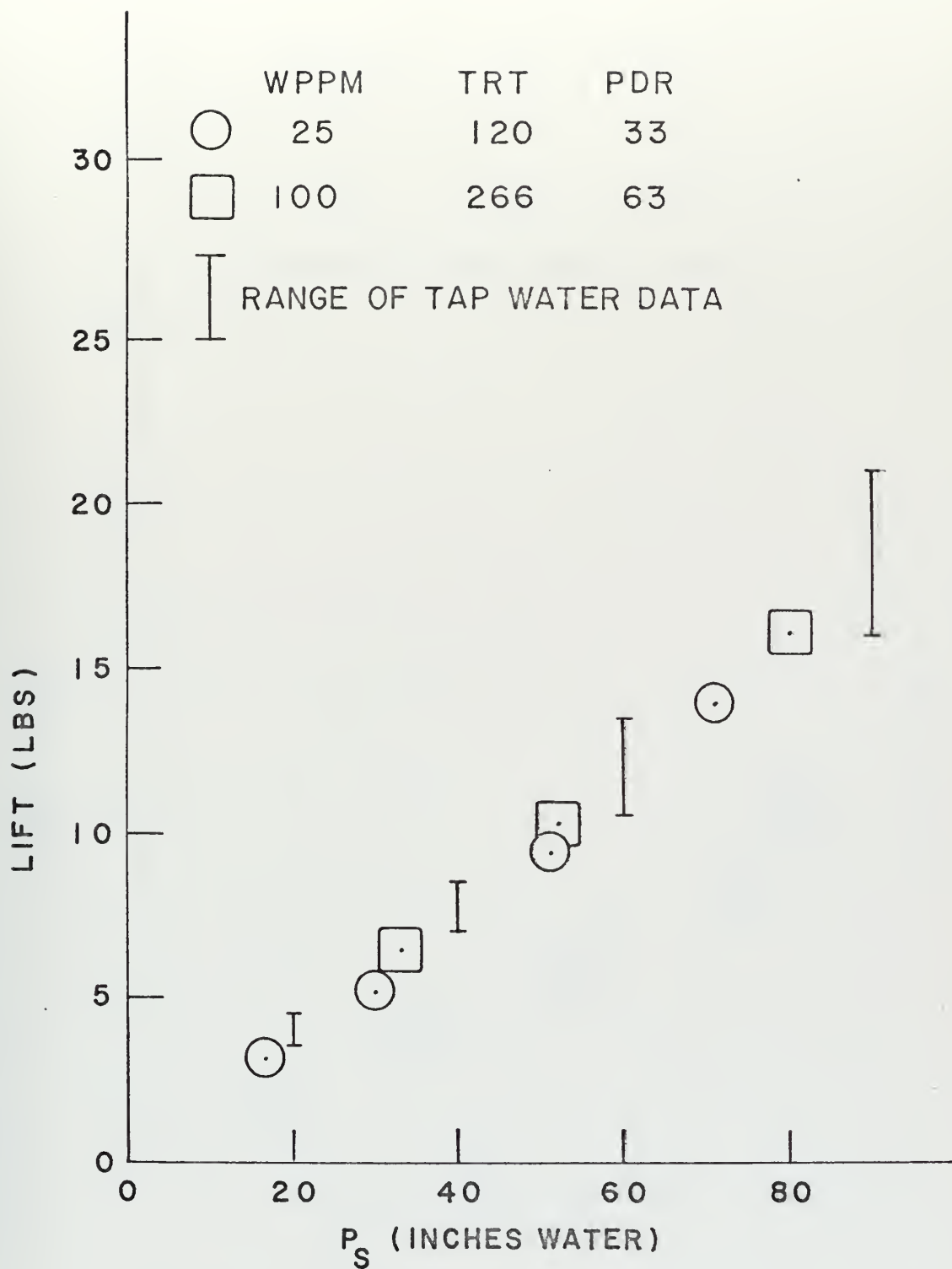
FIGURE 25: LIFT vs P_S

α = 3 DEGREES (NOMINAL)

81
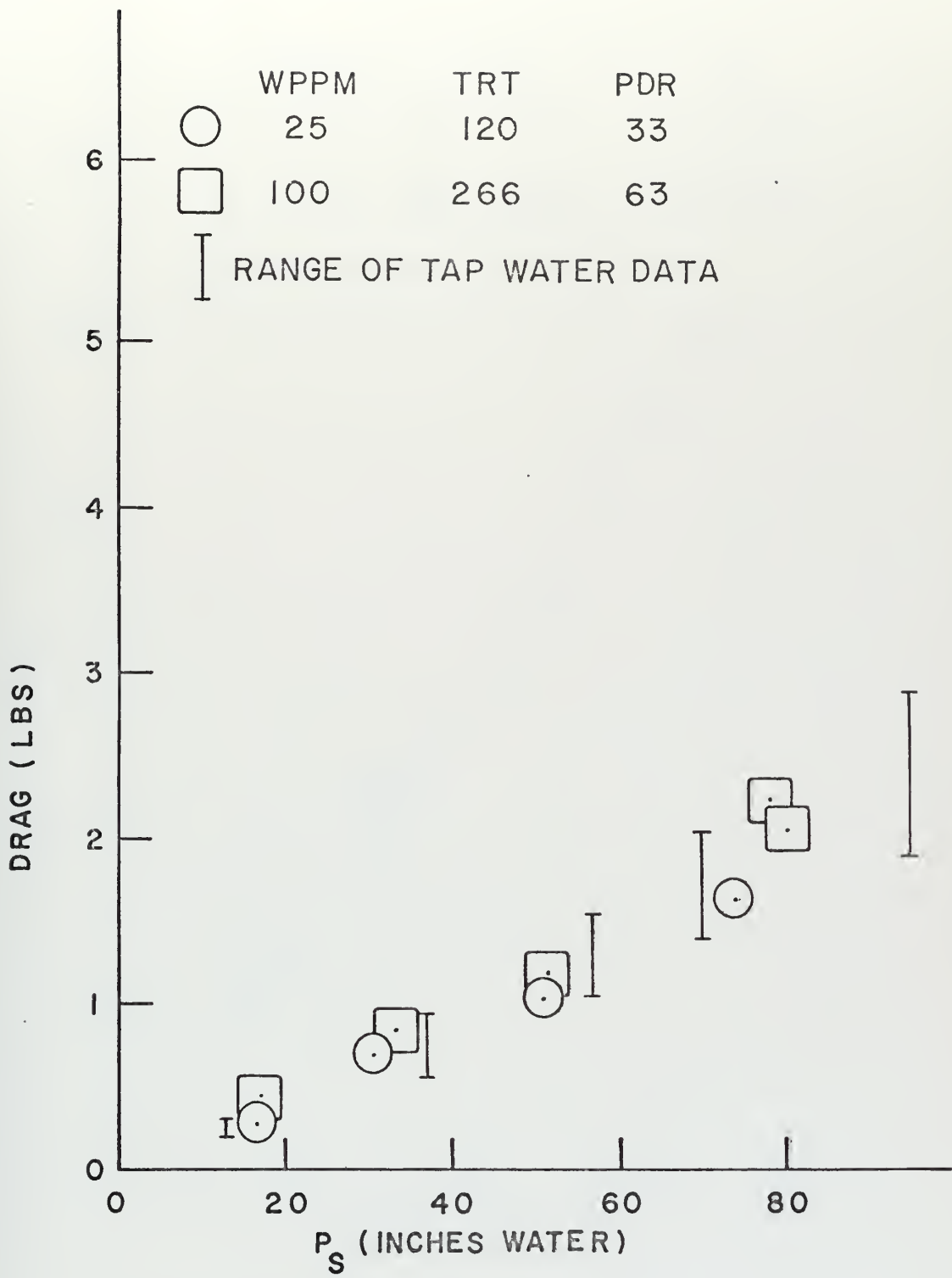
FIGURE 26: DRAG vs. P_S

α = 3 DEGREES (NOMINAL)

82
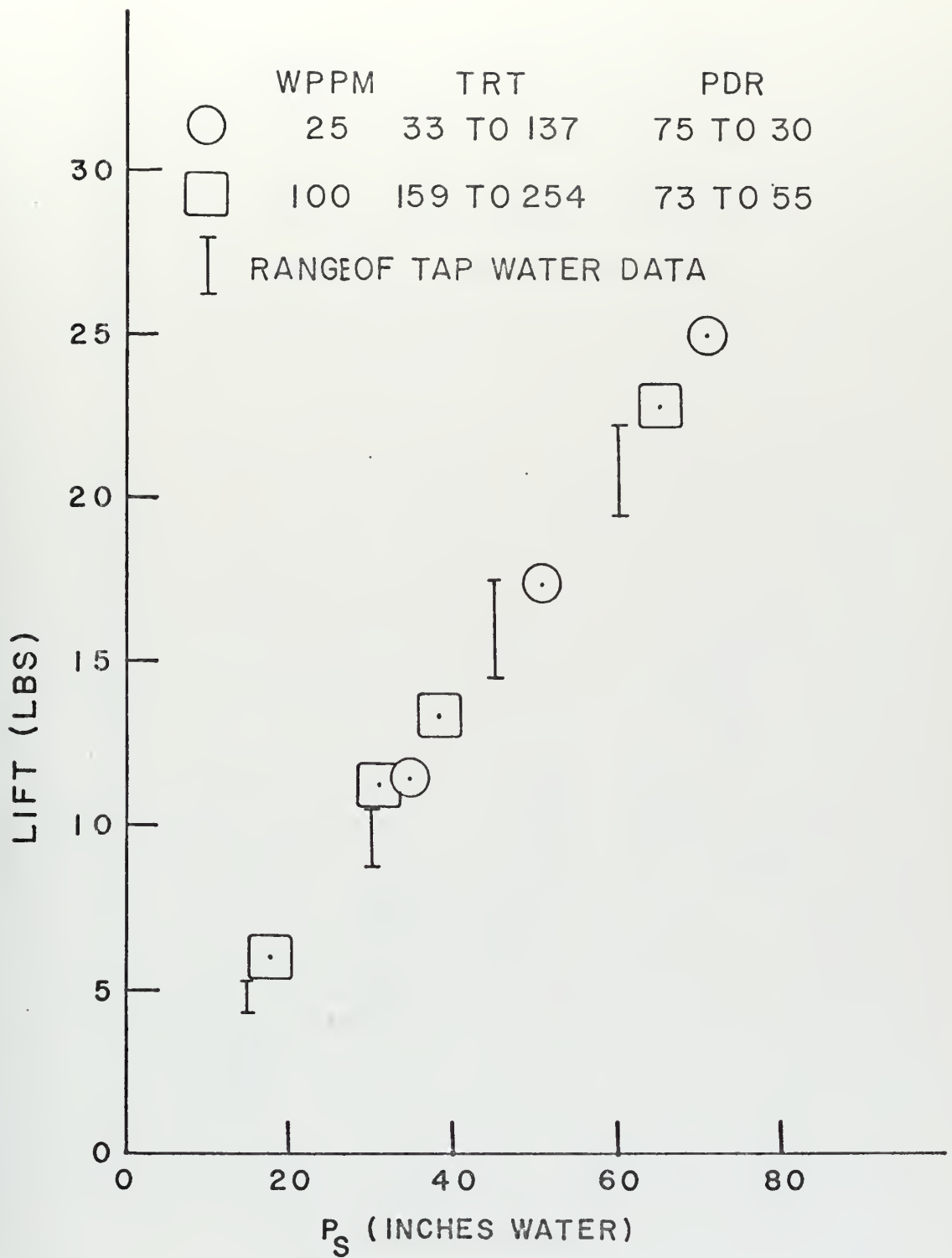
FIGURE 27 : LIFT vs P_S

α = 6 DEGREES (NOMINAL)

83
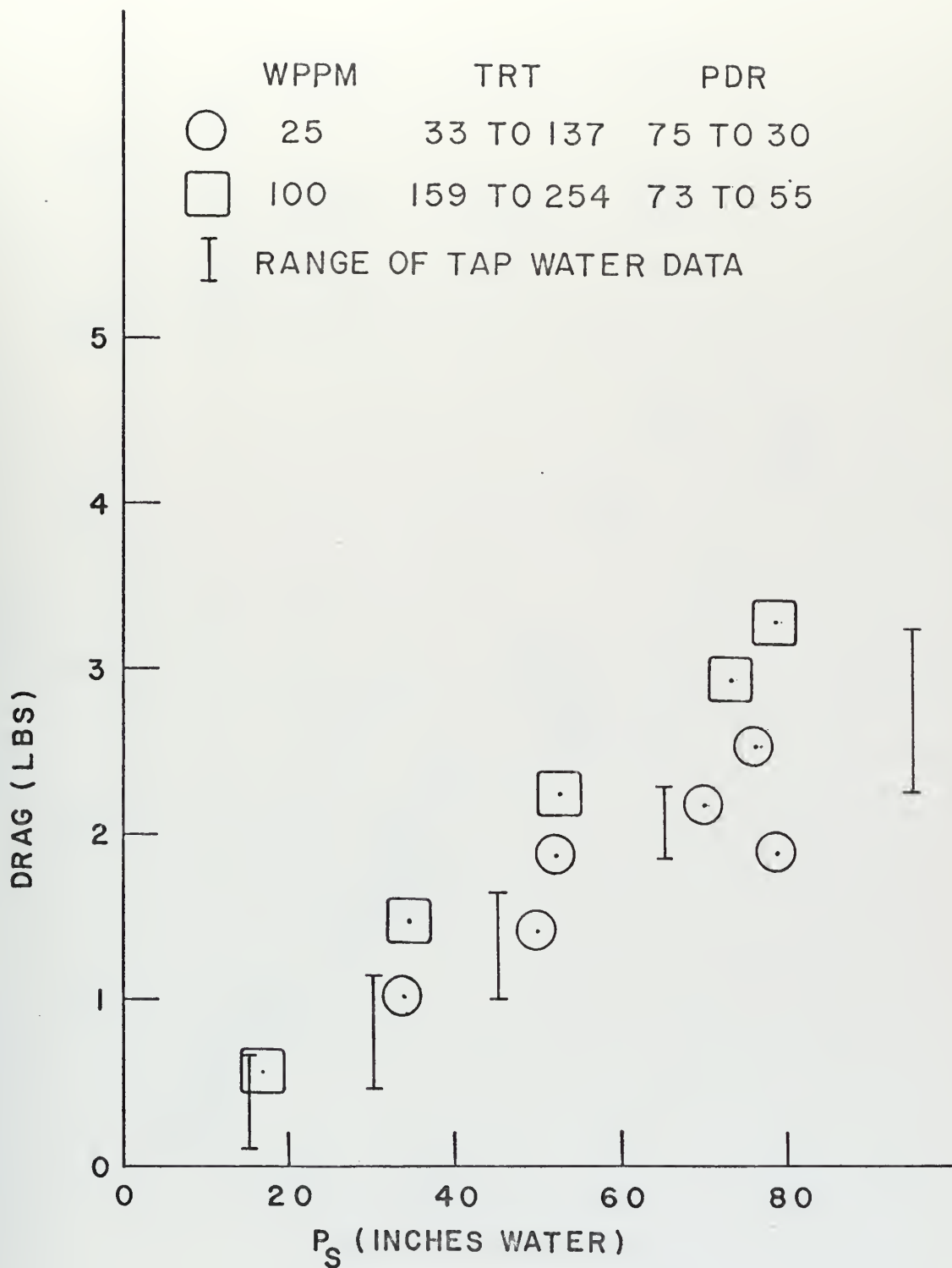
FIGURE 28: DRAG vs P_S
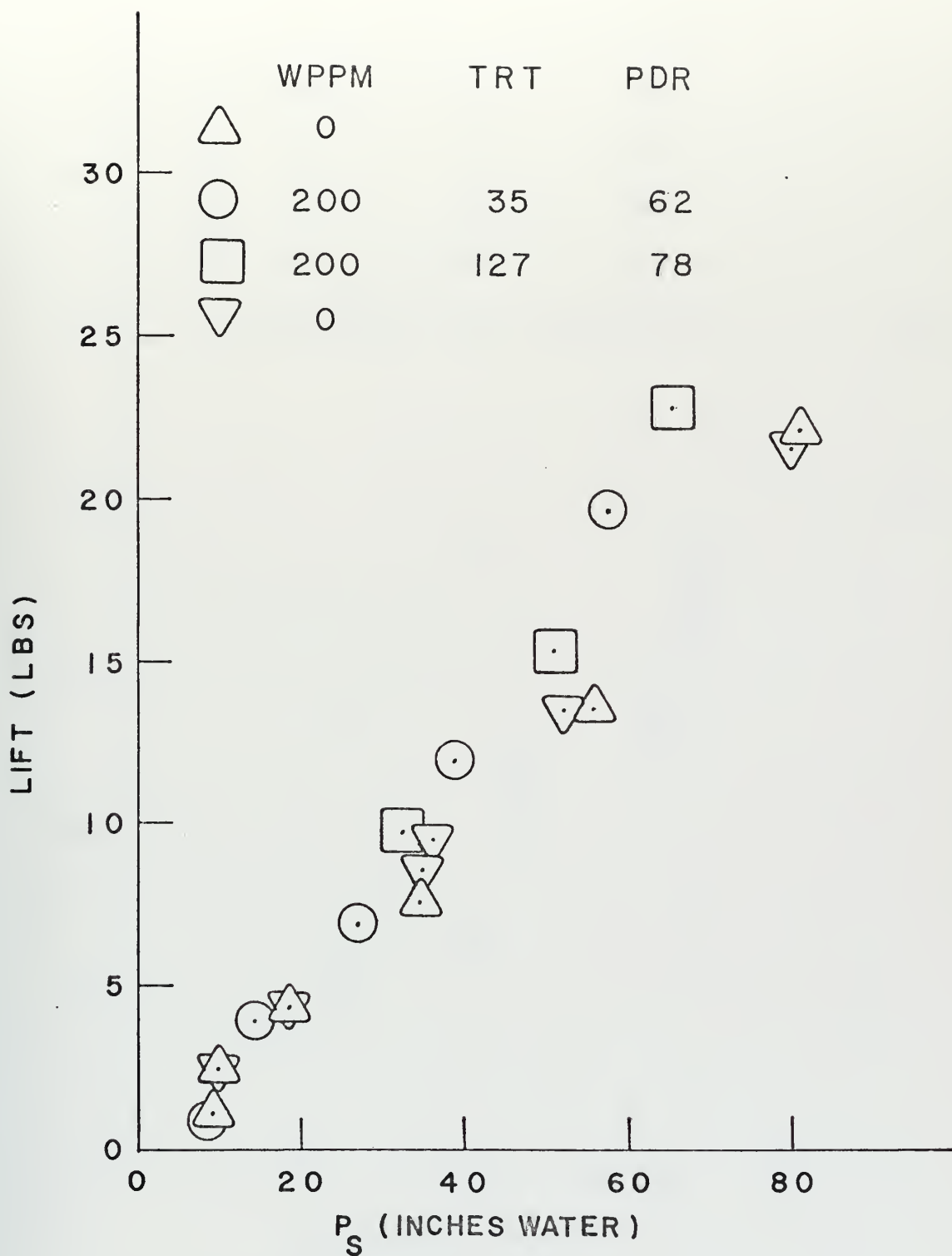
α = 6 DEGREES (NOMINAL)

FIGURE 29: LIFT vs P_S

α = 4.5 DEGREES (MEASURED)
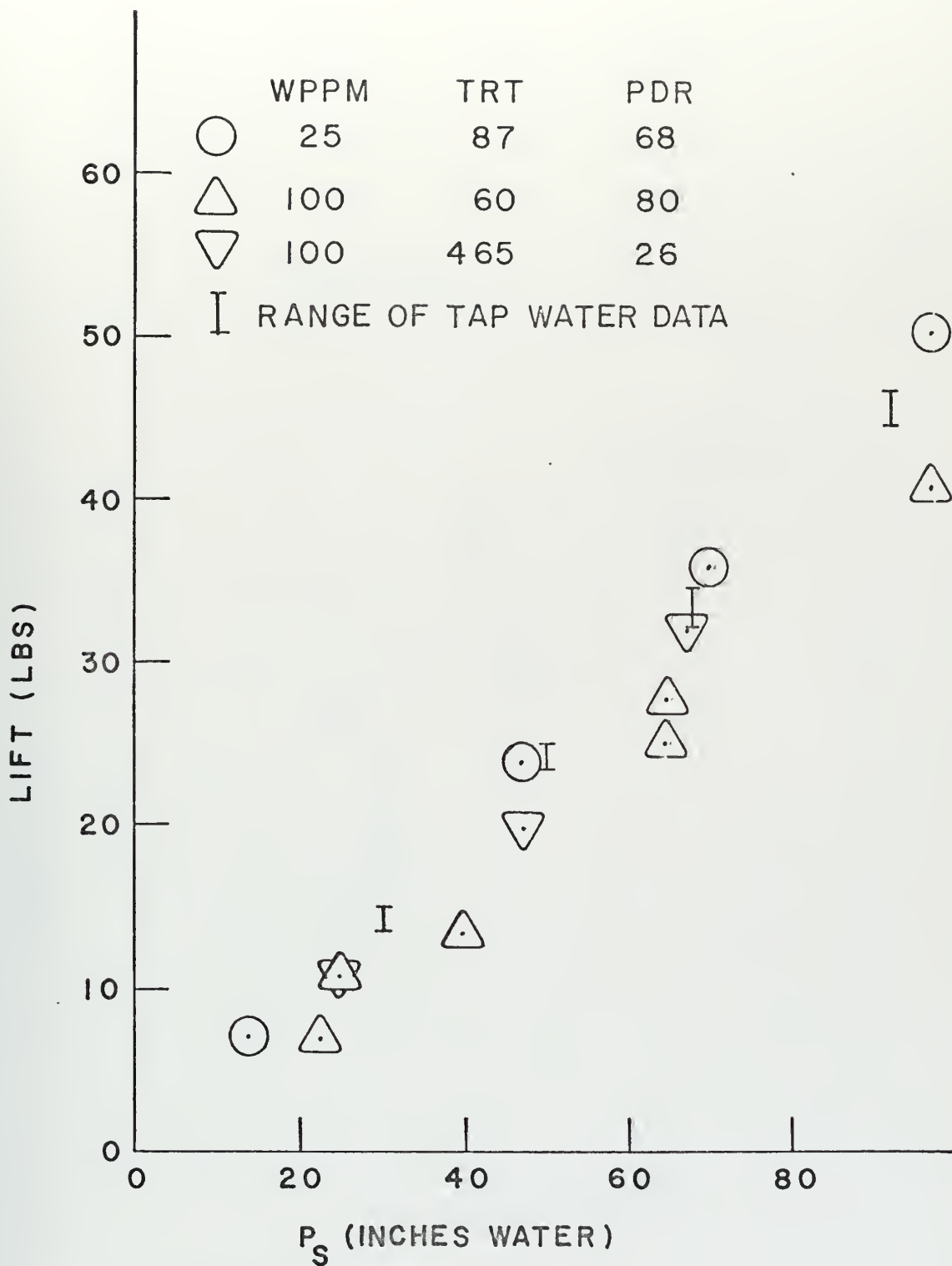
FIGURE 30 : LIFT vs P_S

$\alpha = 9$ DEGREES (NOMINAL)
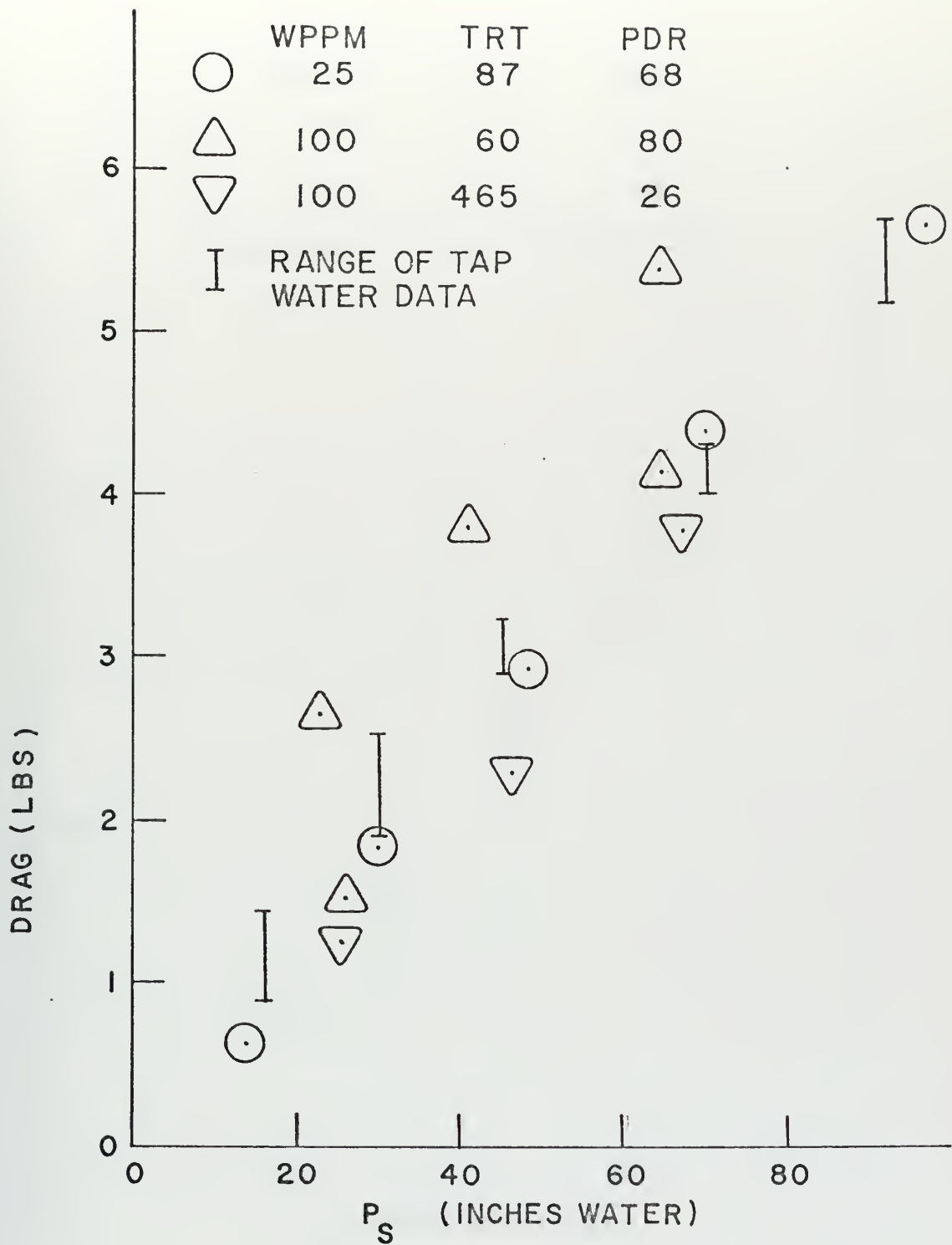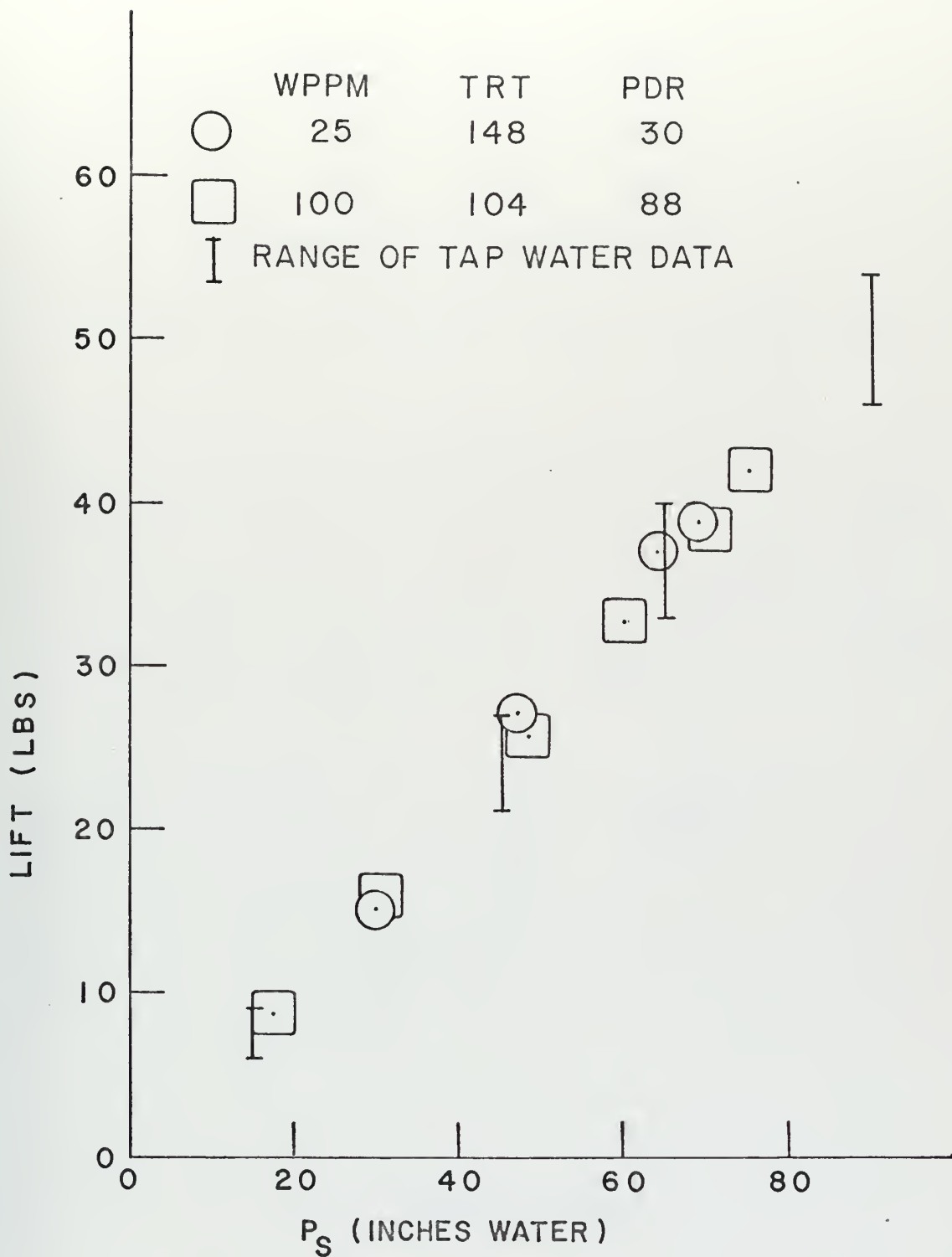
FIGURE 31: DRAG vs P_S

α = 9 DEGREES (NOMINAL)

FIGURE 32 : LIFT vs P_S
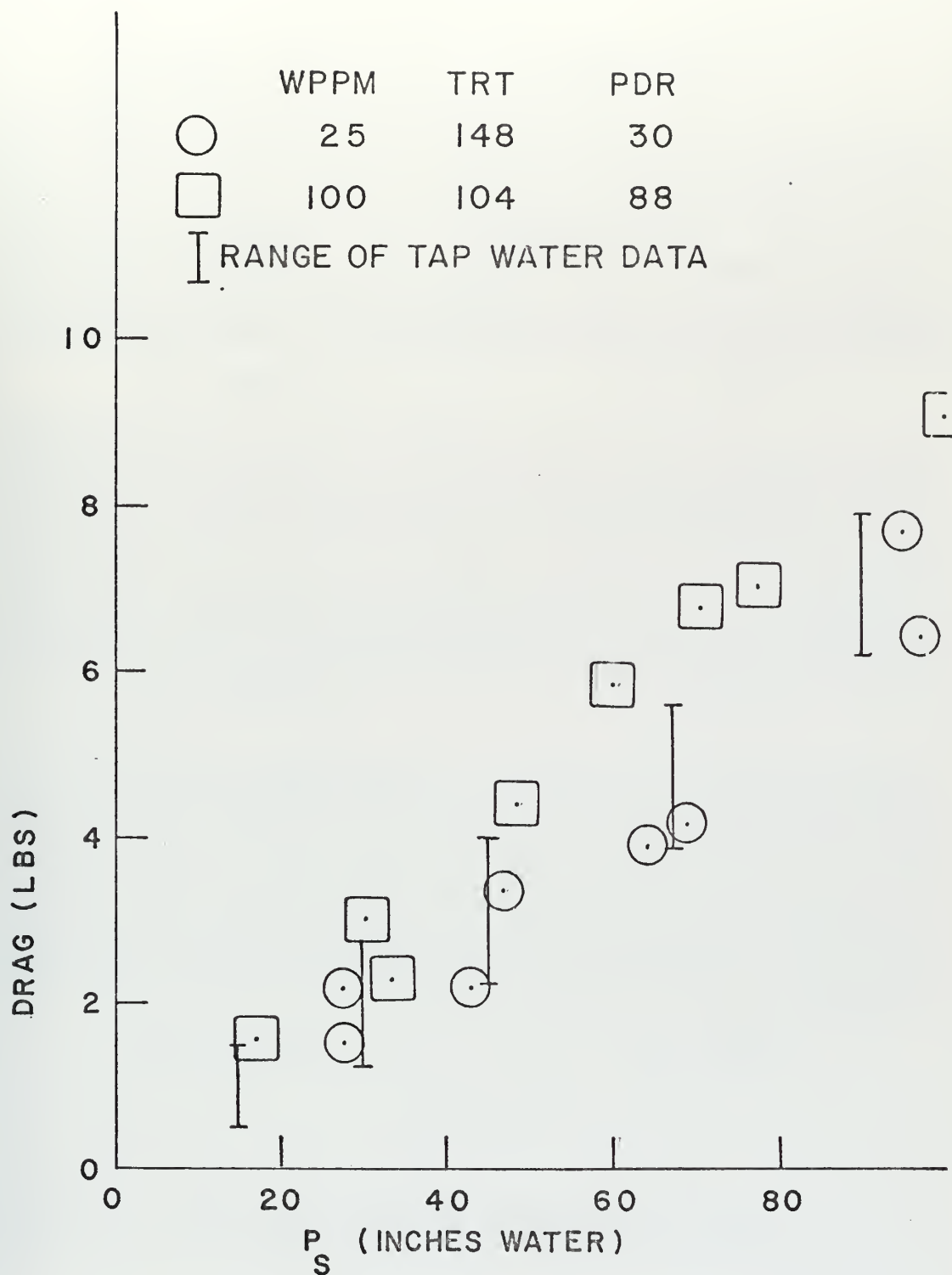
α = 12 DEGREES (NOMINAL)

88

FIGURE 33: DRAG vs P_S
α = 12 DEGREES (NOMINAL)
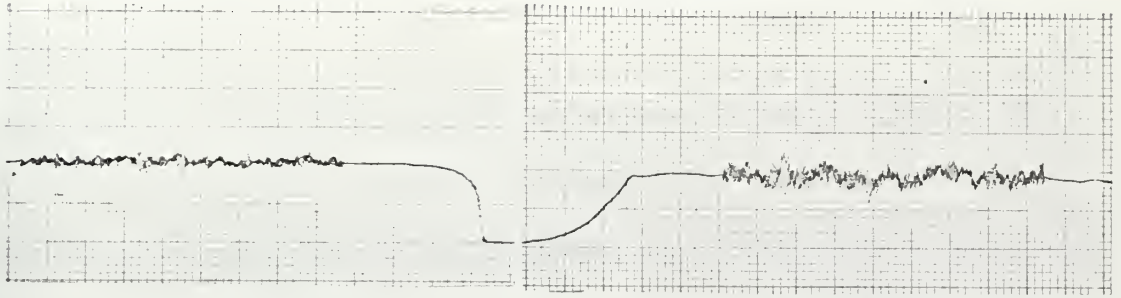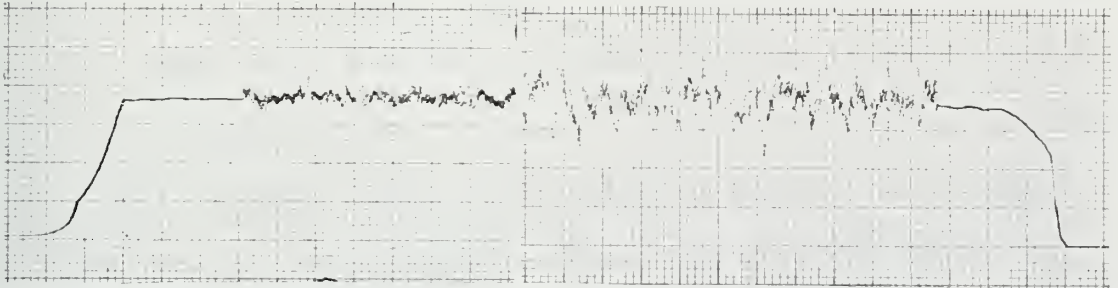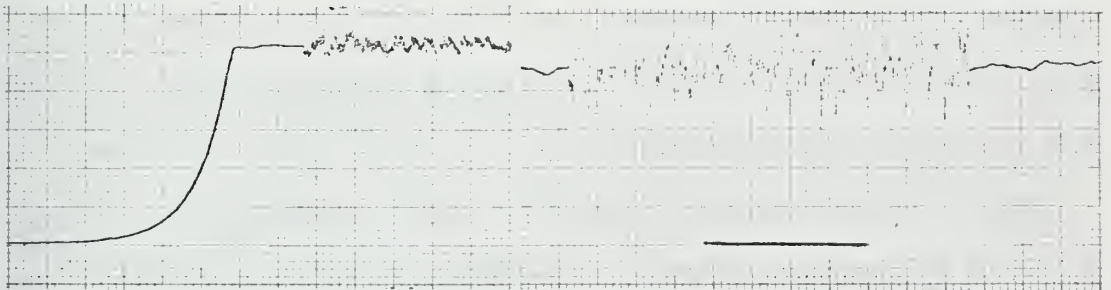
Figure 34: Oscillograph tracings of dynamic lift force

with the same water tunnel [Ref. 38]. Both the drag coefficients and the Reynolds number for all cylinder data have been corrected for tunnel effects.

Transition in tap water is seen to occur at Reynolds numbers of 1.7×10^5 to 3.0×10^5. The data lie between the results obtained on the NPL tunnel and the Göttingen tunnel as illustrated in Section II.A.

Preliminary investigations indicated that at relatively high concentrations of fresh Polyox WSR-301, the characteristics of the C_d versus Re curve are similar to those obtained in sphere drop tests and cylinder tow tank tests. However, very dilute solutions (i.e., 5 to 1.0 wppm) were found to be much more effective in reducing the drag coefficient than the higher concentrations (i.e., 25 to 100 wppm). It was observed that for all concentrations, sufficient pumping time (degradation) decreased the drag coefficient for Reynolds numbers above a certain value which depended upon the cylinder size. With sufficient pumping, a new flow behavior was observed which resulted in a low drag coefficient above a critical Re, a drag coefficient approximately that of water below the critical Re, and a large unsteady secondary flow near the separation line at the critical Reynolds number.

The results of flow about the 3/4-inch, one-inch and 1-1/2-inch cylinders at a concentration of 100 wppm Polyox WSR-301 are presented in Figs. 36-40. The apparent increase of the drag coefficient in fresh solutions, as compared to tap water, at the lowest test velocity is due to the pressure anomaly previously discussed. The value of C_d decreased

91

as velocity increased, approaching a minimum value of approximately 0.7, independent of the cylinder size.

Data were obtained with the 3/4-inch and 1-1/2-inch cylinders as the solution degraded during a four-hour period of pumping. This amount of degradation significantly reduced the drag coefficient at the lower test velocities on all three cylinders. At higher velocities, the difference between fresh solutions which produced 70 P. D. R. in the rheometer and the degraded solution which produced 40 P. D. R. in the rheometer was insignificant.

The test was continued on the one-inch cylinder for a total of 14 hours of pumping time. As degradation increased, measured by decreasing per cent drag reduction in the rheometer, the value of C_d increased toward 1.2 when Re was less than 10^5 and decreased toward 0.6 for Re greater than 10^5 as shown in Fig. 41.

The critical region formed at a total running time (TRT) of 819 minutes. The critical region is defined by two conditions:

(1) The Reynolds number at which the drag force jumps back and forth from a high to a low value;

(2) For a small increase in velocity the drag force becomes steady at the low value.

Once the critical region has formed, the behavior of the flow about the cylinder is quite distinctive. The time of formation is, however, subjective for understandable reasons. As the solution degrades, the critical region occurs at higher Reynolds numbers.

92

A solution of 25 wppm was tested with the one-inch cylinder. As seen in Figs. 42 and 43, the behavior of this solution is approximately identical to that of the 100 wppm solution at equal per cent drag reduction in the rheometer down to 40 P. D. R. This solution degraded faster than the one more concentrated. With continued degradation, this solution produced a lower value of C_d than the 100 wppm solution for Re greater than 10^5. The critical region formed when the solution produced 7.5 ±1 P. D. R. in the rheometer. Drag oscillations were large below Re_c and small above Re_c. As degradation continued, Re_c increased.

An extensive series of tests was conducted with solutions of 5 wppm Polyox WSR-301. The fresh solutions displayed a drag coefficient which monotonically decreased from 1.2 to 0.5 as the velocity increased from 7 to 25 fps for all three sizes of cylinders. The 5 wppm solutions degraded faster than the more concentrated solutions producing the critical region with less pumping time.

The critical region existed on the 1-1/2-inch cylinder at Re = 13 x 10^4 when the solution displayed a 13 P. D. R. in the rheometer. As shown in Fig. 44, the graphs of max C_d'/C_d (the relative maximum amplitude of oscillation of C_d) versus Re indicate that the critical region had initially formed in the Reynolds number range of 11 to 13 x 10^4.

The one-inch cylinder was tested in solutions prepared with tap water and also with distilled water (Figs. 45-47). The only significant difference between solutions with tap water and solutions with distilled water was that the <u>distilled water reduced the rate of degradation</u>.

At equal P. D. R. in the rheometer, both solutions produced drag forces at any given velocity which differed by less than the expected experimental error.

The gradual transition to the dual value drag coefficient region is graphically displayed in Figs. 45 and 46. The critical region initially formed on the one-inch cylinder at $Re = 10.5 \times 10^4$ when the solution produced approximately 11 P. D. R. in the rheometer. Once the critical region formed, C_d remained approximately constant at 0.43 and independent of the amount of degradation for Re greater than Re_c. Increased pumping produced less P. D. R. in the rheometer and raised the critical Reynolds number.

The 3/4-inch cylinder was tested in a 5 wppm Polyox WSR-301 tap water solution which rapidly degraded (Fig. 48). The critical region formed after 78 minutes of pumping, at $Re = 9.9 \times 10^4$ in a solution which produced 12.5 P. D. R. in the rheometer.

The one-inch cylinder was tested in very dilute solutions of 2.5 and 1.0 wppm Polyox to further investigate the increase in critical Reynolds number with increasing pumping time, and to determine if the critical Reynolds number was also relatively independent of concentration at these very low concentrations. As seen in Figs. 49 and 50, the behavior is the same as with the 5 wppm solution at equal P. D. R. in the rheometer. The critical Reynolds number was 10.5×10^4 and occurred in 2.5 and 1.0 wppm solutions which produced 13.5 and 10.2 P. D. R. respectively.

94

Both solutions were pumped until they produced essentially no drag reduction in the rheometer. The critical Reynolds number increased to 18×10^4 (when the test was terminated), the values of C_d increased toward the water curve for Re less than Re_c and remained approximately constant at $C_d = 0.4 \pm .05$ for Re greater than Re_c.

Lower concentrations were not tested due to the increase in degradation rate with decrease in concentration. In the first data run (10 minutes) the 1.0 wppm solution exhibited from 17.5 to 10 P. D. R. in the rheometer.

The characteristics of the drag oscillations are shown in Fig. 51. The relative maximum oscillation of drag coefficient attained its largest value at the critical Reynolds number. The oscillation greatly attenuated at a slightly higher Re. After falling to a minimum just above Re_c, the magnitude of oscillation increased with Reynolds number probably due to increasing turbulence level in the tunnel test section.

Figure 52 is an assemblage of all the data obtained in the critical region. The critical Reynolds number is plotted as a function of P. D. R. in the rheometer for all the previously mentioned data. In addition, two data for a 1/2-inch cylinder, which were obtained from pressure measurements, were included. A 1/4-inch cylinder was tested up to $Re = 0.6 \times 10^5$ in the same solution, but no critical region was found even though the same solution produced a critical region for a 1-1/2-inch cylinder.
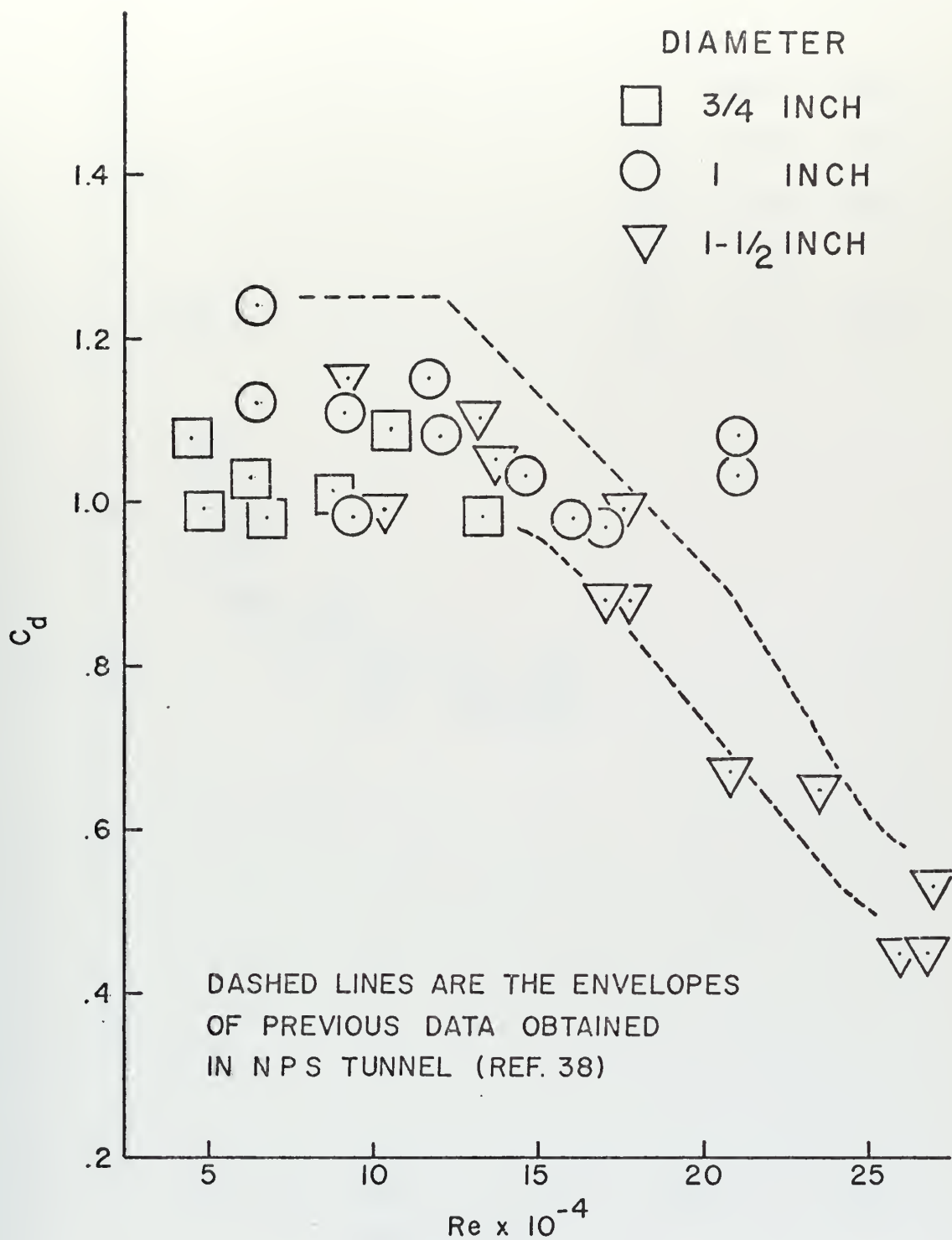
FIGURE 35: C_d vs Re
CYLINDERS IN TAP WATER

DIAMETER
□ 3/4 INCH
○ 1 INCH
▽ 1-1/2 INCH

DASHED LINES ARE THE ENVELOPES
OF PREVIOUS DATA OBTAINED
IN N P S TUNNEL (REF. 38)

C_d

Re x 10^{-4}
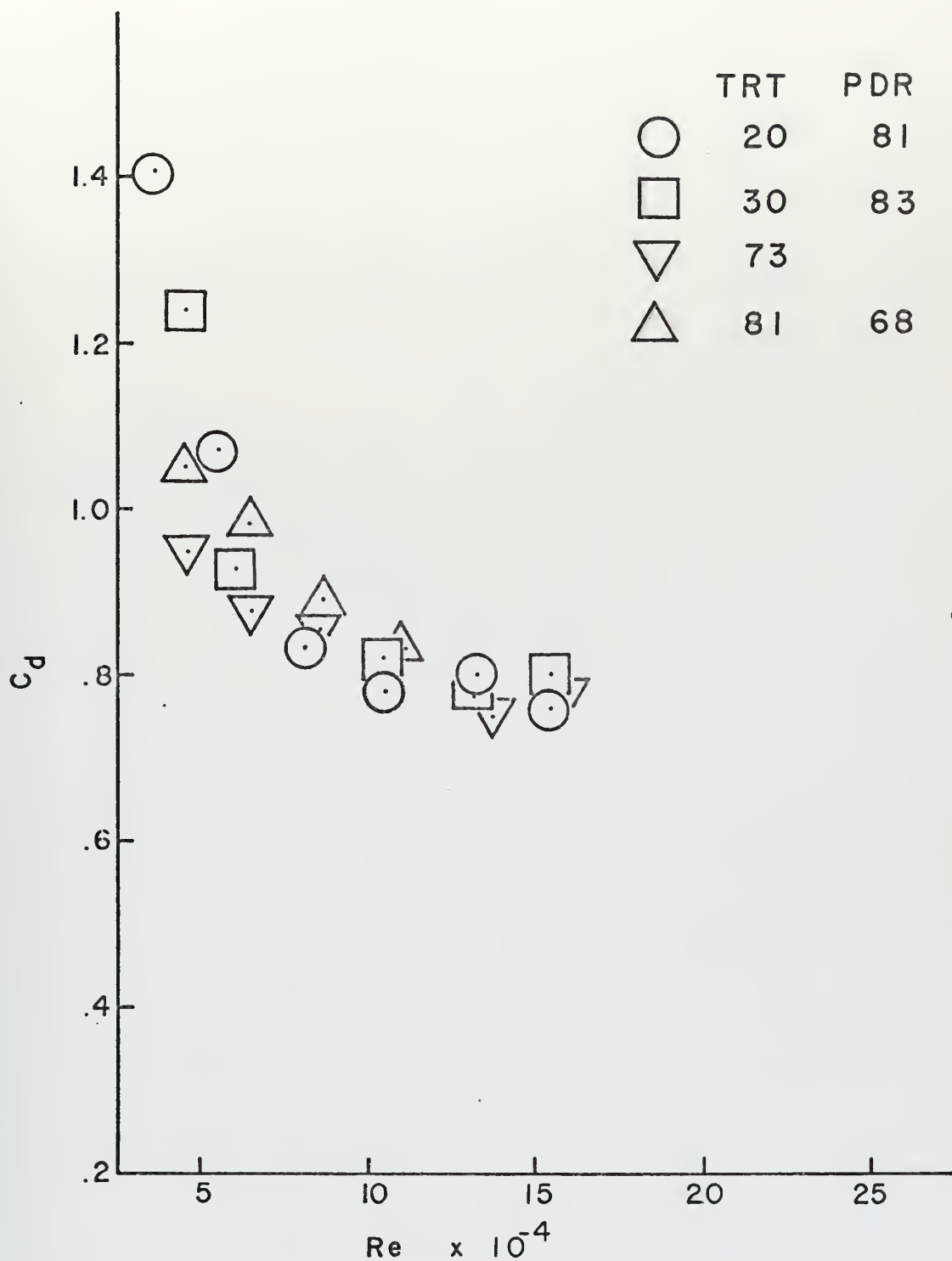
FIGURE 36 : C_d vs Re

$\frac{3}{4}$ IN. DIAMETER CYLINDER
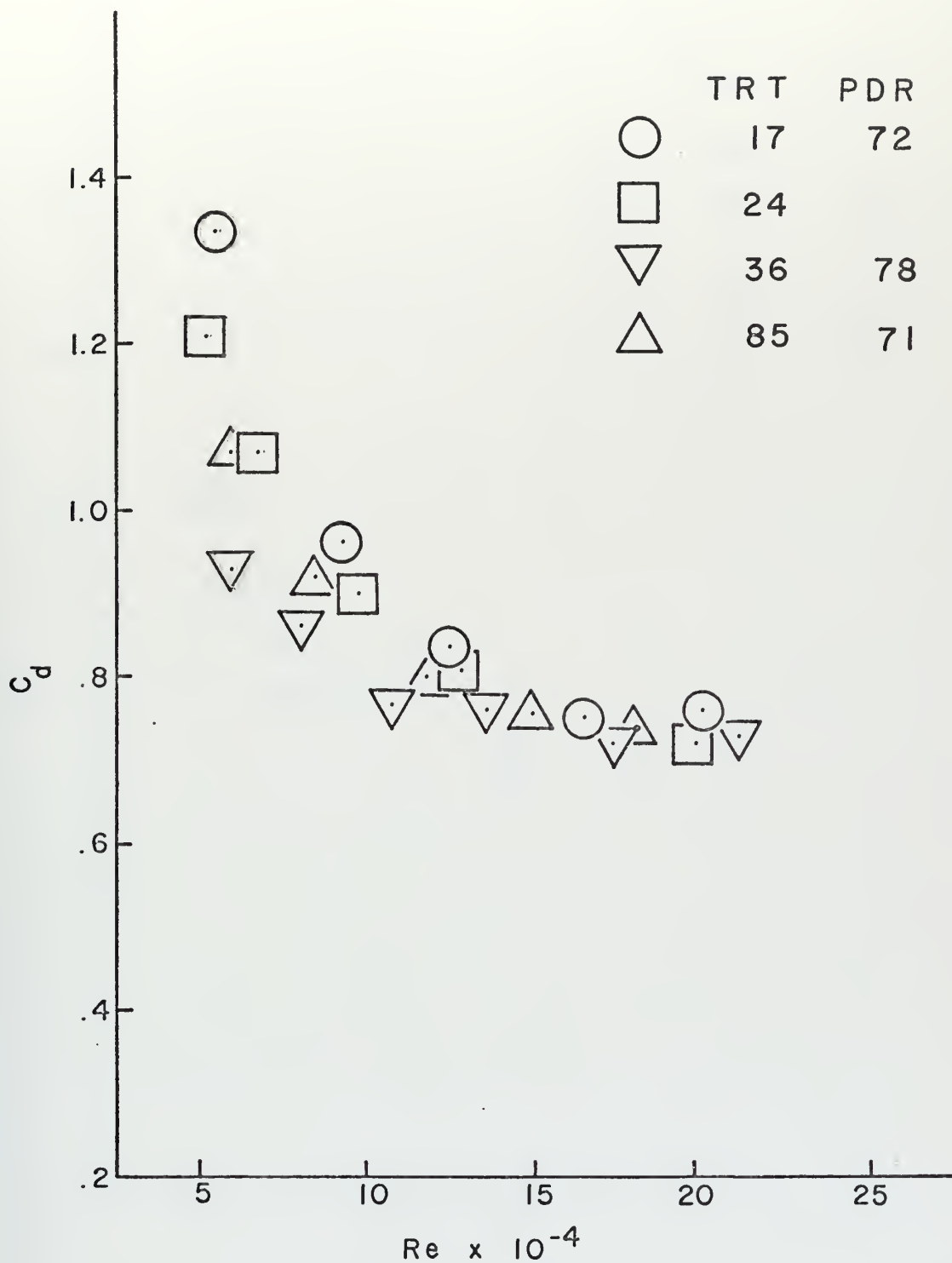
IN 100 WPPM SOLUTION

FIGURE 37: C_d vs Re
¾ IN. DIAMETER CYLINDER
IN 100 WPPM SOLUTION

FIGURE 38 : C_d vs Re

I IN. DIAMETER CYLINDER

IN 100 WPPM SOLUTION

99
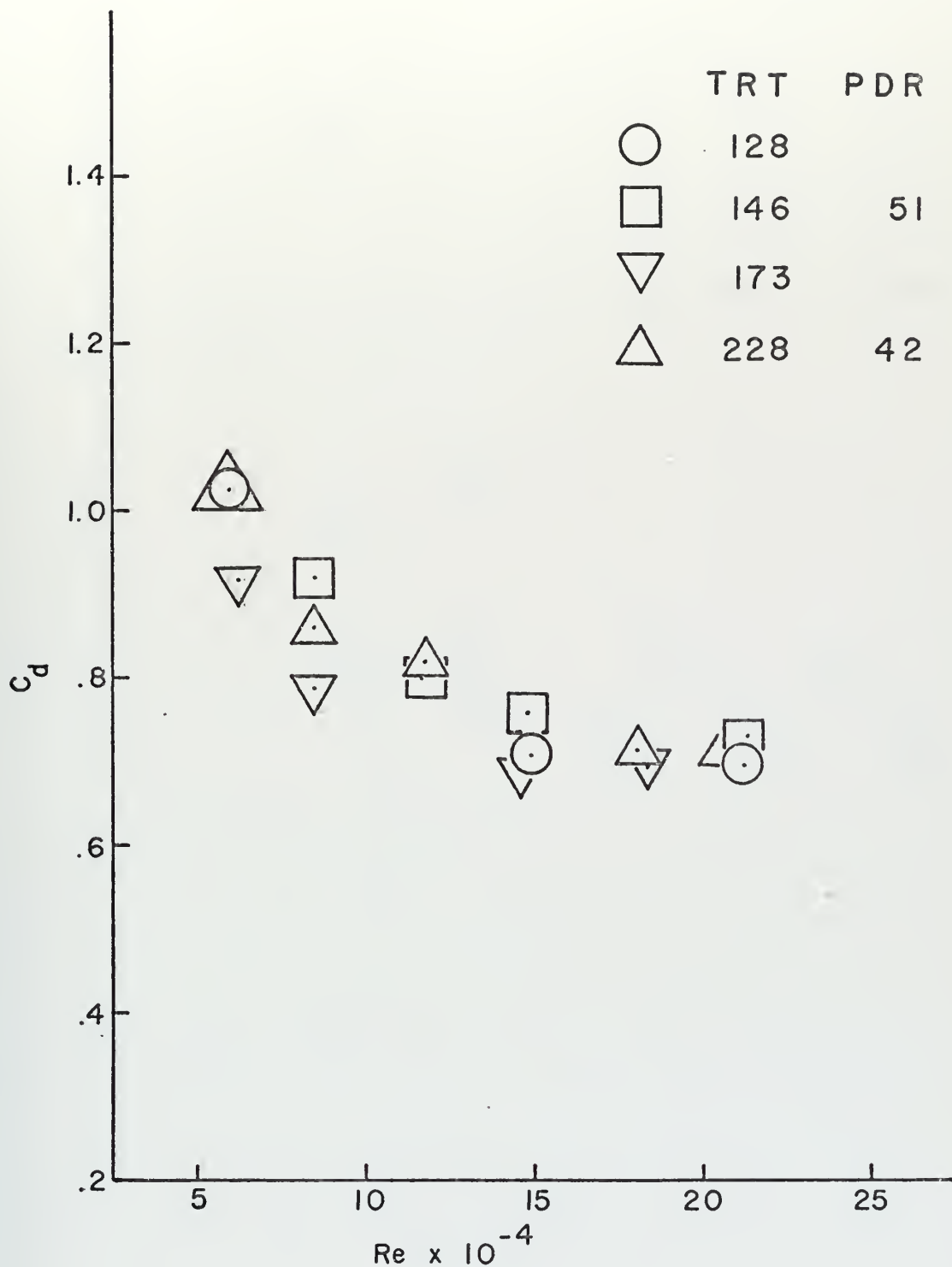
FIGURE 39: C_d vs Re
I IN. DIAMETER CYLINDER
IN 100 WPPM SOLUTION
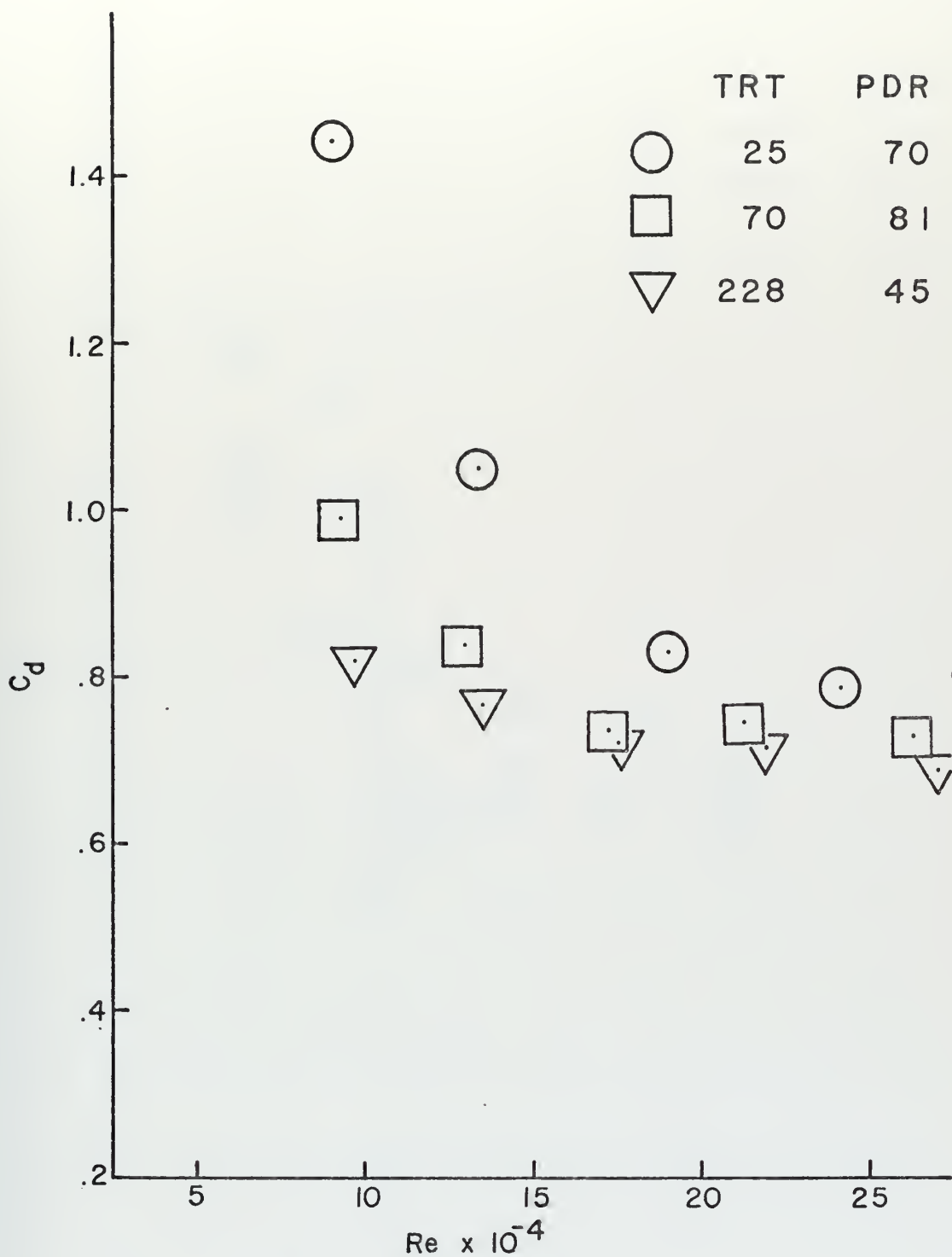
FIGURE 40 : C_d vs Re
1-½ IN. DIAMETER CYLINDER
IN 100 WPPM SOLUTION

101

FIGURE 41: C_d vs Re
I IN. DIAMETER CYLINDER
IN 100 WPPM SOLUTION

102
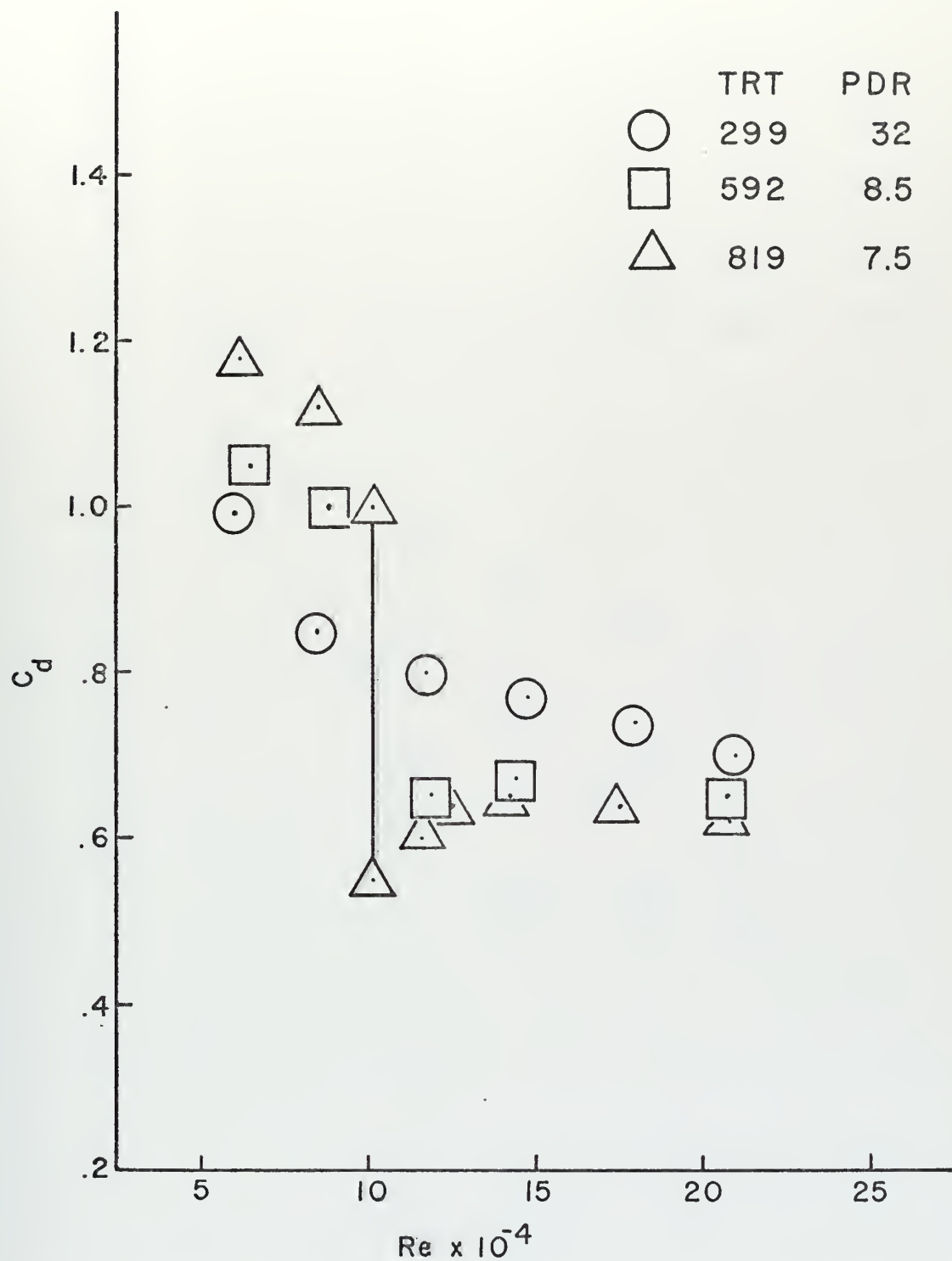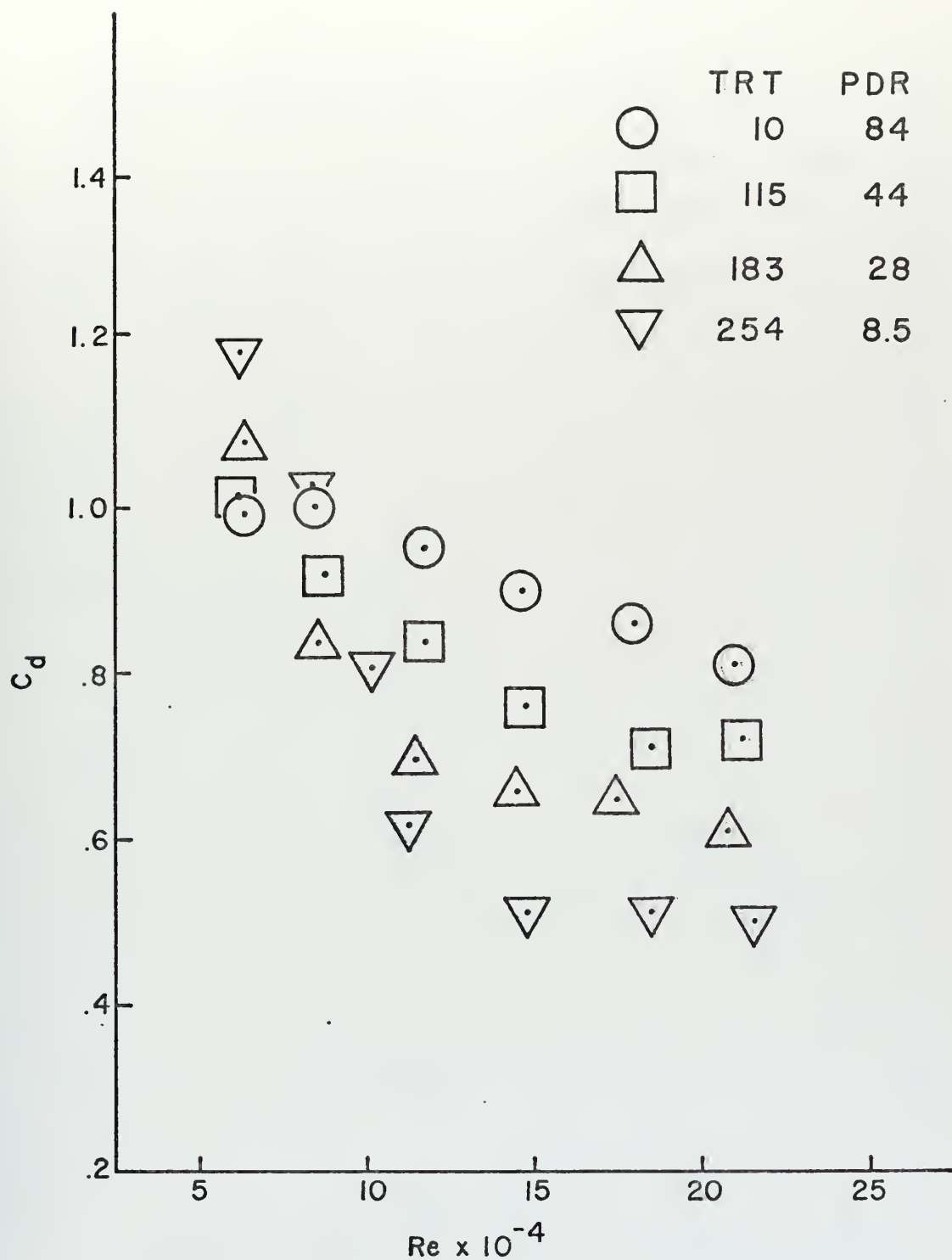
FIGURE 42 : C_d vs Re

1 IN. DIAMETER CYLINDER
IN 25 W P PM SOLUTION
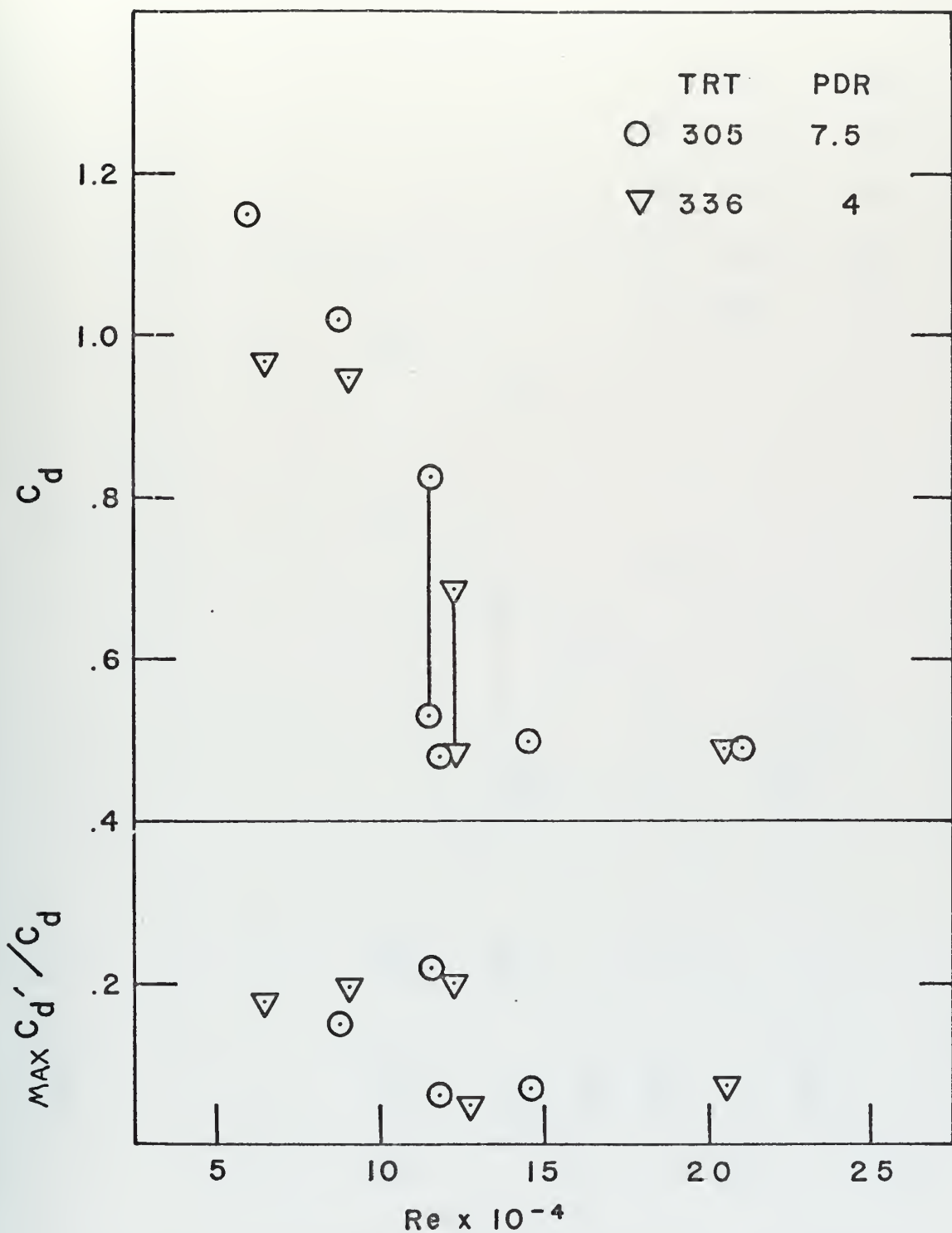
FIGURE 43: 25 WPPM CRITICAL C_d TRANSITION
1 INCH DIAMETER CYLINDER.
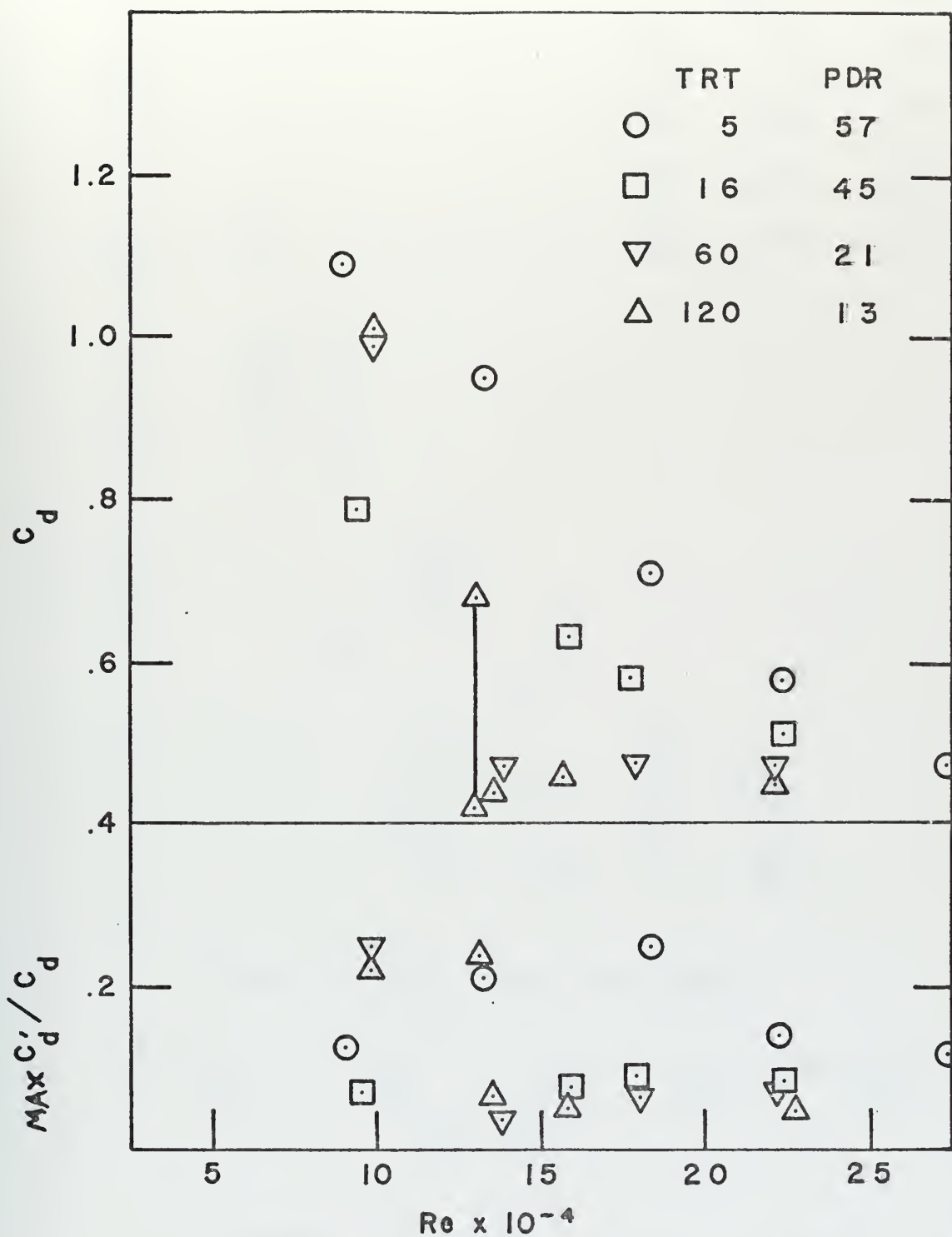
FIGURE 44 : 5 WPPM CRITICAL C_d TRANSITION
1-1/2 INCH DIAMETER CYLINDER.
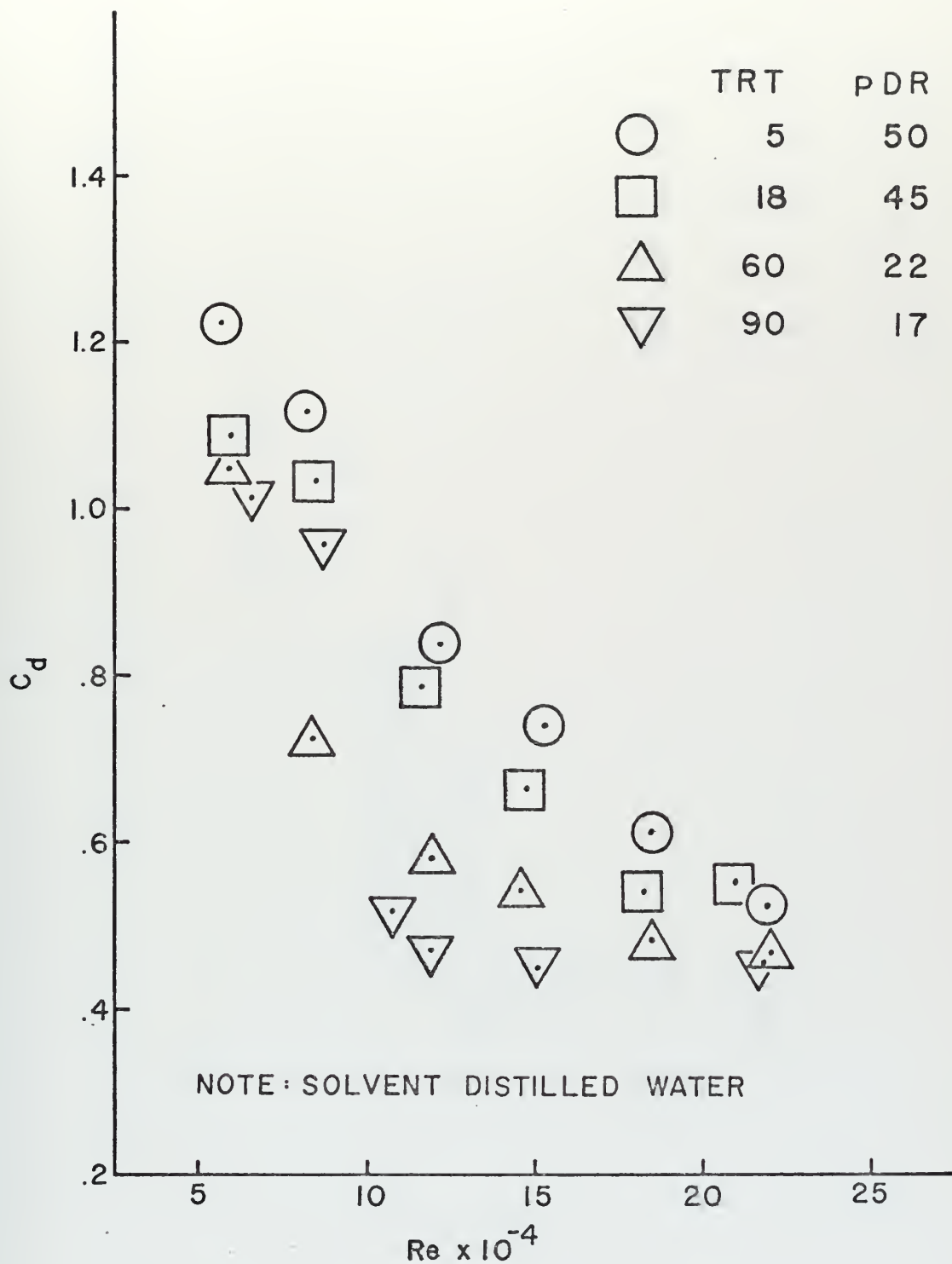
FIGURE 45: C_d vs Re

1 IN. DIAMETER CYLINDER
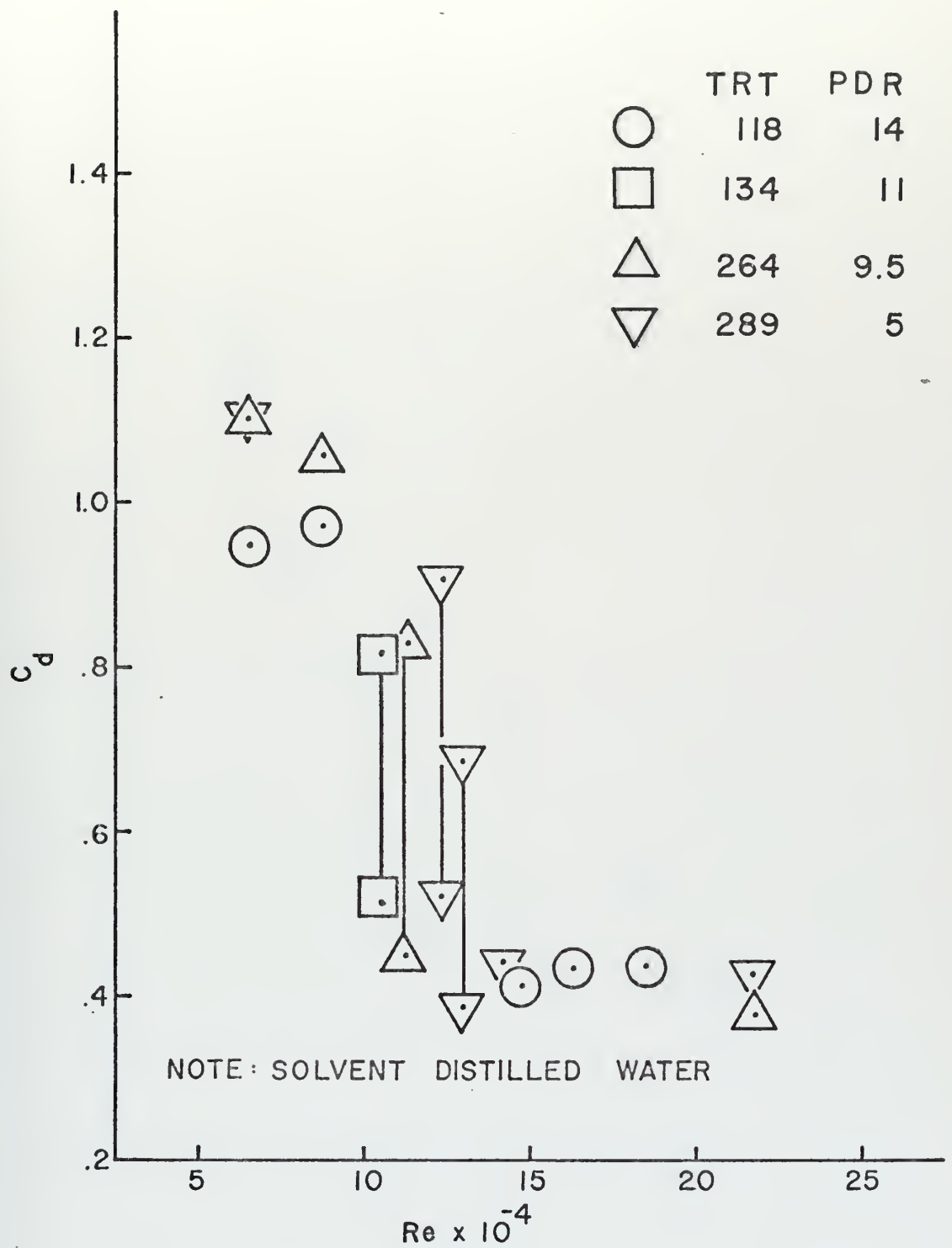
IN 5 WPPM SOLUTION

FIGURE 46: C_d vs Re

1 IN. DIAMETER CYLINDER
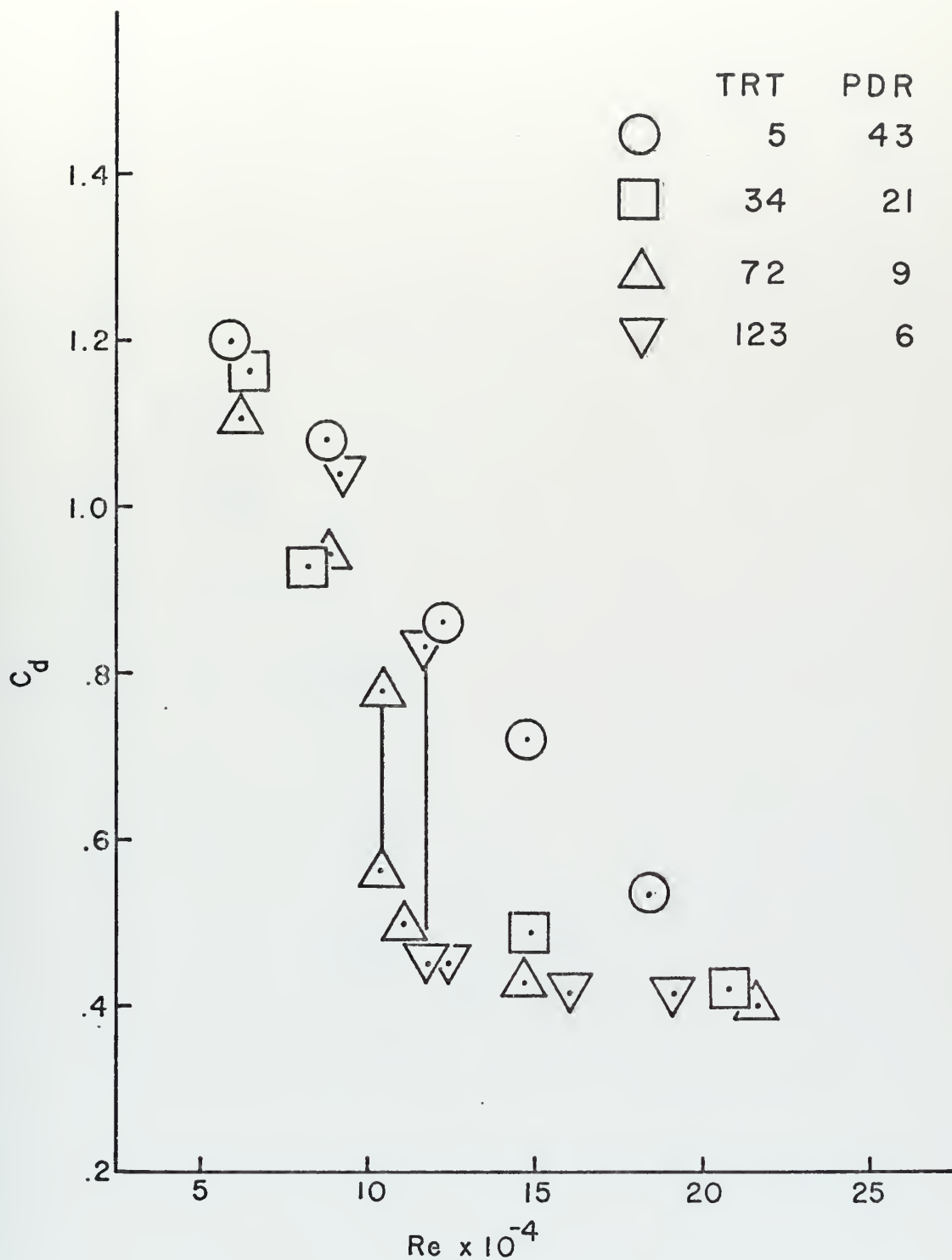
IN 5 WPPM SOLUTION

FIGURE 47: C_d vs Re
1 IN. DIAMETER CYLINDER
IN 5 WPPM SOLUTION

108

FIGURE 48: C_d vs Re

¾ IN. DIAMETER CYLINDER
IN 5 WPPM SOLUTION

109

FIGURE 49: C_d vs Re
I IN. DIAMETER CYLINDER
IN 2.5 WPPM SOLUTION

FIGURE 50: C_d vs Re
1 IN. DIAMETER CYLINDER
IN 1.0 WPPM SOLUTION

111
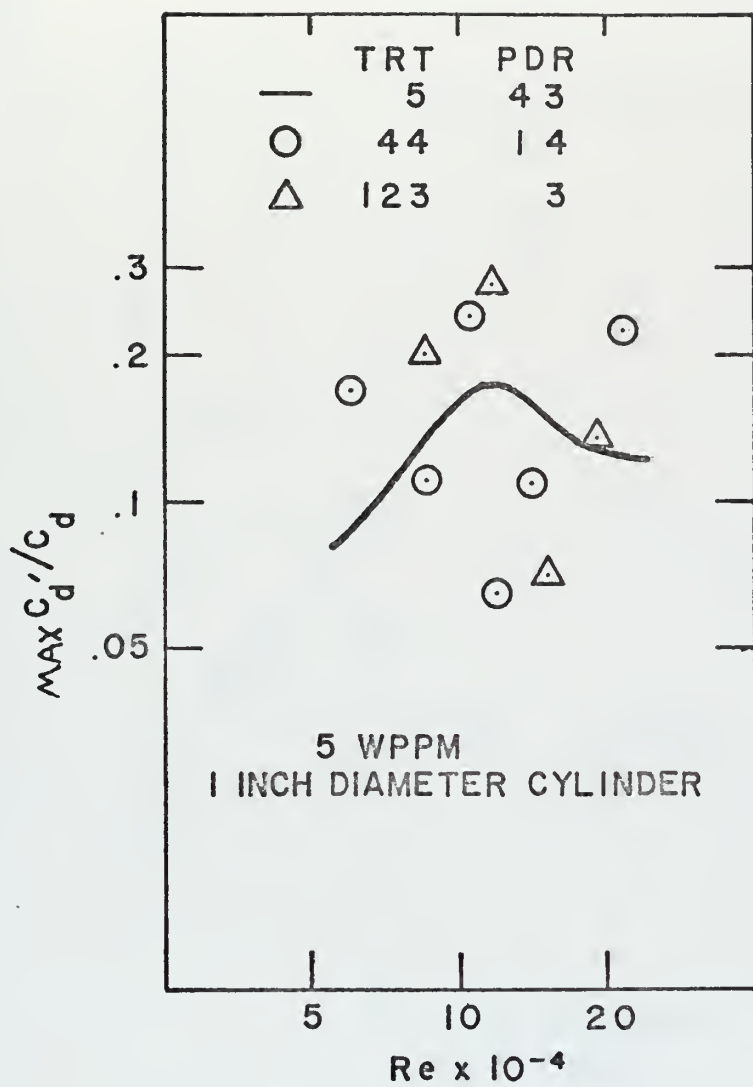
FIGURE 51 : AMPLITUDE OF DRAG
OSCILLATIONS..
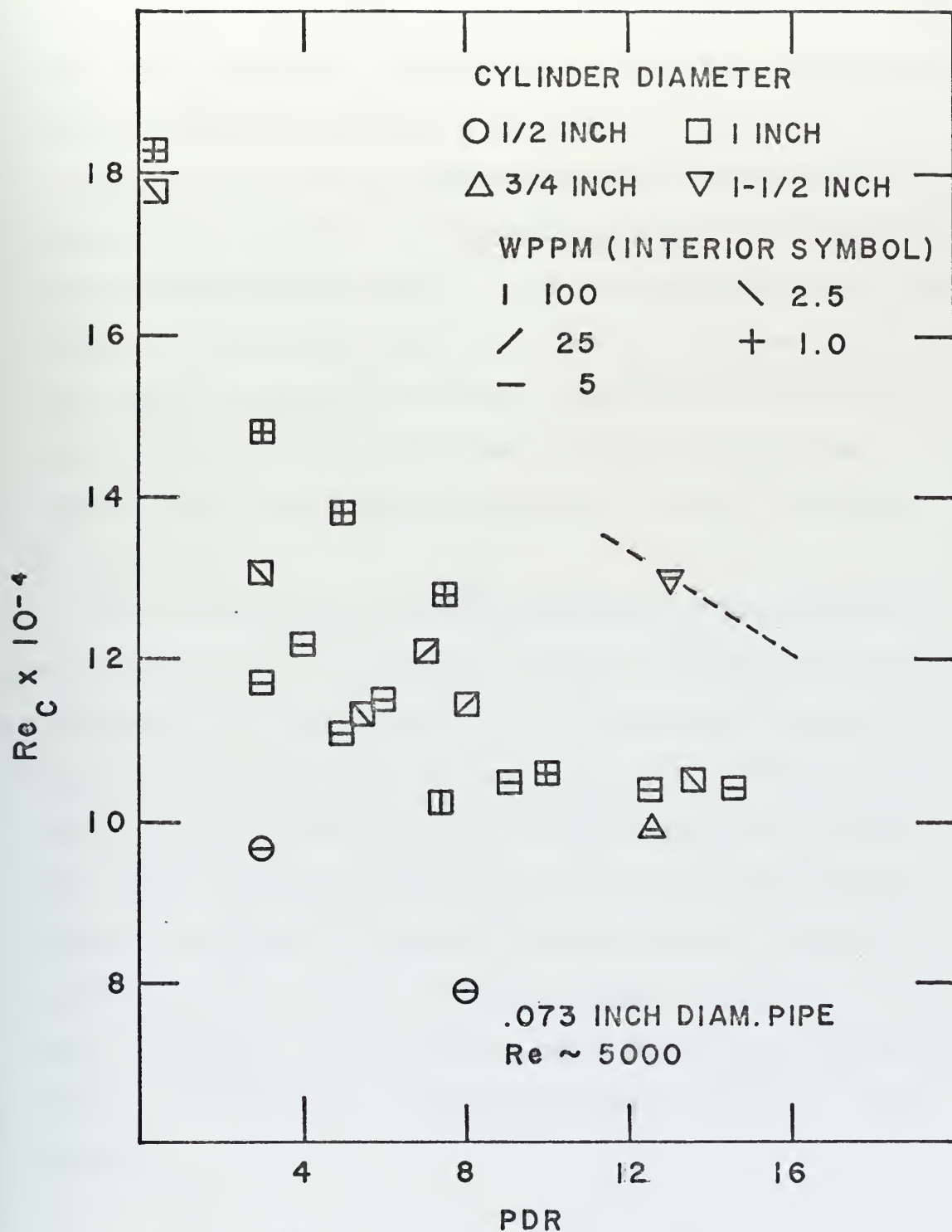
FIGURE 52: CRITICAL Re vs PERCENT (PIPE)
DRAG REDUCTION.

113

It is to be noted that the expected error in the values of P. D. R. is ±2 while the values of Re_c are reliable to within $\pm 0.1 \times 10^5$. The dashed line through the 1-1/2-inch cylinder data indicates the probable trend as evidenced by Fig. 44.

Figure 53 indicates the relative importance of concentration in determining the drag force on a one-inch cylinder for solutions which produce approximately the same P. D. R. in the rheometer, prior to the formation of the critical region. The data fall into two groups: The higher concentrations, 25 and 100 wppm, yielding one curve and the lower concentrations, 2.5 and 5 wppm, yielding a second curve. Apparently, the lower concentrations produce a steeper transition to a lower C_d.

Figure 54 indicates the relative importance of concentration on the characteristics of the critical region. The main effect of concentration is to set the value of C_d at an Re greater than Re_c, the highest concentration producing the largest drag coefficient. The value of the first observed critical Reynolds number for the one-inch cylinder varied only from 10.3×10^4 to 11.4×10^4 while the concentration varied by a factor of 100 and the total pumping time by a factor of 82. The only difference between the tap and distilled water was that the distilled water required twice as much pumping time to form a solution which produced approximately 14 P. D. R. in the rheometer.
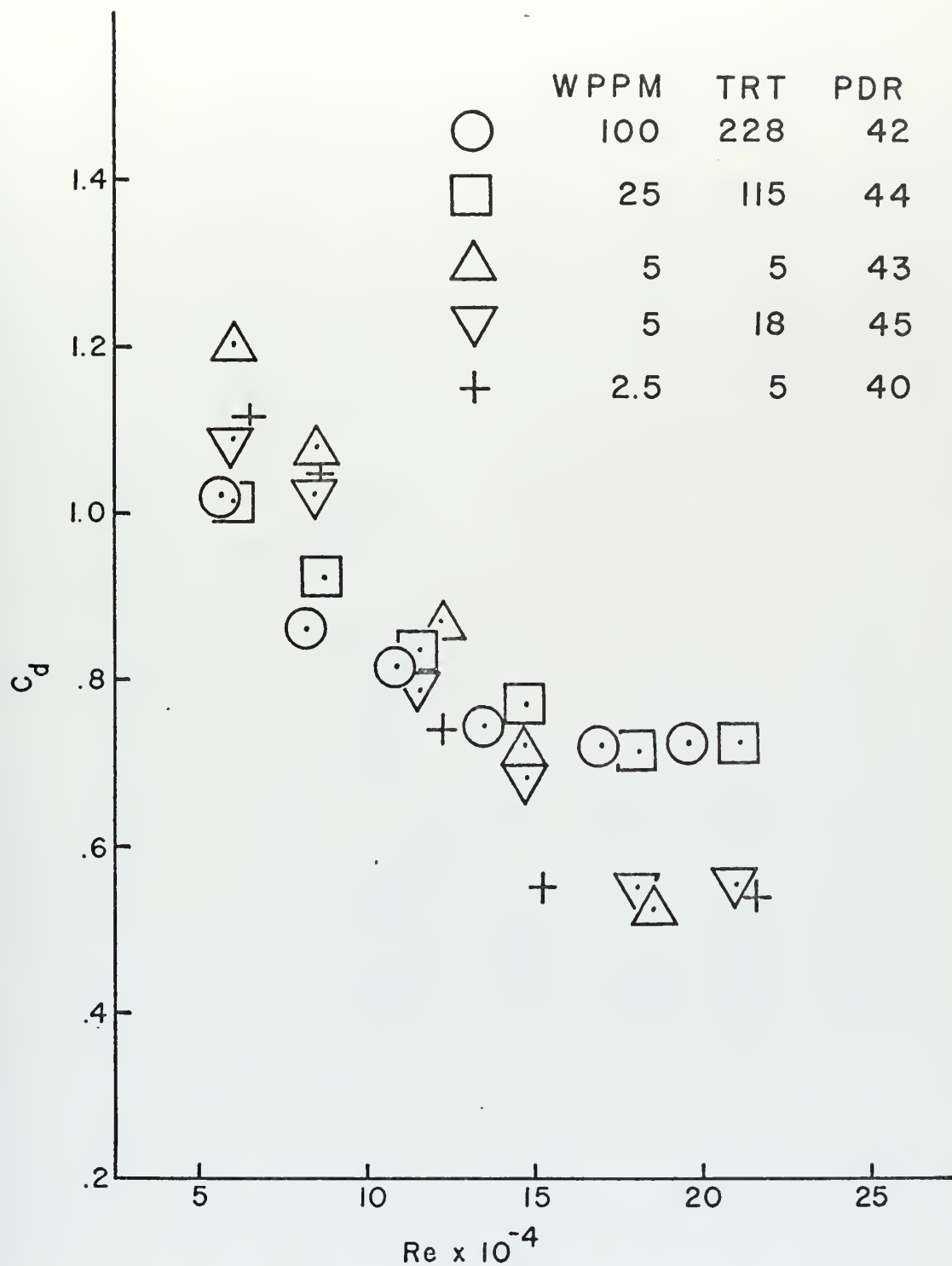
FIGURE 53 : C_d vs Re
1 IN. DIAMETER CYLINDER
PDR ∼ 45

115
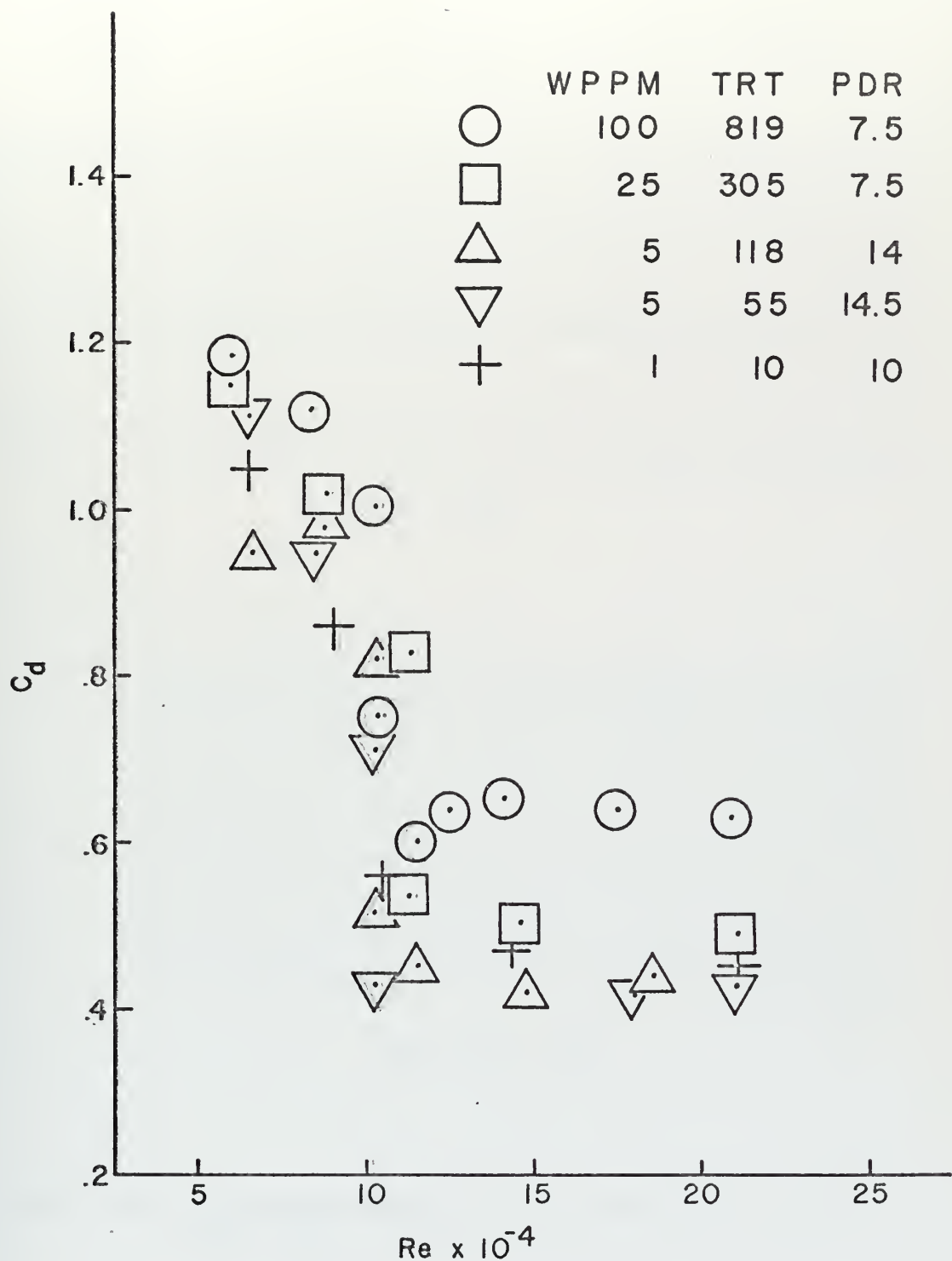
FIGURE 54: C_d vs Re
I IN. DIAMETER CYLINDER
CRITICAL REGION FIRST OBSERVED

116
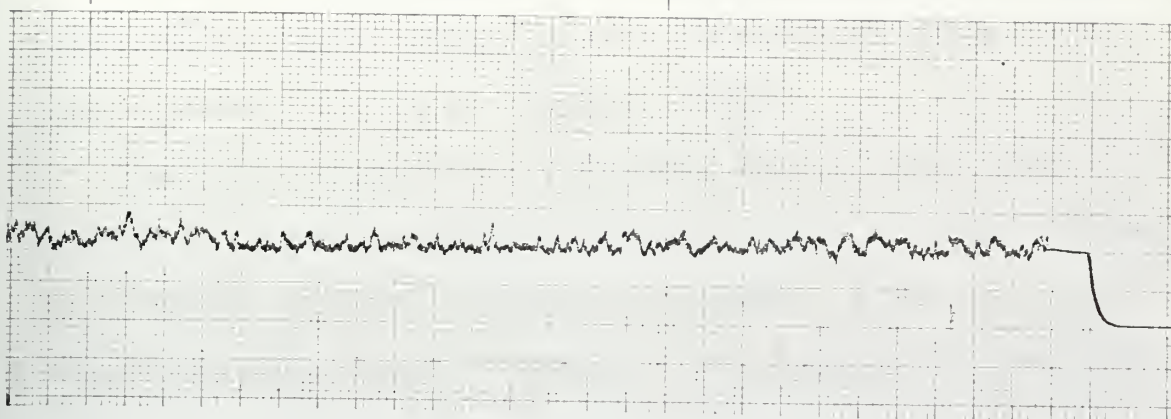
$$Re_c = 12.1 \times 10^4$$
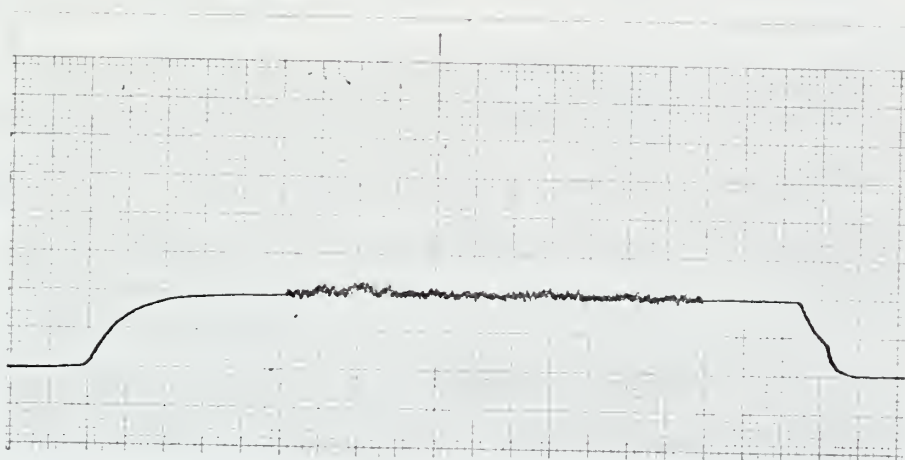
$$Re = 12.4 \times 10^4$$

Figure 55: Oscillograph tracings of drag force at $Re = Re_c$ and $Re > Re_c$

F. PRESSURE DISTRIBUTION ON A CYLINDER IN THE FLOW OF DILUTE POLYMER SOLUTIONS

Preliminary investigations revealed that the pressure distribution about a cylinder in the flow of a dilute polymer solution is quite distinct from that in a Newtonian fluid.

Figure 56 illustrates the (corrected) pressure distribution measured on a one-inch diameter cylinder in the flow of fresh 100 wppm Polyox WSR-301 solution at slow and fast speeds. At Re = 7.2×10^4, the pressure distribution is typical of that found in the subcritical region in Newtonian fluids. The pressure distribution at Re = 2.1×10^5 is typical of that corresponding to the low-drag region in relatively high (25 to 100) concentrations of Polyox. As the Reynolds number increased from 7.2×10^4 to 2.1×10^5, the magnitude of back pressure decreased, the magnitude of minimum C_p increased and its location on the cylinder moved only slightly rearward from 70 to 80 degrees. The value of back pressure, for a given Reynolds number in the test range, was essentially constant from 110 to 180 degrees. In the low drag region of Reynolds numbers, this pressure distribution is markedly different from that produced by plain tap water both at the same Reynolds number and at the Reynolds number in the transition region which would produce the same drag coefficient.

With fresh high-concentration solutions, as the pressure recovery improved (back pressure magnitude decreased) with increasing Re, the separation angle moved gradually rearward and the measured drag coefficient decreased.

The change of pressure distribution at a constant Reynolds number above the critical Reynolds number was studied with a one-inch cylinder in 25 wppm Polyox solution at Re = 1.3×10^5. As shown in Fig. 57,
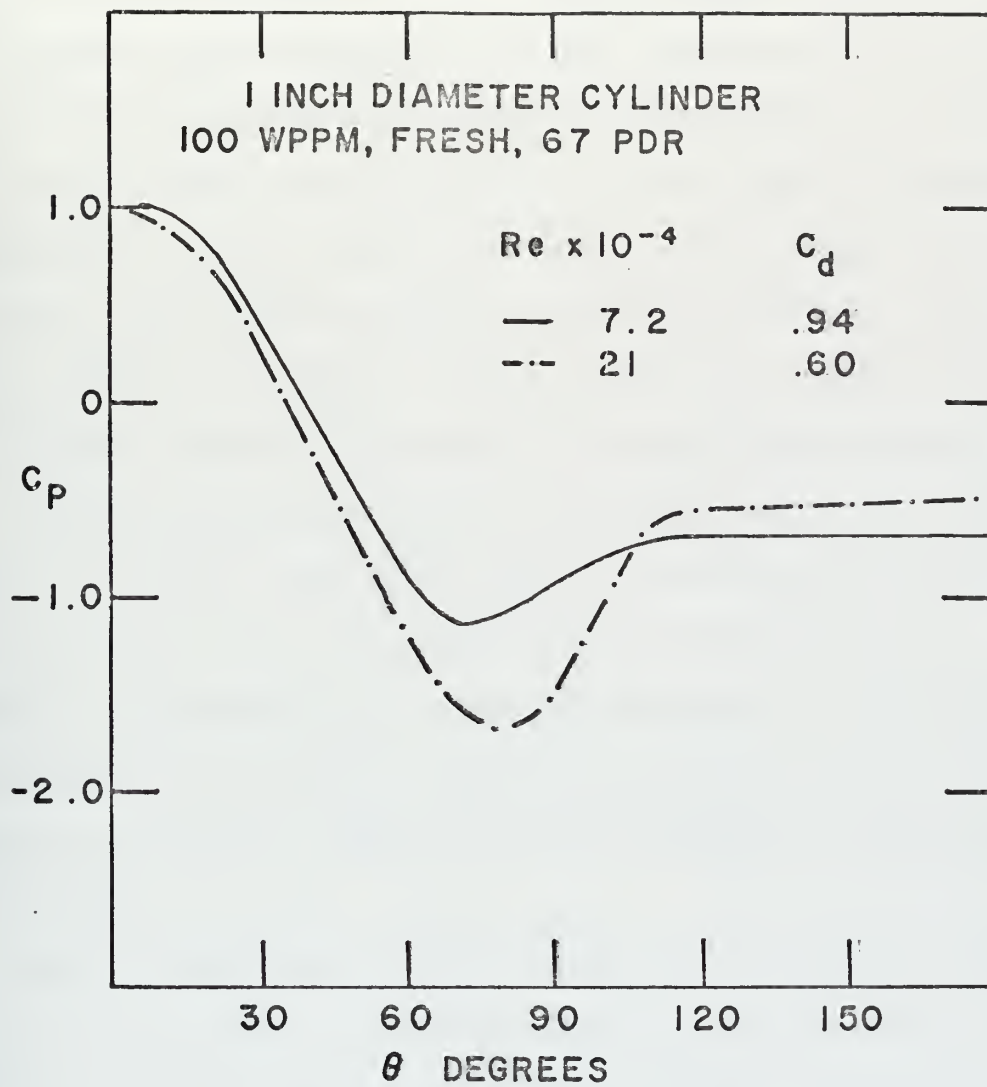
FIGURE 56: CHARACTERISTIC PRESSURE
DISTRIBUTIONS.

the back pressure coefficient changed from -0.67 to -0.30, significantly reducing C_d, while the value and location of minimum C_p were only slightly affected by degradation. The separation angle was measured at intervals between data sets and was found to increase only from 82 to 86 degrees. With increased pumping time, the critical Reynolds number approached 1.3×10^5. The resulting pressure distribution (uncorrected for tunnel effects) is plotted in Fig. 58. It indicates large pressure oscillations in the region of unsteady separation and smaller oscillations in the front and rear of the cylinder. Oscillograph tracings indicated the relatively low frequency (and large amplitude) of these oscillations as compared to the Strouhal frequency in tap water at the same Reynolds number.

Figures 59 through 61 illustrate the local pressure oscillations, at Re = 1.3×10^5, caused by the flow of solutions which produced 37, 20 and 4 P. D. R. The chart speed used for these tracings was 1 mm/sec. The pressure oscillations which occurred at 75, 90 and 110 degrees from the forward stagnation point at the critical Re are presented in Fig. 62. These tracings were recorded at a chart speed of 5 mm/sec.

After a solution has degraded sufficiently to produce a dual value drag coefficient region, two distinct pressure distributions develop, one at Re less than critical and the other for Re greater than critical. Figure 63 illustrates these two types of pressure distributions on a one-inch cylinder in a 5 wppm Polyox solution.

The pressure distributions presented are typical of the pressure distributions measured on 1/2-inch, 3/4-inch, one-inch, and 1-1/2-inch
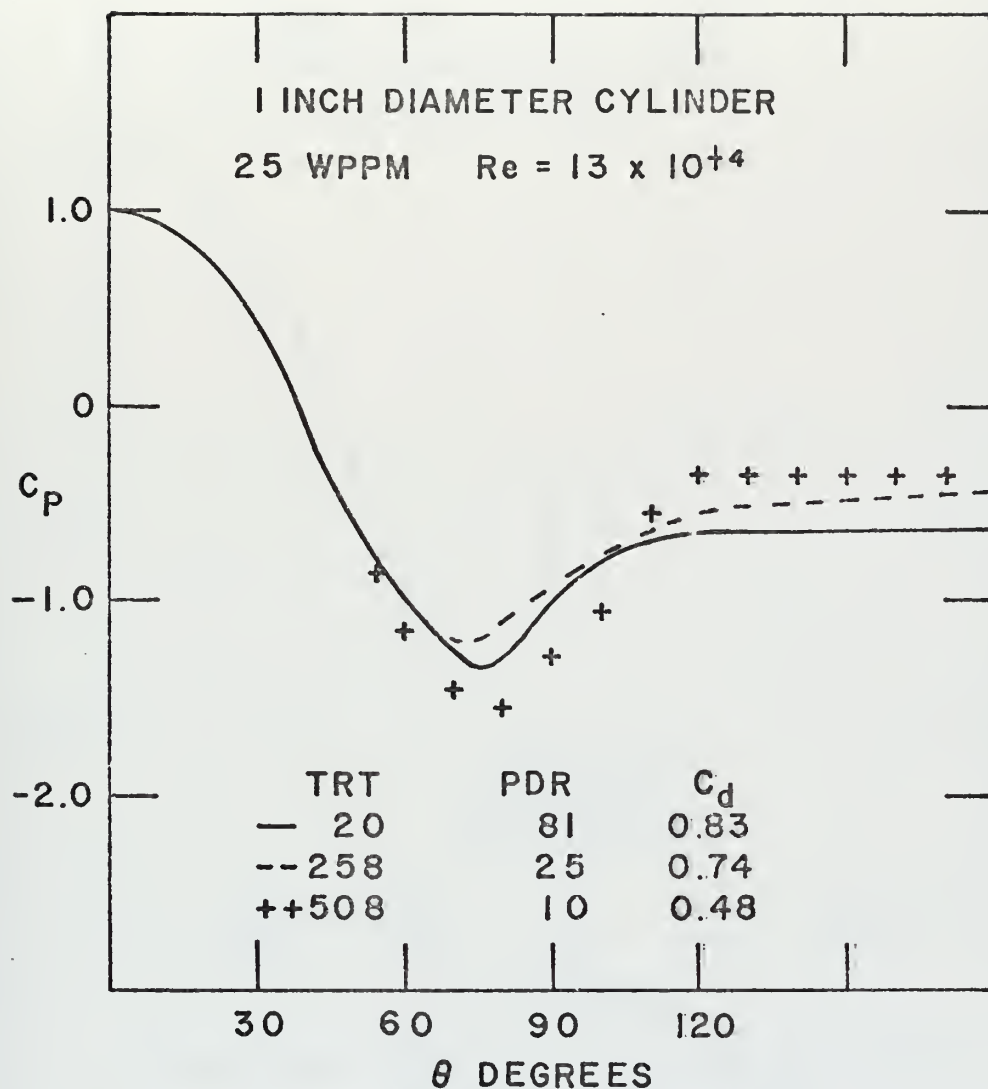
FIGURE 57: CHANGE IN PRESSURE DISTRIBUTION AS SOLUTION DEGRADES.
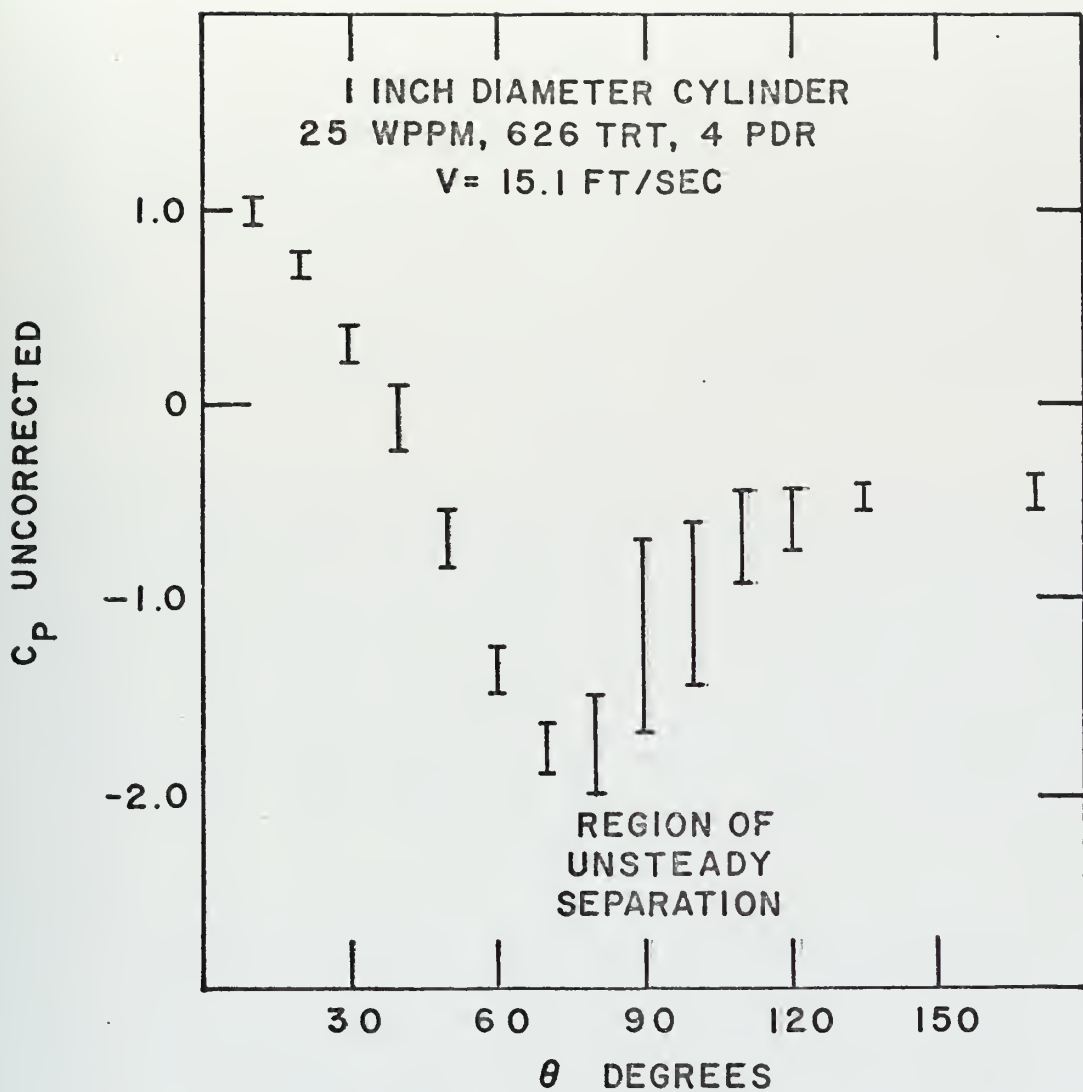
FIGURE 58: PRESSURE DISTRIBUTION AT CRITICAL VELOCITY.

5 WPPM   37 P.D.R.   V = 15.2 FT/SEC

Figure 59: Oscillograph tracings of dynamic pressure

123
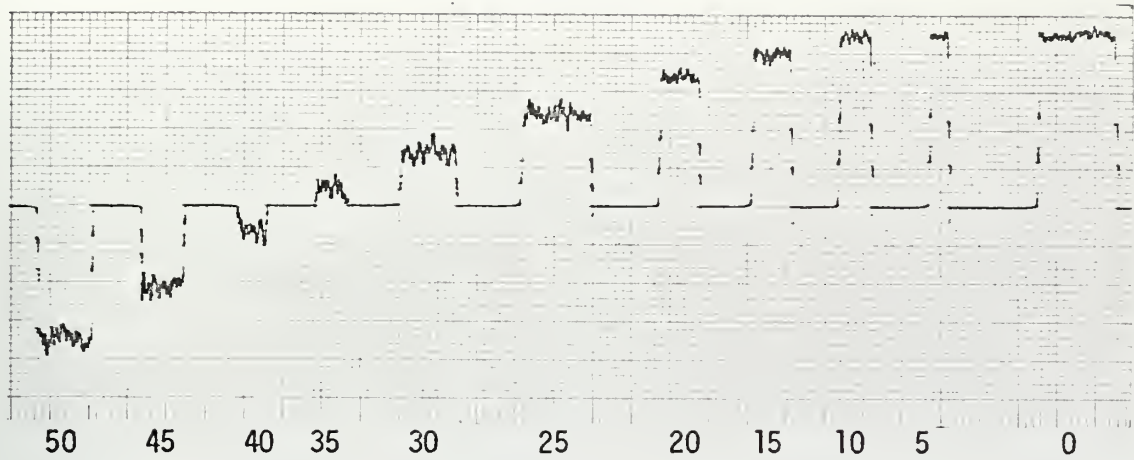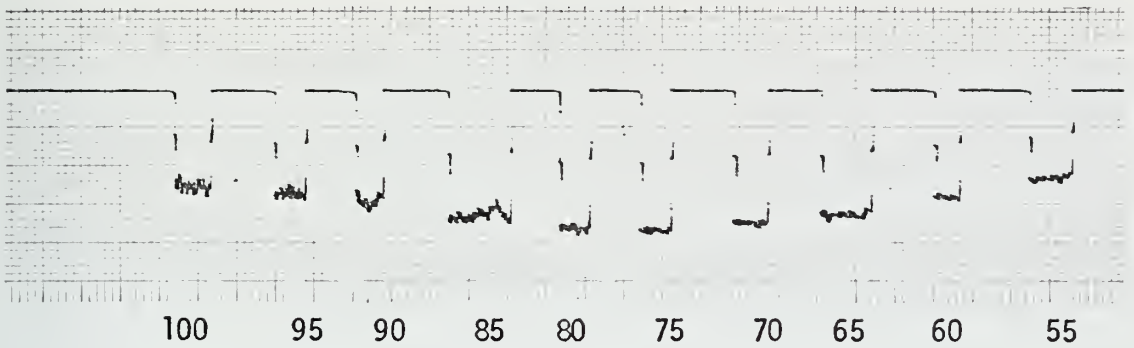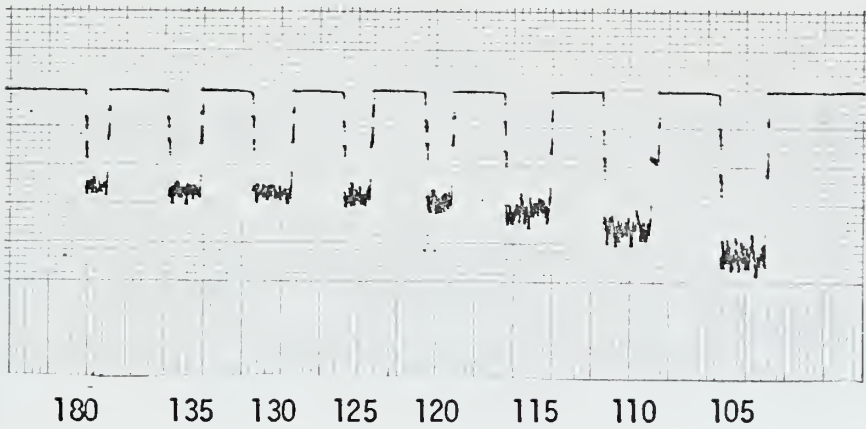
25 WPPM   TRT 332   20 P.D.R.   V = 15.2 FT/SEC

ATT 50
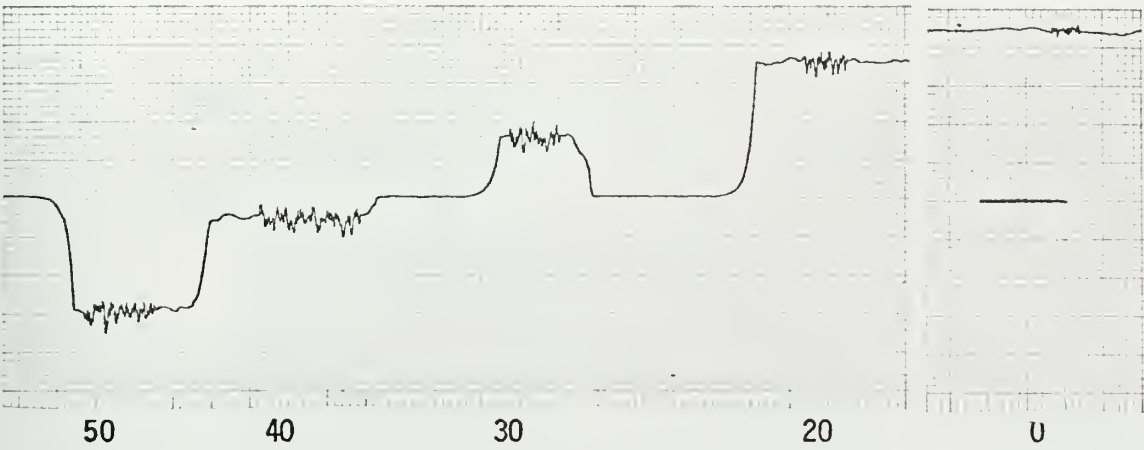
ATT 100
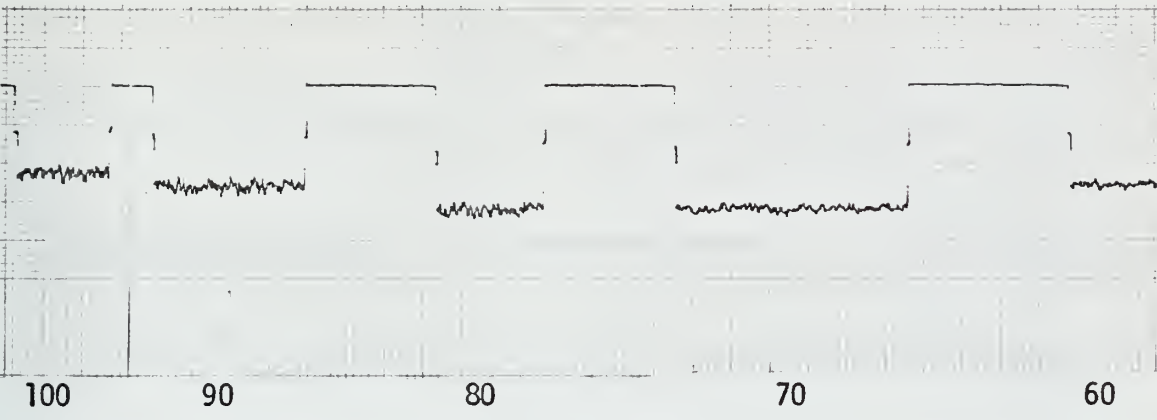
ATT 50
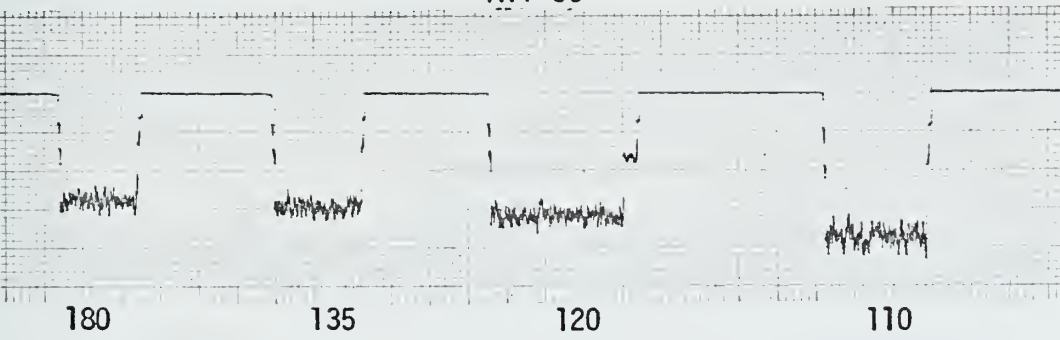
Figure 60:   Oscillograph tracings of dynamic pressure

ATT 50
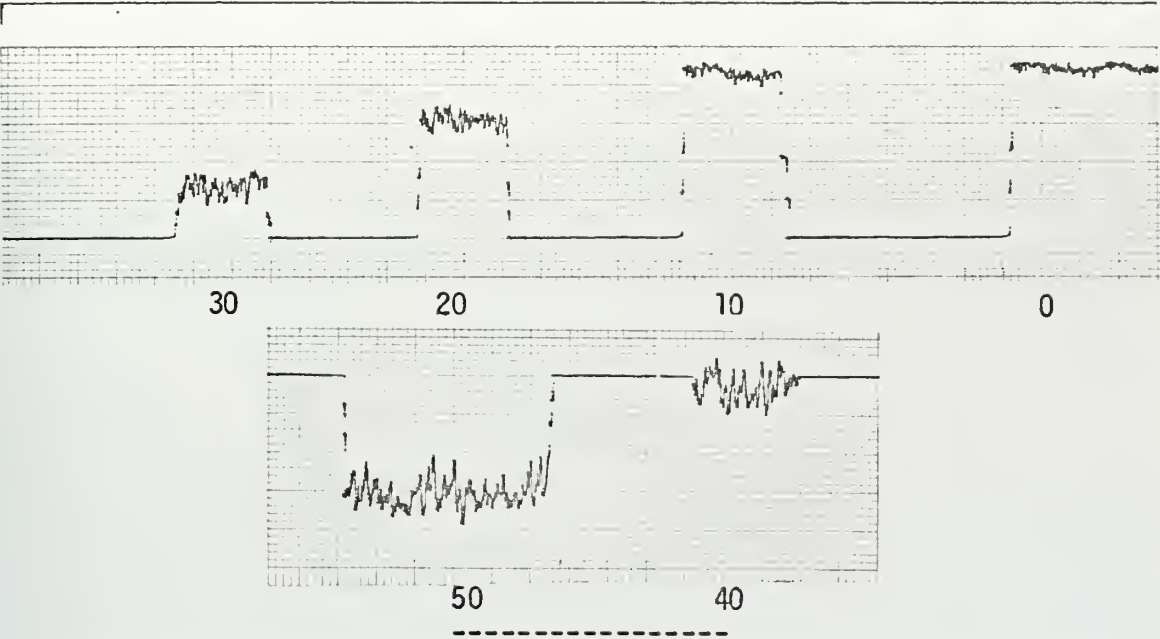
ATT 100
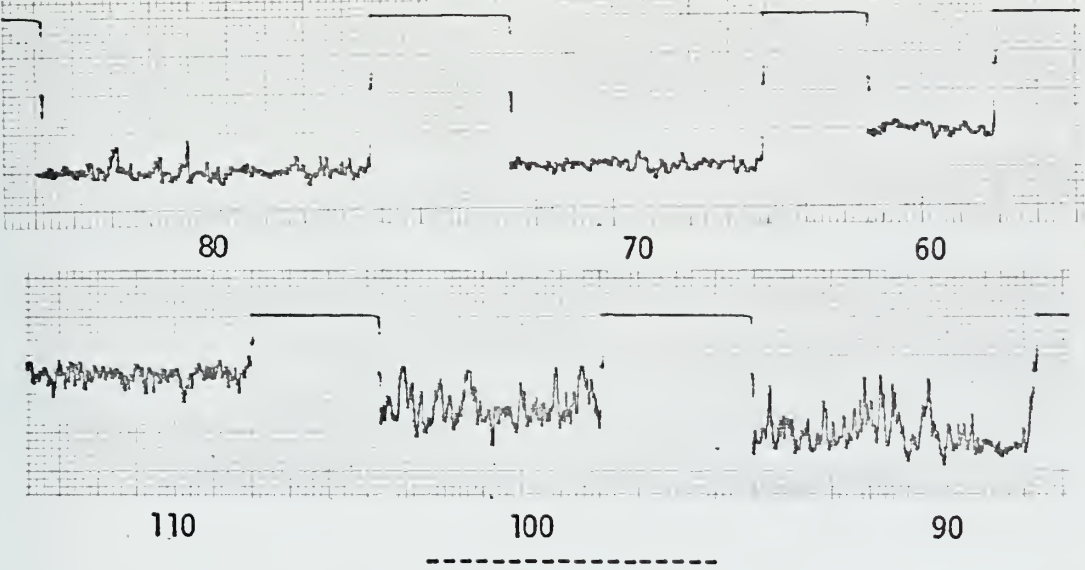
ATT 50
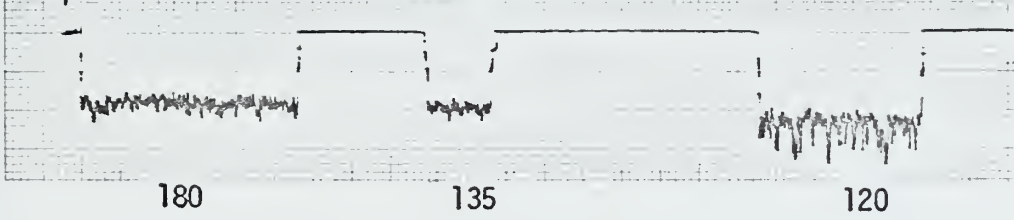
Figure 61: Oscillograph tracings of dynamic pressure

5 WPPM   9.5 P.D.R.   V = 12.8 FT/SEC

ATT 50   CHART SPEED 5 MM/SEC
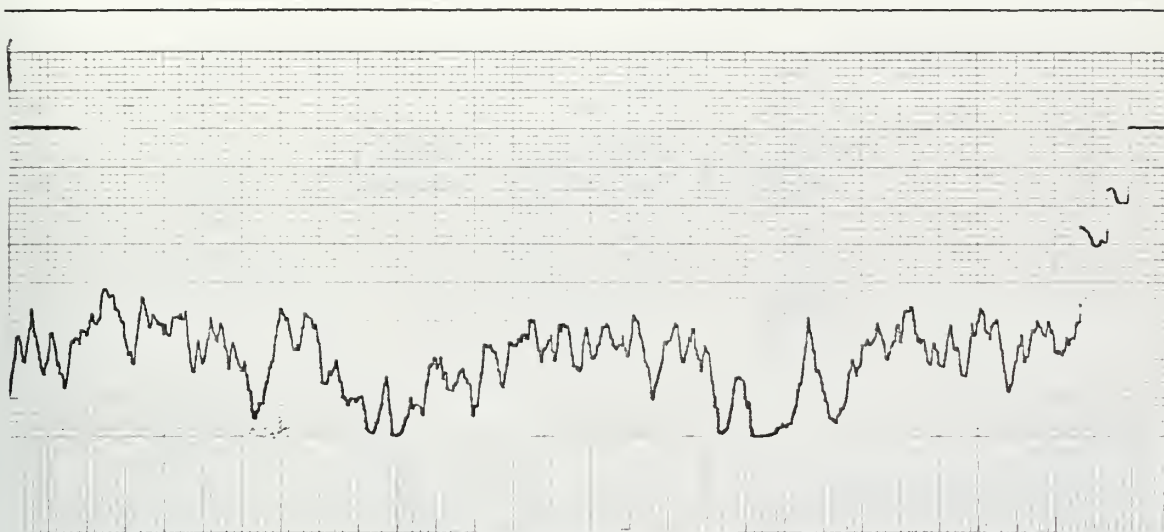
75 DEGREES
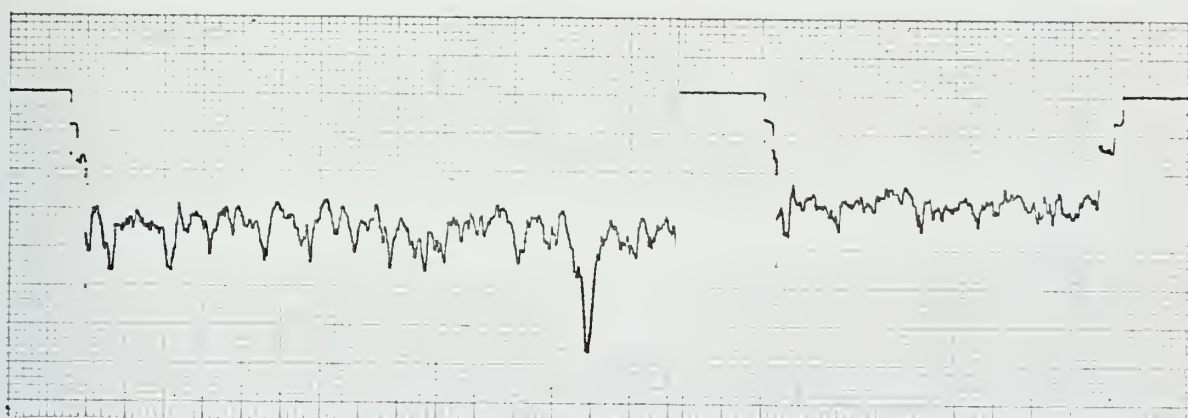
90 DEGREES   **110 DEGREES**

Figure 62: Oscillograph tracings of dynamic pressure at critical
velocity
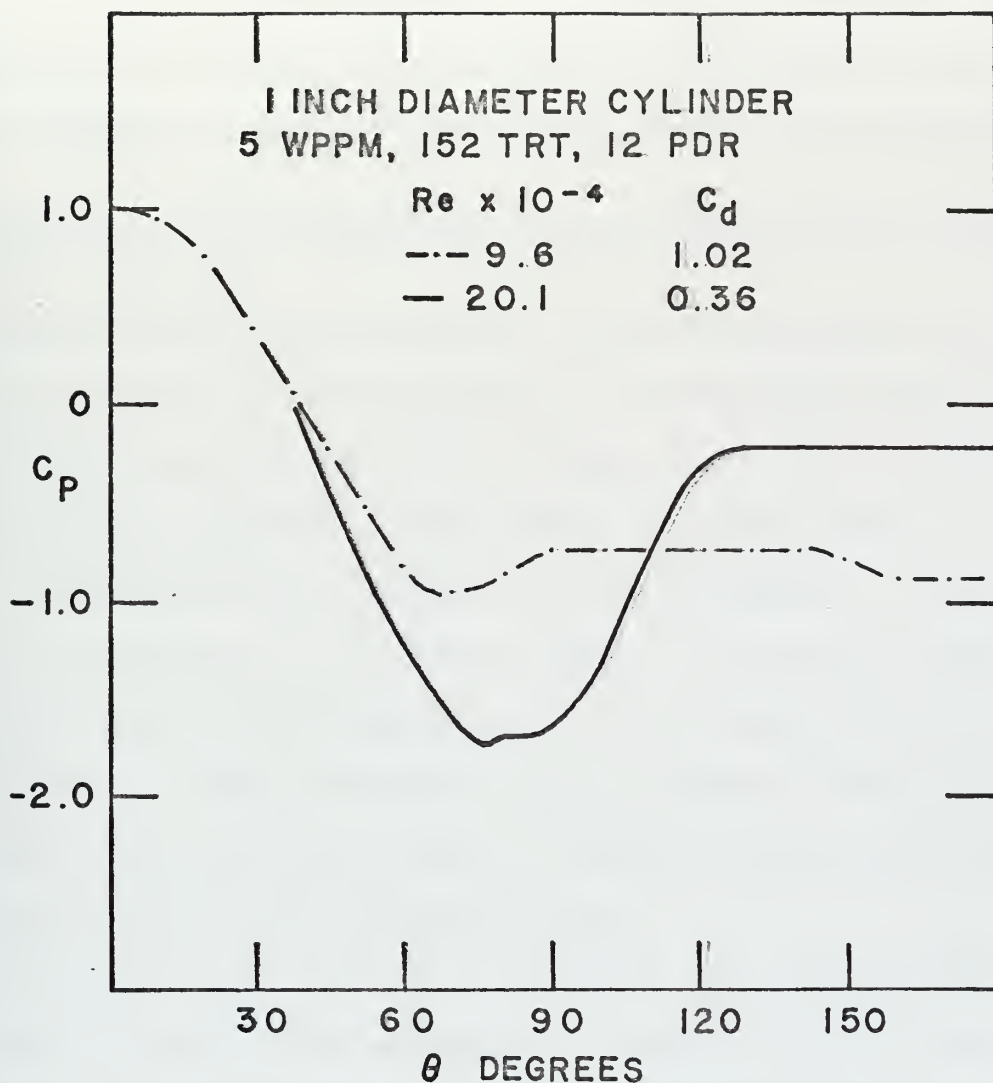
FIGURE 63: PRESSURE DISTRIBUTIONS FOR
$Re < Re_C$ AND $Re > Re_C$.

127

cylinders at comparable velocities, concentrations, and degradations during preliminary investigations. The one-inch cylinder was chosen for the presentation and discussion of the data since the use of this particular size of cylinder maximized the accuracy of separation angle measurement for cylinders which displayed an approximately constant drag coefficient in tap water throughout the range of velocities tested.

G. THE RESULTS OF THE OBSERVATION OF FLOW OF DILUTE POLYMER SOLUTIONS ABOUT A CYLINDER

Separation angles were measured by injecting dye through holes suitably located on a one-inch cylinder. The measurements (Figs. 64 and 65) have shown that for fresh solutions, in the range of velocities tested, higher concentrations yield greater separation angles.

The formation of (or transition to) critical behavior is again graphically revealed. As a solution degrades, the separation angle at Re less than Re_c moves forward, while at Re greater than Re_c it moves rearward. A wavy separation line was observed at Re less than Re_c which coincided with the measured increase in drag and local pressure oscillations, as the solution degraded.

The technique for measuring the separation angle was described in the section dealing with experimental procedure. It must, however, be noted that the separation angle plotted is the most forward angle at which separation was observed on the centerline by dye injection at minimum possible injection velocity.

At the critical velocity, observations made by injecting air, 10 degrees forward of the separation, with the tunnel head pressure reduced to a minimum, indicated wave separation patterns as first

128

reported by Brennen [Ref. 17]. With the dye injection, at minimum injection velocity, the three-dimensional, unsteady, separated flow was revealed.

At first it was thought that a switching from forward (laminar) to rearward (turbulent) separation was being observed. Further observation revealed a three-dimensional unsteady flow which displayed the following characteristics (Fig. 66):: (1) The locus at which the boundary layer detached oscillated over a small range of angles (approximately 74 to 82 degrees); (2) The separated flow fluctuated with low frequency and high amplitude both in the plane normal to the main flow and in the plane parallel to the main flow; (3) Dye streaks which remained close to the cylinder surface actually curved from their plane and became almost perpendicular to the main flow at a cylinder angle of approximately 100 degrees; (4) Streams of dye which did not remain close to the cylinder indicated a strong vorticity the vector of which was parallel to the direction of the main flow; and (5) In addition, to further complicate the subject, fine lines of dye were observed approximately perpendicular to the main stream of dye which resembled the effects produced in sonic compressible fluid flow when a shock line interacts with the boundary layer.

At a slightly (approximately 0.3 fps) higher velocity, the separation line (no longer a wave) switched rearward and remained steady. The dye became blurred a few degrees forward of the separation line indicating a probable transition to turbulent flow in the boundary layer prior to separation. After separation, the dye diffused
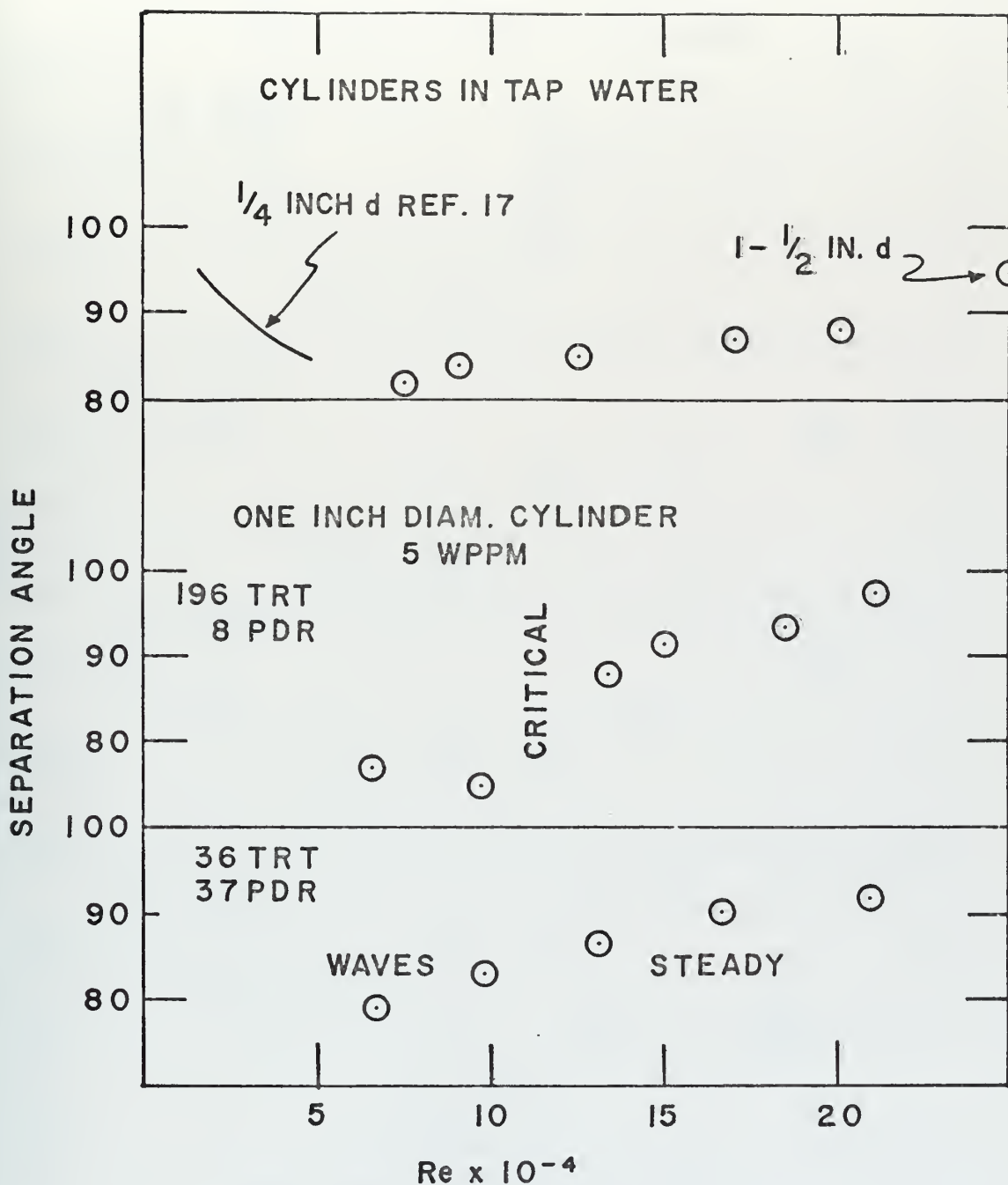
FIGURE 64
SEPARATION ANGLE vs Re.
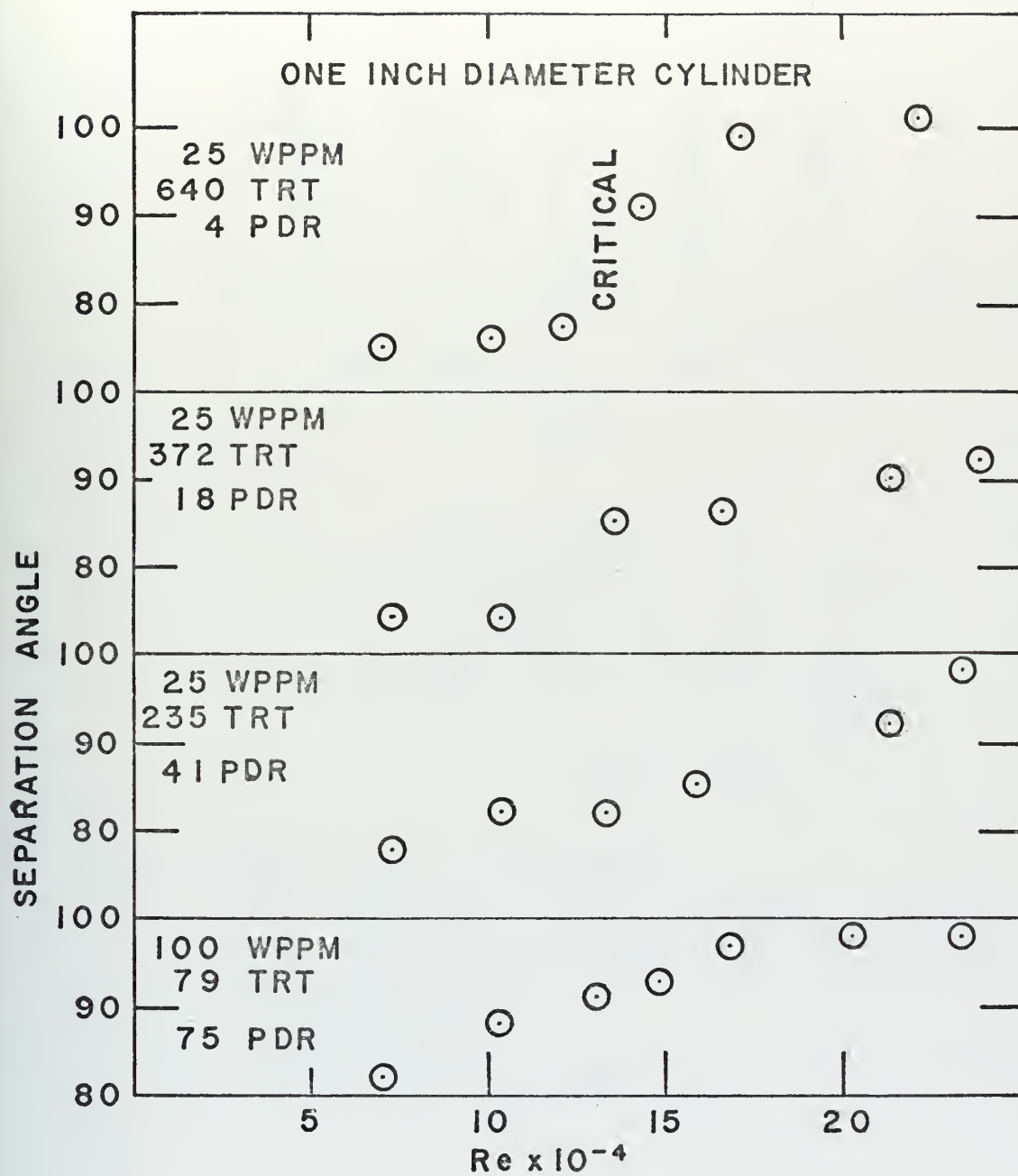
FIGURE 65

SEPARATION ANGLE vs Re.

131

$Re > Re_c$ $Re << Re_c$

$\Uparrow U$

180
90
60
0

$\Uparrow U$ Re_c
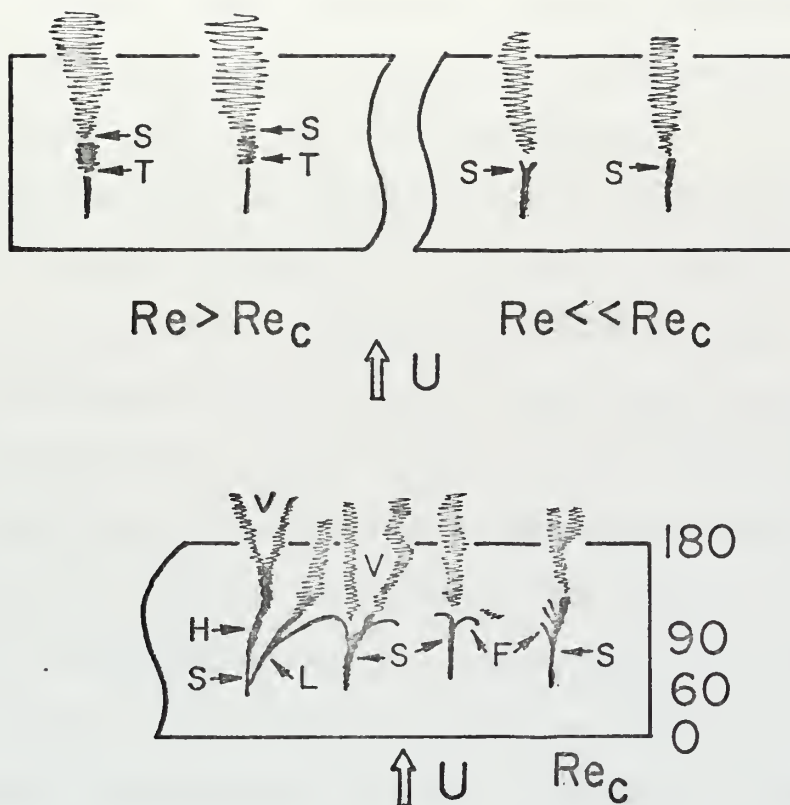
F : FINE DYE STREAKS
H : DYE ENTERS FREE SHEAR LAYER
L : DYE REMAINS CLOSE TO CYL. WALL
S : SEPARATION
T : TRANSITION
V : STREAMWISE VORTEX

FIGURE 66 : SEPARATION FLOW
PATTERN   AT   CRITICAL Re

rapidly in the same manner as in plain water at a high enough Reynolds number to cause a turbulent boundary layer prior to separation.

Because of the high tunnel velocities, low dye injection velocities, and solubility of the dye, it was not possible to observe the flow systematically more than 1/2 inch aft of the cylinder.

Observations made with air bubbles, with the tunnel head reduced to a minimum, indicated a contraction of the wake followed by alternating expansion and contraction for fresh 100 wppm Polyox solutions.

Pressure measurements made on the flat plate placed perpendicular to the flow indicated that fresh solutions of high concentration (100 wppm) significantly alter the flow in the near-wake region. The amplitude of the pressure oscillations, which increased with pumping time, is presented in Fig. 67. When the solution had been pumped for two hours, the oscillograph tracing on the back pressure became identical to that obtained in water, although the solution produced 80 P. D. R. in the rheometer.

No other attempt was made to observe the wake structure. At present an investigation of the wake of bluff bodies in the flow of dilute polymer solutions has been initiated at the Naval Postgraduate School using a free-surface water tunnel designed by Professor Sarpkaya specifically for this purpose.

FRONT (ATT 10)   BACK (ATT 20)

100 WPPM   FRESH   68 P.D.R.

100 WPPM   TRT 41   72 P.D.R.

100 WPPM   TRT 116   80 P.D.R.

WATER
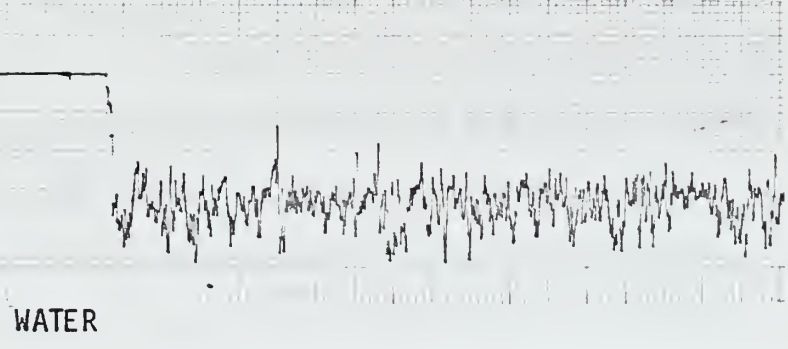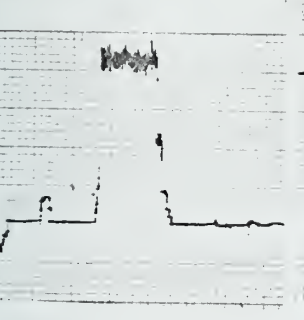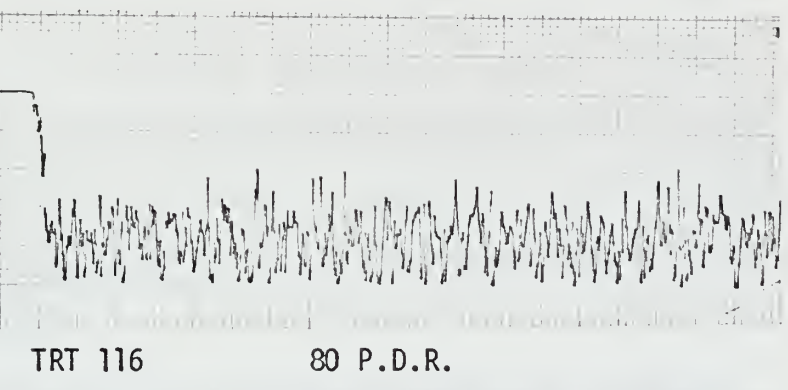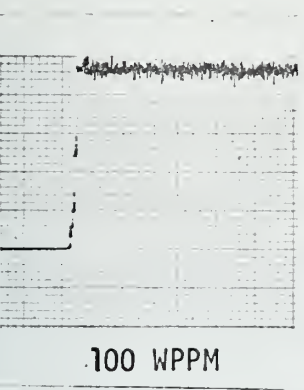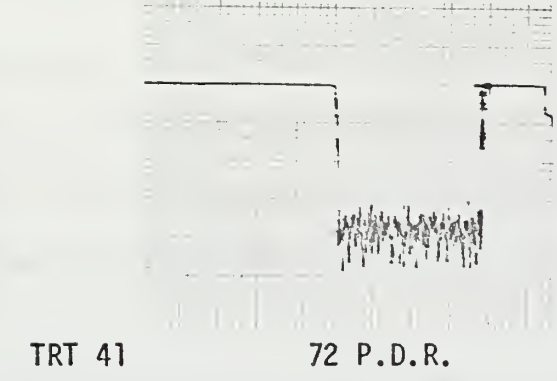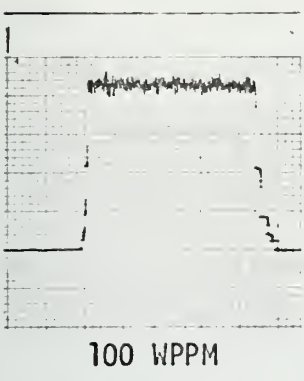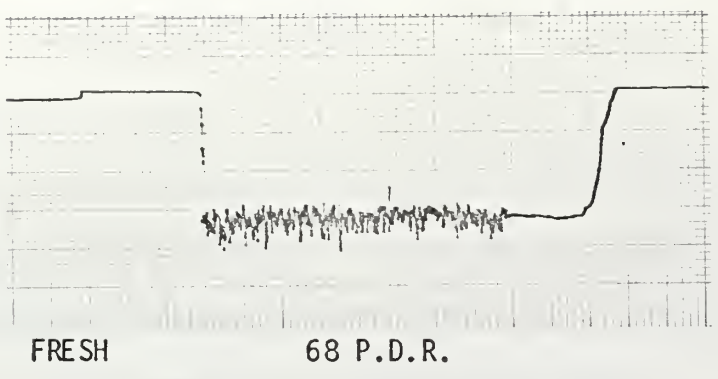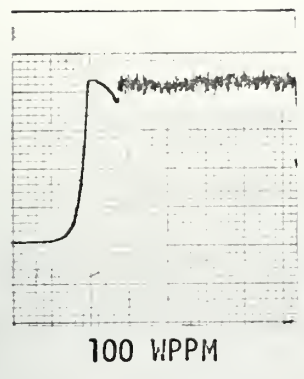
Figure 67: Oscillograph tracings of front and back pressures on a
            flat plate perpendicular to the flow

134

V.   DISCUSSION OF RESULTS

A.   GENERAL DISCUSSION OF THE DATA

The data presented in the previous sections have shown that dilute aqueous polymer (Polyox WSR-301) solutions flowing about a bluff body alter the force coefficients relative to pure water only in the flow regime where there is a drag transition or drag-crisis region.

The mean lift coefficient of the NACA-0024 hydrofoil immersed in dilute Polyox solution did not significantly differ from that for the pure solvent. However, the amplitude of the oscillatory component of the lift force increased significantly in solutions of higher concentrations (200 wppm).

The mean drag coefficient for the cylinders was altered by the presence of the polymer in the flow. The Reynolds number at which transition occurred was shifted and the flow characteristics in this region were modified. The drag-crisis was observed to occur in fresh Polyox solutions at approximately the same free-stream velocity for all the cylinders tested.

As the ability of the polymer solution to reduce pipe friction decreased with degradation, the transition range decreased. When the solution produced approximately 10 per cent drag reduction, independent of concentration, the transition range was so small that a critical Reynolds number in a fairly narrow region was definable. When the free stream velocity was slightly less than the critical value: (1) separation occurred at approximately 74 degrees; (2) a strong secondary flow was observed in the separation region; and

(3) relatively large amplitude pressure oscillations occurred over the entire cylinder. At the critical Reynolds number, the flow was "tripped" to a turbulent boundary layer which delayed separation and caused a decrease in the drag coefficient. As the solution further degraded, the critical Reynolds number increased toward the Newtonian fluid-drag-crisis region.

B. DEPENDENCE OF THE TRANSITION CHARACTERISTICS UPON THE FREE STREAM VELOCITY

There appears to be a strong correlation between the observations made by Brennen [Ref. 17] and the characteristics of the drag force produced by the flow of dilute polymer solutions about bluff bodies. According to Brennen, the flow of fresh 50 wppm Polyox WSR-301 solution past 1/4-inch and 1/2-inch spheres at a free stream velocity of less than 4 fps produced little visible difference from the flow of plain water and velocities from 4 to 7 fps produced three-dimensional cavity surface irregularities, and finally, velocities above 7 fps caused separation line distortion. The published drag coefficients for spheres falling freely through Polyox solutions of comparable concentrations [Refs. 8, 9, 11, 16, 41] were classified into three groups: (1) At a velocity of less than 4 fps, the drag coefficient was similar to the subcritical value in water; (2) In the range of velocities from 4 to 7 fps, the drag transition occurred; and (3) At velocities above 7 fps, the drag coefficient was approximately constant at 0.25.

Cavity surface irregularities behind a 1/4-inch cylinder were observed by Brennen at all speeds. Separation line distortion occurred

above approximately 8 fps. The average velocity at which cylinder drag transition was initiated (U_{tr}) in the flow of fresh dilute Polyox solutions in the NPS water tunnel was also found to be approximately 8 fps.

Figure 68 illustrates the drag transition region for 3/4-inch, one-inch and 1-1/2-inch diameter cylinders in the flow of fresh 100 wppm Polyox solutions. The drag coefficient is determined essentially by the free stream velocity throughout the entire Reynolds number range surveyed. The drag transition range extended from $U/U_{tr} = 1$ to $U/U_{tr} = 2$. At higher values of this ratio, the drag coefficient remained constant at approximately 0.75 even though the drag coefficient of the 1-1/2-inch diameter cylinder at the highest test velocity in plain water was approximately 0.45. The apparent drag increase at the low velocity is probably due to the pressure anomaly previously discussed. The drag transition region for these cylinders after 70 minutes of total pump-running time is also shown in Fig. 68. In addition, as shown in Figs. 36 through 43, the drag coefficient for the 100 wppm solutions was relatively independent of further degradation until the per cent pipe drag reduction decreased to approximately 30%.

At much lower polymer concentrations, the drag coefficient was found to be dependent upon the cylinder diameter as seen in Fig. 69. However, for the fresh 5 wppm solutions, $U/U_{tr} = 1$ did indicate the initiation of transition for all three cylinders tested. The free stream velocity at which transition was initiated for the one-inch and 1-1/2-inch cylinders in the flow of a degraded 5 wppm solution, which displayed 30 per cent pipe drag reduction, could not be determined since it was below the
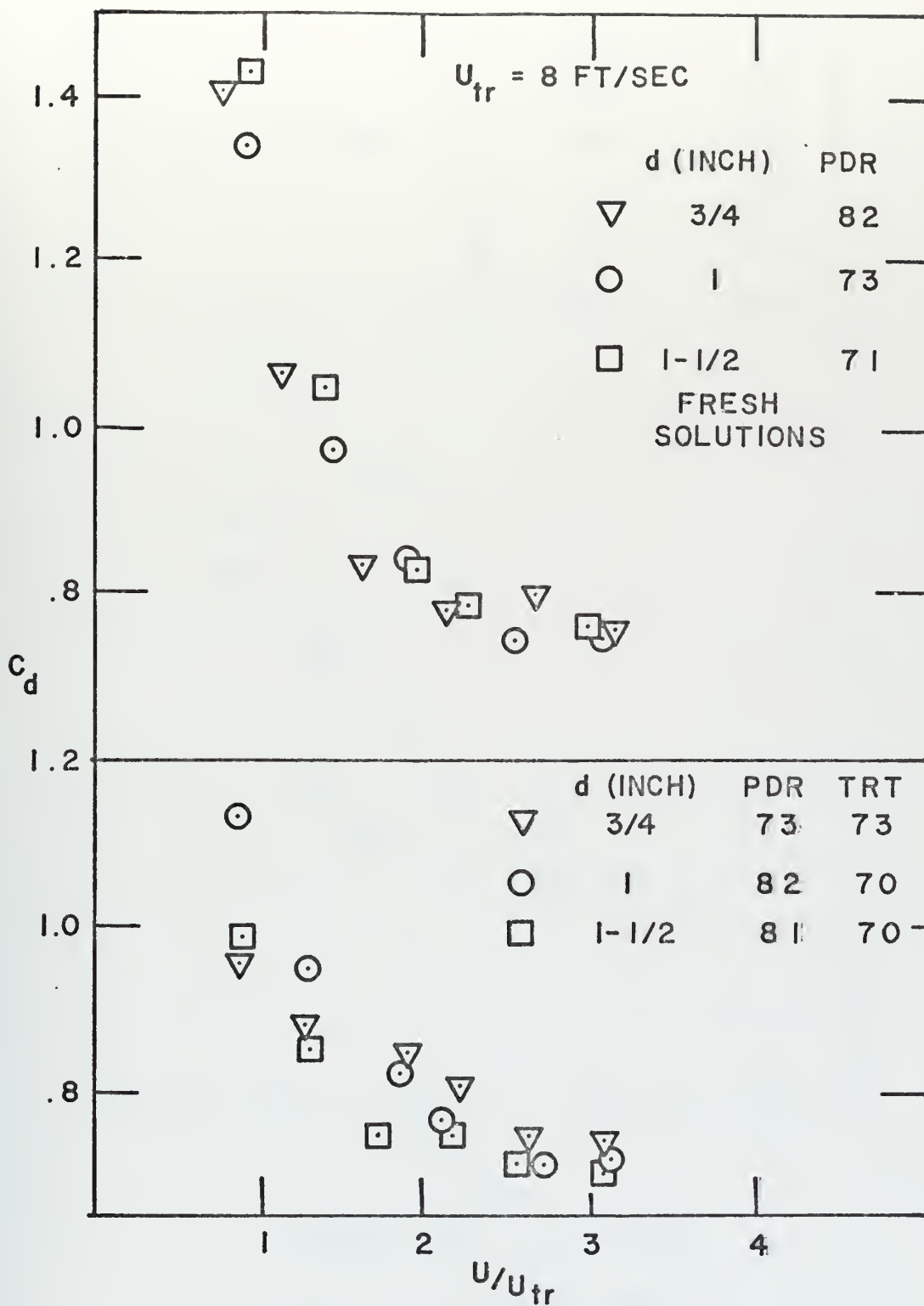
FIGURE 68: C_d vs U/U_{tr}
100 WPPM SOLUTIONS.
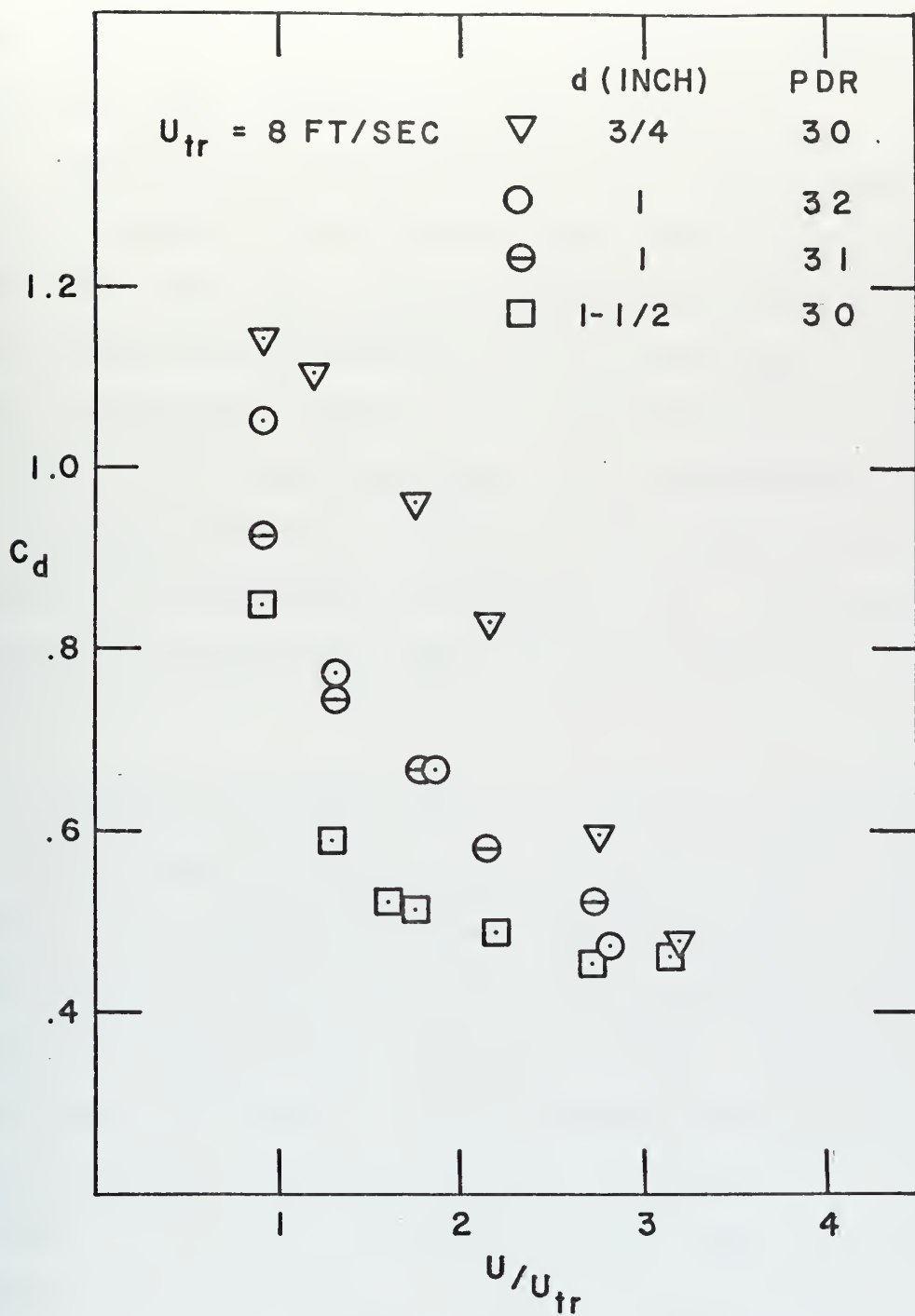
FIGURE 69: C_d vs U/U_{tr}
5 WPPM SOLUTIONS.

minimum attainable tunnel velocity. Thus the evidence suggests that when the concentration and/or the molecular weight of the additive are sufficiently reduced, the velocity at which the transition is initiated becomes dependent also on the cylinder size.

Figures 70 and 71 show that the critical velocity increases as the solution degrades but the transition always occurs at a velocity larger than 8 fps. For similar solutions, equal P. D. R., the critical velocity appeared to be approximately inversely proportional to the square root of the cylinder diameter, i.e., the critical Reynolds number was proportional to the square root of the cylinder diameter.

The drag coefficients obtained with the 5 wppm solutions are plotted in Figs. 72 through 75, as a function of U^2d. The systematic narrowing of the transition range as the polymer degrades is clearly indicated.

C. DEPENDENCE OF THE DRAG COEFFICIENT UPON POLYMER CONCENTRATION

The minimum value of the drag coefficient was found to be determined by the polymer concentration. Without exception, as the solution degraded, the drag coefficient beyond the point of inception of transition decreased until it attained a minimum. The minimum value of the drag coefficient for very low concentrations was the same as that attained with the Newtonian solvent in the drag crisis region. As seen in Fig. 76, for concentrations above 10 wppm, the minimum C_d increased with concentration. It was not determined whether the minimum drag coefficient for 100 wppm and 25 wppm solutions would have continued to decrease as the P. D. R. further decreased. Since, for these solutions the rate of degradation was very low, the test was terminated soon after critical transition was first observed.
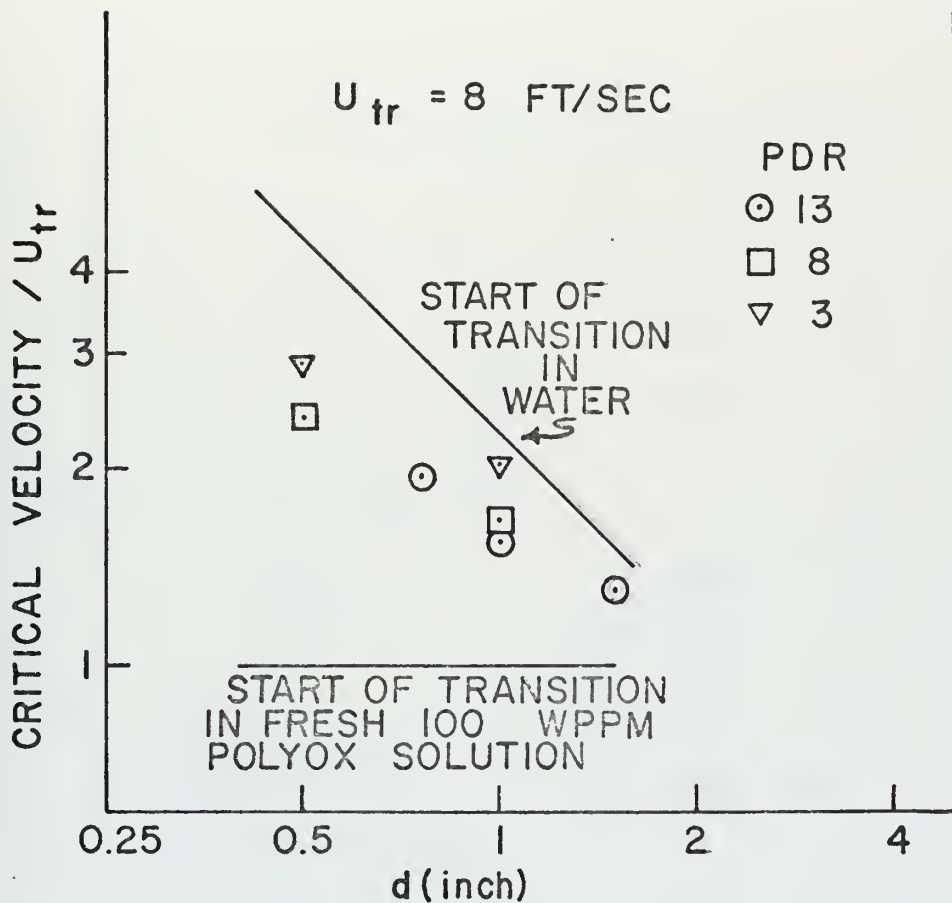
FIGURE 70: CRITICAL VELOCITY VS CYLINDER DIAMETER
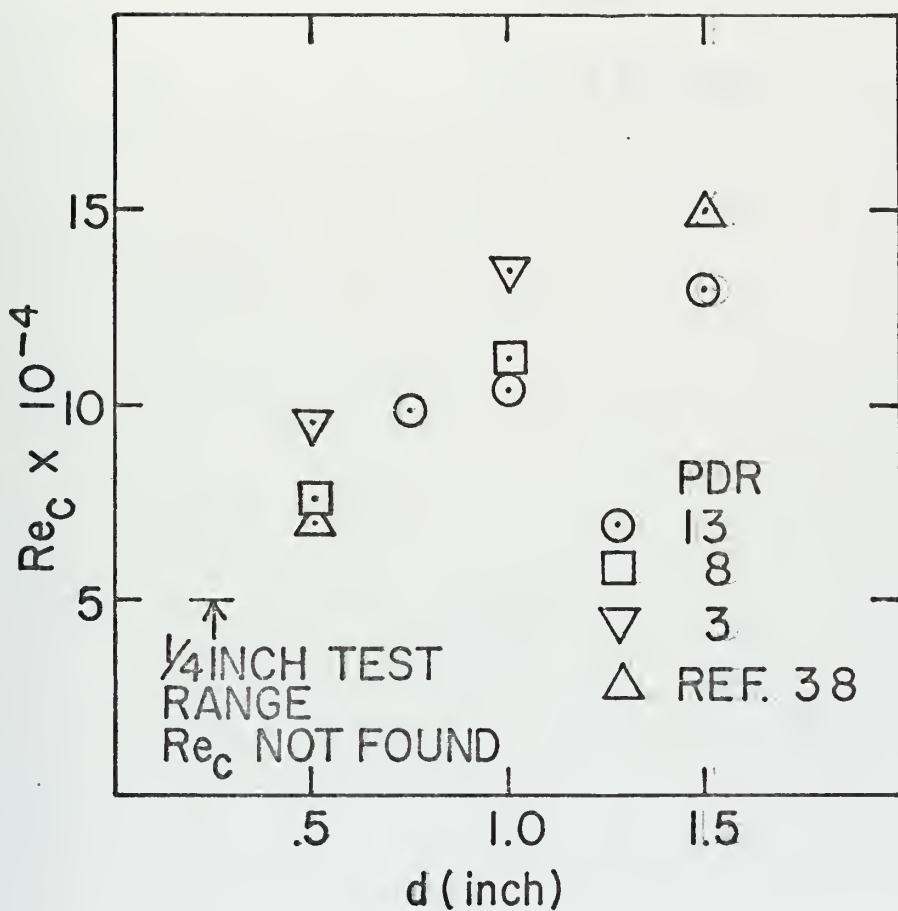
FIGURE 71: CRITICAL Re
vs CYLINDER DIAMETER
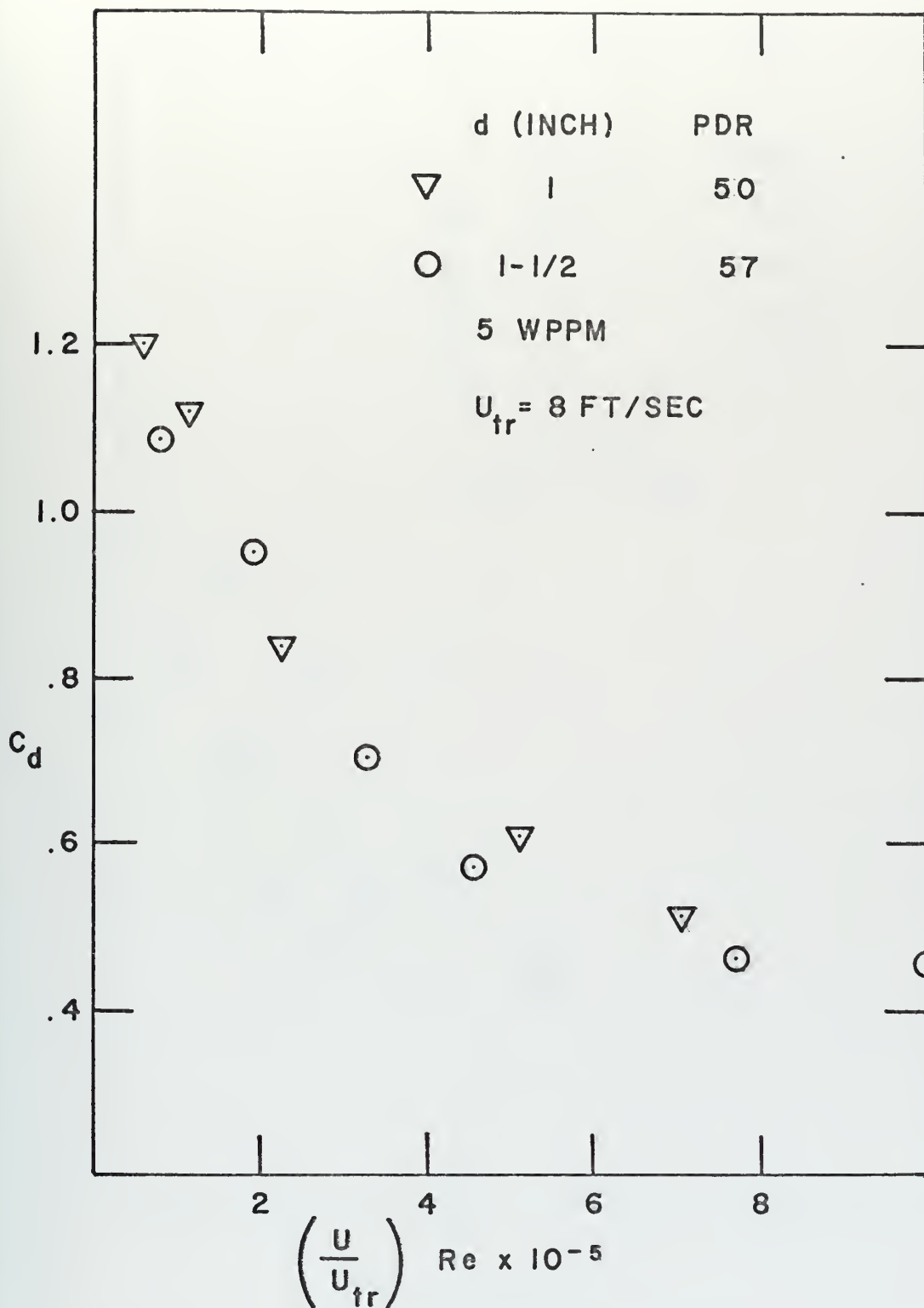
FIGURE 72 : TRANSITIONS IN POLYOX SOLUTION

143
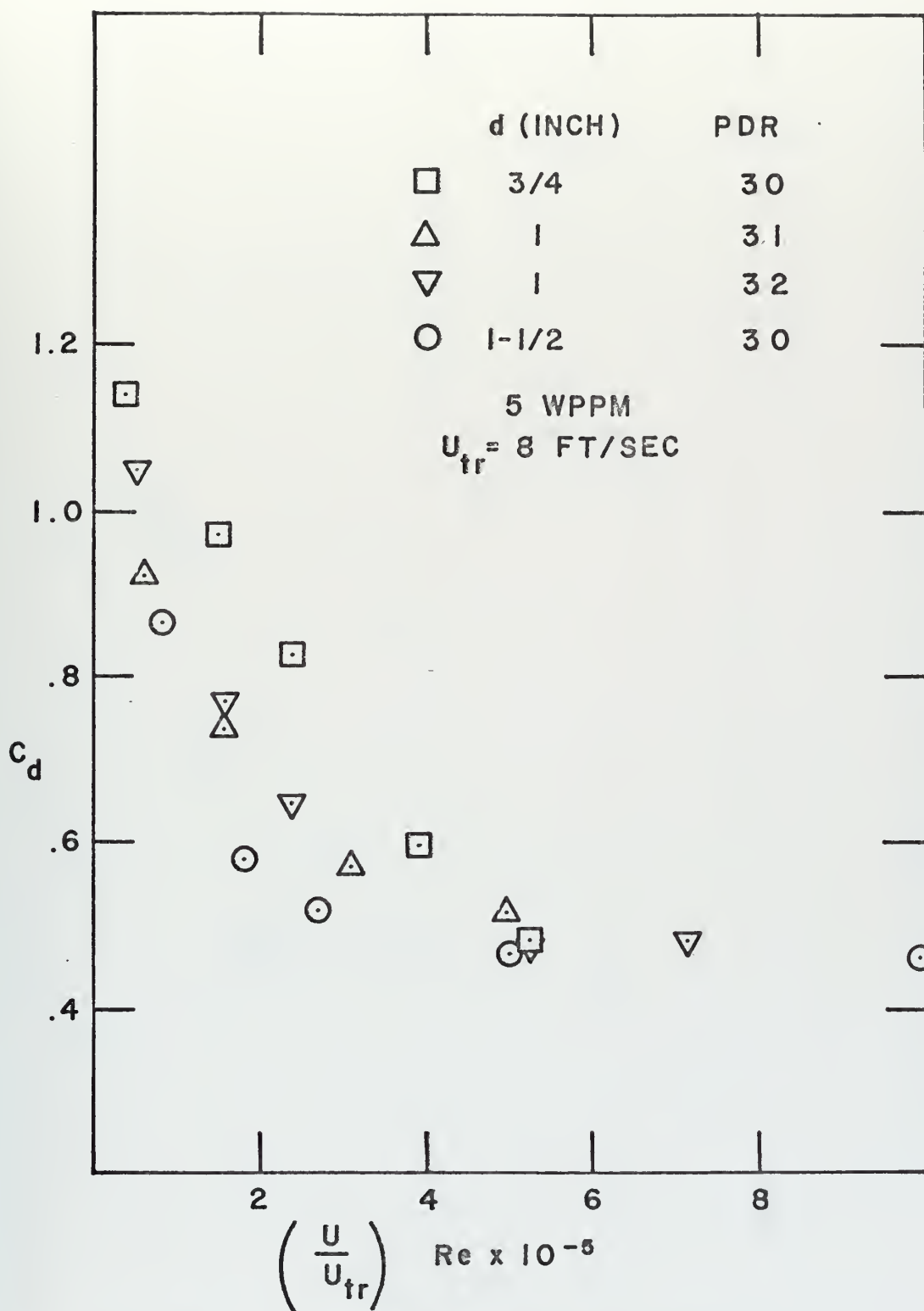
FIGURE 73 : TRANSITION IN POLYOX SOLUTION.
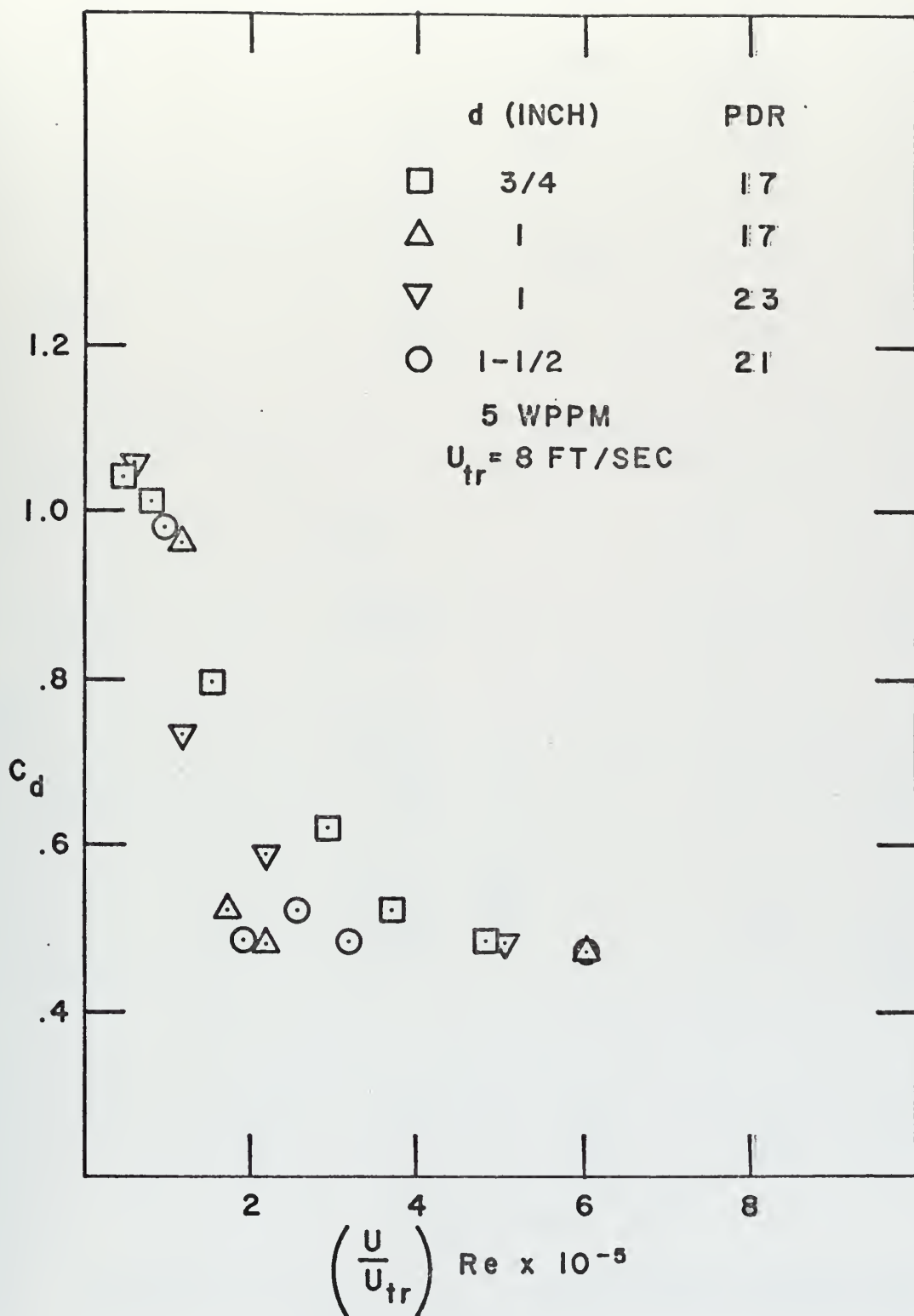
FIGURE 74 : TRANSITION IN POLYOX SOLUTION.
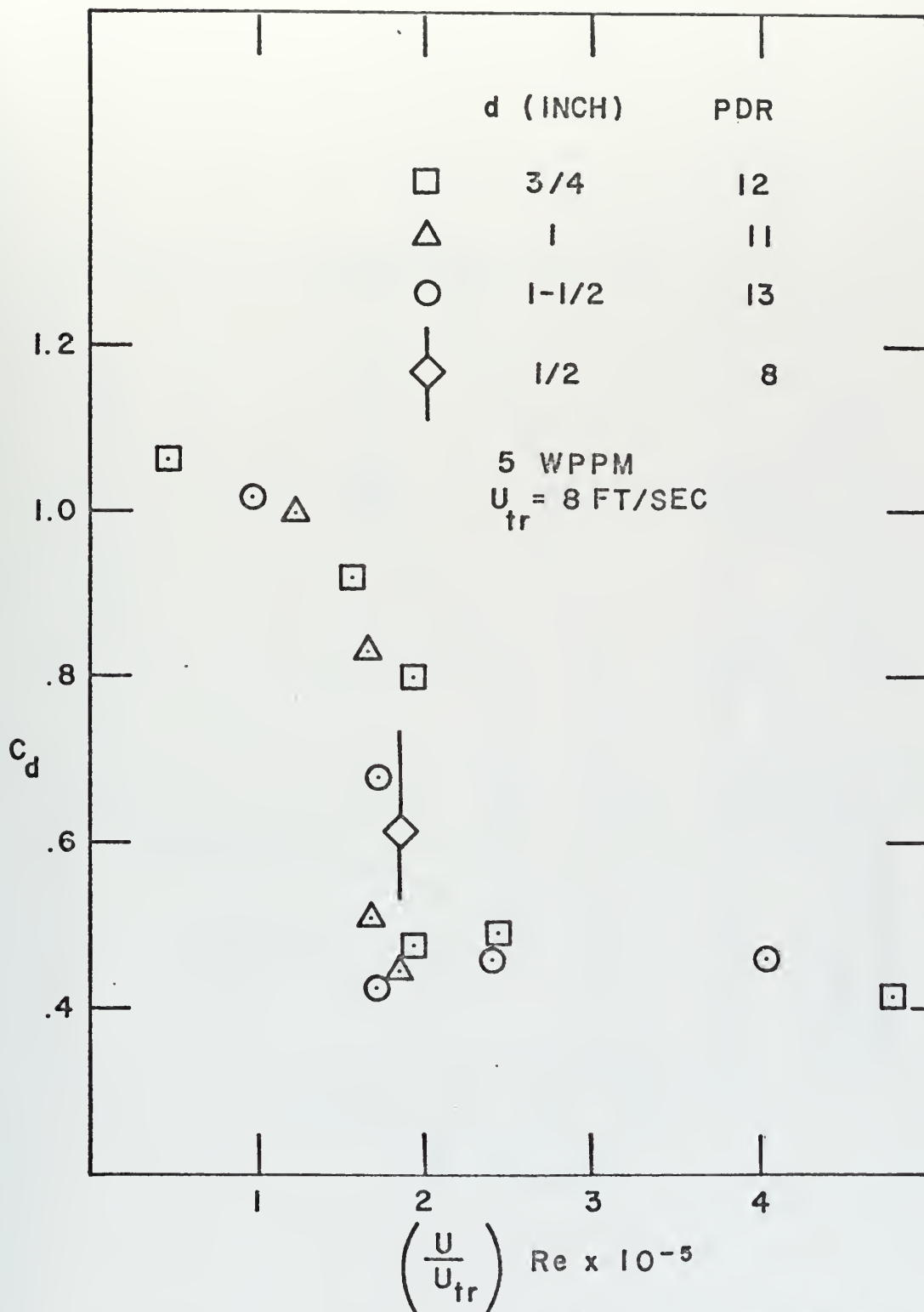
FIGURE 75: CRITICAL TRANSITION IN POLYOX
SOLUTION.

146
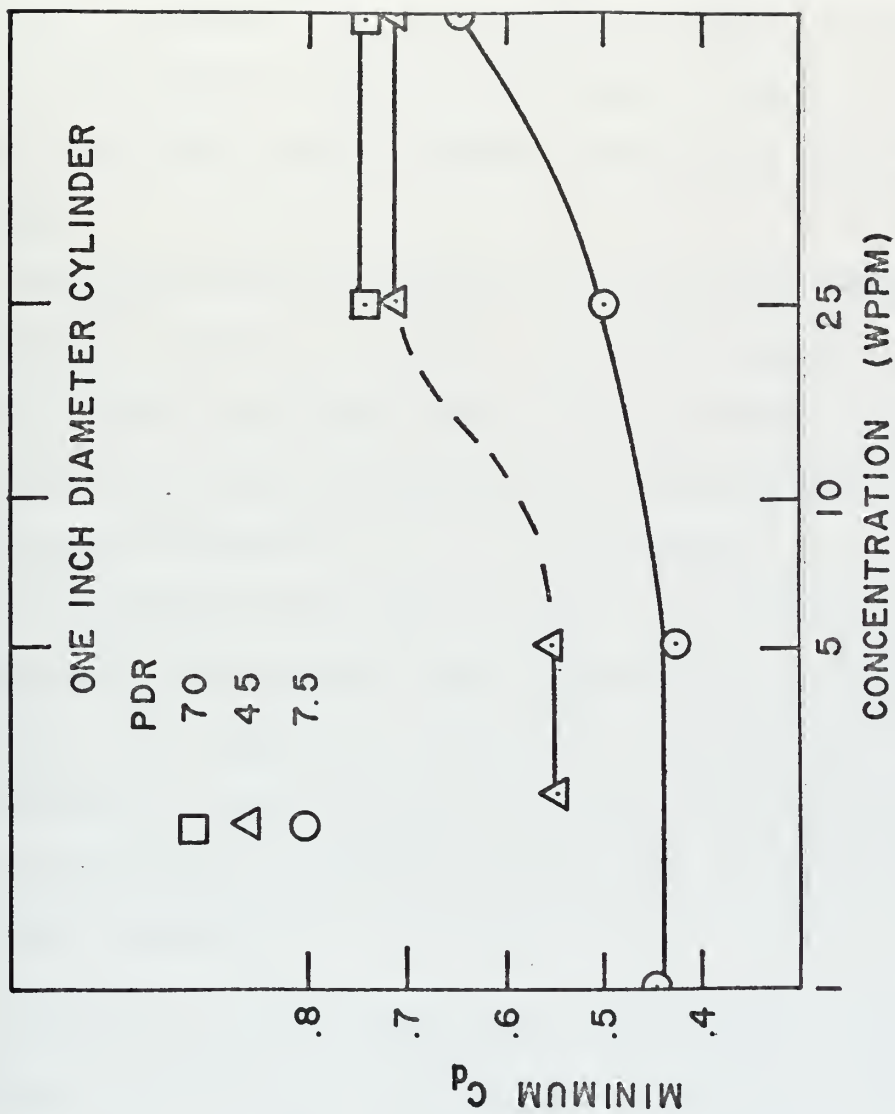
FIGURE 76: EFFECT OF POLYOX CONCENTRA-
TION ON MINIMUM C_d FOR $Re < 3 \times 10^5$

147

D. DEPENDENCE OF THE DRAG COEFFICIENT UPON PER CENT (PIPE) DRAG REDUCTION

As the per cent drag reduction displayed by a Polyox solution in the turbulent pipe rheometer decreased, the transition range narrowed. At 12 ±3 P. D. R., the critical transition occurred independently of the initial value of the concentration (1 to 100 wppm) on the 1/2-inch, 3/4-inch, one-inch and 1-1/2-inch diameter cylinders. A critical velocity was not observed on the 1/4-inch cylinder. However, it is predicted that it will occur at a velocity greater than the maximum test velocity.

For concentrations of 5 wppm and less, the minimum drag coefficient depended only on the P. D. R. Thus, for a given size of cylinder immersed in the flow of Polyox solutions of relatively low concentration, identical transition characteristics were observed in solutions which produced identical P. D. R. in the rheometer.

For concentrations of 25 to 100 wppm, the minimum drag coefficient, although higher than that for lower concentrations, was constant for solutions of the same P. D. R. when the P. D. R. was greater than approximately 40. Thus, for these conditions, the transition curve was also observed to be dependent upon the P. D. R. irrespective of the actual concentration.

E. DEPENDENCE OF THE DRAG COEFFICIENT UPON SEPARATION ANGLE

The drag coefficient is not uniquely determined by the separation angle in the flow of dilute Polyox solutions about cylinders. In the transition region, as shown in Fig. 77, the separation angle shifted rearward as the drag coefficient decreased. At critical transition, the separation point jumped rearward. At higher Reynolds number, it

148

continued to shift further rearward although the drag coefficient remained practically constant.

For a Newtonian fluid, the flow regime in the drag transition region can be characterized by the angle of minimum pressure, i.e., 70 degrees for subcritical and 90 degrees for supercritical. The separation angle is approximately 10 degrees past the minimum pressure angle; and therefore, the separation angle correlates with the drag coefficient. In the flow of Polyox solutions, however, the difference between the angle of minimum pressure and the separation angle is dependent upon concentration, degradation, free stream velocity and the cylinder size. As seen in Fig. 78, under certain conditions the polymer de-stabilizes the boundary layer and in turn causes early separation. The polymer can, under other conditions, delay boundary-layer separation significantly past the minimum pressure angle.

The location of minimum pressure on the cylinder immersed in Polyox solutions, which cause greater than 15 P. D. R., moved from 70 degrees to only 80 degrees as the Reynolds number was increased through the drag transition range. Figure 79 compares the pressure distribution around a one-inch diameter cylinder, in 100 wppm Polyox WSR-301 solution past transition, with a 1-1/2-inch cylinder in tap water at comparable drag coefficient. In addition, the pressure distribution obtained by Roshko [Ref. 30] at Re = 8.4 x 10^6 in air is plotted to illustrate its similarity to that obtained in the polymer solution.

ONE INCH DIAMETER CYLINDER

	WPPM	PDR
O	100	75
△	25	41
□	5	37
▽	25	18
+	5	8

ESTIMATED C_d

CRITICAL
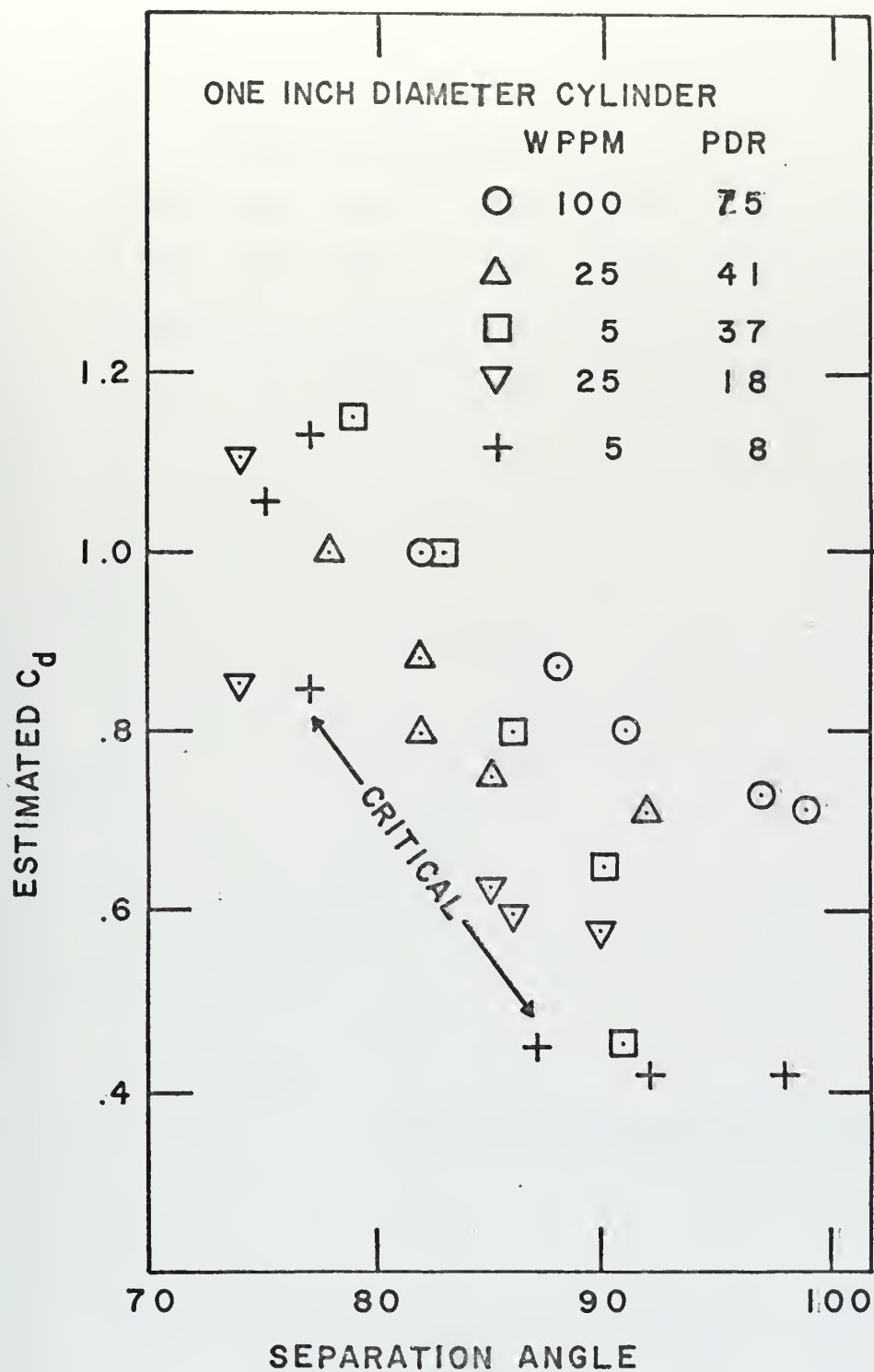
SEPARATION ANGLE

FIGURE 77

C_d vs SEPARATION ANGLE.

150
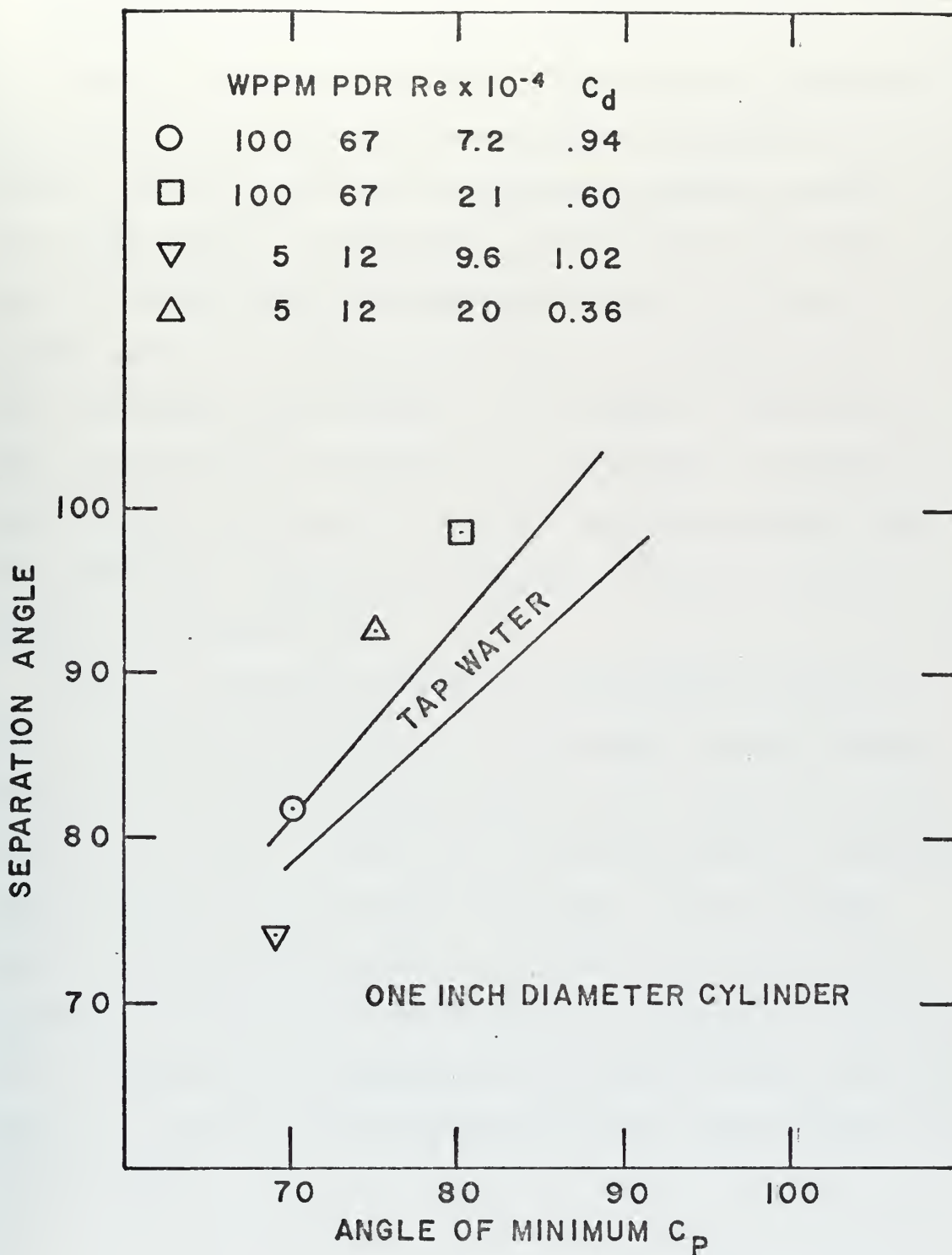
FIGURE 78 · SEPARATION ANGLE vs ANGLE
OF MINIMUM C_P.

151

F. RELATIVE INFLUENCE OF VELOCITY, DIAMETER, POLYMER CONCENTRATION AND SOLUTION PIPE FRICTION REDUCTION UPON THE DETERMINATION OF THE DRAG COEFFICIENT

Figure 80 illustrates the regions of different drag transition characteristics for the range of concentrations investigated. In region-I, the drag coefficient was principally dependent upon the free stream velocity. In region-IIb, the drag coefficient varied with cylinder size, velocity, concentration and P. D. R., with velocity and P. D. R. being dominant factors. In regions-IIa and IIIa, the minimum drag coefficient was independent of concentration. Thus, the transition characteristics were independent of concentration. In regions-IIIa and IIIb, critical transition occurred. The drag coefficients in regions-IIa, IIIa and IIIb were principally a function of U^2d and P. D. R.

Region-IV signifies the Newtonian fluid transition characteristics. It should be noted that even when a polymer solution does not produce any pipe friction reduction, the critical transition can still occur on the cylinder. The wall shear stress and velocity in the pipe were 280 dynes/cm^2 and 250 cm/sec respectively. For the cylinders tested, maximum wall shear stress and maximum local velocity were in the order of 1,000 dynes/cm^2 and 1,000 cm/sec respectively. Therefore, it is not unexpected that degradation past the point of zero pipe drag reduction is necessary before Newtonian transition characteristics are re-established.
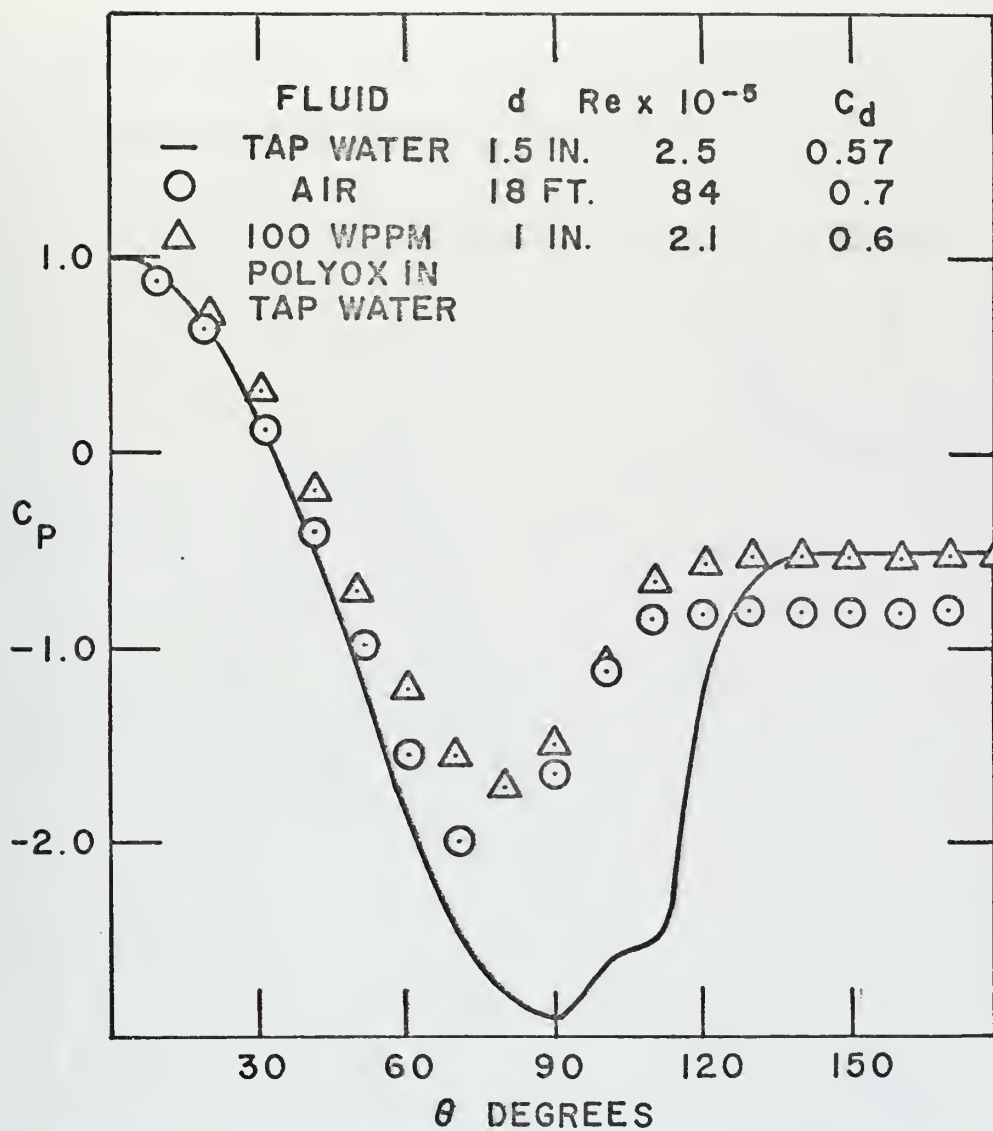
FIGURE 79: PRESSURE DISTRIBUTIONS AT
$C_d \sim 0.6$.
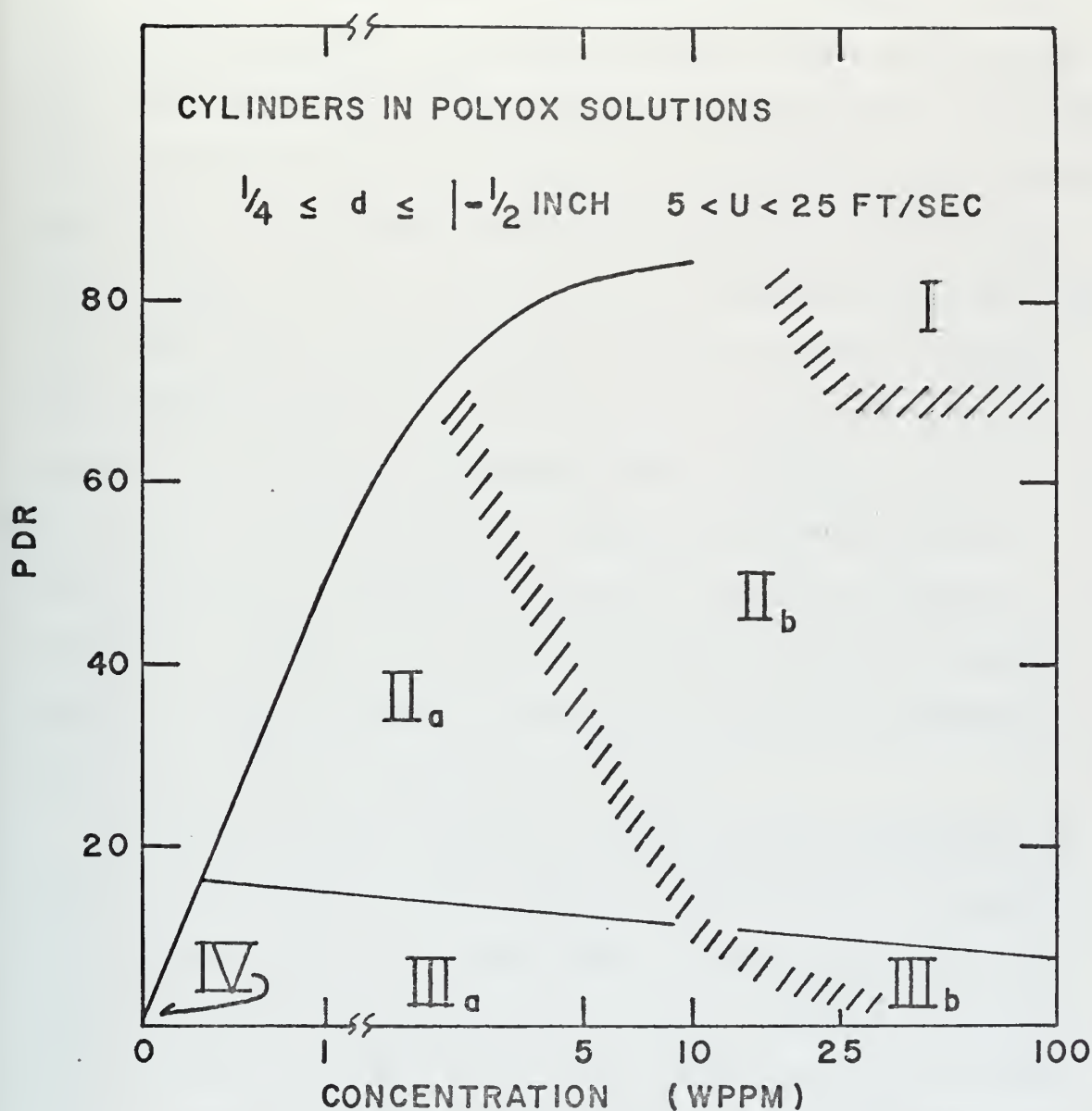
FIGURE 80 : REGIONS OF VARIOUS C_d TRANSITION
CHARACTERISTICS.

154

G. COMPARISON WITH PREVIOUS WORKS

The only previously reported work on direct drag measurements on smoth cylinders of comparable size is that of McClanahan and Ridgely [Ref. 15]. They tested cylinders of length-to-diameter ratios of 5:1 and 10:1 by towing them, in a circular tank, through fresh solutions of Polyox WSR-301. The major difference between their results (for fresh solutions) and those obtained in the NPS tunnel is that the drag transition occurred at a velocity of approximately 4 fps in their experiments. In two cases (solutions of 50 and 200 wppm), the one-inch diameter cylinder of L/d ratio of 5:1 experienced drag transition at a lower velocity than the longer cylinder of identical diameter. End conditions are known to influence the drag force acting on a cylinder in the flow of a Newtonian fluid. In addition, it is reasonable to assume that the end conditions influence the wave separation pattern observed on cylinders in the flow of polymer solutions. Therefore, the higher cylinder drag transition velocity observed in the NPS tunnel is considered to be due to the cylinder extending completely across the test section.

The only previously reported work regarding the determination of the drag coefficient for bluff bodies of comparable size in degraded solutions was the work of A. White [Ref. 9]. He found that the drag coefficient on a 1/2-inch sphere at a free-fall velocity of 4.8 fps increased toward the water value as the solution aged over a six-day period. This is consistent with the results obtained on cylinders at velocities less than the critical velocity.

Brennen [Ref. 17] observed that the velocity at which separation line distortion (on a 1/4-inch cylinder) occurred increased 3 fps by degradation in a 50 wppm Polyox solution. However, he did not observe the tripping to a Newtonian supercritical separation. In the experiments reported herein, such a tripping action was observed in solutions which produced less than 15 P. D. R. His degraded solution produced a turbulent drag of some 92% of water in a rotating wheel rig. The details of that device and the per cent drag reduction versus concentration curve were not given. It is speculated that Brennen's dilute solution would have produced more than 15 P. D. R. in the 0.073-inch rheometer for the following reasons: (1) Fifteen per cent drag reduction relative to laminar flow corresponds to a turbulent friction of 90% of that of water and (2) The work of Hoyt and Fabula [Ref. 2] which demonstrated that a concentration of 5 wppm of Polyox of molecular weight 4×10^6 produced the maximum friction reduction in a 0.109 cm pipe whereas a tenfold increase in concentration, 50 wppm, was necessary to achieve maximum drag reduction in a wheel rig.

No other experiments have been reported in the literature with bluff bodies in either severely degraded or in very low concentration (i.e., 1 wppm) Polyox solutions at velocities near critical. In the NPS water tunnel, however, practically the entire critical range of velocities was covered for the sizes of cylinders tested.

VI. POSSIBLE FLOW MECHANISM(S) FOR BLUFF BODY DRAG REDUCTION

The previous explanations of the observed reduction of the drag
of bluff bodies were based on the limited observations of the rear-
ward shift of the separation line, relative to water, of spheres
dropped into polymer solutions of relatively high concentrations. It
was conjectured that the polymer stabilized the laminar boundary
layer or caused a reattachment rearward of the expected separation
point. The data reported herein clearly indicate the lack of corre-
lation between the separation angle and the drag coefficient in dilute
polymer solutions.

In order to attempt to explain the phenomenon, it seems necessary
to re-examine the basic question of the drag alteration by additives:
The question is not why do the dilute polymer solutions cause drag
reduction on bluff bodies, for in many cases they do not (1-1/2-inch
diameter cylinder in 100 wppm solutions at Re = 2×10^5), but rather
why do the dilute polymer solutions alter the drag-crisis characteris-
tics on bluff bodies for which such a crisis occurs in Newtonian
fluids.

A review of the cylinder drag transition region characteristics
(Section II.A.) directed attention to the fact that the tunnel turbu-
lence intensity, surface roughness and threads, and modified pressure
gradients materially influence the Eiffel-effect Reynolds-number range
and characteristics.

Although the tunnel-turbulence levels were not measured, it may
be inferred from the location of the transition region in tap water

that the turbulence level was <u>of the order of</u> 2%. At this turbulence level, smooth bluff body drag transition is relatively unaffected by <u>slight</u> increases in turbulence level. Based on the works of Fabula [Ref. 42] and Friehe and Schwarz [Ref. 43], it is difficult to conceive that a concentration of 1 wppm Polyox WSR-301, aged 24 hours, could have increased the free stream turbulence to the level necessary to cause a 50% decrease in the drag crisis Reynolds number. If the cause of the "early" drag transition had been principally an increase of the intensity of the free stream turbulence, then the drag coefficient of the 1-1/2-inch cylinder in a 100 wppm solution would not have remained constant at approximately 0.7 as the tunnel velocity was raised above the velocity at which drag transition occurred in tap water. Similar drag characteristics have been reported for spheres dropped into quiescent tanks of fresh Polyox solutions. Therefore, attempting to explain the observed change in drag crisis on the basis of a change in free stream turbulence level is considered to be futile.

On the contrary, an explanation based on the concept of roughness elements or threads in the boundary layer flow and possibly attached to the wall is a physically more realistic line of thought. Even for a concentration of only 1 wppm, there are on the order of 10^{10} large polymer molecules in the cylinder boundary layer. A departure from Reynolds number similarity in the drag crisis region does occur for roughened cylinders. As seen in Fig. 6, the smaller cylinder (larger ε/d) experienced transition at a lower Reynolds number in air flow than the larger cylinders, with the ratio of the transition Reynolds number proportional to the square root of the ratio of cylinder diameters. The drag-crisis Reynolds number in Polyox solutions which

were severely degraded and/or of very low concentration was found to be also proportional to the square root of the ratio of the cylinder diameter. When Humphreys attached threads to the front of a cylinder in air flow at critical Reynolds number, the spanwise cell structure at separation was markedly altered and the transition characteristics changed (Figs. 8 and 10). In a similar manner, the separation cell structure is ordered by the polymer molecules to an extent that Brennen was able to measure their spanwise wave length. In addition, the occurrence of separation-line distortion in polymer solutions is closely and naturally related to the occurrence of drag crisis. However, this analogy cannot be carried too far since, as in turbulent pipe flow, the polymer molecules are many times more effective in altering the flow near a wall than can be justified on the basis of their physical size alone. In addition, this analogy suggests a much greater dependence of drag-crisis characteristics on bluff body size than has been observed in higher concentration solutions. Therefore, it is suggested that there is some other polymer influence imparted to the boundary-layer flow which affects the drag transition characteristics.

This other property is usually given the title of viscoelasticity under which the literature abounds with the concepts of normal stresses, fluid relaxation times, and strain field dependent viscosity, each or all of which would certainly modify the boundary layer in the convective flow about a bluff body. However, it is finally conjectured that it is specifically the finite (but not necessarily constant) critical shear-wave speed (c^*) which is the fundamental polymer property which imparts a significant change in the characteristics of the flow [Refs. 44, 45, 46].

It is significant to note that all mathematical models do not exhibit a finite shear wave speed. Even a model such as the Oldroyd type viscoelastic fluid model [Ref. 46] has a number of different definitions of stress flux, etc., the choice of which alters the predicted boundary layer flow. Thus, the following discussion will deal not so much with the particular characteristics of models that display a finite shear wave speed but rather with the behavior of fluids such as dilute polymer solutions used in the present investigation.

The behavior of the polymer solution flow is governed by the interaction of the viscous boundary layer and a "hydro-polymeric" boundary layer in a manner similar to the interaction of hydrodynamic and thermal boundary layers in convective heat transfer. Above the hydro-polymeric boundary layer, shear waves can propagate and standing waves exist on the characteristic surface similar to the propagation of sound and shock waves in a compressible fluid. When the hydro-polymeric boundary layer is much less than the viscous boundary layer thickness, the viscous boundary layer flow is insensitive to the wall shear stress. This is analogous to the case when the thermal boundary layer thickness is much less than the viscous boundary layer thickness, i.e., the viscous boundary layer flow is insensitive to the wall temperature.

When the wall shear stress exceeds the critical shear stress (ρc^{*2}), the hydro-polymeric boundary layer thickness becomes principally a function of fluid properties, i.e., independent of body size.

When the wall shear stress is much less than the critical shear stress, the locus of the hydro-polymeric boundary layer can be shown to be at $u = c^*$, and thus dependent upon the body size.

160

An approximate solution to the equations of motion for a second-order fluid in stagnation point flow [Ref. 47] have shown that the boundary layer velocity profile and the wall-shear stress are drastically altered when the Weissenberg number Wn (the ratio of the first normal-stress difference to the shear stress) is greater than zero. In fact, as the Weissenberg number increases, critical shear stress decreases, the wall stress increases and inflections occur in the velocity profile. Furthermore, the velocity-over-shoot occurs closer to the wall and increases in magnitude as the Weissenberg number increases.

Based on previous discussions, the following conjectures for the observed anomalous behavior of the flow of dilute polymer solutions about bluff bodies may be offered:

(1) The polymer molecules cause the solution to have a finite critical shear wave speed (c*);

(2) As a result of this finite shear wave speed, a hydro-polymeric boundary layer results;

(3) The entire boundary layer flow is strongly influenced by the hydro-polymeric boundary layer thickness;

(4) The mechanics of the drag crisis are principally unaltered; however, transition characteristics are controlled by the hydro-polymeric boundary layer thickness;

(5) Above the hydro-polymeric boundary layer, shear waves propagate and can have a secondary influence on the transition characteristics;

(6) When the wall shear stress is expected to exceed the critical shear stress, the hydro-polymeric boundary layer thickness is

161

principally determined by the fluid properties (density, dynamic viscosity and critical shear wave speed), independent of the body size;

(7) When the wall shear stress is less than the critical shear stress, the hydro-polymeric boundary layer thickness is principally determined by the distance from the wall at which the streamwise velocity equals the critical shear wave speed;

(8) The ratio of inertial forces to viscous shear forces in the viscous boundary layer, above the hydro-polymeric boundary layer, is altered. This ratio, a generalized Reynolds number, is a function of $\rho U^2/\rho c*^2$ when the critical shear stress is exceeded; and finally,

(9) When the wall shear stress is less than critical and the free stream velocity is greater than the shear wave speed, the shear stress at the interface of the viscous and hydro-polymeric boundary layers ($u = c*$) is a function of $\mu c*/d$. Therefore, the generalized Reynolds number is a function of $\rho U^2/(\mu c*/d)$, i.e., $(U/c*)Re$. In both cases, the generalized Reynolds number is larger than Re.

F. White [Ref. 48] stated that the local friction coefficient (C_f) in (flat plate) polymer flow at a given Rex is equal to the Newtonian C_f evaluated at an effective Reynolds number, Ren, given by

$$Ren = Rex \ (v*/c*)^{ka} \quad \text{for} \quad v* > c*$$

where $v* = (\tau_w/\rho)^{\frac{1}{2}}$, k is equal to 0.4, c* is equal to .08 ±.02 fps for

162

Polyox WSR-301 and "a" is dependent upon concentration. For
concentrations greater than 20 wppm "a" is approximately constant
at 10.

The assumption of a shear wave speed independent of concentration
for the low concentration is invalid. This is reflected by the
dependence of "a" upon concentration for less than 20 wppm Polyox
WSR-301. However, the stated value of critical shear wave speed
does correlate with the other works to be discussed for concentrations
greater than 20 wppm.

Although this effective Reynolds number was developed for turbulent
flow, it is interesting that for laminar boundary layer flow τ_w is
proportional to $\rho U^2 Re^{-\frac{1}{2}}$, with ka = 4, Ren is proportional to $(U/c*)^4$.

Ultman and Denn [Ref. 44] analyzed James' data based on a simple
Oldroyd type fluid model and stated that the onset of anomalous heat
and momentum transfer at <u>low</u> Reynolds numbers (10^{-3} inch diameter
wires) in dilute polymer solutions occurs when the free stream
velocity is equal to the critical shear wave velocity. The onset
for anomalous heat transfer occurred at a free stream velocity of
.08 ±.02 fps for a 52.4 wppm Polyox WSR-301 solution, independent
of wire size (1×10^{-3} to 6×10^{-3} inch diameter).

The data for the onset of the Toms effect in turbulent pipe flow,
from the work of Pruitt and Crawford as reported by Walsh [Ref. 49],
clearly show that for Polyox, the critical shear stress increases
with decreasing concentration and molecular weight.

M. W. x 10^6	Conc. wppm	Onset Stress dynes/cm^2	c* fps
0.5	2	600	.8
0.5	10	120	.36
0.5	50	24	.16
1.6	2	60	.25
1.6	10	15	.125

As a comparison, the maximum shear stress on a 1-1/2-inch diameter cylinder in water flowing at 10 fps is approximately 300 dynes/cm^2, whereas the local free stream velocity at 60 degrees is approximately 17 fps.

For the case of the flow of fresh Polyox WSR-301 solutions with concentrations greater than 10 wppm, the expected wall-shear stress exceeds the critical value over a large portion of the cylinder surface. Thus, the drag coefficient is dependent upon the ratio of the free stream velocity to the critical shear wave speed. As the concentration or molecular weight is decreased, the region where the wall-shear stress exceeds the critical value is decreased. However, the region where the local free stream velocity exceeds the critical shear wave velocity is practically unaffected.

As noted earlier, the critical transition occurred in solutions which produced, at the particular state of degradation, approximately 15 P. D. R. Identical P. D. R. could have been obtained with a fresh solution had it a concentration of 1/3 wppm. Walsh's hypothesis (concentration x onset stress=constant, for a given M. W.) predicts that the 1/3 wppm Polyox WSR-301 solution should have a critical shear stress <u>on the order</u> of 360 dynes/cm^2 and, thus, a critical shear wave speed of 0.6 fps. Therefore, the critical transition occurs not when

the shear exceeds the critical shear stress but when the free stream velocity is an order of magnitude larger than the critical shear-wave speed. Thus the drag coefficient is a function of the product of velocity ratio (U/c*) and the Reynolds number.

This, obviously, does not predict the exact velocity at which drag crisis would occur but it does indicate that the drag crisis occurs at a free stream velocity greater than the shear wave speed and less than the free stream velocity at which the drag crisis would occur on the same body in pure water.

The experimental evidence indicates that the drag transition in fresh solutions of Polyox WSR-301 with concentrations of 25 and 100 wppm is similar to the drag transition in a Newtonian fluid. However, the flow changes from subcritical directly to the transcritical flow observed by Roshko with an 18-foot cylinder in air flow at Re > 3.5 x 10^6.

It is speculated that the critical type drag transition, which occurred in solutions of small concentrations and/or in solutions of drastically reduced molecular weight, is a manifestation of the Coleman-Gurtin [Ref. 45] instability; "...an apparently new type of instability for steady shearing flows of viscoelastic fluids: the breakdown of a steady flow by the rapid growth of a disturbance involving a jump in the acceleration."

Since the bluff bodies were tested in homogeneous solutions, it is not possible to discriminate the effect of the polymer molecules on the boundary layer flow from their effect on the free shear layer and wake flow. However, since both free shear layer and wake flows are dependent upon the boundary layer flow in a Newtonian fluid, it

is conjectured that the direct interaction between free shear layer vortices and wake vortices and the polymer molecules are of secondary importance. The primary effects produced by the polymer molecules in dilute solutions occur near the wall.

VII. SUMMARY OF RESULTS AND CONCLUSIONS

The preceding discussion shows that the effect of polymer molecules on the flow past bluff bodies cannot be considered as drag reduction per se for a given Reynolds number. Small amounts of Polyox WSR-301 in water flowing about a bluff body significantly alter the pressure distribution only in the flow regime where there is a transition region.

The results further indicate that the shift in separation point and the change in back pressure on cylinders, caused by the additive, are not directly related. On the contrary, each depends upon the concentration, degradation, free stream velocity and the cylinder size. Furthermore, the drag coefficient is not uniquely determined by the separation angle.

Two distinct types of drag transition occur: The first is a continuous transition region for fresh solutions, the characteristics of which resemble the drag transition on roughened cylinders. The second is an actual drag "crisis" or "tripping" of the boundary layer at a well defined flow condition for degraded solutions which produce approximately the same friction reduction, in the turbulent-flow pipe rheometer, independent of concentration.

The details of the dependence of cylinder drag coefficient upon the free stream velocity, cylinder diameter, per cent pipe drag reduction and concentration have previously been discussed. In general, it was found that the drag coefficient predominantly depends upon the free stream velocity and per cent pipe drag reduction. There are two significant conclusions which can be drawn from this result: (1) The Reynolds

number similarity does not hold true for flows of dilute polymer solutions past bluff bodies, and (2) there is a relationship between the effect of polymer molecules on fully developed turbulent pipe flow and their effect on convective "laminar" external boundary layer flow. No definitive causal mechanism to explain this relationship and the anomalies produced in the transition flow regime can be offered. Even though conjectures based on viscoelastic phenomenon have been presented, so little data concerning the rheology of dilute Polyox solutions are available that it is not possible to attach specific significance to the predictions of either the Oldroyd or second-order fluid models.

The recirculating fluid tunnel has been demonstrated to be a vital and economical tool for the investigation of external flows of dilute polymer solutions, providing the properties of the solution are monitored. It is vital because the Reynolds number similarity does not apply and the flow velocity must be varied independently of the body size. It is economical because the body is fixed; thus instrumentation is greatly simplified. In addition, with the recirculating tunnel, observation time is neither limited by space nor fluid storage capacity. The implicit assumption is, of course, made that the results obtained in homogeneous solutions can be extrapolated to the case of polymer injection from the wall. It has previously been shown by others that this assumption is fairly valid for turbulent flow over a flat plate. Furthermore, a little reflection shows that whether the polymer solution is injected into the boundary layer or into the entire flow, all of the hydrodynamic effects take place within the boundary layer and thus the presence of polymer in the shear-free flow region does not play, for all intents and purposes, any role on the boundary layer. It is, therefore, justifiable to conclude that the results of the present

168

investigation, attained through the use of a homogeneous solution, should be applicable to cases where polymer solutions of the same molecular weight, type and boundary layer concentration are directly introduced into the flow by injection.

VIII. SUGGESTIONS FOR FURTHER RESEARCH

As is the case with every basic research, the present investigation on the flow of dilute polymer solutions about laboratory size models has discovered certain new flow characteristics and many new areas of investigation. One of the most important problems, both from a theoretical and an experimental point of view, is the acquisition of the ability of both the researcher and designer to determine the governing laws for the extrapolation of the results to large scale objects. On the basis of the present investigation, it appears that the Reynolds number similarity does not hold true for the flows under consideration and thus, the laboratory-scale test studies cannot, at present, be readily extended to desired sizes. Thus, in order to efficiently optimize the properties of boundary-layer flow control offered by these long-chain molecule polymers, it will be necessary to carry out further investigations to establish the physical laws which govern the flow of these solutions.

Secondly, it has been fully realized that the hydrodynamics of polymer solutions requires additional investigation in the area of the rheology of dilute polymer solutions. As pointed out in the conclusion, there appears to be a significant relationship between the propagation of shear waves and the instability of hydro-polymeric boundary layers. Thus, it is recommended that the question of whether the critical wall shear stress (in pipe flow) results from a fluid "stiffness" shear modulus, and as to whether the solution displays a critical finite shear wave speed in laminar flow be resolved. To be more specific,

one must determine for the most effective turbulent-flow pipe-friction reducers in the various flow regimes encountered the essential flow dynamics for both laminar and turbulent flows. It also became apparent that the effect of the intensity of turbulence and the relations between the pipe friction reduction and the drag crisis will have to be more clearly delineated in order to establish stronger ties between the so-called state of degradation of a given solution with its apparent behavior leading to an anomalous stability and earlier transition. The present investigator would suggest that the experiments similar to those carried out by Schubauer and Skramstad [Ref. 51] be repeated with dilute polymer solutions to gain further insights into the stability characteristics of polymerized flows. Furthermore, it suffices to state that these investigations be made for both large and small scale bodies. These recommendations are made with the full recognition of the difficulties involved in their exploration. The difficulties to be encountered in the use of the hot-wire anemometer technique and Pitot tubes due to anomalous heat transfer and normal stress effects in the flow of dilute polymer solutions are apt to render the investigations rather difficult and demand considerable ingenuity on the part of the investigator.

Considering the fact that the understanding of the dilute polymer flow about bluff bodies is considerably less than that for pipe flows, and that one can obtain much reliable data with a water tunnel such as the one used herein, explorations should be continued with similar or larger tunnels where not only the flow path through dye injection techniques could be determined but also and perhaps more significantly, the forces and the pressure distributions be measured. The significance of the last recommendation could not be sufficiently emphasized, recognizing the fact that all of our basic knowledge about the characteristics

171

of flow about bluff bodies came from the measurements of pressure, lift and drag forces, the rms values of their oscillations and the flow measurements in the immediate wake of the bodies.

Additional recommendations concern the investigation of the variation of the convection of vortices by the effects of finite shear wave speed, the exploration of the relationships of the observed phenomena with predictions obtained from various viscoelastic fluid models, and the determination of the dynamics of the deformation and rotation of a given chain of mers whose structure varies from a relatively stiff helical form to a "ball of yarn" like shape. It suffices to say that until the type of experiments cited above are performed and a useful equation-of-state for dilute polymer solutions is established, the application of the known properties of drag transition to large scale bodies will have to remain on a cut and try basis.

APPENDIX A

DATA

Turbulent Flow Pipe Rheometer

Fresh Water Friction Factors

Re	f_t
3951	.0370
4083	.0371
4129	.0378
4129	.0363
4291	.0365
4615	.0366
4654	.0354
4692	.0372
4733	.0364
4733	.0364
4755	.0369
4777	.0364
4796	.0357
4817	.0360
4860	.0353
4920	.0366
5016	.0358
5332	.0350
5465	.0357
5662	.0344

Flat Plate Perpendicular to the Flow

P_s inches water	DRAG lbs.	C_d uncorrected	C_d corrected	Re x 10^{-5} corrected
		Tap water		
23.66	9.52	2.70	2.08	1.07
37.12	14.27	2.58	1.99	1.34
42.92	16.00	2.50	1.94	1.43
53.36	18.94	2.38	1.86	1.59
14.85	5.28	2.38	1.86	.84
7.24	2.81	2.60	2.00	.59
23.66	9.08	2.57	1.98	1.07
55.68	19.54	2.35	1.84	1.62
55.68	20.76	2.50	1.94	1.63
43.61	16.43	2.53	1.96	1.45
35.26	13.41	2.55	1.97	1.31
27.84	10.38	2.50	1.94	1.16
22.73	8.43	2.40	1.93	1.04
19.49	7.22	2.48	1.93	.97
13.46	4.97	2.48	1.93	.80
6.50	2.81	2.81	2.14	.56

100 wppm Polyox WSR-301

TRT 12, 72 PDR

32.48	14.19	2.93	2.22	1.27

TRT 14

32.94	14.70	2.99	2.25	1.28

TRT 17

4.64	2.81	4.06	2.86	.50
7.42	5.10	4.61	3.16	.64
16.70	9.52	3.82	2.73	.94
22.74	11.42	3.37	2.48	1.08
32.02	14.27	2.99	2.25	1.26

TRT 29, 76 PDR

52.20	21.62	2.78	2.13	1.61
37.82	15.44	2.74	2.10	1.38
35.26	14.14	2.69	2.07	1.31
37.58	14.88	2.66	2.05	1.34

174

Flat Plate Perpendicular to the Flow

P_s inches water	DRAG lbs.	C_d uncorrected	C_d corrected	Re x 10^{-5} corrected
		TRT 82, 75 PDR		
42.22	14.27	2.27	1.80	1.41
		100 wppm Polyox WSR-301 TRT 112, 60 PDR		
6.96	2.73	2.63	2.04	.58
12.99	4.97	2.57	1.98	.79
25.06	9.08	2.43	1.90	1.10
40.60	14.01	2.31	1.82	1.38
61.71	20.76	2.26	1.77	1.71
		TRT 137, 58 PDR		
14.66	5.19	2.37	1.87	.83
25.06	9.08	2.43	1.90	1.10
39.44	13.67	2.32	1.83	1.36
47.56	16.43	2.32	1.83	1.50
60.32	20.76	2.31	1.81	1.70
		100 wppm Polyox WSR-301 TRT 12, 69 PDR		
31.32	14.65	3.14	2.34	1.25
		TRT 16		
3.48	2.81	5.42	3.53	.45
7.42	5.26	4.76	3.23	.64
18.75	9.31	3.33	2.46	.98
24.36	12.45	3.43	2.50	1.12
31.08	15.01	3.17	2.36	1.26
		TRT 23, 72 PDR		
53.36	20.87	2.62	2.03	1.60
37.12	15.74	2.85	2.16	1.36
32.48	14.21	2.94	2.22	1.26

Flat Plate Perpendicular to the Flow

P_s inches water	DRAG lbs.	C_d uncorrected	C_d corrected	Re x 10^{-5} corrected
		TRT 63, 80 PDR		
7.42	2.81	2.54	1.98	.60
13.92	5.22	2.52	1.96	.82
25.52	9.40	2.47	1.93	1.10
30.62	11.00	2.41	1.88	1.21
40.60	13.81	2.28	1.80	1.38
48.72	16.86	2.32	1.83	1.52
59.39	19.59	2.21	1.75	1.68

NACA 0024 Hydrofoil, four-inch chord

α = 0 degree nominal, tap water

P_s inches water	LIFT lbs.	DRAG lbs.
16.1	.65	.07
31.4	1.31	.42
49.6	2.49	.78
75.8	3.93	1.36
94.8	6.42	1.92
70.2	4.33	1.40
47.9	2.30	.89
28.5	1.31	.50
18.0	.65	.23
17.5	.96	.31
31.3	2.62	.47
51.0	3.93	.94
60.0	4.06	1.09
74.6	4.91	1.30
79.0	4.91	1.51
99.3	5.57	2.08
104.0	4.91	1.87
80.3	3.60	1.35
70.0	3.27	1.14
53.3	2.62	.89
47.4	2.29	.77
30.8	.97	.47
18.0	.59	.15
30.2	.35	.68
48.0	.70	.99
69.5	1.40	1.45
97.4	1.75	2.18
97.4	2.10	1.87
72.0	1.40	1.45
46.4	.70	.83
29.7	.35	.63

NACA 0024 Hydrofoil, four-inch chord

α = 0 degree (w/shim), 25 wppm Polyox WSR-301

TRT 15, 88 PDR

P_s inches water	LIFT lbs.	DRAG lbs.
17.4	0.0	--
34.8	.49	.31
55.6	1.40	.83
83.5	3.15	1.45
116.0	3.85	1.87
113.0	4.90	2.18
76.5	2.95	1.04
53.5	1.05	.83
33.9	.70	.42
104.5	4.55	1.77
78.8	2.80	1.45
52.5	1.40	.78
113.5	4.90	2.21
75.0	3.15	1.47
50.0	1.40	.81
30.1	1.05	.40
16.7	.56	.13

α = 0 degree, 100 wppm Polyox WSR-301

TRT 326, 44 PDR

P_s inches water	LIFT lbs.	DRAG lbs.
34.0	1.02	.54
51.0	2.38	.86
78.9	3.74	1.43
108.5	4.42	2.32

TRT 352, 27 PDR

P_s inches water	LIFT lbs.	DRAG lbs.
111.00	4.80	2.29
78.0	3.52	1.46
52.3	2.51	.93
31.8	1.15	.52

NACA 0024 Hydrofoil, four-inch chord

α = 3 degrees nominal, tap water

P_s inches water	LIFT lbs.	DRAG lbs.
12.3	2.6	.16
17.6	3.5	.19
28.9	6.4	.39
36.7	7.5	.57
48.3	10.5	.96
56.8	12.8	1.10
70.0	14.5	1.43
94.8	22.2	1.87
97.0	21.5	2.29
71.0	14.7	1.61
53.0	11.2	1.35
46.2	9.5	1.09
37.4	7.5	.83
29.8	5.9	.73
16.3	3.3	.35
12.8	2.3	.29
30.4	6.2	.83
48.2	9.5	1.19
75.9	14.3	1.77
97.3	19.7	2.70
99.5	19.9	2.60
80.5	15.5	2.40
56.9	10.5	1.56
36.0	6.6	.94
30.8	5.6	.83
31.4	5.6	.88
48.2	8.7	1.45
74.3	13.2	2.03
97.5	17.5	2.91
100.0	16.8	3.02
69.5	12.4	2.03
48.6	8.0	1.56
30.1	4.9	1.09

NACA 0024 Hydrofoil, four-inch chord

α = 3 degrees nominal, 100 wppm Polyox WSR-301

TRT 266, 54 PDR

P_s inches water	LIFT lbs.	DRAG lbs.
111.0	23.1	3.06
78.5	16.6	2.24
51.0	10.0	1.40
16.5	3.1	.45
32.5	6.7	.87
51.1	10.4	1.45
79.6	16.2	2.16
109.0	23.9	3.10

α = 3 degrees nominal, 25 wppm Polyox WSR-301

TRT 120, 34 PDR

P_s inches water	LIFT lbs.	DRAG lbs.
50.5	9.4	1.09
71.0	14.1	1.72
106.5	20.7	2.45
30.1	5.3	.75
108.0	21.7	2.48
73.2	13.7	1.64
51.0	9.1	1.12
30.6	5.3	.71
16.9	3.2	.38

NACA 0024 Hydrofoil, four-inch chord

α = 6 degrees nominal, tap water

P_s inches water	LIFT lbs.	DRAG lbs.
18.0	6.4	.10
15.2	5.2	.23
30.8	11.1	.71
48.0	18.2	1.06
73.0	25.6	1.95
94.8	35.4	2.29
66.3	24.3	1.90
45.0	15.7	1.47
28.9	10.2	1.14
14.4	5.1	.57
13.9	4.9	.28
17.1	6.2	.23
28.4	10.6	.44
35.8	13.6	.70
47.1	17.7	1.00
56.9	21.6	1.93
68.6	24.2	2.39
95.5	36.0	2.85
70.0	25.5	2.16
52.0	18.8	1.76
45.5	15.8	1.48
35.5	11.9	1.14
28.4	9.4	1.00
17.0	5.7	.63
11.6	3.6	.40
13.3	4.9	.21
17.0	5.9	.31
29.9	10.3	.80
17.3	5.6	.51
45.5	15.4	1.33
36.7	12.1	1.12
12.5	4.0	.33
29.0	10.5	.92
46.5	14.7	1.56
68.5	22.0	2.34
96.3	33.2	3.26
95.1	33.6	3.12
65.0	21.0	2.29
46.4	14.3	1.61
29.0	8.7	.99

NACA 0024 Hydrofoil, four-inch chord

α = 6 degrees nominal, 25 wppm Polyox WSR-301

TRT 10, 80 PDR
TRT 33

P_s inches water	LIFT lbs.	DRAG lbs.
35.5	11.9	1.19
51.7	17.5	1.92
76.2	27.3	2.55

TRT 45, 70 PDR

109.0	41.2	3.38
106.5	40.4	3.10
78.5	28.0	2.37
51.0	16.8	1.57
34.8	11.2	1.12

TRT 69, 56 PDR

33.7	11.6	.94
50.2	18.2	1.45
79.0	29.4	1.87
109.0	40.6	3.01

TRT 93, 50 PDR

106.0	40.0	3.12
70.5	25.2	2.18
51.8	18.2	1.66
32.0	11.2	.99

TRT 137, 34 PDR

34.8	11.2	1.04
50.5	17.5	1.51
76.0	28.0	2.39
106.0	40.6	3.25

NACA 0024 Hydrofoil, four-inch chord

α = 6 degrees nominal, 100 wppm Polyox WSR-301

P_s inches water	LIFT lbs.	DRAG lbs.
	TRT 159	
106.5	38.1	4.48
49.5	18.3	2.29
16.7	6.1	.62
34.1	11.6	1.51
52.2	18.3	2.29
65.0	23.1	2.70
78.0	29.3	3.33
38.3	13.6	1.66
107.5	40.8	4.37
	TRT 254, 54 PDR	
31.4	11.2	1.40
51.0	18.3	2.13
73.0	27.2	2.96
110.0	40.8	4.10

NACA 0024 Hydrofoil, four-inch chord

α = 6 degrees nominal, 4.5 degrees measured; tap water

P_s inches water	LIFT lbs.
9.02	1.38
18.43	4.52
34.56	7.74
55.68	13.76
80.64	22.36
99.84	30.10
9.41	2.58
18.82	5.07
34.56	7.74
54.72	14.62
76.80	21.50
107.50	31.82
9.60	2.15

200 wppm Polyox WSR-301

TRT 35, 62 PDR

P_s inches water	LIFT lbs.
92.16	32.68
57.60	19.78
38.40	12.04
26.88	7.96
14.21	4.08
8.83	.86

TRT 55, 67 PDR

P_s inches water	LIFT lbs.
8.06	1.08
14.21	3.44
25.92	7.96
40.32	13.33
66.05	21.93
92.16	31.82

NACA 0024 Hydrofoil, four-inch chord

α = 6 degrees nominal, 4.5 degrees measured

200 wppm Polyox WSR-301

TRT 70, 79 PDR

P_s inches water	LIFT lbs.
8.45	2.58
15.36	5.16
25.92	9.46
40.32	15.48
68.35	22.79
92.16	31.82

TRT 86

P_s inches water	LIFT lbs.
9.22	2.58
13.44	4.30
16.90	5.25
23.04	7.96
27.84	9.46
34.56	12.04
46.08	15.48
59.52	20.64
72.96	24.08
82.56	27.52
96.00	33.54

TRT 106, 84 PDR
TRT 127

P_s inches water	LIFT lbs.
8.26	2.36
17.28	5.16
32.06	9.68
50.88	15.48
74.88	22.70
103.7	33.54

NACA 0024 Hydrofoil, four-inch chord

α = 6 degrees nominal, 4.5 degrees measured;. tap water

P_s inches water	LIFT lbs.
9.22	2.24
18.82	4.52
35.52	9.03
51.84	13.50
80.64	21.50
107.5	29.24
9.41	2.11
18.05	4.30
34.56	8.60
51.84	13.50
78.72	21.07
107.5	29.24

NACA 0024 Hydrofoil, four-inch chord

α = 9 degrees nominal, tap water

P_s inches water	LIFT lbs.	DRAG lbs.
13.3	5.8	.62
17.5	7.6	1.45
30.8	14.2	2.50
38.1	18.5	2.80
45.0	21.8	3.21
54.4	26.2	3.54
65.1	31.4	4.06
90.8	45.8	5.20
70.5	35.4	4.15
50.1	24.9	3.22
45.0	22.1	2.92
35.5	16.8	2.39
29.8	14.4	2.00
16.0	7.2	.88
14.0	6.2	.73
30.3	14.0	2.03
45.0	21.0	2.96
68.5	32.7	4.20
97.0	45.8	5.45
94.5	45.0	5.12
74.2	35.0	4.28
68.5	32.2	3.80
51.0	23.6	2.93
45.5	21.0	2.72
31.3	15.2	2.10
26.0	11.9	1.58
29.7	14.0	2.08
44.0	21.7	2.92
68.5	32.9	4.28
92.5	45.5	5.72
92.5	46.2	5.46
67.2	33.6	4.10
45.2	21.7	2.97
27.8	12.6	1.95

NACA 0024 Hydrofoil, four-inch chord

$\alpha = 9$ degrees nominal, 100 wppm Polyox WSR-301

TRT 30, 77 PDR
TRT 60

P_s inches water	LIFT lbs.	DRAG lbs.
16.2	--	--
22.9	7.5	2.70
40.5	13.6	3.85
64.7	25.5	5.40
92.5	40.8	6.65
64.2	27.9	4.15
25.5	11.5	1.56

TRT 75

P_s inches water	LIFT lbs.	DRAG lbs.
92.5	43.3	5.83
64.9	29.2	4.15
48.2	20.4	2.90
36.0	15.3	2.18
30.6	12.5	1.87

TRT 97, PDR 87

P_s inches water	LIFT lbs.	DRAG lbs.
48.2	19.7	3.26
29.7	11.5	2.08
72.5	29.9	4.58
17.0	6.9	1.35
102.0	43.5	6.45

TRT 465

P_s inches water	LIFT lbs.	DRAG lbs.
29.0	12.9	1.14
46.0	21.8	2.28
69.5	33.3	3.95
100.0	46.8	5.82

NACA 0024 Hydrofoil, four-inch chord

α = 9 degrees nominal, 100 wppm Polyox WSR-301

TRT 465

P_s inches water	LIFT lbs.	DRAG lbs.
97.5	48.2	5.75
67.3	32.0	3.80
46.4	19.7	2.34
25.5	12.2	1.25

α = 9 degrees nominal, 25 wppm Polyox WSR-301

TRT 87

P_s inches water	LIFT lbs.	DRAG lbs.
100.0	49.0	6.07
69.5	36.4	4.41
46.4	21.7	2.85
28.3	13.0	1.61
47.5	23.1	2.96
71.2	37.8	4.41
101.0	52.5	5.85
13.9	7.0	.67
97.0	50.5	5.71
29.4	14.8	1.87

NACA 0024 Hydrofoil, four-inch chord

$\alpha = 12$ degrees nominal, tap water

P_s inches water	LIFT lbs.	DRAG lbs.
14.7	8.0	1.56
30.4	17.2	2.45
45.0	26.1	3.17
66.2	40.0	5.56
80.5	50.0	6.70
68.6	41.0	5.72
45.0	26.5	3.70
26.8	17.0	2.44
14.2	9.0	1.41
12.9	5.3	.36
15.2	6.4	.48
29.4	12.9	1.29
35.6	16.3	1.77
45.0	21.0	2.37
55.0	26.2	3.06
66.8	33.8	3.92
89.5	46.4	6.24
70.2	34.3	4.07
52.2	25.8	2.68
45.0	22.2	2.20
33.2	16.2	1.44
28.5	13.7	1.15
16.1	7.4	.65
12.1	5.7	.47
12.8	7.0	--
17.0	9.3	--
29.4	16.8	1.27
44.7	24.7	2.60
67.1	37.9	5.52
75.8	43.0	6.45
85.0	51.0	7.60
12.5	7.1	--
15.6	9.1	--
28.0	16.3	2.72
45.5	24.2	4.05
67.3	38.0	5.62
76.0	41.8	6.45
92.5	52.4	7.90
91.5	53.6	7.70
65.8	38.0	5.50
28.4	17.0	2.33

NACA 0024 Hydrofoil, four-inch chord

α = 12 degrees nominal, tap water

P_s inches water	LIFT lbs.	DRAG lbs.
27.8	15.8	1.46
42.7	23.6	2.70
65.5	37.5	4.80
90.0	51.5	6.85
88.0	50.4	7.42
63.8	35.0	4.73
43.5	24.5	3.05
27.8	15.0	1.82

α = 12 degrees nominal, 25 wppm Polyox WSR-301

TRT 148, 30 PDR

P_s inches water	LIFT lbs.	DRAG lbs.
97.5	58.7	6.45
64.0	37.0	3.85
43.0	24.5	2.29
27.9	16.1	1.56
29.7	15.4	2.18
46.9	26.7	3.34
68.5	39.2	4.25
95.0	58.7	7.80
102.0	60.3	7.70

α = 12 degrees nominal, 100 wppm Polyox WSR-301

88 PDR

P_s inches water	LIFT lbs.	DRAG lbs.
102.0	57.2	9.60
48.7	27.2	5.45
16.9	8.5	1.56
30.5	16.3	3.02
34.8	19.0	3.12
48.7	25.8	4.36
60.2	33.3	5.94
70.5	38.9	6.87
100.0	55.0	9.15

NACA 0024 Hydrofoil, four-inch chord

α = 12 degrees nominal, 100 wppm Polyox WSR-301

88 PDR

P_s inches water	LIFT lbs.	DRAG lbs.
76.3	42.2	7.10
47.5	25.8	3.54
32.5	18.3	2.30

TRT 410

P_s inches water	LIFT lbs.	DRAG lbs.
29.0	14.3	1.58
44.0	24.5	2.55
70.0	36.7	4.12
98.5	53.0	6.81
110.0	59.7	8.11
67.2	36.7	4.50
46.4	24.5	2.70
30.2	15.0	1.45

TRT 430, 26 PDR

CYLINDER DRAG COEFFICIENTS

3/4-inch diameter cylinder, tap water

P_s inches water	DRAG lbs.	C_d uncorrected	C_d corrected	$Re \times 10^{-4}$ corrected
10.21	1.26	1.10	.99	4.9
19.48	2.37	1.09	.98	6.7
32.48	4.00	1.10	.99	8.7
46.40	6.31	1.22	1.09	10.4
74.24	9.05	1.09	.98	13.2
9.22	1.24	1.20	1.08	4.6
17.05	2.17	1.14	1.03	6.2
32.64	4.09	1.12	1.01	8.7

one-inch cylinder, tap water

9.51	1.84	1.30	1.12	6.4
19.30	3.68	1.28	1.11	9.1
34.33	6.31	1.23	1.08	12.1
52.20	9.05	1.16	1.01	14.9
74.24	11.57	1.05	.93	17.7
102.1	17.88	1.18	1.03	20.9
9.74	2.10	1.45	1.24	6.5
31.32	6.21	1.33	1.15	11.6
70.53	11.31	1.08	.97	17.1
20.42	3.42	1.12	.98	9.3
51.04	9.05	1.19	1.04	14.7
102.10	18.94	1.24	1.08	20.9
60.32	10.00	1.11	.98	16.0

1-1/2-inch diameter cylinder, tap water

7.80	2.58	1.48	1.15	9.4
15.78	4.94	1.40	1.10	13.0
30.16	7.36	1.09	.88	17.7
44.08	7.89	.80	.67	20.8
69.60	8.15	.52	.45	26.0
16.70	5.00	1.34	1.05	13.4
95.12	12.10	.57	.49	30.5
28.30	6.84	1.08	.88	17.0
9.84	2.74	1.24	.99	10.2
18.37	5.26	1.28	1.01	14.0
8.12	2.63	1.45	1.13	9.3
29.46	8.15	1.24	.99	17.6
71.92	8.42	.52	.45	26.4
92.80	12.10	.58	.50	30.0

CYLINDER DRAG COEFFICIENTS

1-1/2-inch diameter cylinder, tap water

P_s inches water	DRAG lbs.	C_d uncorrected	C_d corrected	$Re \times 10^{-4}$ corrected
55.68	9.47	.76	.65	23.4
75.17	10.52	.63	.54	27.1
7.89	2.63	1.49	1.15	9.2

CYLINDER DRAG COEFFICIENTS

3/4-inch diameter cylinder, 100 wppm Polyox WSR-301

TRT 20, 82 PDR

P_s inches water	DRAG lbs.	C_d uncorrected	C_d corrected	Re x 10^{-5} corrected
5.76	1.05	1.63	1.41	.37
12.90	1.70	1.18	1.07	.55
28.80	2.94	.91	.83	.81
47.23	4.50	.85	.78	1.04
76.03	7.44	.87	.80	1.32
103.70	9.61	.83	.76	1.54

TRT 30

7.68	1.21	1.41	1.24	.43
16.12	1.86	1.03	.93	.61
29.38	3.01	.91	.83	.82
46.08	4.65	.90	.82	1.03
74.88	7.13	.85	.78	1.31
102.10	9.92	.87	.80	1.53

TRT 40, 83 PDR

9.22	1.08	1.05	.95	.46
18.05	1.95	.97	.88	.64
32.64	3.41	.93	.85	.86
51.07	4.96	.87	.80	1.08
82.56	7.44	.81	.75	1.37
107.50	9.92	.82	.76	1.57

TRT 81, 68 PDR

9.02	1.18	1.17	1.05	.45
17.51	2.11	1.08	.98	.63
32.64	3.56	.98	.89	.87
53.76	5.42	.90	.83	1.11
78.72	7.44	.85	.78	1.34
106.00	9.92	.84	.77	1.56

CYLINDER DRAG COEFFICIENTS

3/4-inch diameter cylinder, 100 wppm Polyox WSR-301

P_s inches water	DRAG lbs.	C_d uncorrected	C_d corrected	Re x 10^{-5} corrected
		TRT 135		
8.83	1.08	1.09	.98	.45
17.28	2.11	1.09	.98	.63
29.76	3.56	1.07	.97	.82
46.08	5.12	.99	.90	1.03
77.57	7.44	.86	.79	1.33
107.50	10.11	.84	.77	1.57
		TRT 146, 50 PDR		
9.22	1.24	1.20	1.07	.46
17.66	2.17	1.10	.99	.63
32.64	3.88	1.06	.96	.86
52.99	5.89	.99	.90	1.10
79.87	8.37	.94	.86	1.35
104.40	10.85	.93	.85	1.55
		TRT 153, 42 PDR TRT 173		
9.22	1.24	1.20	1.07	.46
18.05	2.17	1.08	.98	.64
32.64	3.72	1.02	.92	.86
52.99	5.74	.97	.88	1.10
80.64	8.37	.93	.85	1.36
107.5	10.23	.85	.78	1.57
		TRT 225, 35 PDR		
9.22	1.24	1.20	1.07	.46
17.28	2.11	1.09	.98	.63
32.25	3.72	1.03	.93	.86
51.46	5.64	.98	.89	1.08
76.80	8.06	.94	.86	1.32
107.50	10.66	.89	.82	1.57

CYLINDER DRAG COEFFICIENTS

one-inch diameter cylinder, 100 wppm Polyox WSR-301

P_s inches water	DRAG lbs.	C_d uncorrected	C_d corrected	$Re \times 10^{-5}$ corrected
		TRT 17, 72 PDR		
7.68	1.80	1.57	1.34	.57
20.74	3.41	1.10	.97	.94
36.86	5.18	.94	.84	1.24
67.20	8.37	.84	.75	1.67
96.00	12.09	.85	.76	2.00
		TRT 24		
6.14	1.30	1.42	1.22	.52
10.37	2.02	1.31	1.13	.67
22.08	3.35	1.02	.90	.97
38.78	5.27	.91	.81	1.27
67.97	8.56	.84	.75	1.68
93.70	11.16	.80	.72	1.97
		TRT 36, 78 PDR		
8.26	1.30	1.06	.93	.59
14.98	2.17	.97	.86	.80
27.26	3.50	.86	.77	1.07
44.16	5.58	.85	.76	1.35
72.19	8.56	.80	.72	1.73
99.84	11.78	.79	.71	2.04
		TRT 70, 82 PDR		
8.83	1.71	1.30	1.13	.61
17.66	2.85	1.08	.95	.85
34.37	4.80	.94	.83	1.20
51.46	6.70	.87	.78	1.46
78.72	9.30	.79	.71	1.80
106.00	13.02	.82	.73	2.11

CYLINDER DRAG COEFFICIENTS

one-inch diameter cylinder, 100 wppm Polyox WSR-301

P_s inches water	DRAG Lbs.	C_d uncorrected	C_d corrected	$Re \times 10^{-5}$ corrected
		TRT 85		
9.29	1.71	1.23	1.08	.61
17.66	2.79	1.06	.93	.86
33.60	4.50	.90	.80	1.19
53.76	6.82	.85	.76	1.50
77.57	9.61	.83	.74	1.80
106.00	12.71	.80	.72	2.11
		TRT 95, 71 PDR **TRT 128**		
8.83	1.55	1.18	1.03	.61
17.82	2.79	1.05	.92	.86
32.64	4.28	.88	.79	1.17
54.52	6.51	.80	.72	1.50
77.57	9.30	.80	.72	1.80
109.00	12.71	.78	.70	2.13

TRT 136, 15 Sept. 1970 put in storage
TRT 136, 16 Sept. 1970 filled from storage, 51 PDR
TRT 146

P_s inches water	DRAG Lbs.	C_d uncorrected	C_d corrected	$Re \times 10^{-5}$ corrected
8.83	1.55	1.18	1.03	.61
17.82	2.79	1.05	.92	.86
32.64	4.34	.89	.80	1.17
53.00	6.70	.85	.76	1.48
82.18	9.61	.78	.70	1.86
107.50	13.02	.81	.73	2.12
		TRT 173		
9.14	1.40	1.03	.91	.62
17.66	2.32	.88	.79	.85
33.40	4.34	.87	.78	1.18
52.99	5.58	.71	.64	1.47
80.64	9.30	.77	.69	1.83
108.30	12.71	.79	.71	2.13

CYLINDER DRAG COEFFICIENTS

one-inch diameter cylinder, 100 wppm Polyox WSR-301

P_s inches water	DRAG lbs.	C_d uncorrected	C_d corrected	$Re \times 10^{-5}$ corrected
		TRT 228, 42 PDR		
8.91	1.55	1.17	1.02	.62
17.13	2.48	.97	.86	.85
32.64	4.50	.93	.82	1.17
49.92	6.20	.83	.74	1.44
77.57	9.36	.80	.72	1.80
103.70	12.40	.80	.72	2.08
		TRT 278, 32 PDR TRT 299		
8.75	1.46	1.12	.99	.61
17.28	2.48	.96	.85	.85
33.60	4.50	.90	.80	1.19
52.99	6.82	.86	.77	1.48
77.57	9.61	.83	.74	1.80
106.00	12.40	.78	.70	2.11
		TRT 335, 27 PDR TRT 485		
9.02	1.80	1.34	1.16	.61
17.66	2.33	.88	.79	.86
33.98	3.72	.73	.66	1.18
52.22	6.20	.80	.72	1.47
73.72	8.68	.79	.71	1.75
107.5	12.28	.77	.70	2.10
		TRT 495, 17 PDR TRT 580, 9 PDR TRT 592		
9.60	1.71	1.19	1.04	.64
18.27	3.10	1.14	1.00	.88
34.94	3.72	.71	.64	1.19
51.84	5.58	.72	.66	1.45
78.72	8.06	.69	.63	1.79
106.00	11.16	.71	.65	2.08

199

CYLINDER DRAG COEFFICIENTS

one-inch diameter cylinder, 100 wppm Polyox WSR-301

P_s inches water	DRAG lbs.	C_d uncorrected	C_d corrected	Re x 10^{-5} corrected
		TRT 662, 7 PDR		
10.14	1.80	1.19	1.04	.66
18.28	3.04	1.12	.98	.89
33.02	3.41	.69	.63	1.16
51.07	5.27	.69	.63	1.44
78.34	7.87	.67	.61	1.79
107.52	10.85	.68	.62	2.10
		TRT 737		
9.37	1.80	1.29	1.12	.63
17.66	3.16	1.20	1.05	.87
32.64	3.26	.67	.61	1.16
49.92	4.96	.67	.61	1.43
74.88	7.44	.67	.61	1.75
103.70	10.54	.68	.62	2.06
		TRT 805, 7.4 ±1.4 PDR TRT 819		
8.91	1.80	1.36	1.18	.62
16.13	3.10	1.29	1.12	.83
25.34	3.26	.86	.78	1.02
33.02	3.26	.66	.60	1.16
38.40	4.03	.70	.64	1.25
49.92	5.27	.71	.65	1.43
76.03	7.94	.70	.64	1.76
105.20	10.85	.69	.63	2.07

TRT 836, 3.5 PDR

CYLINDER DRAG COEFFICIENTS

1-1/2-inch diameter cyliner, 100 wppm Polyox WSR-301

P_s inches water	DRAG lbs.	C_d uncorrected	C_d corrected	$Re \times 10^{-5}$ corrected
		TRT 20, 70 PDR		
7.10	3.10	1.93	1.43	.90
16.90	5.02	1.33	1.05	1.34
35.52	8.06	1.01	.83	1.90
57.60	12.40	.96	.79	2.42
86.40	17.61	.91	.76	2.94
		TRT 34, 73 PDR		
6.90	1.95	1.26	1.00	.85
13.05	3.16	1.08	.88	1.16
21.50	5.27	1.10	.89	1.49
35.52	8.18	1.03	.84	1.91
58.37	12.28	.94	.78	2.42
88.32	18.35	.93	.77	2.99
		TRT 43		
7.68	2.32	1.35	1.06	.91
13.06	3.56	1.22	.97	1.17
26.88	6.04	1.00	.82	1.66
41.28	9.30	1.00	.82	2.05
64.52	13.14	.91	.76	2.54
88.32	17.98	.91	.76	3.00
		TRT 70, 81.5 PDR		
8.06	2.23	1.24	.99	.92
16.12	3.72	1.03	.84	1.29
29.76	5.95	.89	.74	1.73
45.69	9.18	.90	.75	2.14
69.12	13.64	.88	.73	2.64
92.16	17.61	.85	.71	3.04

CYLINDER DRAG COEFFICIENTS

1-1/2-inch diameter cylinder, 100 wppm Polyox WSR-301

P_s inches water	DRAG lbs.	C_d uncorrected	C_d corrected	Re x 10^{-5} corrected
		TRT 129, 77 PDR		
8.83	2.48	1.23	.98	.96
17.05	3.88	1.02	.83	1.33
31.10	6.36	.91	.76	1.76
48.00	9.61	.90	.75	2.20
72.96	13.95	.86	.72	2.70
99.84	18.60	.83	.70	3.15
		TRT 146		
8.76	2.33	1.14	.92	.95
16.13	3.66	1.01	.82	1.29
30.34	6.04	.89	.74	1.75
49.15	9.61	.87	.73	2.22
72.96	13.52	.83	.70	2.69
99.84	18.35	.82	.69	3.15
		TRT 197, 55.5 PDR		
9.02	2.02	1.00	.82	.96
17.86	3.72	.93	.77	1.35
30.72	5.89	.86	.72	1.75
48.00	8.99	.84	.71	2.18
72.96	13.33	.82	.69	2.70
99.84	17.98	.80	.67	3.16
		TRT 228		
8.26	1.83	1.00	.82	.92
15.97	3.57	1.00	.82	1.28
30.72	5.89	.86	.72	1.75
50.69	9.30	.82	.69	2.25
74.88	13.64	.81	.68	2.73
99.84	17.98	.80	.67	3.16

TRT 237, 41.5 PDR

CYLINDER DRAG COEFFICIENTS

one-inch diameter cylinder, 25 wppm Polyox WSR-301

P_s inches water	DRAG lbs	C_d uncorrected	C_d corrected	$Re \times 10^{-5}$ corrected
		TRT 15, 84 PDR		
9.60	1.61	1.12	.99	.64
17.28	2.94	1.14	1.00	.86
32.64	5.27	1.08	.95	1.18
51.84	7.90	1.02	.90	1.48
76.80	11.16	.97	.86	1.80
103.7	14.26	.92	.81	2.10
		TRT 115, 43 PDR		
9.02	1.55	1.15	1.01	.62
17.66	2.79	1.06	.93	.87
32.64	4.65	.95	.84	1.17
52.80	6.82	.86	.77	1.48
82.56	9.92	.80	.71	1.86
107.5	13.02	.81	.72	2.12
		TRT 174		
8.83	1.70	1.29	1.13	.61
17.28	2.48	.96	.85	.85
34.56	4.34	.84	.76	1.19
52.80	6.11	.77	.70	1.47
74.88	8.37	.75	.68	1.75
106.00	11.78	.74	.67	2.08
		TRT 183, 28 PDR **TRT 244**		
9.20	1.70	1.24	1.08	.63
18.04	2.54	.94	.84	.86
31.68	3.72	.78	.70	1.14
50.88	5.58	.73	.66	1.44
74.88	8.06	.72	.65	1.75
103.70	10.54	.68	.61	2.06

CYLINDER DRAG COEFFICIENTS

one-inch diameter cylinder, 25 wppm Polyox WSR-301

P_s inches water	DRAG lbs.	C_d uncorrected	C_d corrected	Re $\times 10^{-5}$ corrected
		TRT 254, 20 PDR		
		Aged 72 hours		
		TRT 254, 8.5 PDR		
9.02	1.86	1.38	1.19	.62
17.05	2.95	1.16	1.02	.85
24.96	3.41	.91	.81	1.01
30.72	3.10	.68	.62	1.12
53.76	4.50	.56	.51	1.48
82.56	6.82	.55	.51	1.84
111.40	8.99	.54	.50	2.14
		TRT 305, 7 PDR		
8.64	1.70	1.32	1.15	.61
17.66	3.10	1.17	1.02	.87
27.26	3.56	.87	.78	1.06
34.56	2.63	.51	.48	1.17
30.72	4.34	.94	.83	1.14
to	2.63	.57	.53	1.14
50.88	4.18	.55	.50	1.44
107.50	8.68	.54	.49	2.10
		TRT 315, 8 ±1.5 PDR		
		TRT 336		
10.37	1.70	1.10	.97	.66
19.20	3.10	1.08	.95	.90
35.52	4.03	.76	.69	1.21
to	2.79	.52	.48	1.21
38.40	3.04	.53	.49	1.24
107.5	8.37	.52	.48	2.08

TRT 351, 3.5 ±1.5 PDR

CYLINDER DRAG COEFFICIENTS

1-1/2-inch diameter cylinder, 5 wppm Polyox WSR-301

P_s inches water	DRAG lbs.	C_d uncorrected	C_d corrected	$Re \times 10^{-5}$ corrected
TRT 5, 57 PDR				
7.49	2.33	1.39	1.09	.89
16.51	4.34	1.18	.95	1.31
32.64	6.20	.85	.71	1.81
49.92	7.75	.69	.58	2.23
78.72	9.30	.53	.47	2.73
107.50	12.71	.53	.47	3.19
TRT 16				
8.64	1.86	.96	.79	.94
17.66	3.26	.82	.69	1.33
24.96	4.18	.75	.63	1.58
31.68	4.80	.68	.58	1.76
49.92	6.66	.60	.51	2.22
76.80	9.30	.54	.48	2.69
103.70	12.09	.52	.46	3.13
TRT 26, 30 PDR				
7.87	1.86	1.06	.86	.90
16.90	2.64	.70	.59	1.30
24.96	3.41	.61	.52	1.57
31.68	4.34	.61	.52	1.76
49.92	6.20	.55	.48	2.19
78.72	8.99	.51	.45	2.73
103.70	12.40	.53	.46	3.16
TRT 60, 21 PDR				
9.02	2.48	1.23	.98	.97
18.04	2.17	.54	.47	1.32
25.34	3.41	.60	.52	1.57
32.64	4.03	.55	.48	1.77
49.92	6.05	.54	.47	2.19
76.80	8.99	.52	.45	2.73
103.70	12.30	.53	.46	3.16

CYLINDER DRAG COEFFICIENTS

1-1/2-inch diameter cylinder, 5 wppm Polyox WSR-301

P_s inches water	DRAG lbs.	C_d uncorrected	C_d corrected	$Re \times 10^{-5}$ corrected
TRT 73, 18.5 PDR				
9.98	2.79	1.25	.99	1.03
19.20	2.02	.47	.41	1.36
32.64	3.72	.51	.44	1.78
49.92	5.89	.53	.46	2.20
72.96	8.68	.53	.46	2.65
103.70	12.40	.53	.46	3.16
TRT 120				
9.14	2.64	1.29	1.02	.98
17.28	3.10	.80	.68	1.31
to	1.86	.48	.42	1.29
24.96	2.94	.53	.46	1.55
49.92	5.89	.53	.46	2.20
103.70	12.40	.53	.46	3.16
19.20	2.17	.50	.44	1.35
TRT 130, 13 PDR				

CYLINDER DRAG COEFFICIENTS

3/4-inch diameter cylinder, 5 wppm Polyox WSR-301

P_s inches water	DRAG lbs.	C_d uncorrected	C_d corrected	Re x 10^{-5} corrected
		TRT 5, 30 PDR		
8.64	1.24	1.28	1.14	.45
15.74	2.17	1.23	1.10	.61
32.64	3.88	1.05	.96	.87
50.69	5.12	.90	.82	1.08
83.71	5.98	.64	.60	1.37
115.20	6.51	.51	.48	1.60
		TRT 16		
9.6	1.24	1.16	1.04	.47
17.66	2.11	1.07	.97	.64
31.10	3.16	.91	.83	.85
53.76	4.40	.73	.68	1.10
82.56	5.27	.57	.54	1.35
115.20	6.14	.48	.45	1.60
		TRT 24, 17 PDR		
9.6	1.24	1.16	1.04	.47
17.28	2.17	1.12	1.01	.63
33.60	3.26	.87	.80	.87
53.76	3.97	.66	.62	1.09
81.40	4.96	.55	.52	1.34
103.70	5.95	.51	.48	1.52
		TRT 57, 13 PDR		
9.6	1.24	1.16	1.04	.47
19.20	2.32	1.08	.98	.67
33.60	3.56	.95	.87	.88
53.76	3.41	.57	.54	1.09
84.48	4.65	.49	.46	1.37
111.40	5.58	.45	.43	1.56

CYLINDER DRAG COEFFICIENTS

3/4-inch diameter cylinder, 5 wppm Polyox WSR-301

P_s inches water	DRAG lbs.	C_d uncorrected	C_d corrected	Re x 10^{-5} corrected
		TRT 78		
9.37	1.24	1.18	1.06	.47
18.05	2.32	1.15	1.03	.65
33.22	3.78	1.02	.92	.88
44.16	4.30	.88	.80	.99
to	2.50	.50	.47	.99
52.99	3.10	.52	.49	1.08
81.41	4.28	.47	.45	1.33
115.20	5.58	.43	.41	1.59

TRT 89, 12 PDR

CYLINDER DRAG COEFFICIENTS

one-inch diameter cylinder, 5 wppm Polyox WSR-301

P_s inches water	DRAG lbs.	C_d uncorrected	C_d corrected	$Re \times 10^{-5}$ corrected
TRT 5, 43.5 PDR				
8.64	1.80	1.40	1.20	.61
17.66	3.26	1.25	1.08	.87
35.52	5.12	.97	.86	1.22
51.84	6.20	.80	.72	1.47
83.71	7.29	.58	.53	1.85
TRT 16, 32.5 PDR				
8.45	1.52	1.21	1.06	.60
17.89	2.17	.81	.77	.84
36.48	4.03	.74	.67	1.23
55.30	5.27	.64	.58	1.51
83.71	6.51	.52	.48	1.84
115.20	8.68	.51	.47	2.16
TRT 34, 21.5 PDR				
9.22	1.86	1.35	1.17	.63
16.74	2.63	1.06	.93	.84
33.60	3.41	.68	.62	1.17
53.76	4.40	.55	.50	1.48
80.64	5.89	.49	.44	1.83
108.30	7.44	.46	.43	2.08
TRT 55, 14.5 PDR				
8.83	1.70	1.30	1.12	.62
17.28	2.79	1.08	.95	.86
23.42	2.88	.83	.75	.98
26.88	2.48	.62	.57	1.04
33.60	2.79	.56	.51	1.17
53.37	4.03	.51	.47	1.47
80.64	5.42	.45	.42	1.79
111.40	7.56	.46	.43	2.11

CYLINDER DRAG COEFFICIENTS

one-inch diameter cylinder, 5 wppm Polyox WSR-301

P_s inches water		DRAG lbs.	c_d uncorrected	c_d corrected	$Re \times 10^{-5}$ corrected
			TRT 72, 9 PDR		
9.41		1.80	1.28	1.11	.64
18.82		2.94	1.05	.94	.88
26.88		3.41	.85	.76	1.06
	to	2.48	.62	.57	1.04
30.72		2.48	.54	.50	1.11
34.56		2.63	.51	.47	1.18
54.14		3.72	.46	.43	1.47
80.64		5.58	.46	.43	1.79
115.20		7.44	.43	.40	2.15
			TRT 85		
9.22		1.70	1.24	1.08	.63
17.51		3.10	1.19	1.04	.86
25.92		3.72	.96	.86	1.04
32.64		4.03	.83	.75	1.16
	to	2.48	.51	.47	1.15
34.94		2.48	.48	.45	1.18
52.80		3.72	.47	.44	1.45
82.56		5.83	.47	.44	1.81
			TRT 123, 4.5 ±1.5 PDR		
9.22		1.86	1.35	1.17	.63
17.28		3.10	1.20	1.05	.86
33.02		4.65	.94	.84	1.17
	to	2.48	.50	.46	1.16
38.40		2.79	.49	.46	1.23
65.28		4.34	.45	.42	1.61
92.16		6.20	.45	.42	1.92

CYLINDER DRAG COEFFICIENTS

one-inch diameter cylinder

distilled water, 5 wppm Polyox WSR-301

P_s inches water	DRAG lbs.	C_d uncorrected	C_d corrected	Re x 10^{-5} corrected
TRT 5, 50 ±1.5 PDR				
8.06	1.70	1.41	1.22	.59
16.13	3.10	1.29	1.12	.83
35.52	4.96	.94	.84	1.22
55.68	6.82	.82	.74	1.52
83.32	8.37	.67	.61	1.85
115.20	9.92	.58	.53	2.17
TRT 18, 45 PDR				
8.83	1.63	1.25	1.09	.61
17.66	3.10	1.18	1.03	.87
32.64	4.28	.88	.79	1.16
53.76	5.89	.73	.67	1.48
81.40	7.13	.59	.54	1.82
107.50	9.61	.60	.55	2.09
TRT 32, 31 PDR				
9.10	1.39	1.03	.91	.62
17.66	2.17	.82	.74	.85
34.17	3.78	.74	.67	1.19
53.76	5.12	.64	.58	1.49
80.64	6.82	.57	.52	1.81
115.20	9.30	.54	.50	2.15
TRT 60, 22.5 ±2.5 PDR				
9.98	1.80	1.21	1.06	.65
18.05	2.17	.81	.73	.86
34.94	3.41	.65	.59	1.20
51.84	4.65	.60	.54	1.46
82.56	6.51	.53	.48	1.84
115.20	9.00	.52	.47	2.18

CYLINDER DRAG COEFFICIENTS

one-inch diameter cylinder

distilled water, 5 wppm Polyox WSR-301

P_s inches water	DRAG lbs.	C_d uncorrected	C_d corrected	Re x 10^{-5} corrected
TRT 90, 16.5 ± 1 PDR				
9.60	1.86	1.30	1.13	.64
18.05	2.79	1.04	.92	.87
26.88	2.54	.63	.57	1.05
32.64	3.10	.64	.58	1.16
53.76	4.34	.54	.49	1.49
80.64	6.04	.50	.45	1.83
115.20	8.68	.51	.46	2.18
TRT 118, 13.7 ±.3 PDR				
9.98	1.70	1.15	1.01	.65
18.05	2.94	1.09	.96	.87
27.26	2.32	.57	.52	1.06
34.94	2.73	.52	.47	1.20
54.53	3.97	.49	.45	1.49
63.36	4.50	.48	.44	1.60
84.48	6.20	.49	.45	1.85
115.20	8.68	.51	.46	2.18
9.60	1.55	1.08	.95	.64
17.66	2.94	1.12	.98	.87
24.96	2.48	.67	.61	1.01
33.60	2.48	.50	.45	1.18
53.76	3.72	.46	.42	1.48
65.28	4.65	.48	.44	1.63
84.48	6.04	.48	.44	1.85
25.92	3.56	.92	.82	1.04
to	2.17	.56	.51	1.04
31.68	2.32	.49	.45	1.13
TRT 144, 11 PDR TRT 181, 10.5 PDR TRT 264, 9.5 PDR				
9.60	1.80	1.26	1.10	.64
18.05	3.26	1.21	1.06	.88
29.76	4.03	.91	.82	1.11
to	2.17	.49	.45	1.11

212

CYLINDER DRAG COEFFICIENTS

one-inch diameter cylinder

distilled water, 5 wppm Polyox WSR-301

P_s inches water	DRAG lbs.	C_d uncorrected	C_d corrected	Re x 10^{-5} corrected
		TRT 144, 11 PDR		
		TRT 181, 10.5 PDR		
		TRT 264, 9.5 PDR		
34.56	2.32	.45	.41	1.19
84.48	5.74	.46	.42	1.86
115.20	7.44	.43	.39	2.18
		aged four days		
		TRT 278, 5 PDR		
		TRT 289		
9.83	1.86	1.27	1.10	.65
17.51	2.94	1.13	.99	.86
34.56	4.96	.96	.85	1.21
35.52	5.58	1.05	.92	1.23
to	2.94	.56	.51	1.21
39.94	4.34	.73	.66	1.28
to	2.48	.42	.38	1.28
50.69	3.72	.49	.45	1.43
82.56	5.58	.45	.41	1.84
113.70	8.06	.48	.44	2.15

TRT 317, 3 PDR

CYLINDER DRAG COEFFICIENTS

P_s inches water	DRAG lbs.	C_d uncorrected	C_d corrected	Re x 10^{-5} corrected

one-inch diameter cylinder, 2.5 wppm Polyox WSR-301

TRT 10, 39 ±1 PDR

P_s inches water	DRAG lbs.	C_d uncorrected	C_d corrected	Re x 10^{-5} corrected
9.20	1.77	1.28	1.11	.63
17.28	3.10	1.20	1.05	.86
35.52	4.40	.83	.74	1.22
56.06	5.12	.61	.55	1.52
84.48	6.35	.50	.46	1.85
115.20	8.06	.47	.44	2.14

TRT 30, 19 PDR

9.02	1.70	1.26	1.10	.63
17.66	2.79	1.06	.94	.86
33.98	2.79	.55	.50	1.18
53.76	3.76	.46	.43	1.46
78.72	5.58	.47	.44	1.77
115.20	8.06	.47	.44	2.14

TRT 38, 13.5 ±1.5 PDR

9.22	1.39	1.01	.90	.62
18.43	2.63	.96	.85	.88
26.88	3.10	.77	.70	1.05
to	1.86	.46	.43	1.05
34.56	2.17	.42	.39	1.18
53.76	3.56	.44	.41	1.47
86.40	5.58	.43	.40	1.86
115.20	7.44	.43	.40	2.14

TRT 61, 5.5 ±1.5 PDR

8.91	1.39	1.05	.93	.61
18.27	2.94	1.08	.95	.88
30.72	3.72	.81	.72	1.13
to	1.86	.40	.37	1.13
36.48	2.23	.41	.38	1.21
72.96	4.49	.49	.38	1.71

CYLINDER DRAG COEFFICIENTS

P_s inches water	DRAG lbs.	C_d uncorrected	C_d corrected	$Re \times 10^{-5}$ corrected
		one-inch diameter cylinder, 2.5 wppm Polyox WSR-301		
		TRT 72		
19.58	3.25	1.11	.98	.91
26.88	4.34	1.08	.95	1.07
34.56	4.96	.96	.85	1.21
42.24	4.34	.69	.63	1.31
to	2.79	.44	.41	1.31
48.00	3.41	.48	.45	1.38
107.50	7.44	.46	.43	2.07

215

CYLINDER DRAG COEFFICIENTS

P_s inches water	DRAG lbs.	C_d uncorrected	C_d corrected	Re x 10^{-5} corrected
one-inch diameter cylinder, 2.5 wppm Polyox WSR-301				
TRT 83				
9.98	1.86	1.25	1.09	.65
18.82	3.26	1.16	1.02	.89
35.52	5.12	.96	.85	1.22
54.72	6.66	.81	.73	1.50
74.88	5.89	.53	.49	1.74
103.70	7.75	.50	.47	2.03
TRT 100				
76.80	9.30	.81	.73	1.78
to	5.58	.48	.45	1.78
one-inch diameter cylinder, 1.0 wppm Polyox WSR-301				
TRT 0, 17.5 ±.5 PDR				
12.67	2.02	1.06	.93	.73
16.89	2.17	.86	.77	.84
34.56	2.79	.54	.50	1.18
55.68	4.09	.49	.46	1.49
84.48	6.04	.48	.45	1.83
TRT 10, 10 ±1 PDR				
9.98	1.80	1.20	1.05	.65
19.20	2.79	.97	.86	.90
26.88	3.41	.85	.76	1.06
to	2.48	.62	.57	1.06
36.09	2.63	.49	.46	1.20
52.80	4.33	.51	.48	1.45
80.64	5.58	.46	.43	1.79
111.40	8.06	.48	.45	2.10

CYLINDER DRAG COEFFICIENTS

P_s inches water	DRAG lbs.	C_d uncorrected	C_d corrected	$Re \times 10^{-5}$ corrected
one-inch diameter cylinder, 1.0 wppm Polyox WSR-301				
TRT 21, 7.5 ±.5 PDR				
9.79	1.86	1.27	1.10	.65
18.43	3.10	1.13	.99	.88
27.84	4.34	1.04	.92	1.08
40.32	4.65	.77	.69	1.29
to	2.79	.46	.43	1.29
46.08	3.41	.49	.46	1.35
52.80	3.97	.50	.47	1.45
92.16	6.51	.47	.45	1.89
TRT 32, 5 PDR				
9.79	1.86	1.27	1.10	.65
17.66	3.25	1.23	1.07	.87
34.56	4.96	.96	.85	1.21
46.08	6.20	.90	.80	1.39
46.08 to	3.10	.45	.42	1.39
51.84	3.97	.51	.47	1.45
72.96	5.58	.51	.47	1.72
107.50	8.06	.50	.46	2.09
TRT 44				
9.60	1.80	1.25	1.09	.64
18.43	3.41	1.24	1.08	.89
32.64	5.27	1.08	.95	1.17
51.83	7.44	.96	.85	1.48
to	4.96	.64	.58	1.48
61.44	8.06	.88	.79	1.60
to	4.34	.47	.44	1.60
74.88	5.70	.62	.56	1.76
103.70	8.06	.52	.48	2.05
TRT 139				
10.18	1.86	1.22	1.07	.66
18.05	3.41	1.26	1.10	.88
33.60	5.89	1.17	1.02	1.20
53.76	8.06	1.00	.88	1.51
78.72	10.54	.90	.80	1.83
to	6.20	.53	.49	1.83
105.90	8.06	.51	.47	2.01

Cylinder "critical drag transition

U ft/sec	d inch	Re_c x 10^{-5}	Conc. wppm	PDR ±2
12.2	1	1.02	100	7.4
13.6	1	1.14	25	8.0
14.5	1	1.21	25	7.5
10.4	1-1/2	1.30	5	13.0
15.8	3/4	.99	5	12.5
12.5	1	1.04	5	12.5
13.3	1	1.11	5	5.0
14.6	1	1.22	5	4.0
12.5	1	1.04	5	14.5
12.6	1	1.05	5	9.0
13.8	1	1.15	5	6.0
14.0	1	1.17	5	3.0
12.6	1	1.05	2.5	13.5
13.6	1	1.13	2.5	3.5
15.8	1	1.31	2.5	3.0
21.4	1	1.78	2.5	0.0
12.7	1	1.06	1.0	10.0
15.5	1	1.29	1.0	7.5
16.7	1	1.39	1.0	5.0
17.7	1	1.48	1.0	3.0
21.9	1	1.83	1.0	0.0
18.5	1/2	1.11	5.0	8.0
22.9	1/2	1.37	5.0	3.0
>30.0	1/4	> .90	5.0	13.0

Pressure Distribution on One Inch Cylinder

100 wppm Polyox WSR-301, TRT 73, 75 PDR
Cd = 0.94
Re = 0.72×10^5

ANGLE DEGREES	MEASURED CP	ACTUAL CP
0.0	1.00	1.000
5.	0.98	0.983
10.	0.97	0.974
15.	0.87	0.887
20.	0.77	0.800
25.	0.55	0.608
30.	0.34	0.425
35.	0.10	0.216
40.	-0.13	0.016
45.	-0.40	-0.220
50.	-0.68	-0.463
55.	-0.90	-0.655
60.	-1.13	-0.855
65.	-1.27	-0.977
70.	-1.44	-1.125
75.	-1.42	-1.108
80.	-1.40	-1.091
85.	-1.31	-1.012
90.	-1.21	-0.925
95.	-1.14	-0.864
100.	-1.10	-0.829
105.	-1.03	-0.768
110.	-0.97	-0.716
115.	-0.97	-0.716
120.	-0.97	-0.716
125.	-0.97	-0.716
130.	-0.97	-0.716
135.	-0.97	-0.716
140.	-0.97	-0.716
145.	-0.97	-0.716
150.	-0.97	-0.716
155.	-0.97	-0.716
160.	-0.97	-0.716
165.	-0.97	-0.716
170.	-0.97	-0.716
175.	-0.97	-0.716
180.	-0.97	-0.716

Pressure Distribution on One-Inch Cylinder

100 wppm Polyox WSR-301, TRT 60, 70 PDR

$C_d = 0.60$

$Re = 2.1 \times 10^5$

ANGLE DEGREES	MEASURED CP	ACTUAL CP
0.0	1.00	1.000
5.0	0.98	0.982
10.0	0.94	0.946
15.0	0.83	0.846
20.0	0.69	0.718
25.0	0.47	0.519
30.0	0.25	0.319
35.0	0.00	0.092
40.0	-0.33	-0.208
45.0	-0.65	-0.498
50.0	-0.91	-0.735
55.0	-1.20	-0.998
60.0	-1.43	-1.207
65.0	-1.67	-1.425
70.0	-1.81	-1.552
75.0	-1.88	-1.615
80.0	-1.96	-1.688
85.0	-1.85	-1.588
90.0	-1.74	-1.488
95.0	-1.52	-1.289
100.0	-1.25	-1.043
105.0	-0.98	-0.798
110.0	-0.81	-0.644
115.0	-0.74	-0.580
120.0	-0.71	-0.553
125.0	-0.69	-0.535
130.0	-0.69	-0.535
135.0	-0.69	-0.535
140.0	-0.69	-0.535
145.0	-0.68	-0.526
150.0	-0.68	-0.526
155.0	-0.67	-0.517
160.0	-0.67	-0.517
165.0	-0.67	-0.517
170.0	-0.66	-0.508
175.0	-0.65	-0.498
180.0	-0.65	-0.498

Pressure Distribution on One Inch Cylinder

25 wppm Polyox WSR-301, TRT 20, 81 PDR
Cd = 0.83
Re = 1.4×10^5

ANGLE DEGREES	MEASURED CP	ACTUAL CP
0.0	1.00	1.000
5.	1.00	1.000
10.	0.94	0.947
15.	0.83	0.850
20.	0.72	0.753
25.	0.55	0.603
30.	0.33	0.409
35.	0.05	0.162
40.	-0.23	-0.085
45.	-0.51	-0.332
50.	-0.81	-0.596
55.	-1.02	-0.781
60.	-1.28	-1.011
65.	-1.46	-1.169
70.	-1.57	-1.266
75.	-1.66	-1.346
80.	-1.62	-1.310
85.	-1.49	-1.196
90.	-1.28	-1.011
95.	-1.11	-0.861
100.	-1.02	-0.781
105.	-0.95	-0.720
110.	-0.94	-0.711
115.	-0.91	-0.684
120.	-0.89	-0.667
125.	-0.89	-0.667
130.	-0.89	-0.667
135.	-0.89	-0.667
140.	-0.89	-0.667
145.	-0.89	-0.667
150.	-0.89	-0.667
155.	-0.89	-0.667
160.	-0.89	-0.667
165.	-0.89	-0.667
170.	-0.89	-0.667
175.	-0.89	-0.667
180.	-0.89	-0.667

Pressure Distribution on the One Inch Cylinder

25 wppm Polyox WSR-301, TRT 258, 25 PDR
Cd = 0.73
Re = 1.4×10^5

ANGLE DEGREES	MEASURED CP	ACTUAL CP
0.0	1.00	1.000
5.	0.99	0.991
10.	0.98	0.982
15.	0.88	0.893
20.	0.77	0.795
25.	0.57	0.616
30.	0.38	0.447
35.	0.14	0.233
40.	-0.09	0.028
45.	-0.36	-0.213
50.	-0.65	-0.472
55.	-0.90	-0.695
60.	-1.15	-0.918
65.	-1.31	-1.061
70.	-1.44	-1.177
75.	-1.44	-1.177
80.	-1.35	-1.097
85.	-1.26	-1.016
90.	-1.17	-0.936
95.	-1.08	-0.856
100.	-0.99	-0.775
105.	-0.94	-0.731
110.	-0.85	-0.650
115.	-0.82	-0.624
120.	-0.74	-0.552
125.	-0.73	-0.543
130.	-0.72	-0.535
135.	-0.72	-0.535
140.	-0.71	-0.526
145.	-0.69	-0.508
150.	-0.68	-0.499
155.	-0.67	-0.490
160.	-0.65	-0.472
165.	-0.65	-0.472
170.	-0.65	-0.472
175.	-0.65	-0.472
180.	-0.65	-0.472

Pressure Distribution on One Inch Cylinder

25 wppm Polyox WSR-30T, TRT 508, 9.6 PDR
Cd = 0.49
Re = 1.3 x 10^5

ANGLE DEGREES	MEASURED CP	ACTUAL CP
0.0	1.00	1.000
5.	0.99	0.991
10.	0.98	0.982
15.	0.84	0.853
20.	0.73	0.752
25.	0.54	0.577
30.	0.36	0.412
35.	0.09	0.164
40.	-0.17	-0.075
45.	-0.44	-0.323
50.	-0.71	-0.571
55.	-1.02	-0.856
60.	-1.33	-1.141
65.	-1.51	-1.306
70.	-1.69	-1.471
75.	-1.73	-1.508
80.	-1.78	-1.554
85.	-1.64	-1.425
90.	-1.51	-1.306
95.	-1.38	-1.187
100	-1.24	-1.058
105.	-0.98	-0.819
110.	-0.71	-0.571
115.	-0.60	-0.470
120.	-0.49	-0.369
125.	-0.47	-0.351
130.	-0.46	-0.341
135.	-0.44	-0.323
140.	-0.44	-0.323
145.	-0.44	-0.323
150.	-0.43	-0.314
155.	-0.43	-0.314
160.	-0.43	-0.314
165.	-0.42	-0.305
170.	-0.42	-0.305
175.	-0.42	-0.305
180.	-0.42	-0.305

Pressure Distribution on One-Inch Cylinder

25 wppm Polyox WSR-301, TRT 626, 4 PDR, at "critical" speed 15.2 ft/sec

Angle degrees	C_p measured
0	.96 to 1.04
10	.91 to 1.04
20	.62 to .75
30	.18 to .41
40	.13 to - .23
50	- .50 to - .82
60	-1.27 to -1.45
70	-1.64 to -1.90
80	-1.46 to -2.00
90	-0.73 to -1.73
100	-0.64 to -1.45
110	- .45 to - .91
120	- .45 to - .77
135	- .41 to - .50
180	- .36 to - .55

Pressure Distribution on One Inch Cylinder

5 wppm Polyox WSR-301, TRT 151, 12 PDR
Cd = 1.02
$Re = .96 \times 10^5$

ANGLE DEGREES	MEASURED CP	ACTUAL CP
0.0	1.00	1.000
5.	1.00	1.000
10.	0.97	0.974
15.	0.86	0.879
20.	0.73	0.767
25.	0.54	0.603
30.	0.27	0.370
35.	0.09	0.214
40.	-0.23	-0.062
45.	-0.45	-0.252
50.	-0.68	-0.450
55.	-0.95	-0.683
60.	-1.14	-0.848
65.	-1.27	-0.960
70.	-1.27	-0.960
75.	-1.23	-0.925
80.	-1.18	-0.882
85.	-1.09	-0.804
90.	-1.00	-0.727
95.	-1.00	-0.727
100.	-1.00	-0.727
105.	-1.00	-0.727
110.	-1.00	-0.727
115.	-1.00	-0.727
120.	-1.00	-0.727
125.	-1.00	-0.727
130.	-1.00	-0.727
135.	-1.00	-0.727
140.	-1.00	-0.727
145.	-1.00	-0.727
150.	-1.09	-0.804
155.	-1.09	-0.804
160.	-1.18	-0.882
165.	-1.18	-0.882
170.	-1.18	-0.882
175.	-1.18	-0.882
180.	-1.18	-0.882

Pressure Distribution on One Inch Cylinder

5 wppm Polyox WSR-301, TRT 161, 12 PDR
Cd = 0.36
Re = 2.0 x 10^5

ANGLE DEGREES	MEASURED CP	ACTUAL CP
0.0	1.00	1.000
5.	1.00	1.000
10.	0.98	0.981
15.	0.88	0.888
20.	0.73	0.748
25.	0.51	0.543
30.	0.31	0.357
35.	0.07	0.133
40.	-0.23	-0.147
45.	-0.50	-0.399
50.	-0.88	-0.753
55.	-1.19	-1.042
60.	-1.46	-1.294
65.	-1.69	-1.508
70.	-1.77	-1.583
75.	-1.96	-1.760
80.	-1.92	-1.723
85.	-1.92	-1.723
90.	-1.85	-1.657
95.	-1.69	-1.508
100.	-1.54	-1.368
105.	-1.31	-1.154
110.	-0.85	-0.725
115.	-0.58	-0.473
120.	-0.42	-0.324
125.	-0.35	-0.259
130.	-0.31	-0.221
135.	-0.31	-0.221
140.	-0.31	-0.221
145.	-0.31	-0.221
150.	-0.31	-0.221
155.	-0.31	-0.221
160.	-0.31	-0.221
165.	-0.31	-0.221
170.	-0.31	-0.221
175.	-0.31	-0.221
180.	-0.31	-0.221

APPENDIX B

DISCUSSION OF EXPERIMENTAL ERRORS

Since the study of the flow of dilute Polyox solutions past bluff bodies was principally a comparison of the body forces produced in tap water with the body forces produced in polymer solutions, it was essential to estimate the minimum magnitude of the change of these forces that could be reliably determined.

Two sources of error were common to the measured stagnation pressure and lift and drag forces: calibration and the balance and zero shift in the transducer-recorder system. The first was estimated to have introduced a relative error of 3%. The latter was assumed to have an error of 3%. In addition, the estimated error in reading of the recorder chart was approximately 0.3 mm which corresponded to an error of approximately 3% since the strip chart recorder attentuation was usually set at a value which provided at least 10 mm deflection. This, however, was not always possible for the force measurements at the lowest velocity and for the lift force measurements at zero nominal angle of attack.

Two additional errors were applicable to the measured hydrofoil drag force. The lift force caused deflections in the drag-force sensing beam equal to an apparent drag force of 1% of the applied lift force. Due to bearing friction, a minimum of 0.25 pounds drag force was necessary to cause reproducible strain gage output.

The expected total error is defined as the square root of the sum of the individual errors squared. Therefore, the expected total error

was estimated to be 5% for the pressure and lift and cylinder drag forces at the higher velocities. The expected total error for the hydrofoil lift force at zero nominal angle of attack and for the cylinder drag force at the lowest velocity was estimated to be 9%. The expected error for the hydrofoil drag force was estimated to vary at the high velocities from 7% at zero angle of attack to 12% at six degrees and larger. At low velocities, the hydrofoil drag force was expected to be unreliable.

Since the error in drag coefficient is due to errors in both stagnation pressure and drag force, the expected total relative error in C_d varied from 10% at the lowest velocity to 7% at the higher velocities. The expected relative error for the Reynolds number (based on the viscosity of water) was one-half the relative error for stagnation pressure, exclusive of any pressure anomaly in the polymer solutions.

LIST OF REFERENCES

1. Toms, B. A., "Some Observations on the Flow of Linear Polymers through Straight Tubes at Large Reynolds Numbers," Proc. Int'l. Cong. Rheol. Part II, 1949.

2. Hoyt, J. W. and Fabula, A. G., "The Effect of Additives on Fluid Friction," 5th Symposium Naval Hydrodynamics ACR-112, p. 947-974, Sept. 1964.

3. Deavours, C. A., A Critical Survey of Literature Concerning the Toms' Effect, Div. of Applied Mathematics, Brown U. Tech. Report No. 1, Project No. NR062-179/8-2-65, May 1966.

4. Lumley, J. L., "The Toms Phenomenon: Anomalous Effects in Turbulent Flow of Dilute Solutions of High Molecular Weight Linear Polymers," Applied Mechanics Reviews, V. 20, no. 12, p. 1139-49, Dec. 1967.

5. White, A., "Some Observations on the Flow Characteristics of Certain Dilute Macromolecular Solutions," Proceedings of the Symposium on Viscous Drag Reduction, Dallas Texas, Sept. 1968, p. 107-130, Plenum Press, 1969.

6. Crawford, H. R. and Pruitt, G. T., Symposium Non-Newtonian Fluid Mechanics, 56th Annual Meeting Inst. Chem. Eng., Houston, Texas, Dec. 1963.

7. Ruszczycky, M. A., "Sphere Drop Tests in High-polymer Solutions," Nature, v. 206, p. 614-15, May 1965.

8. White, A., "Effect of Polymer Additives on Boundary Layer Separation and Drag of Submerged Bodies," Nature, v. 211, p. 1390, Sept. 1966.

9. White, A., "Drag of Spheres in High Polymer Solutions," Nature, v. 216, p. 994, Dec. 1967.

10. Brennen, C. and Gadd, G. E., "Aging and Degradation in Dilute Polymer Solutions," Nature, v. 215, p. 1368, 1967.

11. Lang, T. G. and Patrick, H. V. L., Drag of Blunt Bodies in Polymer Solutions, Naval Ordnance Test Station Tech. Report 4379, July, 1967.

12. Hayes, M. F., Drag Coefficients of Spheres Falling in Dilute Aqueous Solutions of Long-Chain Macromolecules, M.S. Thesis, Naval Postgraduate School, Monterey, 1966.

13. Chenard, J. H., Drag of Spheres in Dilute Aqueous Solutions of Poly(ethylene oxide) within the Region of the Critical Reynolds, M.S. Thesis, Naval Postgraduate School, Monterey, 1967.

14. James, D. F., _Laminar Flow of Dilute Polymer Solutions Around Circular Cylinders_, Ph. D. Thesis, California Institute of Technology, Pasadena, 1967.

15. McClanahan, T. and Ridgely, P. J., _Drag of Circular Cylinders in Dilute Solutions of Poly(ethylene oxide) for Flows Characterized by Laminar Boundary Layer Separation_, M.S. Thesis, Naval Postgraduate School, Monterey, 1968.

16. Sanders, J. V., "Drag Coefficients of Spheres in Poly(ethylene oxide) Solutions," _Int'l. Shipbuilding Progress_, v. 14, p. 140-157, Apr. 1967.

17. Brennen, C., "Some Cavitation Experiments with Dilute Polymer Solutions," J. Fluid Mech., v. 44, p. 51-63, 1970.

18. Luikov, A. V., Shul'man, Z. P. and Puris, B. I., "Mass Transfer of a Cylinder in Forced Flow of a Non-Newtonian Viscoelastic Fluid," _Heat-Transfer-Soviet Research_, v. 1, no. 1, p. 121-32, 1969.

19. Barenblatt, G. I., Bulina, I. G. and Myasnikov, V. P., "Drag Reducing Effect of Solutions of Some High-Molecular Compounds in Turbulent Flow Past Bodies," _Zhurnal Prikladnoi Mekh. i Tekhn. Fiziki_, no. 3, p. 95-6, 1965.

20. Paterson, R. W., _Turbulent Flow Drag Reduction and Degradation with Dilute Polymer Solutions_, Div. of Eng. and Applied Physics, Eng. Sci. Lab., Harvard University, 1969.

21. Virk, P. S., Mickley, H. S. and Smith, K. A., "The Ultimate Asymptote and Mean Flow Structure in Toms' Phenomenon," _Trans. of the ASME, J. of Applied Mechanics_, p. 488-93, June 1970.

22. Sarpkaya, T., _Resistance to the Flow of Dilute Aqueous Polymer Solutions_, Research Proposal submitted to NSRDC, 15 Feb., 1968.

23. Lienhard, J. H., _Synopsis of Lift, Drag and Vortex Frequency Data for Rigid Circular Cylinders_, College of Eng. Research Div., Washington State University, Bulletin 300, 1966.

24. Schlichting, H., _Boundary Layer Theory_, Pergamon Press, 1955.

25. Fage, A., "The Drag of Circular Cylinders and Spheres at High Values of Reynolds Number," _A.R.C. R&M 1370_, 1930.

26. Fage, A. and Falkner, V. M., "Further Experiments on the Flow Around a Circular Cylinder," _A.R.C. R&M 1369_, 1931.

27. Fage, A. and Warsap, "The Effects of Turbulence and Surface Roughness on the Drag of a Circular Cylinder," _A.R.C. R&M 1283_, 1930.

28. Delany, N. K. and Sorensen, N. E., Low Speed Drag of Circular Cylinders of Various Shapes, NACA TN 3038, 1953.

29. Humphreys, J. S., "On a Circular Cylinder in a Steady Wind at Transition Reynolds Numbers," J. Fluid Mech., v. 9, pt. 4, p. 603-12, 1960.

30. Roshko, A., "Experiments on the Flow Past a Circular Cylinder at Very High Reynolds Number," J. Fluid Mech., v. 10, pt. 3, p. 345-56, 1961.

31. Luthander, S. and Rydberg, A., "Experimentelle Untersuchungen uber den Luftwiderstand bei einer um eine mit der Windrichtung parallelen Anhse rotierrenden Kugel," Phys. Z., v. 36, p. 552, 1935.

32. Peterka, J. A. and Richardson, P. D., "Effects of Sound on Separated Flows," J. Fluid Mech., v. 37, pt. 2, p. 265-87, 1969.

33. Dale, J. R. and Holler, R. A., "Secondary Vortex Generation in the Near Wake of Circular Cylinders," J. Hydronautics, v. 4, no. 1, p. 10-15, Jan. 1970.

34. Kestin, J. and Wood, R. T., "On the Stability of Two-Dimensional Stagnation Flow," J. Fluid Mech., v. 44, p. 461-79, 1970.

35. Gadd, G. E., "Effects of Long-Chain Molecule Additives in Water on Vortex Streets," Nature, v. 211, p. 169-70, 1966.

36. Kalashnikov, V. W. and Kudin, A. M., "Karman Vortices in the Flow of Drag Reducing Polymer Solutions," Nature, v. 225, p. 445, 1970.

37. White, W. C. and McEligot, D. M., "Transition of Mixtures of Polymers in a Dilute Aqueous Solution," presented at Winter Annual, ASME, Los Angeles, paper no. 69-WA/FE-20, Nov. 1969.

38. Hendricks, R. L., Flow of Dilute Polymer Solutions about Submerged Bodies, M.S. Thesis, Naval Postgraduate School, Monterey, 1970.

39. Maskell, E. C., A Theory of the Blockage Effects on Bluff Bodies and Stalled Wings in a Closed Wind Tunnel, A.R.C., R. No. 3400, 1965.

40. Roshko, A., On the Drag and Shedding Frequency of Two-Dimensional Bluff Bodies, NACA TN 3169, 1954.

41. White, D. A., "Drag Coefficients for Spheres in High Reynolds Number Flow of Dilute Solutions of High Polymers," Nature, v. 212, p. 277, 1966.

42. Fabula, A. G., An Experimental Study of Grid Turbulence in Dilute High-Polymer Solutions, Ph.D. Thesis, Pennsylvania State U., 1966.

43. Friehe, C. A. and Schwarz, W. H., "Grid-Generated Turbulence in Dilute Polymer Solutions," J. Fluid Mech., v. 44, pt. 1, p. 173-93, 1970.

44. Ultman, J. S. and Denn, M. M., "Anomalous Heat Transfer and a Wave Phenomenon in Dilute Polymer Solutions," Trans. of the Society of Rheology, v. 14, pt. 3, p. 307-17, 1970.

45. Coleman, B. D. and Gurtin, M. E., "On the Stability against Shear Waves of Steady Flows of Non-Linear Visco-Elastic Fluids," J. Fluid Mech., v. 33, pt. 1, p. 165-181, 1968.

46. Tlapa, G. A., Elastic Recovery and the Toms Effect--A Simple Model, Illinois Inst. of Tech., Dept. of Mathematics TR4, July 1968.

47. Beard, D. B. and Walters, K., "Elastico-Viscous Boundary-Layer Flows, I. Two-Dimensional Flow near a Stagnation Point," Proc. Camb. Phil. Soc., v. 60, p. 667, 1964.

48. White, F. M., "A Theory of Boundary-Layer Flow Noise with Application to Pressure Gradients and Polymer Solutions," J. Hydronautics, v. 3, no. 2, Apr. 1969.

49. Walsh, A. M., On the Turbulent Flow of Dilute Polymer Solutions, Ph.D. Thesis, California Inst. of Tech., Pasadena, 1967.

50. Woolery, E. F., Drag of Free-Falling Spheres in Dilute Aqueous Solutions of Poly(Ethylene oxide) for Reynolds Numbers above the Critical Value, M.S. Thesis, Naval Postgraduate School, 1968.

51. Schubauer, G. B. and Skramstad, H. K., "Laminar Boundary Layer Oscillations and Stability of Laminar Flow," J. Aero. Sci., v. 14, p. 69, 1947.

INITIAL DISTRIBUTION LIST

No. Copies

1. Defense Documentation Center   2
   Cameron Station
   Alexandria, Virginia   22314

2. Library, Code 0212   2
   Naval Postgraduate School
   Monterey, California   93940

3. Professor T. Sarpkaya, Code 59Sl   3
   Department of Mechanical Engineering
   Naval Postgraduate School
   Monterey, California   93940

4. LT Peter Garland Rainey, USN   2
   223 West 148th Place
   Dolton, Illinois   60419

233

DOCUMENT CONTROL DATA - R & D

(Security classification of title, body of abstract and indexing annotation must be entered when the overall report is classified)

1 ORIGINATING ACTIVITY (Corporate author)	2a. REPORT SECURITY CLASSIFICATION
Naval Postgraduate School Monterey, California 93940	Unclassified
	2b. GROUP

3 REPORT TITLE

The Flow of Dilute Polymer (Polyox WSR-301) Solutions past Bluff Bodies in the Drag Transition Region

4 DESCRIPTIVE NOTES *(Type of report and inclusive dates)*
Doctoral Thesis; March 1971

5 AUTHOR(S) *(First name, middle initial, last name)*

Peter Garland Rainey, Lieutenant, United States Navy

6 REPORT DATE	7a. TOTAL NO. OF PAGES	7b. NO. OF REFS
March 1971	235	51

8a. CONTRACT OR GRANT NO	9a. ORIGINATOR'S REPORT NUMBER(S)
WR-0-7008	
b. PROJECT NO.	
c.	9b. OTHER REPORT NO(S) *(Any other numbers that may be assigned this report)*
d.	

10 DISTRIBUTION STATEMENT

Approved for public release; distribution unlimited.

11. SUPPLEMENTARY NOTES	12. SPONSORING MILITARY ACTIVITY
	Naval Postgraduate School Monterey, California 93940

13. ABSTRACT

Flow of aqueous solutions of Polyox WSR-301, with concentrations of 1.0 to 200 wppm, past bluff bodies was investigated in the cylinder drag transition region of Reynolds numbers. Lift and drag forces were measured on a NACA-0024, four-inch chord hydrofoil. Drag force, pressure distribution and separation angle were measured on circular cylinders (diameters from 1/4 to 1-1/2 inch).

The polymer additive was found to alter only those drag coefficients which have a Reynolds number transition region. Two distinct types of cylinder drag transition were observed: (1) At high concentrations, transition from sub-critical to a transcritical flow occurred at the same free stream velocity independent of body diameter; and (2) at low concentrations and/or molecular weights, tripping from a sub-critical to a super-critical flow occurred at a well defined flow condition which was a function of free stream velocity, body diameter and turbulent pipe-flow friction reduction. In all cases, transition occurred earlier than that in the pure solvent. The polymer had a de-stabilizing effect on the boundary layer flow.

14.

KEY WORDS	LINK A		LINK B		LINK C	
	ROLE	WT	ROLE	WT	ROLE	WT
POLYMER						
CIRCULAR CYLINDER						
DRAG REDUCTION						
FLOW ABOUT CIRCULAR CYLINDERS						

DD FORM 1473 (BACK)
1 NOV 65

S/N 0101-807-6821

235

UNCLASSIFIED
Security Classification

A-3140